

ИНСТИТУТ ЗА ФИЗИКУ			
ПРИМЉЕНО:		26. 04. 2021	
Рад.јед.	б р о ј	Арх.шифра	Прилог
0801	320/1		

Образложење предлога Др Јадранке Васиљевић за добитника Студентске награде Института за физику у Београду за 2021. годину

Др Јадранка Васиљевић је докторску дисертацију под називом **“Propagation, localization and control of light in Mathieu lattices”** (срп. **„Простирање, локализација и контрола светлости у Матјеовим решеткама“**) урадила у Лабораторији за нелинеарну фотонику Института за физику под менторством Др Драгане Јовић Савић и коменторством Др Дејана Тимотијевића, а одбринила је на Физичком факултету Универзитета у Београду. Истраживања у оквиру њене дисертације усмерена су на изучавање Матјеових зрака: феномена који су везани за простирање различитих Матјеових зрака у нелинеарној средини, као и формирање нових врста аperiодичних фотонских решетки помоћу њих, затим неуређених решетки и вођење таласа у њима а у циљу изучавања ефеката локализације светлости.

Сва истраживања у оквиру докторске дисертације резултат су **теорјетског, нумеричког и експерименталног** истраживања. Кандидаткиња је најпре развила одговарајући тероријски модел, затим направила нумерички код и тако добила нумеричка решења, која су поређена са експерименталним резултатима, како би се квалитативно и квантитативно објаснили фундаментални феномени нелинеарне фотонику у оваквим срединама. Нумеричке симулације је урадила у оквиру Лабораторије за нелинеарну фотонику Института за физику, а потом је добијене резултате експериментално реализовала делом на Институту за физику а делом на Институту за примењену физику, Универзитета у Минстеру. У оквиру својих посета Институту за примењену физику, Универзитета у Минстеру, Јадранка је усавршила експерименталну технику оптичке индукције која омогућава генерисање фотонских решетки коришћењем недифрагујућих зрака и проучавања феномена простирања светлости у фотонским решеткама.

Резултати које је кандидаткиња приказала у својој дисертацији подељени су у три целине. У *провој* целини испитивала је нелинеарну само-интеракцију појединачног Матјеовог зрака у кристалу стронцијум баријум ниобату. Пронашла је да зраци најнижег реда показују понашање слично дискретној дифракцији у једнодимензионалној решетки у линеарном режиму, док Матјеови зраци вишег реда показују ефекте дискретне дифракције приликом преласка са једно- на дводимензионални систем. Испитала је и елиптичне Матјеове зраке у разним нелинеарним режимима и показала да су погодни за реализацију динамичких структура које ротирају током пропагације у правцу протока енергије. Такве ротирајуће динамичке структуре погодне су за израду закривљених таласовода са могућношћу контролисања закривљености као и броја таласовода. Ово истраживање представља значајан допринос у области јер уводи потпуно нови приступ за реализацију хиралних дводимензионалних фотонских решетки са подесивим особинама. Друга целина њене тезе односи се на испитивање простирања елиптичног вортексног зрака у фотонским решеткама креираним помоћу појединачних Матјеових зрака. Пронашла је врсту дискретних вортексних зрака, тзв. елиптичне огрлице и показала да се променом реда решетке као и њеног елиптицитета, могу контролисати облик и величина оваквих огрлица. У *трећој* целини кандидаткиња је увела потпуно нови приступ за генерисање дводимезионих аperiодичних решетки коришћењем интерференције више Матјеових зрака. У зависности од конфигурације зрака, њиховог међусобног растојања и угла ротације

или фазне релације међу њима, добијене су различите класе сложених фотонских структура. Експериментална техника је базирана на методи оптичке индукције у једном паралелном процесу уписивања и простирања. У таквим решеткама испитивала је простирање уског Гаусијанског пробног зрака као и како локално окружење утиче на дифракцију пробног зрака и услове за формирање јако локализованих стања као што су просторни солитони. Изучавала је још један степен слободе контроле протока и локализације светлости додавањем неуређености у аперидичну Матјеову решетку. Показала је да у оваквим неуређеним решеткама најпре долази до појачаног транспорта а затим и до Андерсонове локализације светлости.

Најбољи показатељ квалитета Јадранкиног истраживања као и њеног доктората јесу категорије часописа у којима су њени резултати објављени. Такође треба нагласити и њен висок ниво компетентности у својој области. О томе најбоље сведочи то што су сви њени радови у часописима који су концентрисани на јасно дефинисану област оптике. Поједини часописи су њене резултате издвојили као значајан допринос и сврстали их међу најбоље у тој години:

1. Рад „*Visualizing the Energy Flow of Tailored Light*“ објављен у часопису *Advanced Optical Materials* одабран је као један од најбољих за 2018. годину. Као такав уврштен је у специјално издање часописа *Best of Advanced Optical Materials 2018*.

<https://onlinelibrary.wiley.com/page/journal/21951071/homepage/best-of-advanced-optical-materials-2018.html>

2. Резултати њених истраживања под називом „*Expanding Discrete Optics with Mathieu Beams*“ објављени су у специјалном децембарском издању *Optics & Photonics News-a. Optics & Photonics News* је специјални месечни магазин најпознатијег издавача у области оптике – *Optical Society of America*, који као такав нема импакт фактор али објављује најновија детаљна достигнућа на пољу оптике. Његово посебно (децембарско) издање *Optics in 2019*, издваја најзначајнија рецензирана истраживања оптике која су се појавила током протекле године.

https://www.osa-opn.org/home/articles/volume_30/december_2019/features/optics_in_2019/

Осим тога Јадранка је и добитник награде за најбољи студентски постер на конференцији PHOTONICA 2019, Београд 26-30 Август, 2019.

Имајући у виду квалитет њеног научно-истраживачког рада, достигнути степен истраживачке компетентности, лични допринос кандидата као и квалитет докторске дисертације изузетно ми је задовољство да предложим Др Јадранку Васиљевић за студенстку награду Института за физику за ову годину.

Предлаже:



Др Драгана Јовић Савић

Научни саветник

Руководилац Лабораторије за нелинеарну фотонику

Биографија кандидата:

Јадранка Васиљевић рођена је у Краљеву 1990. године где је завршила основну и средњу школу. Основне академске студије уписала је 2009. а завршила их 2013. године на Природно-математичком факултету Универзитета у Крагујевцу, смер Физика, са просечном оценом 9,51. Исте године уписала је мастер академске студије на Природно-математичком факултету Универзитета у Крагујевцу, смер Физика, које је завршила 2014. године са просечном оценом 9,5. Завршни рад под називом: **”Простирање и локализација светлости у квазипериодичним фотонским решеткама”**, који је урадила на Институту за физику у Лабораторији за нелинеарну фотонику под менторством Др Драгане Јовић Савић, одбранила је 2014. године на Природно-математичком факултету Универзитета у Крагујевцу.

Школске 2014/2015. године Јадранка је уписала Докторске академске студије на Физичком факултету Универзитета у Београду, студијски програм *Квантна оптика и ласери*. Докторску дисертацију под називом **“Propagation, localization and control of light in Mathieu lattices”** урадила је под менторством Др Драгане Јовић Савић и коменторством Др Дејана Тимотијевића у Лабораторији за нелинеарну фотонику на Институту за физику и одбранила је 30. 9. 2020. на Физичком факултету Универзитета у Београду.

Добитник је стипендије Фонда за младе таленте Републике Србије, Министарства омладине и спорта - „Доситеја“, школске 2012-2013 године, током завршне године основних академских студија. На докторским студијама била је стипендиста Министарства просвете, науке и технолошког развоја (2015-2017). Од новембра 2017. године запослена је на Институту за физику у Београду као истраживач приправник у Лабораторији за нелинеарну фотонику, где је била ангажована на пројекту основних истраживања ОИ171036 *„Нелинеарна фотоника нехомогених средина и површина“* Министарства просвете, науке и технолошког развоја Републике Србије чији руководицац је била Др Драгана Јовић Савић. У звање истраживач сарадник изабрана је 9. 7. 2019. године, а у звање научни сарадник 22. 1. 2021. године.

Учествовала је и на DAAD билатералном пројекту између Републике Србије и Републике Немачке *„Контрола светлости помоћу детерминистичких аperiodичних и комплексних фотонских решетки“* (2016-2017 године), у оквиру ког је више пута посетила Институт за примењену физику, Универзитета у Минстеру, Немачка.

Њена област истраживања је нелинеарна фотоника. Резултате свог досадашњег истраживања публиковала је у шест радова. Радови који су ушли у докторску дисертацију публиковани су у следећим категоријама: један рад је у међународном часопису категорије M21a, четири рада публикована су у три часописа категорије M21. На три рада Јадранка је први аутор, а на два други. Према бази Scopus, радови су до сада цитирани 12 пута. Према овој бази Хиршов индекс кандидата је 2. Поред тих радова има и један рад категорије M22, једно предавање по позиву са међународног скупа штампано у изводу (M32), као и 4 саопштења са међународних скупова штампана у изводу (M34). Дисертација је изузетно концизна, темељна и прегледна. Написана је на енглеском језику на 65 страна.

Списак радова Др Јадранке Васиљевић

(* резултати докторске дисертације)

2.1. Радови у међународним часописима изузетних вредности (M21a)

1. * Alessandro Zannotti, **J. M. Vasiljević**, D. V. Timotijević, D. M. Jović Savić and Cornelia Denz, "Visualizing the Energy Flow of Tailored Light", *Advanced Optical Materials* 6(8), 1701355-1 – 1701355-6 (2018). **M21a, IF=7.430, Optics: 7/95.**

2.2. Радови у врхунским међународним часописима (M21)

1. * **J. M. Vasiljević**, Alessandro Zannotti, D. V. Timotijević, Cornelia Denz and D. M. Jović Savić, "Light propagation in aperiodic photonic lattices created by synthesized Mathieu–Gauss beams", *Appl. Phys. Lett.* **117**, 041102-1 - 041102-5 (2020). **M21, IF=3.597, Physics, Applied: 37/154.**
2. * Alessandro Zannotti, **J. M. Vasiljević**, D. V. Timotijević, D. M. Jović Savić, and Cornelia Denz, "Morphing discrete diffraction in nonlinear Mathieu lattices", *Optics Letters*, Vol. 44(7), 1592 - 1595, (2019). **M21, IF= 3.714, Optics: 20/97.**
3. * **J. M. Vasiljević**, Alessandro Zannotti, D. V. Timotijević, Cornelia Denz and D. M. Jović Savić, "Elliptical vortex necklaces in Mathieu lattices", *Phys. Rev. A* 97, 033848-1 - 033848-5 (2018). **M21, IF= 2.909, Optics (2017): 23/94.**
4. * **J. M. Vasiljević**, Alessandro Zannotti, D. V. Timotijević, Cornelia Denz and D. M. Jović Savić, "Creating aperiodic photonic structures by synthesized Mathieu-Gauss beams", *Phys. Rev. A* 96, 023840-1 – 023840-5 (2017). **M21, IF= 2.909, Optics (2017): 23/94.**

2.3. Радови у истакнутим међународним часописима (M22)

1. N. M. Lučić, D. M. Jović Savić, A. Piper, D. Ž. Grujić, **J. M. Vasiljević**, D. V. Pantelić, B. M. Jelenković, and D. V. Timotijević, "Light propagation in quasi-periodic Fibonacci waveguide arrays", *Journal of the Optical Society of America B* 32, 1510 -1513 (2015). **M22, IF= 1.731, Optics (2015): 41/90.**

2.4. Предавање по позиву са међународног скупа штампано у изводу (M32)

1. * Jadranka M. Vasiljević, „Localization of Light in Mathieu Aperiodic Photonic Lattices“, Book of abstracts of Webinar on Laser, Optics & Photonics October 21-22, pp 21, (2020).

2.5. Саопштења са међународних скупова штампана у изводу (M34)

1. * **J. M. Vasiljević**, Alessandro Zannotti, D. V. Timotijević, Cornelia Denz and D. M. Jović Savić, „Waveguiding in Mathieu photonic lattices“, VII International School and Conference of Photonics, Belgrade, Serbia, August 26-30 (2019). ISBN 978-86-7306-153-5.

2. * Marius Rimmner, Alessandro Zannotti, **J. M. Vasiljević**, D. V. Timotijević, D. M. Jović Savić, Cornelia Denz, „*Chirality and discrete diffraction in nonlinear Mathieu lattices*“, SPIE Photonics Europe, Strasbourg, France, April 22-26, pp 75 (2018).
3. * **J. M. Vasiljević**, Alessandro Zannotti, D. V. Timotijević, Cornelia Denz and D. M. Jović Savić, „*Realizing aperiodic photonic lattices by synthesized Mathieu-Gauss beams*“, VI International School and Conference of Photonics, Belgrade, Serbia, August 28-September 1 (2017). ISBN 978-86-82441-46-5
4. **J. M. Vasiljević**, N. M. Lučić, D. V. Timotijević, A. Piper, D. Ž. Grujić, D. V. Pantelić, B. M. Jelenković and D. M. Jović Savić, „*Light propagation in deterministic aperiodic Fibonacci waveguide arrays*“, V International School and Conference on Photonics, Belgrade, Serbia, August 24-28 (2015). ISBN 978-86-7306-131-3





2.6. Одбрањена докторска дисертација (M70)

1. Јадранка М. Васиљевић “Propagation, localization and control of light in Mathieu lattices”, Универзитет у Београду, Физички факултет (2020).

Light propagation in aperiodic photonic lattices created by synthesized Mathieu–Gauss beams

Cite as: Appl. Phys. Lett. **117**, 041102 (2020); <https://doi.org/10.1063/5.0013174>

Submitted: 08 May 2020 . Accepted: 14 July 2020 . Published Online: 27 July 2020

Jadranka M. Vasiljević , Alessandro Zannotti, Dejan V. Timotijević , Cornelia Denz , and Dragana M. Jović Savić 



View Online



Export Citation



CrossMark

Lock-in Amplifiers
up to 600 MHz



Watch



Light propagation in aperiodic photonic lattices created by synthesized Mathieu–Gauss beams

Cite as: Appl. Phys. Lett. **117**, 041102 (2020); doi: [10.1063/5.0013174](https://doi.org/10.1063/5.0013174)

Submitted: 8 May 2020 · Accepted: 14 July 2020 ·

Published Online: 27 July 2020







View Online



Export Citation



CrossMark

Jadranka M. Vasiljević,^{1,a)}  Alessandro Zannotti,² Dejan V. Timotijević,¹  Cornelia Denz,² 
and Dragana M. Jović Savić¹ 

AFFILIATIONS

¹Institute of Physics, University of Belgrade, P.O. Box 68, 11001 Belgrade, Serbia

²Institute of Applied Physics and Center for Nonlinear Science (CeNoS), University of Muenster, 48149 Muenster, Germany

^{a)} Author to whom correspondence should be addressed: jadranka@ipb.ac.rs

ABSTRACT

We investigate light propagation in a two-dimensional aperiodic refractive index lattice realized using the interference of multiple Mathieu–Gauss beams. We demonstrate experimentally and numerically that such a lattice effectively hinders linear light expansion and leads to light localization, compared to periodic photonic lattices in a photorefractive crystal. Most promisingly, we show that such an aperiodic lattice supports the nonlinear confinement of light in the form of soliton-like propagation that is robust with respect to changes in a wide range of intensities.

Published under license by AIP Publishing. <https://doi.org/10.1063/5.0013174>

Diffraction is a fundamental feature of wave dynamics in any branch of physics that involves waves: optics, acoustics, quantum mechanics, etc. However, in many applications, propagation-invariant transverse intensity distributions, referred to as nondiffracting beams, are needed. Nondiffracting beams are exact solutions of the Helmholtz equation, which exist in different coordinate systems:¹ superposition of plane waves in Cartesian, Bessel beams in circular cylindrical,² Mathieu beams in elliptic cylindrical,³ and parabolic beams in parabolic cylindrical coordinates.⁴

The potential of nondiffracting structures is well recognized in modern photonic research.^{5–9} Among them, the propagation of light through tailored refractive index modulations optically fabricated in photosensitive media by propagation-invariant intensity profiles became the subject of extensive theoretical and experimental investigations since the resulting refractive index structure represents a pure 2D material.^{10–14} This field of linear and nonlinear optics in photonic lattices typically uses simple nondiffracting Cartesian beam configurations, often hexagonal light structures, to modulate the refractive index since this allows mimicking features of 2D graphene,¹⁵ its famous bandgap structure,¹⁶ or its nonlinear light matter interaction, leading to spatial soliton formation.¹⁷ In a few recent studies, solitons, elliptically shaped vortex solitons, or even vortex necklaces are observed in optically induced photonic lattices by nondiffracting Mathieu beams.^{12,18–20} Moreover, the superposition of this kind of elliptic nondiffracting beam allows the formation of different aperiodic photonic structures.²¹

Although the physics of periodic photonic systems is of fundamental interest, deviation from periodicity is important as it leads to higher complexity. One such deviation in optics results in the realization of photonic quasicrystals,⁸ structures with a reduced degree of order between periodic and disordered ones.

The localization of waves is an intriguing research subject observed in a variety of classical and quantum systems,^{22,23} including light waves,^{24–27} Bose–Einstein condensates,²⁸ and sound waves.²⁹ Although the transverse expansion properties in periodic photonic lattices,^{30–33} as well as in disordered ones,^{34–36} have been investigated extensively, light localization and transverse expansion in photonic quasicrystals^{37,38} is still an open question.

In this paper, we investigate the effects of light propagation in aperiodic photonic structures created by synthesized Mathieu–Gauss (MG) beams in a photorefractive crystal,²¹ experimentally and numerically. We investigate how various input beam positions influence the diffraction and compare them with appropriate periodic waveguide arrays. We find that our approach effectively suppresses the beam expansion depending on the refractive index modulation Δn . Most importantly, in the nonlinear regime, we find localized states that are robust with respect to changes in the probing light intensities and propagation distance. Such stable solitary states are, thus, much more appealing for applications than typical spatial solitons, especially gap solitons, which react sensitively on changes in the strength of the nonlinearity.³⁹

Figure 1 shows the experimental setup to fabricate and probe MG beam-based photonic lattices. A frequency-doubled, expanded, and collimated Nd:YVO₄ laser with a wavelength of $\lambda = 532$ nm is split into two separate beams—an ordinary polarized writing and an extraordinary polarized probe beam. Both beams are spatially tailored in intensity and phase by phase-only spatial light modulators (SLMs), Holoeye Pluto VIS. For this purpose, pre-encoded digital holograms are addressed to the SLMs, and their diffraction patterns are bandpass filtered in Fourier space (FF₁ and FF₂).⁴⁰ The ordinarily polarized structure beam optically induces a refractive index modulation in a photorefractive cerium-doped strontium barium niobate (SBN:Ce) crystal, thereby addressing the weaker electro-optic coefficient $r_{13} = 47$ pm/V. Probing the artificial photonic structure with extraordinarily polarized probe beams addresses the stronger electro-optic coefficient $r_{33} = 237$ pm/V. Although the electro-optic coefficients differ roughly by a factor of 5, the ordinary writing process of two-dimensional lattices can be considered to be fairly linear. Previous studies that applied the same technique for the optical induction of photonic lattices demonstrated a neglectable self-action and, thus, longitudinally invariant refractive index modulations.^{6,7,9,15,41} The birefringent crystal with dimensions of $5 \times 5 \times 20$ mm³ has refractive indices of $n_o = 2.325$ and $n_e = 2.358$ and is externally biased with an electric field of $E_{\text{ext}} = 2000$ V/cm aligned along the optical $c = x$ -axis, perpendicular to the direction of propagation, the z -axis parallel to the long axis of the crystal. An imaging system consisting of a microscope objective (MO) and a camera detects transverse intensity distributions of writing and/or probing beams at the backface of the crystal. When we are recording the intensity distribution of the Gaussian probe beam at the backface of the crystal, the writing beam is turned off.

We model our experiment by solving the nonlinear Schrödinger equation for an initial scalar electric field $A(\mathbf{r})$ numerically by using a spectral split-step beam propagation method⁴² of the equation

$$i\partial_z A(\mathbf{r}) + \frac{1}{2k_z} \Delta_{\perp} A(\mathbf{r}) + \frac{k_z}{2n_{o,e}^2} \delta n^2(|A(\mathbf{r})|^2) A(\mathbf{r}) = 0. \quad (1)$$

By this, the nonlinear propagation of the field $A(\mathbf{r})$ with longitudinal wave vector k_z in a photorefractive nonlinearity is evaluated. While the writing beam is a complex nondiffracting aperiodic light field, we use Gaussian beams as probe beams. The wave number

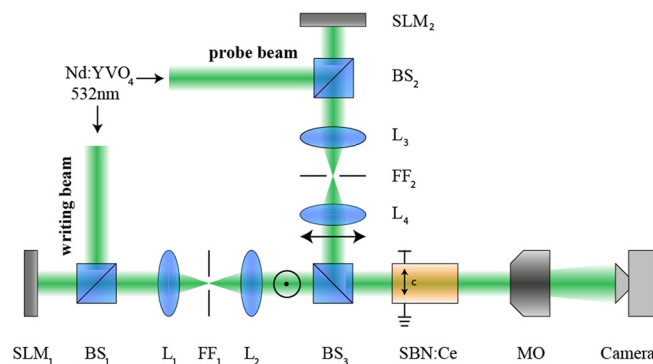


FIG. 1. Scheme of the experimental setup. BS: beam splitter, FF: Fourier filter, L: lens, MO: microscope objective, SBN: photorefractive strontium barium niobate crystal, and SLM: phase-only spatial light modulator.

$k = 2\pi/\lambda = \sqrt{(k_x^2 + k_z^2)}$ is defined by wavelength λ . The potential is given by $\delta n^2(|A(\mathbf{r})|^2) = -n_{o,e}^4 r_{13,33} E$. The electric field $E = E_{\text{ext}} + E_{\text{sc}}$ that builds up inside the SBN crystal is a superposition of an external electric field E_{ext} and an internal space charge field E_{sc} , which is due to the incident intensity distribution $I_p = |A(\mathbf{r})|^2$. In order to take the electric bias of the SBN crystal into account, we use an anisotropic model to calculate the refractive index modulation by solving the potential equation,⁴³

$$\begin{aligned} \Delta_{\perp} \phi_{\text{sc}} + \nabla_{\perp} \ln(1+I) \cdot \nabla_{\perp} \phi_{\text{sc}} \\ = E_{\text{ext}} \partial_x \ln(1+I) + \frac{k_B T}{e} [\Delta_{\perp} \ln(1+I) + (\nabla_{\perp} \ln(1+I))^2], \end{aligned} \quad (2)$$

which yields $E_{\text{sc}} = \partial_x \phi_{\text{sc}}$. Based on the probe beam power, we denote the scenario in which the lattice is fabricated by intensity $I = I_g$ and subsequently illuminated by the low power probe beam as the linear regime. For higher powers of the probe beam, we take into account mutual nonlinear interaction of the probe and writing beams by including them together in the term $I = I_g + I_p$, which we denote as the nonlinear regime. $I_g(\mathbf{r})$ is the writing beam intensity of the MG beams²¹ and $I_p(\mathbf{r})$ the Gaussian probe beam intensity. Note that the intensities used in the simulations are normalized by a dark current intensity I_{dark} , which can be determined experimentally.⁴⁴ However, in most cases, the intensities used in the simulations and in the experiment are conformed by comparing the light propagation in variously realized refractive index modulations.

We investigate the influence of an aperiodic photonic lattice created by synthesized MG beams²¹ on the beam propagation and compare our experimental results with numerical simulations. The lattice writing beam is synthesized using a combination of the spatially shifted patterns created by the interference of two second-order even MG beams with an ellipticity of $q = 25$ and a structure size of $a = 25$ μm , oriented at 90° with respect to each other and π out-of-phase configuration, with a detailed description of fabrication given in Ref. 21. The pattern is created with a finite number of MG beams (elliptic shape, each MG beam has no translational symmetry), the “repeating” area is finite, the lattice has boundaries; in general, the synthesized lattice has no translational symmetry as well. The “typical patterns” only look similar, but they are never identical. In Figs. 2(a) and 2(b), the aperiodic lattice and the characteristic lattice typical patterns are depicted. The lattice writing beam has an invariant transverse intensity profile during propagation, and hence, its Fourier

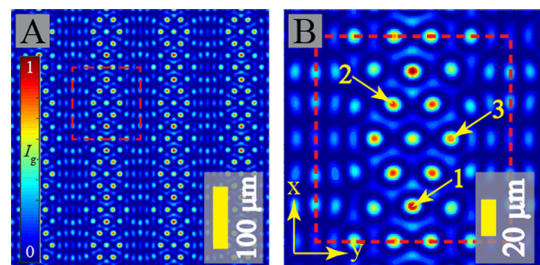


FIG. 2. (a) Transverse aperiodic lattice structure fabricated with synthesized MG beams. (b) Typical pattern, where the yellow arrows indicate some of the probe beam excitation sites.

components are located on a ring with radius $k_{\perp} = 2\pi/a$ related to the structure size a of the MG beams. The nondiffracting character of such a Mathieu lattice in the 20 mm long SBN crystal is demonstrated in Ref. 21. In order to characterize the light-matter interaction within such a medium, a probe beam is launched into a single site. The probe beam experiences lateral transport within the lattice as it propagates along its axis, resulting in a diffraction pattern characteristic of the local structure. While in a simple periodic lattice, each site looks like any other and discrete diffraction looks the same irrespective of the initial site of excitation, in an aperiodic lattice, however, different local environments exist, so that the transport behavior is expected to vary significantly from site to site.⁴⁵ The chosen points differ from each other by their local interaction since some have a higher local symmetry than others.

We investigate this behavior in the suggested aperiodic photonic lattice by comparing the linear diffraction for different probe beam excitation positions, numerically and experimentally. The lattice is fabricated with an experimental laser power of $P_0 = 50 \mu\text{W}$, which corresponds to a simulated maximum lattice intensity of $I_g = I_0 = 0.7$. Subsequently, after the lattice writing beam and the external electric field E_{ext} are switched off, the Gaussian probe beam with a FWHM of $w_0 = 8 \mu\text{m}$ illuminates the lattice. Its power of a few $10 \mu\text{W}$ is chosen to be sufficiently low so that it does not change the refractive index modulation but is only affected by it. Figure 3 shows the transverse intensity distributions of the probe beam after propagating through the lattice as a function of the excitation sites marked by numbers 1, 2, and 3 in Fig. 2(b). The first column shows transverse intensity distributions obtained at the backface of the SBN crystal in the linear regime. The importance of which local lattice site is excited is clearly visible in the simulated and experimentally obtained intensity distributions, where discrete diffraction is clearly visible as in D2, unlike for other two excitation sites. We note a clear agreement between the experimentally and numerically obtained results.

Further, we perform a series of experiments and numerical calculations to observe nonlinear localization of the discrete diffraction pattern. Therefore, in both numerical simulations and experiment, with the external electric field switched on, we increase the lattice and probe beam maximum intensities, which now interact and create a common refractive index pattern, resulting in the lattice modified by nonlinear self- and cross action. The second column of Fig. 3 shows the transverse intensity distribution of only the probe beam when propagating through the commonly fabricated lattice with a beam power of $P_0 = 50 \mu\text{W}$ or a maximum intensity of $I_p = I_0 = 0.7$. Subsequently, we increase the strength of the nonlinearity by doubling the beam power $2P_0$ in the experiment and simulation. The corresponding intensity distributions are shown in the third column of Fig. 3. For input position 1 and sufficiently high beam powers, we observe a spatial soliton in the aperiodic lattice, shown in Figs. 3(c1) and 3(c2). Other input positions 2 and 3 do not support this localized state, depicted in Figs. 3(e), 3(f), 3(h), and 3(i).

To verify the robustness of the spatial soliton, in numerical simulations, we change the nonlinearity strength by increasing the maximum intensities of the writing and probe beams, while keeping all other parameters fixed. We find that the output intensity distribution of the soliton at the exit crystal face remains largely unchanged with an up to three times higher beam power. The results are shown in Fig. 4. For even higher intensities, the localized state starts to

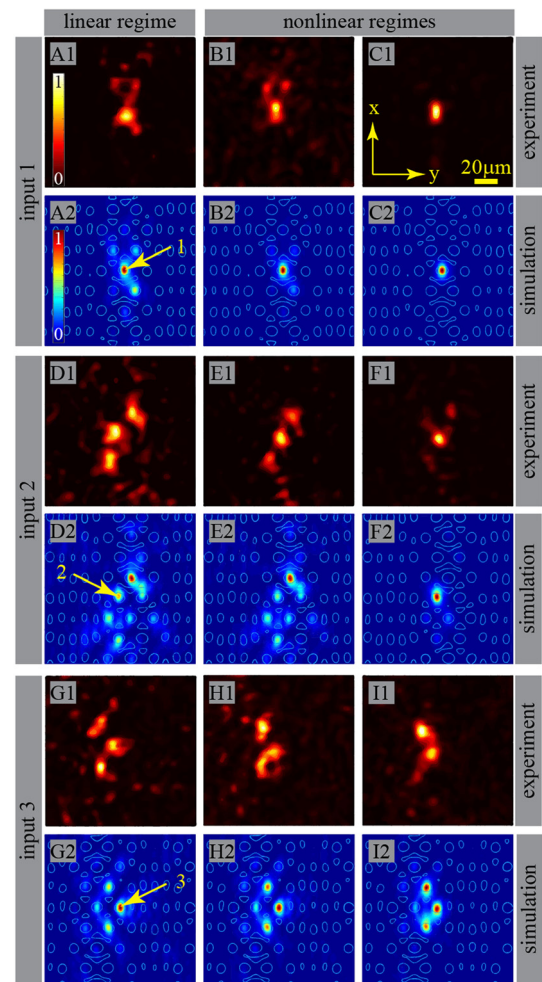


FIG. 3. Probe beam propagation in an aperiodic photonic lattice. Numerically and experimentally observed transverse intensity distributions at the crystal's backface in the linear regime (the first column) and two nonlinear regimes: (the second column) numerical probe beam maximum intensity of $I_p = I_0 = 0.7$ and appropriate experimental beam power of $P_0 = 50 \mu\text{W}$ and (the third column) numerical probe beam maximum intensity of $I_p = 2I_0$ and experimental beam power of $2P_0$. The yellow arrows indicate the probe beam excitation sites, while the blue contour denotes the layout of the lattice beams.

experience modulation instabilities, leading to a breakup of the beam into filaments. Further, numerical simulations for propagation distances longer than the length of our crystal are performed, obtaining stable output intensity distributions up to 10 cm (not shown here).

In order to examine the localization properties of the aperiodic Mathieu lattice in general, independent of the concrete excitation site, we simulate the light propagation in the lattice coming from 100 different probe beam excitation positions and average their expansion. For that purpose, the probe beam excitation positions are selected at an equidistant spacing to cover one complete typical pattern depicted in Fig. 2(b). Figure 5 presents these results, with a gradual transition from suppressed discrete diffraction to nonlinear localization, using the same intensities as in Fig. 3. The output averaged transverse

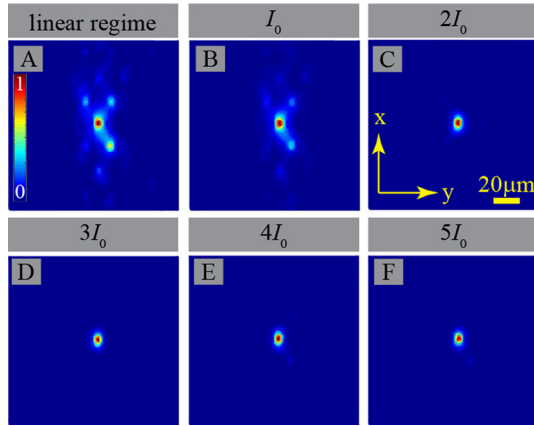


FIG. 4. The robustness of the lattice soliton in the case of input 1. Simulated transverse intensity distributions at the crystal's backface in linear and five different nonlinear cases. Parameters are as shown in Fig. 3.

intensity profiles in Figs. 5(a)–5(c) narrow with increasing nonlinearity. Still, due to the diverse contributions that are averaged, nonlinear profiles shown in (d) do not show the soliton shape as typically known from spatial bright solitons in the bulk.

For a more quantitative analysis and to characterize the amount of beam expansion, we introduce the effective beam width $\omega_{\text{eff}} = \text{PR}(z)^{-1/2}$, where

$$\text{PR}(z) = \frac{\int |A(x, y, z)|^4 dx dy}{\left(\int |A(x, y, z)|^2 dx dy \right)^2} \quad (3)$$

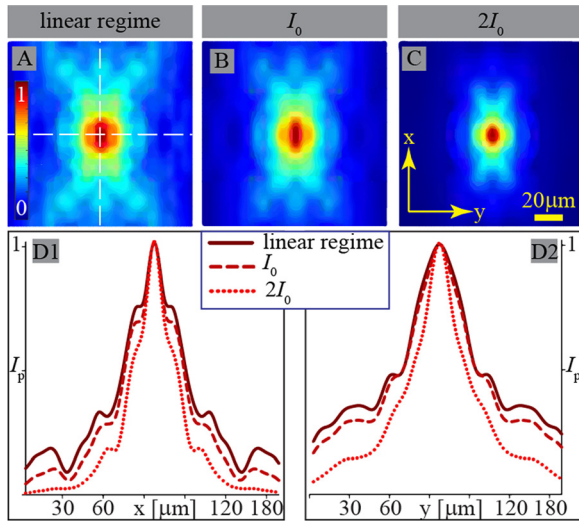


FIG. 5. Averaged intensity distributions at the lattice output, for 100 different probe beam excitation sites, in (a) linear and (b) and (c) nonlinear cases. (d1) and (d2) present averaged intensity profiles, taken along the horizontal and vertical transverse directions [indicated with the white lines in (a)], respectively. Parameters are as shown in Fig. 3.

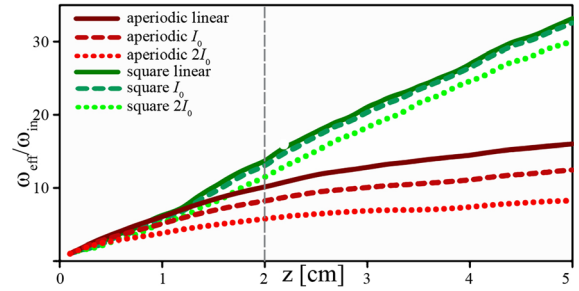


FIG. 6. Comparison between beam spreading in linear and two nonlinear regimes inside the aperiodic lattice and an periodic square lattice. Numerical simulation of the averaged normalized effective width (averaged over 100 excitation positions) along the propagation distance. ω_{in} is the initial effective width. Parameters are as shown in Fig. 3.

is the inverse participation ratio.²⁵ In such a structure, we perform averaging over different incident beam positions in order to remove effects of the local environment, i.e., the influence of the neighboring waveguides. The averaged normalized effective beam width is calculated along the propagation distance for the propagation length longer than the crystal length. We perform statistical analysis of the normalized effective beam width for the cases demonstrated in Fig. 3. These results are shown in Fig. 6 and reveal that the beam expansion during propagation is hindered when increasing the input beam power. We compare propagation of light in our aperiodic lattice with a periodic square lattice. The square lattice is created with period d equal to the characteristic structure size $a = 2\pi/k_{\perp}$ of MG beams used to create the aperiodic Mathieu lattice, $d = a = 25 \mu\text{m}$. We observe the tendency of this aperiodic lattice to suppress diffraction, especially for longer propagation distances. In these cases, light is less localized in the periodic square lattice than in the aperiodic Mathieu lattice.

In summary, we demonstrate various propagation effects in an aperiodic lattice created by synthesized Mathieu–Gauss beams. The aperiodic structure hinders the beam expansion during propagation, compared to the propagation of light in comparable periodic lattices. Even stronger light localization, which can be interpreted as robust spatial soliton formation with respect to intensity changes, can be observed for nonlinearly propagating probe beams in such aperiodic lattices. Our experimental results pave the way for exploiting light propagating in a broad range of aperiodic photonic lattices and will find applications in capacity-enhanced optical information processing.

The authors acknowledge partial support from the Ministry of Education, Science, and Technological development, Republic of Serbia (Project No. OI 171036), and support from the German Academic Exchange Service (Project No. 57219089).

DATA AVAILABILITY

The data that support the findings of this study are available from the corresponding author upon reasonable request.

REFERENCES

¹E. G. Kalnins and J. W. Miller, *J. Math. Phys.* **17**, 331 (1976).
²J. Durnin, J. J. Miceli, and J. H. Eberly, *Phys. Rev. Lett.* **58**, 1499 (1987).
³J. C. Gutiérrez-Vega, M. D. Iturbe-Castillo, and S. Chávez-Cerda, *Opt. Lett.* **25**, 1493 (2000).

- ⁴M. A. Bandres, J. C. Gutiérrez-Vega, and S. Chávez-Cerda, *Opt. Lett.* **29**, 44 (2004).
- ⁵S. Chávez-Cerda, U. Ruiz, V. Arrizón, and H. M. Moya-Cessa, *Opt. Express* **19**, 16448 (2011).
- ⁶N. M. Lucić, B. M. Bokić, D. Z. Grujić, D. V. Pantelić, B. M. Jelenković, A. Piper, D. M. Jović, and D. V. Timotijević, *Phys. Rev. A* **88**, 063815 (2013).
- ⁷F. Diebel, B. M. Bokić, M. Boguslawski, A. Piper, D. V. Timotijević, D. M. Jović, and C. Denz, *Phys. Rev. A* **90**, 033802 (2014).
- ⁸B. Freedman, G. Bartal, M. Segev, R. Lifshitz, D. N. Christodoulides, and J. Fleisher, *Nat.* **440**, 1166 (2006).
- ⁹F. Diebel, B. M. Bokić, D. V. Timotijević, D. M. J. Savić, and C. Denz, *Opt. Express* **23**, 24351 (2015).
- ¹⁰Y. V. Kartashov, V. A. Vysloukh, and L. Torner, *Phys. Rev. Lett.* **93**, 093904 (2004).
- ¹¹Y. V. Kartashov, V. A. Vysloukh, and L. Torner, *Phys. Rev. Lett.* **94**, 043902 (2005).
- ¹²Y. V. Kartashov, A. A. Egorov, V. A. Vysloukh, and L. Torner, *Opt. Lett.* **31**, 238 (2006).
- ¹³Y. V. Kartashov, V. A. Vysloukh, and L. Torner, *Opt. Lett.* **33**, 141 (2008).
- ¹⁴R. Fisher, D. N. Neshev, S. Lopez-Aguayo, A. S. Desyatnikov, A. A. Sukhorukov, W. Krolikowski, and Y. S. Kivshar, *Opt. Express* **14**, 2825 (2006).
- ¹⁵B. Terhalle, T. Richter, A. S. Desyatnikov, D. N. Neshev, W. Krolikowski, F. Kaiser, C. Denz, and Y. S. Kivshar, *Phys. Rev. Lett.* **101**, 013903 (2008).
- ¹⁶N. K. Efremidis, J. Hudock, D. N. Christodoulides, J. W. Fleischer, O. Cohen, and M. Segev, *Phys. Rev. Lett.* **91**, 213906 (2003).
- ¹⁷J. W. Fleischer, M. Segev, N. K. Efremidis, and D. N. Christodoulides, *Nature* **422**, 147 (2003).
- ¹⁸F. Ye, D. Mihalache, and B. Hu, *Phys. Rev. A* **79**, 053852 (2009).
- ¹⁹A. Ruelas, S. Lopez-Aguayo, and J. C. Gutiérrez-Vega, *Opt. Lett.* **33**, 2785 (2008).
- ²⁰J. V. Vasiljević, A. Zannotti, D. V. Timotijević, C. Denz, and D. M. J. Savić, *Phys. Rev. A* **97**, 033848 (2018).
- ²¹J. V. Vasiljević, A. Zannotti, D. V. Timotijević, C. Denz, and D. M. J. Savić, *Phys. Rev. A* **96**, 023840 (2017).
- ²²P. Sheng, *Scattering and Localization of Classical Waves in Random Media*, 2nd ed. (World Scientific, 1990).
- ²³A. Legendijk, B. Tiggelen, and D. S. Wiersma, *Phys. Today* **62**(8), 24 (2009).
- ²⁴T. Pertsch, U. Peschel, J. Kobelke, K. Schuster, H. Bartelt, S. Nolte, A. Tünnermann, and F. Lederer, *Phys. Rev. Lett.* **93**, 053901 (2004).
- ²⁵T. Schwartz, G. Bartal, S. Fishman, and M. Segev, *Nature* **446**, 52 (2007).
- ²⁶S. Gentilini, A. Fratolocci, L. Angelani, G. Ruocco, and C. Conti, *Opt. Lett.* **34**, 130 (2009).
- ²⁷C. Conti and A. Fratolocci, *Nat. Phys.* **4**, 794 (2008).
- ²⁸G. Roati, C. D'Errico, L. Fallani, M. Fattori, C. Fort, M. Zaccanti, G. Modugno, M. Modugno, and M. Inguscio, *Nature* **453**, 895 (2008).
- ²⁹J. D. Maynard, *Rev. Mod. Phys.* **73**, 401 (2001).
- ³⁰H. S. Eisenberg, Y. Silberberg, R. Morandotti, and J. S. Aitchison, *Phys. Rev. Lett.* **85**, 1863 (2000).
- ³¹T. Pertsch, T. Zentgraf, U. Peschel, A. Bräuer, and F. Lederer, *Phys. Rev. Lett.* **88**, 093901 (2002).
- ³²D. N. Christodoulides, F. Lederer, and Y. Silberberg, *Nature* **424**, 817 (2003).
- ³³A. Fratolocci and G. Assanto, *Opt. Lett.* **31**, 1489 (2006).
- ³⁴D. M. Jović, Y. S. Kivshar, C. Denz, and M. R. Belić, *Phys. Rev. A* **83**, 033813 (2011).
- ³⁵D. M. Jović, M. R. Belić, and C. Denz, *Phys. Rev. A* **84**, 043811 (2011).
- ³⁶Y. Lahini, A. Avidan, F. Pozzi, M. Sorel, R. Morandotti, D. N. Christodoulides, and Y. Silberberg, *Phys. Rev. Lett.* **100**, 013906 (2008).
- ³⁷E. Maciá, *Rep. Prog. Phys.* **69**, 397 (2006).
- ³⁸P. Wang, Y. Zheng, X. Chen, C. Huang, Y. V. Kartashov, L. Torner, V. V. Konotop, and F. Ye, *Nature* **577**, 42 (2020).
- ³⁹F. Lederer, G. I. Stegeman, D. N. Christodoulides, G. Assanto, M. Segev, and Y. Silberberg, *Phys. Rep.* **463**, 1 (2008).
- ⁴⁰J. A. Davis, D. M. Cottrell, J. Campos, M. J. Yzuel, and I. Moreno, *Appl. Opt.* **38**, 5004 (1999).
- ⁴¹A. Zannotti, F. Diebel, M. Boguslawski, and C. Denz, *Adv. Opt. Mater.* **5**, 1600629 (2017).
- ⁴²G. P. Agrawal, *Nonlinear Fiber Optics*, 5th ed. (Academic Press, 2012).
- ⁴³A. A. Zozulya and D. Z. Anderson, *Phys. Rev. A* **51**, 1520 (1995).
- ⁴⁴M. Segev, *Opt. Quantum Electron.* **30**, 503 (1998).
- ⁴⁵M. Boguslawski, N. M. Lucić, F. Diebel, D. V. Timotijević, C. Denz, and D. M. J. Savić, *Optica* **3**, 711 (2016).



Optics Letters

Morphing discrete diffraction in nonlinear Mathieu lattices

ALESSANDRO ZANNOTTI,^{1,*} JADRANKA M. VASILJEVIĆ,² DEJAN V. TIMOTIJEVIĆ,^{2,3}
DRAGANA M. JOVIĆ SAVIĆ,² AND CORNELIA DENZ¹

¹Institute of Applied Physics and Center for Nonlinear Science (CeNoS), University of Muenster, 48149 Muenster, Germany

²Institute of Physics, University of Belgrade, P.O. Box 68, 11001 Belgrade, Serbia

³Science Program, Texas A&M University at Qatar, P.O. Box 23874 Doha, Qatar

*Corresponding author: a.zannotti@uni-muenster.de

Received 14 January 2019; revised 20 February 2019; accepted 22 February 2019; posted 22 February 2019 (Doc. ID 357502); published 20 March 2019

Discrete optical gratings are essential components to customize structured light waves, determined by the band structure of the periodic potential. Beyond fabricating static devices, light-driven diffraction management requires nonlinear materials. Up to now, nonlinear self-action has been limited mainly to discrete spatial solitons. Discrete solitons, however, are restricted to the eigenstates of the photonic lattice. Here, we control light formation by nonlinear discrete diffraction, allowing for versatile output diffraction states. We observe morphing of diffraction structures for discrete Mathieu beams propagating nonlinearly in photosensitive media. The self-action of a zero-order Mathieu beam in a nonlinear medium shows characteristics similar to discrete diffraction in one-dimensional waveguide arrays. Mathieu beams of higher orders show discrete diffraction along curved paths, showing the fingerprint of respective two-dimensional photonic lattices. © 2019 Optical Society of America

<https://doi.org/10.1364/OL.44.001592>

Manipulating waves by customizing their interaction with functional materials enables a variety of photonic applications, e.g., tailored diffraction at gratings to discretize the waves' spectral components [1,2]. Waves in periodically structured media show dynamics that cannot be realized in homogeneous media, determined by the media's band structure. Propagation of light in dielectric media with a periodically varying refractive index can mimic the spatio-temporal characteristics that are typically encountered in discrete systems, and the underlying field evolution effectively becomes "discretized" [1]. Most importantly, the vision to control light with light is realizable only by exploiting nonlinear materials as mediators [3]. Thus, shaping the periodically varying refractive index structure allows for diffraction management to control in turn the light distribution [4].

Different types of periodic photonic structures, including arrays of evanescently coupled optical waveguides [5], optically induced lattices in photorefractive materials [6], and photonic crystals [7], have been employed to engineer and control

fundamental properties of wave propagation. Arrays or lattices of evanescently coupled waveguides are prime examples of structures in which *discrete diffraction* [2,5,8] can be observed. These arrays consist of equally spaced identical waveguide elements or sites, possessing all essential characteristics of a photonic crystal structure (Brillouin zones, band structure, etc.). In such a physical setting, light couples between waveguides through tunneling, showing its diffraction characteristics. When low intensity light is injected into one or a few neighboring waveguides, it couples to more and more waveguides, broadening its spatial distribution. Fundamentally new physics occur in contrast to diffraction in homogeneous media. High-intensity light producing nonlinear responses in the refractive index is capable of forming *discrete spatial solitons* [9]. A renewed interest in nonlinear light-matter interaction goes beyond soliton formation. It is devoted to physical systems with dimensionality morphing, e.g., the continuous transformation of the lattice structure from 1D to 2D [10–12].

Nondiffracting beams, having propagation-invariant intensity distributions, allow creating 1D and 2D photonic lattices in photosensitive media. Particularly in the areas of optics and atom physics, these beams enable novel applications [13–16]. Among the variety of different nondiffracting beams, Mathieu beams [15,17] solve the Helmholtz equation in elliptic cylindrical coordinates [18]. They are used for a new type of optical lattice-writing light [19–23] allowing solitons or even elliptically shaped vortex solitons, and are beneficially used for particle manipulation [24]. However, their elliptical characteristics allow going far beyond soliton investigations and extending applications of nonlinear self-action.

In this Letter, we exploit Mathieu beams as lattice-writing light to fabricate discrete waveguide structures and investigate their nonlinear self-action in these structures, leading to morphing discrete diffraction. We investigate Mathieu beams of different orders in a photorefractive crystal, experimentally and numerically. We link linear discrete diffraction with nonlinear self-effects and demonstrate gradual transition from one to two dimensions. We use the term *morphing diffraction* to describe the nonlinear behavior similar to discrete diffraction.

We observe discrete diffraction similar to the typical discrete diffraction observed in 1D waveguide arrays, with Mathieu beams of zeroth order propagating in nonlinear media. For lower nonlinearity, we observe a behavior similar to broad Gaussian beam diffraction in waveguide arrays. Increasing the order of Mathieu beams, we demonstrate dimensionality morphing of discrete diffraction, with a gradual transition from 1D to 2D waveguiding geometries. With higher-order Mathieu beams, we observe discrete diffraction along each layer. For higher nonlinearities, we observe reflection along one transverse direction and asymmetric intensity distributions due to the thermal diffusive effects.

To experimentally investigate the nonlinear propagation of Mathieu beams, we use the setup shown in Fig. 1. A frequency-doubled Nd:YVO₄ laser illuminates a spatial light modulator (SLM) “Holoeye Pluto” and is modulated in both amplitude and phase [25]. An appropriate Fourier filter (FF) is implemented. The extraordinary polarized structure beam interacts with the photorefractive strontium barium niobate (SBN) crystal, which has dimensions of 5 × 5 × 15 mm³. It is externally biased with an electric field $E_{\text{ext}} = 1600 \text{ Vcm}^{-1}$ parallel to the optical c axis, directed along one of the shorter axes, parallel to the x axis. The propagation of the paraxial light fields is mainly in z direction. An adjustable microscope objective and a camera build the imaging system to scan the entire intensity volume by recording single transverse slices. In order to measure the phase of the structure beam, we superimpose a tilted plane wave as a reference beam and use a standard digital holographic method.

We simulate the light propagation in a nonlinear photorefractive medium by solving the nonlinear Schrödinger equation (1) numerically using a spectral split-step propagation method [26]:

$$i\partial_z\psi(\mathbf{r}) + \frac{1}{2k_z}[\Delta_{\perp} + V(I)]\psi(\mathbf{r}) = 0. \quad (1)$$

The nonlinear light-matter interaction is calculated by assuming a light-induced refractive index modulation as proposed in [27]. The paraxial scalar light field $\psi(\mathbf{r})$ with longitudinal wave vector k_z propagates in a nonlinear potential $V(I) = -k_z^2 n_e^2 r_{33} E_{sc}(I)$ defined by photorefractive nonlinearity. The laser wavelength $\lambda = 532 \text{ nm}$ defines the wave number $k = 2\pi/\lambda = \sqrt{k_x^2 + k_z^2}$. $n_e = 2.358$ is the extraordinary bulk refractive index and $r_{33} = 237 \text{ pmV}^{-1}$ the corresponding linear electro-optic coefficient. The electric space charge field $E_{sc}(I)$ builds up inside the SBN crystal and depends on the intensity $I = |\psi(\mathbf{r})|^2$. We model the nonlinear optical induction of the intensity-dependent, saturable, non-local, and anisotropic refractive index modulation [28], as shown in our previous works [23,29].

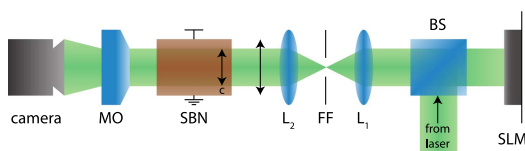


Fig. 1. Scheme of experimental setup. BS, beam splitter; FF, Fourier filter; L, lens; MO, microscope objective; SLM, phase-only spatial light modulator.

We use even Mathieu beams $\psi_m(\xi, \eta)$ [15], mathematically described as a product of radial c_{em} and angular J_{em} Mathieu functions of order m :

$$\psi_m(\xi, \eta) = C_m(q)J_{em}(\xi; q)c_{em}(\eta; q), \quad (2)$$

where $C_m(q)$ is a weighting constant that depends on $q = f^2 k_t^2/4$, a parameter of ellipticity which is related to the positions f of the two foci and the transverse wave number $k_t = 2\pi/a$, where a is a characteristic structure size. ξ and η are elliptical coordinates and their relation with spatial coordinates x, y is given by $x + iy = f \cosh(+i\eta)$. Here we choose $a = 25 \mu\text{m}$.

Before investigating the nonlinear propagation of Mathieu beams, we exemplarily characterize the free-space propagation of a zeroth-order even Mathieu writing beam with $q = 25$ experimentally. The quasi 1D discrete intensity distribution is shown in Fig. 2(A1), accompanied by the phase pattern (A2). It propagates invariantly (A3) over a distance of 6.36 mm in free space, which corresponds to 15 mm in the homogeneous SBN crystal. The same conclusions are worthy for higher-order Mathieu beams used later to demonstrate intermediate and 2D discrete diffraction.

Their discrete intensity distribution with a complex transverse curvature makes Mathieu beams highly suited to investigate morphing diffraction in self-induced waveguides. We find that the lattice-fabricating Mathieu beam in Fig. 2 shows *nonlinear discrete diffraction* as a consequence of its self-action in dependence of the beam power P that influences the strength of the nonlinearity, shown in Fig. 3. The first row depicts the

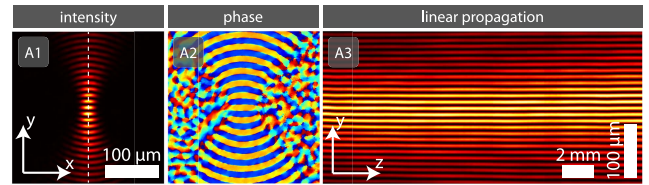


Fig. 2. Experimental characterization of a zeroth-order lattice fabricating even Mathieu beam. (A1) Transverse intensity and (A2) phase distributions. (A3) Cross section through the intensity volume at the orientation indicated with the white line in (A1).

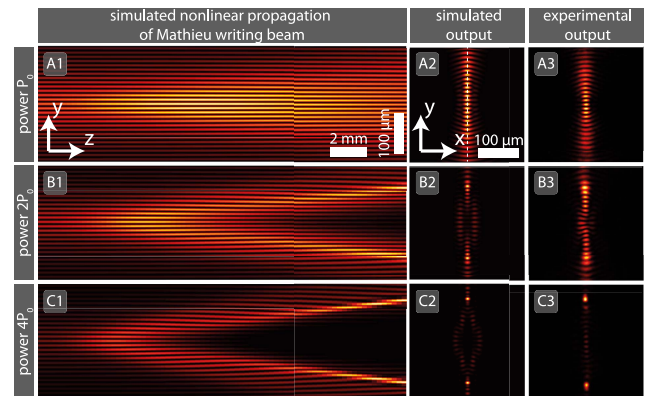


Fig. 3. (1) Simulated nonlinear propagation of Mathieu beams shows morphing discrete diffraction for increasing beam powers P . (2) Simulated and (3) experimentally observed intensity distributions at the crystal's back face.

simulated yz cross section through the intensity volume (A1), and further the simulated (A2) and the experimentally obtained (A3) transverse intensity distributions at the back face of the SBN crystal for $P = P_0 = 10 \mu\text{W}$, showing that the waveguides are well fabricated. The observed discrete diffraction has similarities to that of a broad Gaussian beam propagating in 1D periodic waveguide arrays [2]. By doubling the beam power twice [Figs. 3(B) and 3(C)], we observe a spreading of highest intensities away from the center and towards the outer parts along the y axis. This effect is the nonlinear counterpart of linear discrete diffraction in 1D waveguide arrays. Since the envelope of the 1D intensity distribution along the y axis of an initial zeroth-order Mathieu beam has its maximum in the origin, the refractive index modulation and thus the self-action of the writing beam is strongest in the center. Very high beam powers of $4P_0$ increase diffusive effects [23,29] along the optical c axis, parallel to the x axis, apparent at the shift in intensity in (B3) and (C3).

Beyond 1D nonlinear discrete diffraction, we realize morphing discrete diffraction along curved 2D paths at the example of Mathieu lattices showing dimensionality crossover. We chose

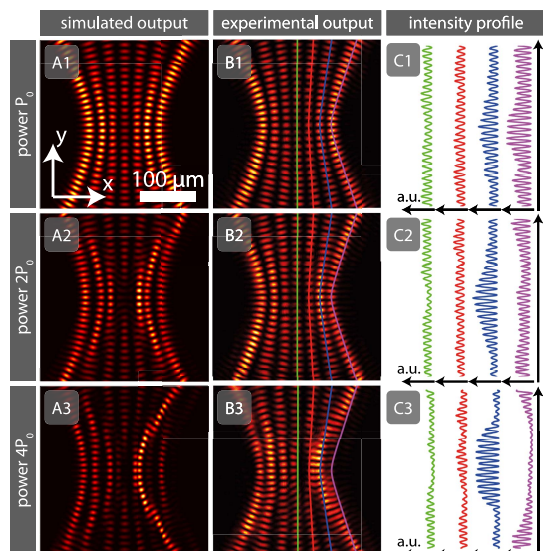


Fig. 4. Morphing discrete diffraction on curved paths based on the self-action of sixth-order even Mathieu beams: (A) simulated and (B) experimentally observed transverse intensity distributions at the crystal's back face. (C) Intensity profiles along the hyperbolic waveguide layers indicated in (B).

the sixth-order even Mathieu beam with $q = 325$ [10–12], imaged in Fig. 4, for demonstration of dimensionality crossover. The figure shows the simulated (A) and experimentally observed (B) transverse intensity distributions at the back face of the SBN crystal in dependence of a successive doubling of the initial beam power $P_0 = 10 \mu\text{W}$. We observe intensity distributions that reflect the fingerprint of linear discrete diffraction; however, the outward directed intensity transport in the nonlinear lattices follows mainly along each hyperbolic layer of the Mathieu beam (C).

For the lowest power P_0 , the highest intensities located in the center of an initial sixth-order Mathieu beam are redistributed towards the outer parts in y direction, shown by the intensity profile along the green line (B1) and (C1). Increasing the power P , we observe that further hyperbolic arms of the Mathieu lattice are affected. Central intensities spread outwards along 2D curves (2 and 3). Additionally, a diffusion driven shift in x direction and merging intensities due to modulation instabilities influence the intensity redistribution; however, the pure effect of 2D nonlinear discrete diffraction along hyperbolic paths is predominantly observable.

To demonstrate that discrete Mathieu lattices themselves imprint the intensity distribution on probing light that is typical for discrete diffraction, we simulate linear propagation of narrow Gaussian beams in the lattices presented above. Figure 5(A) images the intensity distribution of such a Gaussian probe beam inside the Mathieu lattice in Fig. 3(A). The initial plane in Fig. 5(A) indicates the lattice. The perpendicularly launched probe beam couples from waveguide to waveguide, presenting diffraction characteristics as in 1D waveguide arrays. Further configurations are launching probe beams in the 2D lattice in Fig. 4(A1) in the center and the outermost layer [purple hyperbola in Fig. 4(B1)]. The intensity of the central excitation diffracts discrete in central and neighboring layers, shown in (B). The outer excitation evolves to discrete diffraction along the hyperbolic waveguide layer, imaged in (C).

In summary, we demonstrated morphing diffraction of Mathieu beams with transition from 1D to 2D. These nondiffracting beams allow realizing discrete lattices in general elliptic geometries. We showed that discrete diffraction on unconventional paths is possible as a result of the self-action of Mathieu beams in nonlinear material. We observed discrete diffraction similar to that observed in 1D waveguide arrays using Mathieu beams of zeroth order, or discrete diffraction similar to the one in 2D photonic lattices with higher-order Mathieu beams. Increasing the nonlinearity, reflections along one transverse direction are observed as well as asymmetric intensity distributions due to thermal diffusive effects. Thus, nonlinear discrete

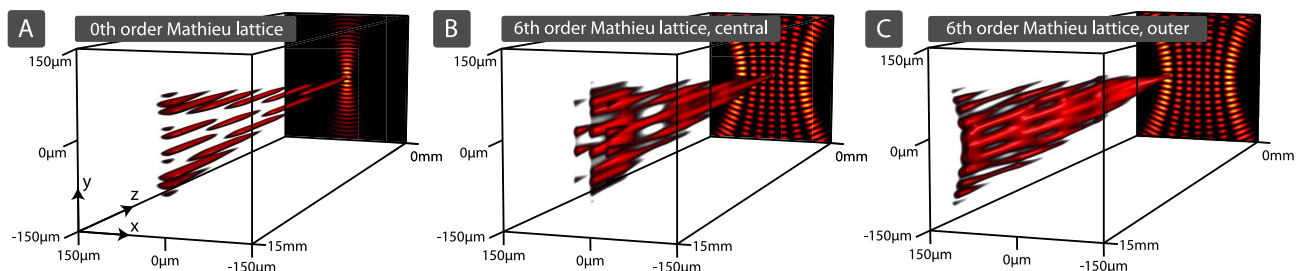


Fig. 5. Gaussian probe beam in Mathieu lattice potentials from: (A) Fig. 3(A1); (B) Fig. 4(B1) central waveguides; (C) Fig. 4(B1) purple waveguide layer.

diffraction allows controlling the light dynamics in lattices by light itself, providing a simple technique to create novel gratings and nonlinear switches.

Funding. Deutscher Akademischer Austauschdienst (DAAD) (57219089); Ministarstvo Prosvete, Nauke i Tehnološkog Razvoja (OI 171036); Qatar National Research Fund (QNRF) (NPRP 8-028-1- 001).

REFERENCES

1. H. S. Eisenberg, Y. Silberberg, R. Morandotti, and J. S. Aitchison, *Phys. Rev. Lett.* **85**, 1863 (2000).
2. T. Pertsch, T. Zentgraf, U. Peschel, A. Brauer, and F. Lederer, *Phys. Rev. Lett.* **88**, 093901 (2002).
3. J. Hudock, N. K. Efremidis, and D. N. Christodoulides, *Opt. Lett.* **29**, 268 (2004).
4. D. N. Christodoulides, F. Lederer, and Y. Silberberg, *Nature* **424**, 817 (2003).
5. H. S. Eisenberg, Y. Silberberg, R. Morandotti, A. R. Boyd, and J. S. Aitchison, *Phys. Rev. Lett.* **81**, 3383 (1998).
6. J. W. Fleischer, M. Segev, N. K. Efremidis, and D. N. Christodoulides, *Nature* **422**, 147 (2003).
7. J. D. Joannopoulos, S. G. Johnson, J. N. Winn, and R. D. Meade, *Photonic Crystals: Molding the Flow of Light*, 2nd ed. (Princeton University, 1995).
8. T. Pertsch, U. Peschel, F. Lederer, J. Burghoff, M. Will, S. Nolte, and A. Tünnermann, *Opt. Lett.* **29**, 468 (2004).
9. F. Lederer, G. I. Stegeman, D. N. Christodoulides, G. Assanto, M. Segev, and Y. Silberberg, *Phys. Rep.* **463**, 1 (2008).
10. A. Szameit, Y. V. Kartashov, F. Dreisow, M. Heinrich, T. Petrisch, S. Nolte, A. Tünnermann, V. A. Vysloukh, F. Lederer, and L. Torner, *Phys. Rev. Lett.* **102**, 063902 (2009).
11. D. M. Jović, M. R. Belić, and C. Denz, *Phys. Rev. A* **84**, 043811 (2011).
12. U. Naether, Y. V. Kartashov, V. A. Vysloukh, S. Nolte, A. Tünnermann, L. Torner, and A. Szameit, *Opt. Lett.* **37**, 593 (2012).
13. J. Durnin, J. J. Miceli, and J. H. Eberly, *J. Opt. Soc. Am.* **4**, 651 (1987).
14. J. Durnin, J. J. Miceli, and J. H. Eberly, *Phys. Rev. Lett.* **58**, 1499 (1987).
15. J. C. Gutiérrez-Vega, M. D. Iturbe-Castillo, and S. Chávez-Cerda, *Opt. Lett.* **25**, 1493 (2000).
16. M. A. Bandres, J. C. Gutiérrez-Vega, and S. Chávez-Cerda, *Opt. Lett.* **29**, 44 (2004).
17. J. C. Gutiérrez-Vega, M. D. Iturbe-Castillo, G. A. Ramírez, E. Tepichín, R. M. Rodríguez-Dagnino, S. Chávez-Cerda, and G. H. C. New, *Opt. Commun.* **195**, 35 (2001).
18. J. C. Gutiérrez-Vega, M. A. Meneses-Neva, and S. Chávez-Cerda, *Am. J. Phys.* **71**, 233 (2003).
19. P. Rose, M. Boguslawski, and C. Denz, *New J. Phys.* **14**, 033018 (2012).
20. Y. I. Kartashov, A. A. Egorov, V. A. Vysloukh, and L. Torner, *Opt. Lett.* **31**, 238 (2006).
21. F. Ye, D. Mihalache, and B. Hu, *Phys. Rev. A* **79**, 053852 (2009).
22. A. Ruelas, S. Lopez-Aguayo, and J. C. Gutiérrez-Vega, *Opt. Lett.* **33**, 2785 (2008).
23. J. V. Vasiljević, A. Zannotti, D. V. Timotijević, C. Denz, and D. M. Jović, *Phys. Rev. A* **96**, 023840 (2017).
24. C. Alpmann, R. Bowman, M. Woerdemann, M. Padgett, and C. Denz, *Opt. Express* **18**, 26084 (2010).
25. J. A. Davis, D. M. Cottrell, J. Campos, M. J. Yzuel, and I. Moreno, *Appl. Opt.* **38**, 5004 (1999).
26. G. Agrawal, *Nonlinear Fiber Optics*, 5th ed. (Academic, 2012).
27. N. V. Kukhtarev, V. B. Markov, S. G. Odulov, M. S. Soskin, and V. L. Vinetskii, *Ferroelectrics* **22**, 949 (1979).
28. A. A. Zozulya and D. Z. Anderson, *Phys. Rev. A* **51**, 1520 (1995).
29. A. Zannotti, J. V. Vasiljević, D. V. Timotijević, C. Denz, and D. M. Jović, *Adv. Opt. Mater.* **6**, 1701355 (2018).

Visualizing the Energy Flow of Tailored Light

Alessandro Zannotti,* Jadranka M. Vasiljević, Dejan V. Timotijević, Dragana M. Jović Savić, and Cornelia Denz

Exploiting the energy flow of light fields is an essential key to tailor complex optical multistate spin and orbital angular momentum (OAM) dynamics. With this work, the energy flow is identified and quantified by a novel approach that is based on the symmetry breaking induced by nonlinear light–matter interaction of OAM carrying beams at the example of Mathieu beams, showing transverse invariant intensity distributions. These complex scalar nondiffracting beams exhibit outstanding transverse energy flows on elliptic paths. Although their energy is continuously redistributed during linear propagation in homogeneous media, the beams stay nondiffracting. This approach to visualize the energy flow of light is based on the nonlinear self-action in a nonlinear crystal. By this, the sensitive equilibrium is perturbed and accumulation of rotating high-intensity spots is enabled. Intensity distributions on elliptic, chiral paths are demonstrated as a manifestation of the energy flow. Furthermore, the formation of corresponding refractive index modulations that may be implemented as chiral waveguides, is controlled via the beam power and structure size.

1. Introduction

The energy flow of light is determined by both, its spin angular momentum and its orbital angular momentum (OAM), and is generally described by the Poynting vector.^[1] Controlling the spatial polarization and phase structure of light, the combination of binary spin states and multistate orbital angular momentum dynamics is an essential key to further establish modern high-dimensional singular optics. These abilities enabled breakthrough research in the areas of spatial polarization modulation,^[2] classical entanglement,^[3] high-density signal transmission,^[4] or optical micromanipulation.^[5,6]

In order to investigate two-dimensional energy flows in the transverse plane, in particular nondiffracting beams with

transverse invariant intensity distributions and continuously modulated phase distributions are suited. The class of nondiffracting beams has attracted considerable interest and features not only applications in optics, but also in solid state and atom physics.^[7–11] A detailed understanding of their energy flows therefore is of high importance in many communities. However, the energy flow of continuously modulated nondiffracting beams withstands a direct observation because it is hidden for the case of linear propagation in homogeneous media. The transverse intensity distribution stays invariant and the energy flow is continuously redistributed.

Four nondiffracting beam families exist as solutions of the paraxial as well as the nonparaxial Helmholtz equation in different coordinate systems:^[12–17] Discrete beams in Cartesian, Bessel beams^[8] in spherical, Mathieu beams in elliptic, and

Weber beams in parabolic coordinates. Among these diverse families, Mathieu beams^[9,10,18,19] may be interpreted as a generalized beam class, capable to interpolate between Cartesian and spherical coordinates. In contrast to parabolic Weber beams, their transverse spatial intensity distributions can form closed paths on ellipses, with spatially structured orbital angular momenta^[6,20] showing periodic boundaries.

Mathieu beams are highly appealing to access fundamental physical effects in elliptical coordinates.^[21] In several studies, they have been beneficially used for particle manipulation,^[5] and served as lattice-writing light,^[22–26] featuring the nonlinear propagation of (vortex) solitons in these previously linearly induced elliptic lattices. However, the self-action of Mathieu beams in nonlinear media was not investigated until now.

Scalar even and odd Mathieu beams exhibit only real-valued field distributions. Their transverse Poynting vector therefore vanishes. In contrast, the complex superposition of even and odd Mathieu beams leads to generalized elliptic Mathieu beams, showing outstanding continuously modulated spatial phase distributions, i.e., OAM.^[5,6,20] Thus, for these beams a transverse energy flow is present. Until today, only a few works have addressed the energy flow in these complex spatially modulated beams with its unique OAM characteristics, e.g., using the OAM structure of Mathieu beams to transfer orbital angular momentum to particles that start to rotate.^[5,6,20]

With this work, we present an approach to visualize the energy flow of light at the example of elliptic Mathieu beams. We demonstrate experimentally and numerically that the

A. Zannotti, Prof. C. Denz
Institute of Applied Physics and Center for Nonlinear Science (CeNoS)
Westfälische Wilhelms-Universität Münster
48149 Münster, Germany
E-mail: a.zannotti@uni-muenster.de

J. M. Vasiljević, Prof. D. V. Timotijević, Prof. D. M. Jović Savić
Institute of Physics
University of Belgrade
P.O. Box 68, 11001 Belgrade, Serbia
Prof. D. V. Timotijević
Science Program
Texas A&M University at Qatar
P.O. Box 23874, Doha, Qatar

DOI: 10.1002/adom.201701355

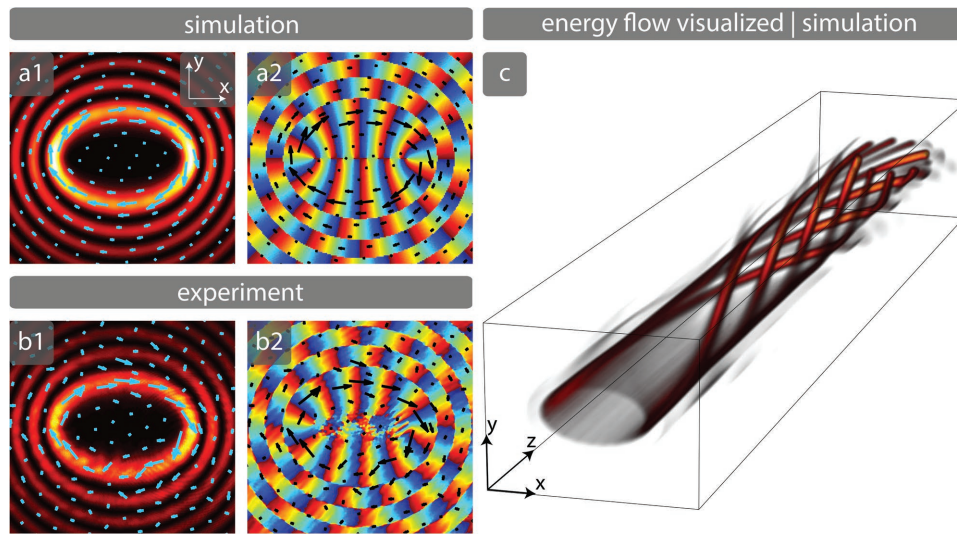


Figure 1. a,b) Poynting vector of the elliptic Mathieu beam and c) its nonlinear propagation. The energy flow, characterized by the Poynting vector (indicated by arrows), is (a) calculated and (b) observed experimentally for the initial beam profiles, shown in (a1, b1) intensity and (a2, b2) phase. The formation of rotating high-intensity filaments due to the nonlinear self-interaction is illustrated in (c).

energy flow of elliptic Mathieu beams becomes observable by propagating in a nonlinear photorefractive crystal. The nonlinearity breaks the sensitive equilibrium of the energy redistribution of the beam and enables the formation of high-intensity spots that encircle a common center, driven by the OAM in the direction of the energy flow. Due to the nonlinear interaction, the intensity distribution is transferred to a correspondingly twisted refractive index modulation. We demonstrate that we can control the formation and rotation of high-intensity spots by increasing the strength of the nonlinearity or by tailoring the size of the initial beam. Note, that by this, photonic structures can be implemented as chiral waveguides, supporting the actual and rich field of research on chiral photonic structures.^[27–31]

2. Characteristics of Elliptic Mathieu Beams

Fundamental Mathieu beams are solutions of the Helmholtz equation in elliptical cylindrical coordinates (ξ, η, z) . They are mathematically described by a product of radial and angular Mathieu functions and exist either as even or odd solutions.^[9] Elliptic Mathieu beams represent a complex linear superposition of even and odd Mathieu beams of the same order m . For a monochromatic, scalar elliptic Mathieu beam of order m , the light field is given by^[21]

$$\psi(\xi, \eta) = C_m(q) J_{e_m}(\xi; q) c_{e_m}(\eta; q) + i S_m(q) J_{o_m}(\xi; q) s_{e_m}(\eta; q) \quad (1)$$

where J_{e_m} and J_{o_m} are the even and odd radial Mathieu functions, and c_{e_m} and s_{e_m} are the even and odd angular Mathieu functions of order m , respectively. $C_m(q)$ and $S_m(q)$ are weighting constants that depend on $q = f^2 k_t^2 / 4$ that in turn determines the ellipticity of the Mathieu beams. It is related to the positions f of the two foci and the transverse wave number $k_t = 2\pi/a$ that corresponds to a characteristic structure size a .

The transverse time-averaged Poynting vector $\langle S \rangle$ of a linearly polarized, transverse light field ψ is determined by the spatial OAM distribution and given by^[32]

$$\langle S \rangle = \frac{i\omega\epsilon_0}{2} (\psi^* \nabla \psi - \psi \nabla \psi^*) \quad (2)$$

where $\omega = ck$ is the angular-frequency that connects the speed of light c with the wave number $k = 2\pi/\lambda$, defined by the wavelength λ . ϵ_0 is the vacuum permittivity.

Figure 1 exemplarily shows an elliptic Mathieu beam of order $m = 10$ with an ellipticity of $q = 25$ (Panels (a,b)), and our concept to visualize its energy flow (Panel (c)). The numerically calculated transverse field as well as the experimentally obtained field are shown in intensity and phase at the initial plane in Figure 1a,b, respectively. While it is natural to calculate numerically an electric field ψ , experimentally only the transverse intensity (I) and phase (ϕ) are accessible. From these, we construct the experimentally obtained electric field $\psi = \sqrt{I} \exp[i\phi]$. Using Equation (2), we calculate and image the transverse Poynting vector of this beam, indicated with overlying arrows. Figure 1c shows a characteristic numerical simulation that illustrates how the main intensity that is distributed on an ellipse enters the front of a nonlinear crystal, optically induces a photonic structure that yields to the formation of high-intensity spots which start to rotate in the direction of the energy flow. At the back face of the crystal several spots remain that prove the existence of the initial energy flow.

In the following, we present our approach to visualize numerically and experimentally the energy flow of elliptic Mathieu beams and thus tailor the realization of chiral waveguides. We further demonstrate that we can control the rotation and the degree of filamentation mainly by the strength of the nonlinearity and the structure sizes of the Mathieu beams. In this work, we exemplarily demonstrate our results for an elliptic Mathieu beam of order $m = 10$ and ellipticity $q = 25$. However,

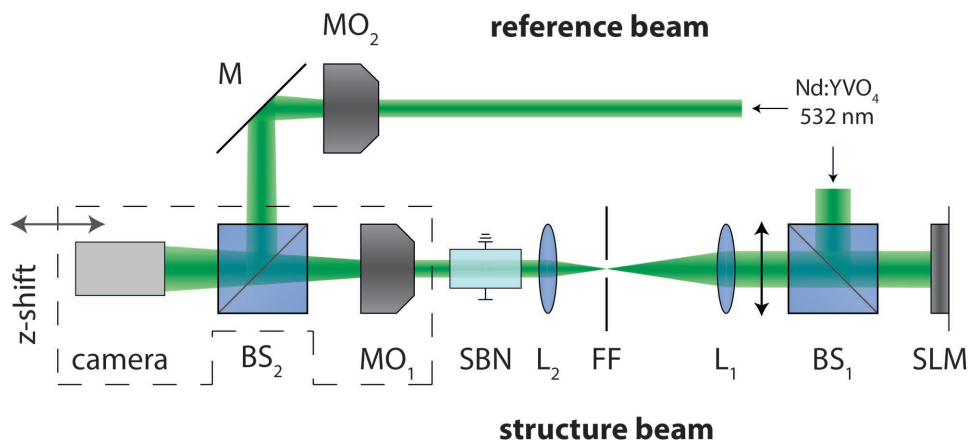


Figure 2. The experimental setup. BS: beam splitter, FF: Fourier filter, L: lens, M: mirror, MO: microscope objective, SLM: spatial light modulator.

realizations with elliptic Mathieu beams that differ in their order or ellipticity are possible within a certain parameter range that also depends on the further properties of the beam and the nonlinearity.

3. Details on the Numerical Simulations and the Experimental Setup

In the experiment, which is shown in **Figure 2**, we use a frequency-doubled Nd:YVO₄ laser. The broad laser beam illuminates as a plane wave a spatial light modulator “Holoeye Pluto VIS.” We adopt the method of Ref. [33] to modulate both, amplitude and phase of the initial transverse (*x*-*y*-plane) light field with one phase-only modulator. An appropriate Fourier filtering is required. The extraordinary polarized structure beams interact with a nonlinear Strontium Barium Niobate (SBN) crystal which has geometrical dimensions of 5 × 5 × 15 mm³. It is biased with an external electric field *E*_{ext} along the optical *c*-axis, directed along one of the shorter axis, parallel to the *x*-axis. The paraxial structured light field propagates mainly in *z*-direction. The intensity distribution at the back face of the SBN crystal is magnified with a microscope objective and imaged by a camera. In order to measure the phase of the structure beam, we superimpose a tilted plane wave as reference beam and use a digital holographic method.^[34]

Numerically, we solve the nonlinear Schrödinger Equation (3) by applying a spectral split step propagation method^[35,36]

$$i \partial_z \psi(\mathbf{r}) + \frac{1}{2k_z} [\Delta_{\perp} + V(I)] \psi(\mathbf{r}) = 0 \quad (3)$$

It describes the paraxial propagation of a scalar light field $\psi(\mathbf{r})$ with longitudinal wave vector k_z in a potential $V(I) = -k_z^2 n_e^2 r_{33} E(I)$ due to the photorefractive nonlinearity. $k = 2\pi/\lambda = (k_x^2 + k_z^2)^{1/2}$ is the wave number and defined by the wavelength $\lambda = 532$ nm. $n_e = 2.358$ is the extraordinary bulk refractive index, and $r_{33} = 237$ pm V⁻¹ is the corresponding electro-optic coefficient.

Photorefractive SBN provides a strong nonlinearity at comparatively low power levels and the ability of reversible

inductions. The electric field $E(I) = E_{\text{ext}} + E_{\text{sc}}(I)$ that builds up inside the SBN crystal is a superposition of a static external electric field $E_{\text{ext}} = 1600$ V cm⁻¹ and an internal space charge field $E_{\text{sc}}(I)$ that results due to the incident intensity distribution $I(r) = |\psi(r)|^2$.^[37] We calculate the resulting intensity-dependent, saturable, nonlocal, and anisotropic refractive index modulation via $E_{\text{sc}} = \partial_x \phi_{\text{sc}}$ by solving the modeling potential Equation (4) numerically^[38]

$$\Delta \phi_{\text{sc}} + \nabla \phi_{\text{sc}} \nabla \ln(1+I) = E_{\text{ext}} \partial_x \ln(1+I) \quad (4)$$

4. Visualizing the Energy Flow of Elliptic Mathieu Beams

The balanced intensity redistribution of elliptic Mathieu beams is only present for their linear propagation in homogeneous media. We break this sensitive equilibrium by controlling the nonlinear self-action of elliptic Mathieu beams in a photorefractive crystal. When interacting with the optically induced refractive index modulation, the energy flow is altered. This leads to the accumulation of intensity at defined spots, where in turn the refractive index is increased. In this way, helically twisted refractive index lattices form and rotate in a predetermined direction.

Observing experimentally the formation and accumulation of high-intensity spots at the back face of the SBN crystal that are substantiated by corresponding numerical simulations and additionally controllable by the power and structure size of the writing beam represents our concept to visualize the energy flow of Mathieu beams. Furthermore, this method features the fabrication of chiral waveguide arrays.

We investigate the nonlinear self-action of the Mathieu beams with a structure size of $a = 15$ μm in the SBN crystal and reveal their energy flow by optically inducing a refractive index modulation with the structure beams. Based on the comparison with the numerical simulations, we estimate that the optically induced refractive index depth is in the order of 10⁻⁴. Systematically, we increase the initial beam power $P_0 \approx 20$ μW and double it in two steps in both, numerical simulation and

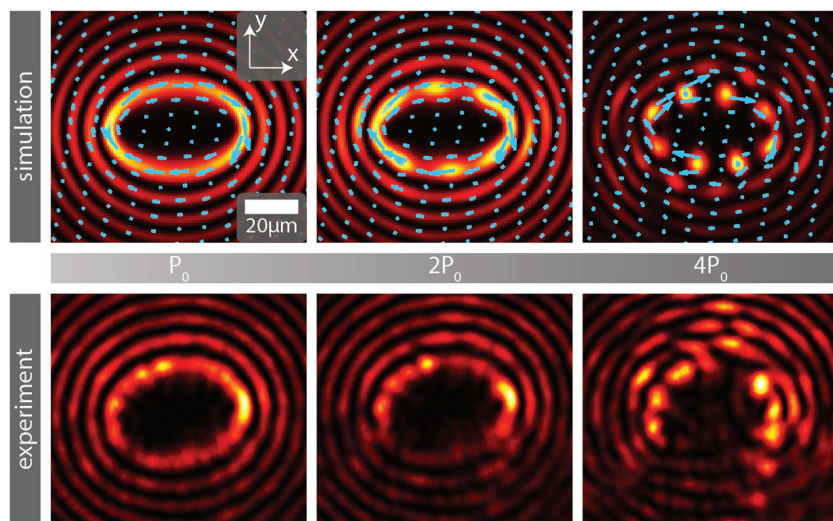


Figure 3. The transverse intensity distributions of elliptic Mathieu beams ($a = 15 \mu\text{m}$) at the back face of the SBN crystal, nonlinearly inscribed with increasing beam powers. Compared are numerical simulations (calculated Poynting vector indicated by arrows) with experimental results.

experiment. **Figure 3** shows the transverse intensity distributions at the back face of the SBN crystal. For the numerical simulations, we indicated with arrows that the Poynting vector (the energy flow) is still directed along the initial ellipse. Our construction scheme to experimentally obtain the complex electric field ψ and thus calculate the Poynting vector is not applicable here, since the spatial phase distribution ϕ is not accessible by using holographic techniques when imaging through the inhomogeneous refractive index modulation. As well, an experimental glance inside the crystal to see the 3D intensity distribution is not possible, since the light in the observing plane would be refracted by the inhomogeneous photonic structure in an unpredictable manner. Thus, we show that the experimental intensity distribution obtained at the back face of the crystal is tunable by changing the beam power so that spots of high intensity can be realized with changing positions and connect their individual manifestation with the formation of chiral lattices inside the crystal. The back face intensity distributions of simulation and experiment are in high agreement and substantiate our numerical simulations for the 3D distribution of the intensity inside the volume.

In particular, we show the transition from quasi linear propagation to a strong nonlinear self-interaction which introduces a symmetry breaking of the energy flow. For a weak beam power P_0 the beam propagates almost linearly, apparent at an almost unchanged output intensity distribution, indicating that the beam is still nondiffracting. When doubling the power, modulations emerge in form of occurring accumulations of intensity along the beforehand smoothly modulated ellipse. The writing beam thus can no longer be considered as nondiffracting nor as Mathieu beam. For the highest beam power of $4P_0$, separated spots of high intensity appear and rotate in the direction indicated by the Poynting vector, thereby forming rotating refractive index strands in analogy to the simulation in Figure 1c. The spots that occur at the back face of the SBN crystal are a consequence of modulation instabilities^[39] on an ellipse. Thus,

the amount of spots does not only depend on the order m of the elliptic Mathieu beams, but is influenced by several parameters, like the strength of the nonlinearity, the structure size, or the propagation distance.

Due to the modulation of the intensity distribution along the innermost ellipse and the anisotropic medium, the refractive index modulation is predominantly established in the direction of the optical c -axis. Subsequently, the energy flow, which is typically located on an ellipse, is now preferentially directed perpendicular to the c -axis where the refractive index modulation is weak, but is especially hindered to flow parallel to the c -axis due to the strong variations in the potential. Thus, conglomerations of high intensity form in particular at the trough of high refractive index where enough intensity is accumulated to create solitary strands of increased refractive index.

Note that these twisted photonic structures may act as waveguides for further probe beams and guide light on elliptical, chiral paths. Our numerical simulations and the experimental results both indicate that the period of rotation changes during formation as well as the radius from the central axis. Moreover, some streams of intensity branch and multiple intensity maxima occur (cf. Section 5). Our approach therefore provides a flexible and easy to implement method to realize chiral photonic media. Further investigations could potentially show advanced light–matter interactions, e.g., when probing these diverse chiral structures with chiral light.

5. Tailored, Nonlinear Mathieu Lattices

Additional to the previously discussed dependence of the formation of rotating waveguides on the strength of the nonlinearity, we demonstrate the control of the induction of elliptic Mathieu lattices in the nonlinear medium by changing the characteristic structure size $a = 2\pi/k_t$. Different elliptic Mathieu beams show a very rich rotating behavior with different spot characteristics.

Figure 4 shows the nonlinear control of the beam rotation by changing the beam size parameter a , whereby the beam power is constant at $P_0 \approx 20 \mu\text{W}$. We apply characteristic beam sizes of $a = [15, 20, 25] \mu\text{m}$. Compared are our experimental results with corresponding numerical simulations. Arrows again indicate the Poynting vector. We found that by increasing the structure size a of elliptic Mathieu beams, the local slope of the helix of the emerging rotating strands of higher refractive index is decreased. We also observe a coupling of the rotation to the quantity of spots. For $a = 15 \mu\text{m}$ in Figure 4, we hardly see conglomerations of intensity. For $a = 20 \mu\text{m}$ similar rotating waveguides occur as we have observed them for the structure size of $a = 15 \mu\text{m}$ with a power P that is comparable to be between $2P_0$ and $4P_0$, shown in Figure 3. By this, we find a regime where the strength of the nonlinearity is suited to

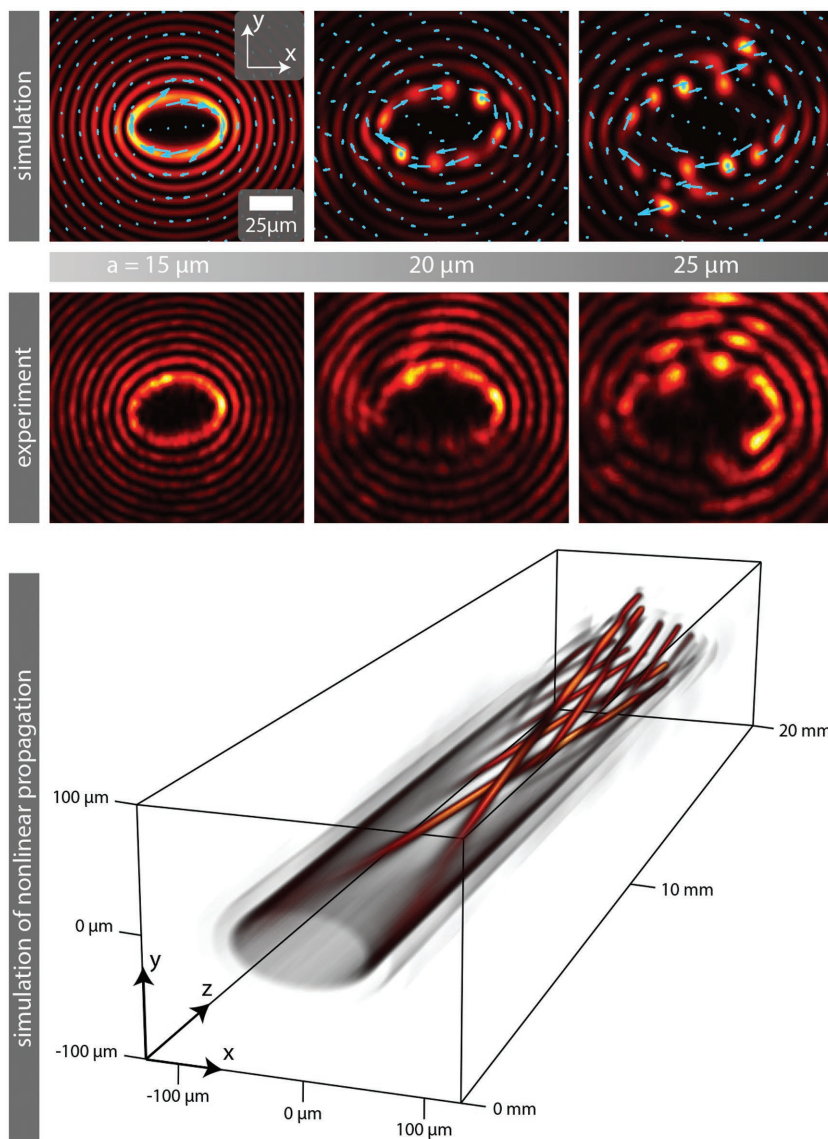


Figure 4. Numerically calculated (top) and experimentally measured (middle) transverse intensity distributions at the back face of the SBN crystal after nonlinear and self-interacting propagation of elliptic Mathieu beams ($P \approx 20 \mu\text{W}$), for beams with different structure sizes a . Arrows indicate the Poynting vector. The 3D intensity volume (bottom) visualizes the branching to due modulation instabilities on an ellipse for the case that $a = 25 \mu\text{m}$.

host the rotating photonic structures. This in turn is justified by the fact that for $a = 25 \mu\text{m}$ the self-action is strong and tends to become stronger for larger structure sizes a , also recognizable by the Poynting vector that directs outward for the outer high-intensity spots. Figure 4 shows the numerically simulated 3D intensity volume for $a = 25 \mu\text{m}$, and demonstrates exemplary for this borderline case the enhanced degree of branching for increased beam sizes. In the presented case, new branches of high intensity start to form after a propagation distance of about 10 mm and rotate. Further branches appear after longer propagation distances. Note that for larger structure sizes, the intensity spreads to ellipses located more outside due to increasing modulation instabilities of the broader beam. Thus,

rotating strands of high intensity can only induce chiral refractive index strands for these proper parameters.

6. Conclusion

We presented an approach to identify and visualize the energy flow of light based on the symmetry breaking by nonlinear light-matter interaction of OAM carrying beams. As an example, we chose elliptic Mathieu beams with outstanding continuously modulated OAM distributions. We used a nonlinearity introduced in form of a photorefractive SBN crystal in order to break the sensitive equilibrium, which is present for linear propagation of nondiffracting beams. We demonstrated exemplarily that the nonlinear self-action of elliptic Mathieu beams leads to the formation of high-intensity filaments, which rotated in the direction determined by the energy flow. The dependence of these emerging photonic structures on the strength of the nonlinearity and the structure size of the Mathieu beams was investigated and we pointed out that the twisted refractive index formation could act as chiral waveguides. We worked out that the formation of chiral Mathieu lattices is possible only in this limited regime with proper parameters for the nonlinearity and structure size. Corresponding numerical simulations substantiate our results. For elliptic Mathieu beams, our approach furthermore is well suited to fabricate rotating photonic structures with elliptic trajectories, thereby considerably advancing the field of chiral light and photonic structures.

Note that chiral lattices created by our approach show longitudinally increasing “helix slopes”, and additionally tailored transverse ellipticities. Both properties may be considered as novel degree of freedom to design unique band structures and realize artificial photonic media with new topologies.

Acknowledgements

The authors acknowledge support by the German Academic Exchange Service (Project 57219089), the Ministry of Education, Science, and Technological development, Republic of Serbia (Projects OI 171036), as well as the Qatar National Research Fund (NPRP 7-665-1-125).

Conflict of Interest

The authors declare no conflict of interest.

Keywords

chiral media, energy flow, Mathieu beams, nonlinear optics, photorefractive optics

Received: December 13, 2017

Revised: January 26, 2018

Published online:

-
- [1] M. Born, E. Wolf, *Principles of Optics*, 7th ed., Cambridge University Press, Cambridge, UK **1999**.
- [2] E. Otte, C. Alpmann, C. Denz, *J. Opt.* **2016**, *18*, 074012.
- [3] F. Töppel, A. Aiello, C. Marquardt, E. Giacobino, G. Leuchs, *New J. Phys.* **2014**, *16*, 073019.
- [4] J. Leach, M. J. Padgett, S. M. Barnett, S. Franke-Arnold, J. Courtial, *Phys. Rev. Lett.* **2002**, *88*, 257901.
- [5] C. Alpmann, R. Bowman, M. Woerdemann, M. Padgett, C. Denz, *Opt. Express* **2010**, *18*, 26084.
- [6] C. López-Mariscal, J. C. Gutiérrez-Vega, G. Milne, K. Dholakia, *Opt. Express* **2006**, *14*, 4182.
- [7] J. Durnin, *J. Opt. Soc. Am. A* **1987**, *4*, 651.
- [8] J. Durnin, J. J. Miceli, J. H. Eberly, *Phys. Rev. Lett.* **1987**, *58*, 1499.
- [9] J. C. Gutiérrez-Vega, M. D. Iturbe-Castillo, S. Chávez-Cerda, *Opt. Lett.* **2000**, *25*, 1493.
- [10] M. A. Bandres, J. C. Gutiérrez-Vega, S. Chávez-Cerda, *Opt. Lett.* **2004**, *29*, 44.
- [11] R. Stützle, M. C. Göbel, T. Hörner, E. Kierig, I. Mourachko, M. K. Oberthaler, M. A. Efremov, M. V. Fedorov, V. P. Yakovlev, K. A. H. van Leeuwen, W. P. Schleich, *Phys. Rev. Lett.* **2005**, *95*, 110405.
- [12] Z. Bouchal, *Czech J. Phys.* **2003**, *53*, 537.
- [13] P. Rose, M. Boguslawski, C. Denz, *New J. Phys.* **2012**, *14*, 033018.
- [14] U. Levy, S. Derevyanko, Y. Silberberg, *Prog. Opt.* **2016**, *61*, 237.
- [15] P. Zhang, Y. Hu, T. Li, D. Cannan, X. Yin, R. Morandotti, Z. Chen, X. Zhang, *Phys. Rev. Lett.* **2012**, *109*, 193901.
- [16] P. Aleahmad, M.-A. Miri, M. S. Mills, I. Kaminer, M. Segev, D. N. Christodoulides, *Phys. Rev. Lett.* **2012**, *109*, 203902.
- [17] M. Bandres, M. A. Alonso, I. Kaminer, M. Segev, *Opt. Express* **2013**, *21*, 13917.
- [18] J. C. Gutiérrez-Vega, M. D. Iturbe-Castillo, G. A. Ramírez, E. Tepichín, R. M. Rodríguez-Dagnino, S. Chávez-Cerda, G. H. C. New, *Opt. Commun.* **2001**, *195*, 35.
- [19] C. L. López-Mariscal, M. A. Bandres, J. C. Gutiérrez-Vega, S. Chávez-Cerda, *Opt. Express* **2005**, *13*, 2364.
- [20] S. Chávez-Cerda, M. J. Padgett, I. Allison, G. H. C. New, J. C. Gutiérrez-Vega, A. T. O'Neil, I. MacVicar, J. Courtial, *J. Opt. B: Quantum Semiclassical Opt.* **2001**, *195*, 35.
- [21] J. C. Gutiérrez-Vega, R. M. Rodríguez-Dagnino, M. a. Meneses-Nava, S. Chávez-Cerda, *Am. J. Phys.* **2003**, *71*, 233.
- [22] Y. V. Kartashov, V. A. Vysloukh, L. Torner, *Phys. Rev. Lett.* **2004**, *93*, 093904.
- [23] R. Fischer, D. N. Neshev, S. Lopez-Aguayo, A. S. Desyatnikov, A. A. Sukhorukov, W. Krolikowski, Y. S. Kivshar, *Opt. Express* **2006**, *14*, 2825.
- [24] Y. V. Kartashov, A. A. Egorov, V. A. Vysloukh, L. Torner, *Opt. Lett.* **2006**, *31*, 238.
- [25] F. Ye, D. Mihalache, B. Hu, *Phys. Rev. A* **2009**, *79*, 053852.
- [26] A. Ruelas, S. Lopez-Aguayo, J. C. Gutiérrez-Vega, *Opt. Lett.* **2008**, *33*, 2785.
- [27] A. Zannotti, F. Diebel, M. Boguslawski, C. Denz, *Adv. Opt. Mater.* **2016**, *5*, 1600629.
- [28] J. Becker, P. Rose, M. Boguslawski, C. Denz, *Opt. Express* **2011**, *19*, 9848.
- [29] J. Xavier, S. Vyas, P. Senthilkumaran, C. Denz, J. Joseph, *Opt. Lett.* **2011**, *36*, 3512.
- [30] A. Kuzky, R. Schreiber, H. Zhang, A. Govorov, T. Liedl, N. Liu, *Nat. Mater.* **2014**, *13*, 862.
- [31] M. C. Rechtsman, J. M. Zeuner, Y. Plotnik, Y. Lumer, D. Podolsky, F. Dreisow, S. Nolte, M. Segev, A. Szameit, *Nature* **2013**, *496*, 196.
- [32] L. Allen, M. Padgett, M. Babiker, *Prog. Opt.* **1999**, *39*, 291.
- [33] J. A. Davis, D. M. Cottrell, J. Campos, J. Yzuel, I. Moreno, *Appl. Opt.* **1999**, *38*, 5004.
- [34] J. Zhao, P. Zhang, J. B. Zhou, D. X. Yang, D. S. Yang, E. P. Li, *Chin. Phys. Lett.* **2003**, *20*, 1748.
- [35] G. P. Agrawal, *Nonlinear Fiber Optics*, 5th ed., Academic Press, Oxford, UK **2013**.
- [36] F. Diebel, B. M. Bokic, D. V. Timotijevic, D. M. Jovic Savic, C. Denz, *Opt. Express* **2015**, *23*, 24351.
- [37] N. V. Kukhtarev, V. B. Markov, S. G. Odulov, M. S. Soskin, V. L. Vinetskii, *Ferroelectrics* **1979**, *22*, 949.
- [38] A. A. Zozulya, D. Anderson, *Phys. Rev. A* **1995**, *51*, 1520.
- [39] C. Denz, M. Schwab, C. Weillnau, *Transverse-Pattern Formation in Photorefractive Optics*, 1st ed., Springer-Verlag, Berlin, Heidelberg, New York **2003**.

Elliptical vortex necklaces in Mathieu lattices

Jadranka M. Vasiljević,¹ Alessandro Zannotti,² Dejan V. Timotijević,^{1,3} Cornelia Denz,² and Dragana M. Jović Savić¹

¹*Institute of Physics, University of Belgrade, P.O. Box 68, 11001 Belgrade, Serbia*

²*Institut für Angewandte Physik and Center for Nonlinear Science, Westfälische Wilhelms-Universität Münster, 48149 Münster, Germany*

³*Science Program, Texas A&M University at Qatar, P.O. Box 23874, Doha, Qatar*



(Received 25 December 2017; published 27 March 2018)

We demonstrate unusual kinds of discrete vortex beams, elliptical necklaces, realized by Mathieu photonic lattices. Varying the order of the Mathieu lattices and their ellipticity, we can control the shape and size of such necklaces. Besides stable vortex states, we observe oscillatory dipole states or dynamical instabilities and study their orbital angular momentum. Dynamical instabilities occur for higher beam power and higher-order vortices. Also the decay of higher-order phase singularities and their separation is observed in dependence on the ellipticity.

DOI: [10.1103/PhysRevA.97.033848](https://doi.org/10.1103/PhysRevA.97.033848)

I. INTRODUCTION

An optical vortex that possesses a phase singularity and a rotational flow around the singular point in a given direction can be found in physical systems of different nature and scale, ranging from water whirlpools and atmospheric tornadoes to quantized vortices in superfluids and quantized lines of magnetic flux in superconductors [1]. The study of optical vortices and associated localized vortex states is important for both fundamental and applied physics, leading to applications in many areas that include optical data storage, distribution and processing, optical interconnects between electronic chips and boards, and free-space communication links [2–4]. They also have potential uses in optical tweezers [5], optical manipulation and trapping [6,7], microscopy [8], and quantum information processing [9,10].

The evolution of nonlinear excitations in systems whose properties are modulated is especially interesting and in optics can be realized when an intense laser beam propagates in the material with a suitable transverse refractive index modulation that can be fabricated in nonlinear materials including semiconductors, liquid crystals, fused silica, polymers, and photorefractive media [11–18]. The combination of diffractive and nonlinear effects with transverse refractive index modulation in photonic lattices opens the possibility to produce spatially localized states of light [19,20]. To optically induce two-dimensional photonic lattices it is appropriate to use nondiffracting light beams that are exact solutions of the Helmholtz equation in different coordinate systems [21,22]: plane waves in Cartesian, Bessel beams in circular cylindrical [23], Mathieu beams in elliptic cylindrical [24], and parabolic beams in parabolic cylindrical coordinates [25].

In this paper we report on the existence of elliptical necklace beams in photonic lattices optically induced by Mathieu nondiffracting beams, using vortices as a probe beam. These necklace beams show discrete intensity spots on elliptical curves, associated with discrete phase vortices. We investigate the conditions for their existence as well as their properties, both experimentally and theoretically. Changing the lattice ellipticity and choosing Mathieu lattices of appropriate order, we control the shape and the size of an elliptical necklace, as well

as the number of the “pearls” in the necklace. We investigate the breakup of higher-order vortices (topological charge $C_T = 2, 3, 4$) into $C_T = 1$ vortices and their rate of separation during propagation. Phase singularity distances increase with C_T , higher lattice ellipticity, and propagation distance. Further, we study the stability of such elliptic necklaces. Supported by the strong nonlinearity, we show the formation of oscillating dipole states in the intensity distribution for very long propagation distances and discuss our results by investigating additionally the transfer of orbital angular momentum (AM) to the lattice. Finally, a high intensity of the probe beam leads to nonlinear dynamical instabilities observable in the intensity distribution of the necklaces.

II. EXPERIMENTAL METHOD AND MODELING OF VORTEX BEAM PROPAGATION IN MATHIEU LATTICES

Figure 1 shows the experimental setup to realize elliptical necklaces. A frequency-doubled, expanded, and collimated Nd:YVO₄ laser with wavelength $\lambda = 532$ nm is split into two separate beams: an ordinary polarized writing and an extraordinary polarized probe beam. Both are spatially tailored in intensity and phase by a phase-only spatial light modulator Holoeye Pluto VIS. For this purpose, special Fourier filters (FF1 and FF2) are required [26]. The structure beam optically induces refractive index modulations in the 15-mm-long photorefractive Strontium Barium Niobate crystal doped by Cerium (SBN:Ce), thereby addressing the weaker electro-optic coefficient $r_{13} = 47$ pm/V. The birefringent crystal has refractive indices $n_o = 2.325$ and $n_e = 2.358$ and is externally biased with an electric field $E_{\text{ext}} = 1600$ V/cm aligned along the optical $c = x$ axis, perpendicular to the direction of propagation (z axis). Probing the artificial photonic structure is done with the extraordinary polarized probe beam that addresses the stronger electro-optic coefficient $r_{33} = 237$ pm/V. An imaging system consisting of a microscope objective and camera detects transverse intensity distributions at the back of the crystal.

We model our experiment by solving the nonlinear Schrödinger equation for an initial scalar electric field $A(\mathbf{r})$

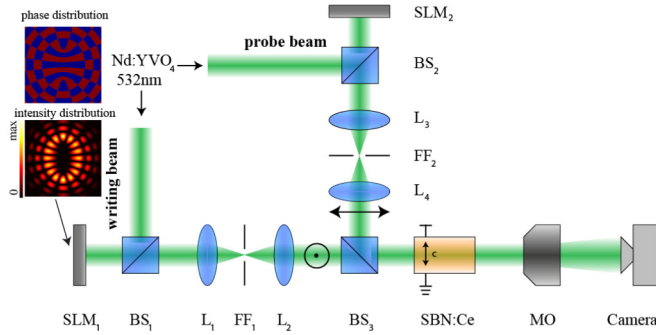


FIG. 1. Experimental setup for the investigation of vortex beams in a Mathieu lattice optically induced in a photorefractive SBN crystal: BS, beam splitter; FF, Fourier filter; L, lens; M, mirror; MO, microscope objective; and SLM, spatial light modulator.

numerically by using a beam propagation method [27]:

$$i \partial_z A(\mathbf{r}) + \frac{1}{2k_z} \Delta_{\perp} A(\mathbf{r}) + \frac{k_z}{2n_{o,e}^2} \delta n^2[|A(\mathbf{r})|^2] A(\mathbf{r}) = 0. \quad (1)$$

By this, the nonlinear propagation of the field $A(\mathbf{r})$ with longitudinal wave vector k_z in a photorefractive nonlinearity is evaluated. The wave number $k = 2\pi/\lambda = \sqrt{k_{\perp}^2 + k_z^2}$ is defined by the wavelength λ . We use elliptical Laguerre Gaussian vortex beams as probe beams [28]. The potential is given by $\delta n^2[|A(\mathbf{r})|^2] = -n_{o,e}^4 r_{13,33} E$. The electric field $E = E_{\text{ext}} + E_{\text{sc}}$ that builds up inside the strontium barium niobate (SBN) crystal is a superposition of an external electric field E_{ext} and an internal space charge field E_{sc} that results due to the incident intensity distribution $I(\mathbf{r}) = |A(\mathbf{r})|^2$. Owing to the biased SBN crystal, we use an anisotropic approximation to calculate the refractive index modulation and solve the potential equation [29]

$$\Delta \phi_{\text{sc}} + \nabla \phi_{\text{sc}} \nabla \ln(1 + I + I_{\text{latt}}) = E_{\text{ext}} \partial_x \ln(1 + I + I_{\text{latt}}), \quad (2)$$

where $E_{\text{sc}} = \partial_x \phi_{\text{sc}}$ and I_{latt} is the lattice intensity according to the corresponding Mathieu beams. We use Mathieu beams $M_m(\xi, \eta)$ mathematically described as the product of radial c_{em} and angular J_{em} Mathieu functions of order m ,

$$M_m(\xi, \eta) = C_m(q) J_{em}(\xi; q) c_{em}(\eta; q), \quad (3)$$

where $C_m(q)$ is a weighting constant. The functions depend on $q = f^2 k_{\perp}^2 / 4$, a parameter of ellipticity which is related to the positions f of the two foci and the transverse wave number $k_{\perp} = 2\pi/a$, where a is the characteristic structure size; here $I_{\text{latt}} = |M_m(\xi, \eta)|^2$ and $a = 90 \mu\text{m}$. We present results with even Mathieu functions, but our conclusions are the same for odd Mathieu functions.

III. ELLIPTICAL NECKLACE STRUCTURES

To systematically investigate the propagation of vortex beams in Mathieu lattices, we start our studies by considering the Mathieu lattices optically induced with even Mathieu function of order $m = 8$, dependent on different ellipticity parameters q . We examine the conditions of existence of spatially localized vortex states. It is well known that the presence of

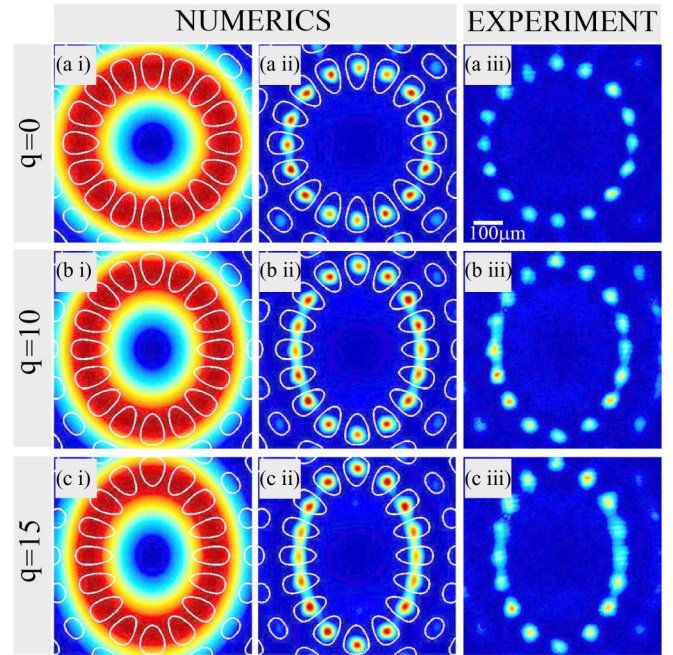


FIG. 2. Elliptical necklaces in Mathieu lattices with different ellipticity parameter q and $C_T = 1$. The input vortex beam is shown with the layout of the lattice beams indicated by open circles (the first column). The corresponding intensity distributions are shown at the exit crystal face in numerics (the second column) and experiment (the third column). The parameters are $E_0 = 1600 \text{ V/cm}$, numerical lattice intensity $I_{\text{latt}} = 0.3$, and input vortex intensity 0.005 ; the experimental lattice power $P_{\text{latt}} = 20 \mu\text{W}$ and input vortex power $8 \mu\text{W}$.

the lattice during vortex breakup induces confinement of the filaments approximately at the location of the incident vortex ring and the surrounding lattice sites. We choose the input vortex beam with $C_T = 1$ to cover the lattice sites of the inner lattice elliptical ring.

Figure 2 summarizes our results for three different values of ellipticity parameter q . At the beginning, we consider the case with no ellipticity ($q = 0$) and observe a stable necklace beam for very low nonlinearity (almost linear). Increasing the lattice ellipticity for the same experimental conditions, we observe elliptical necklaces, with lobes slightly closer to each other, owing to the shape and distribution of the lattice sites in that lattice area. Investigating the stability of these necklaces, we find that these vortex states are stable during propagation along the crystal. With Mathieu lattices of higher order ($m > 8$), we observe elliptical necklaces with a larger number of pearls, staying stable along the length of the crystal. With broader vortex beams we find vortex solutions with two necklaces, covering the inner and next ring of the Mathieu lattice. These states are not stable during the propagation.

Next we investigate higher-order vortex beams in Mathieu lattices. We choose the same input ring vortex beam with different C_T (Fig. 3). Energy flow inside the inner lattice ring causes an increase in asymmetry when incrementing C_T . In the overall phase distribution, we observe a central area having the expected vortex state. However, on the inner lattice ring, we observe a vortex state corresponding to the input C_T , but circularly shifted with respect to the central vortex area.

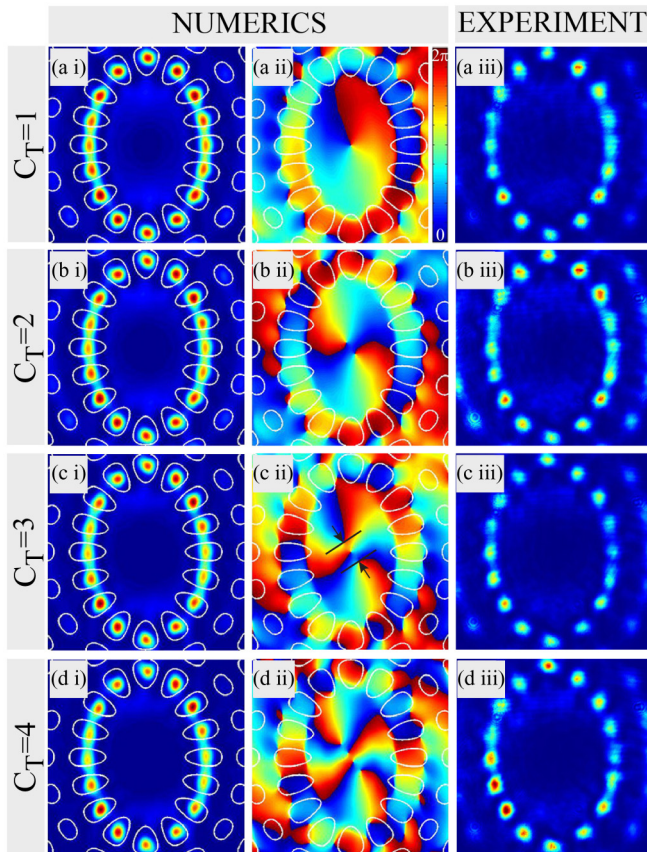


FIG. 3. Single- and multiple-charged elliptical necklaces for the numerically observed intensity (the first column) and phase distributions (the second column). The third column presents experimentally observed intensity distributions. The lattice ellipticity $q = 15$ and other parameters are as in Fig. 2.

Considering phase distributions along the propagation, we observe the phase distribution shifting along the inner lattice ring, as well as in the central part of the phase distributions.

For higher-order vortices we observe a spatial separation of several single-charged phase singularities [30], unlike the conventional multiple-charged vortex where the embedded phase singularity is multiply folded. The elliptical necklaces show an unfolded behavior in the phase distribution, with the

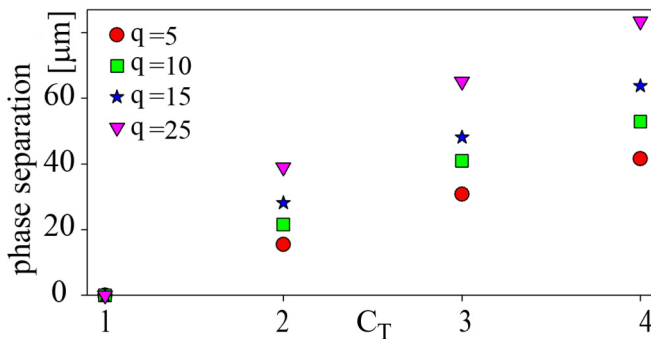


FIG. 4. Phase singularity separation versus C_T for various lattice ellipticities after a 15-mm propagation distance. Separations are measured as the Euclidean distance between the two singularities.

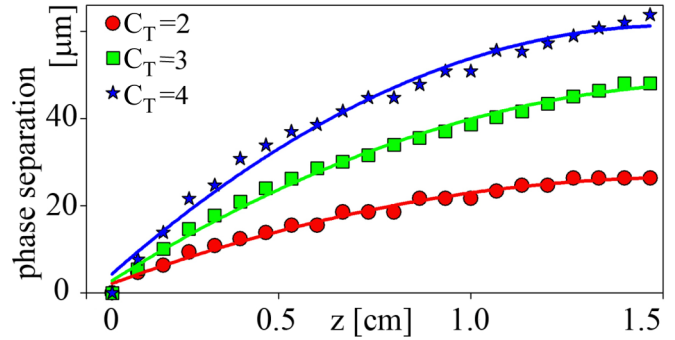


FIG. 5. Phase singularity separation versus propagation distance for various C_T . Separations are measured between the two singularities for lattice ellipticity $q = 15$ as a Euclidean distance. The parameters are as in Fig. 3.

appearance of multiple single-charged phase singularities separated by a finite distance. We found that the phase singularity separation depends on the lattice ellipticity, as well as the input vortex C_T . We measure the Euclidean distance between the two furthest singularities [as indicated in Fig. 3(cii)] for different lattice ellipticity and presented results in Fig. 4. Higher values of separations are observed for higher ellipticities q . Phase singularity separation distances also increase with propagation distance, for higher $C_T = 2, 3, 4$ and $q = 15$ (Fig. 5). Higher values of separations are observed for higher C_T .

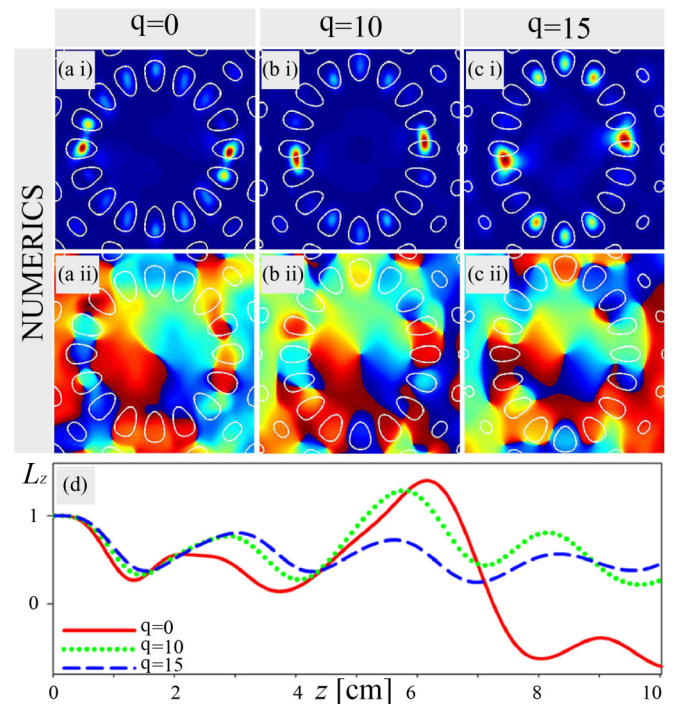


FIG. 6. Dipole states in Mathieu lattices of various ellipticity (a) $q = 0$, (b) $q = 10$, and (c) $q = 15$. Intensity and phase distributions are presented after 10-cm propagation. (d) Normalized z component of the angular momentum along the propagation distance. Other parameters are as in Fig. 2.

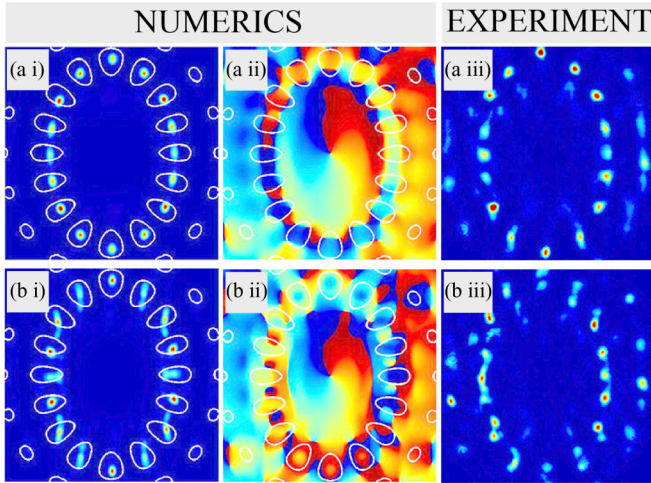


FIG. 7. Nonlinear vortex propagation in Mathieu lattices. The first and third columns present intensity distributions, and the second column presents the corresponding phase distributions at the exit face of crystal. Input vortex intensities in numerics are (a i) 0.01 arb. units and (b i) 0.1 arb. units, and input vortex power in experiment are (a iii) 20 μ W and (b iii) 30 μ W. The other parameters are as in Fig. 2(c).

IV. ELLIPTICAL NECKLACE INSTABILITIES

Finally, we discuss in detail the (in)stability of elliptical necklaces. We demonstrated in Sec. III that these vortex states observed in linear and very low nonlinear regimes (Fig. 2) are stable during propagation in our nonlinear photorefractive crystal. We also further investigate their stability for longer propagation distances numerically, in order to address length scales that are not accessible in the experiment. While the elliptical necklaces remain stable for propagation length a few times longer than our crystal size, after 10 cm they transform to oscillating dipole states (Fig. 6). Their phase distributions remain unchanged in the center, but along the inner lattice ring their initial phase distribution for stable states is broken. Higher-order vortex states, observed in the form of slightly asymmetric necklaces [Figs. 3(b)–3(d)] with lower powers, are stable only for short propagation distances (crystal size).

Also, we investigate the orbital AM of necklace beams during propagation [31,32]. The standard definition for the (normalized) z component of the orbital AM is adopted [32]:

$$L_z = -\frac{i}{2} \iint dx dy A^*(x,y)(x\partial_y - y\partial_x)A(x,y) + c.c. \quad (4)$$

Figure 6(d) presents the mean orbital AM L_z per transverse plane dependent on the propagation distance z of the necklace states along the propagation distance for different ellipticity parameters q . Less pronounced AM transfer is observed for higher lattice ellipticity. For lower ellipticities, the neighboring lobes exchange more power during the propagation and the transfer of angular momentum from the vortex to the photonic lattice is more pronounced (red plot).

Increasing the input vortex power, we investigate the stability of vortex states. The most illustrative cases are presented in Fig. 7 for vortex states with $C_T = 1$ and lattice ellipticity $q = 15$. With lower powers, neighboring lobes exchange some power, the stable elliptical necklace is broken, and regular oscillations along the propagation take place [Fig. 7(a)]. When increasing the beam power, irregular oscillations take place which are more pronounced for longer propagation distances [Fig. 7(b)]. With higher beam powers, phase distributions stay unchanged only in the central part and are broken along the inner lattice ring.

V. CONCLUSION

In summary, we have demonstrated experimental and numerical investigations of the elliptical necklace in a photorefractive medium with optically induced Mathieu lattices. We have analyzed how various orders of Mathieu lattices and their ellipticities could control the shape and the size of the elliptical necklace, as well as the number of pearls in them. Phase singularity separations were investigated for higher-order vortices. We have observed that such separations increase with C_T , higher lattice ellipticities, and the propagation distance. The stability of elliptical necklaces was studied as well as their AM. Stable vortex states were observed for lower beam powers and shorter distances, but oscillatory dipole states or dynamical instabilities were observed for longer propagation distances, higher beam power, and higher-order vortices. Our results enable further investigations of vortex beam control in photonic lattices optically induced by other than Mathieu beams and could find applications in the field of optical micromanipulation to guide, trap, and sort objects.

ACKNOWLEDGMENTS

This work was supported by the German Academic Exchange Service (Project No. 57219089), the Ministry of Education, Science and Technological Development, Republic of Serbia (Project No. OI 171036), and the Qatar National Research Fund (Grant No. NPRP 7-665-1-125).

[1] L. M. Pismen, *Vortices in Nonlinear Fields* (Clarendon, Oxford, 1999).
 [2] A. Desyatnikov, Y. Kivshar, and L. Torner, in *Progress in Optics*, edited by E. Wolf (Elsevier, Amsterdam, 2005), Vol. 47, pp. 291–391.
 [3] J. Wang, *Photon. Res.* **4**, B14 (2016).
 [4] A. E. Willner, L. L. Guodong Xie, Y. Ren, H. Huang, Y. Yue, N. Ahmed, M. J. Willner, A. J. Willner, Y. Yan, Z. Zhao, Z. Wang, C. Liu, M. Tur, and S. Ashrafi, *Photon. Res.* **4**, B5 (2016).
 [5] M. J. Padgett and R. Bowman, *Nat. Photonics* **5**, 343 (2011).

[6] K. Dholakia and T. Čižmár, *Nat. Photonics* **5**, 335 (2011).
 [7] L. Paterson, M. P. MacDonald, J. Arlt, W. Sibbett, P. E. Bryant, and K. Dholakia, *Science* **292**, 912 (2001).
 [8] S. Bernet, A. Jesacher, S. Fürhapter, C. Maurer, and M. Ritsch-Marte, *Opt. Express* **14**, 3792 (2006).
 [9] A. Mair, A. Vaziri, G. Weihs, and A. Zeilinger, *Nature (London)* **412**, 313 (2001).
 [10] J. Leach, B. Jack, J. Romero, A. K. Jha, A. M. Yao, S. Franke-Arnold, D. G. Ireland, R. W. Boyd, S. M. Barnett, and M. J. Padgett, *Science* **329**, 662 (2010).

- [11] H. S. Eisenberg, Y. Silberberg, R. Morandotti, A. R. Boyd, and J. S. Aitchison, *Phys. Rev. Lett.* **81**, 3383 (1998).
- [12] D. Mandelik, H. S. Eisenberg, Y. Silberberg, R. Morandotti, and J. S. Aitchison, *Phys. Rev. Lett.* **90**, 053902 (2003).
- [13] T. Pertsch, T. Zentgraf, U. Peschel, A. Brauer, and F. Lederer, *Phys. Rev. Lett.* **88**, 093901 (2002).
- [14] K. A. Brzdakiewicz, M. A. Karpierz, A. Fratolocchi, G. Assanto, and E. Nowinowski-Kruszelnicki, *Opto-Electron. Rev.* **13**, 107 (2005).
- [15] F. Chen, M. Stepic, C. E. Rüter, D. Runde, D. Kip, V. Shandarov, O. Manela, and M. Segev, *Opt. Express* **13**, 4314 (2005).
- [16] H. Trompeter, T. Pertsch, F. Lederer, D. Michaelis, U. Streppel, A. Brauer, and U. Peschel, *Phys. Rev. Lett.* **96**, 023901 (2006).
- [17] A. Szameit, D. Blomer, J. Burghoff, T. Schreiber, T. Pertsch, S. Nolte, and A. Tunnerman, *Opt. Express* **13**, 10552 (2005).
- [18] P. Rose, M. Boguslawski, and C. Denz, *New J. Phys.* **14**, 033018 (2012).
- [19] D. N. Christodoulides, F. Lederer, and Y. Silberberg, *Nature (London)* **424**, 817 (2003).
- [20] J. W. Fleischer, M. Segev, N. K. Efremidis, and D. N. Christodoulides, *Nature (London)* **422**, 147 (2003).
- [21] P. Zhang, Y. Hu, T. Li, D. Cannan, X. Yin, R. Morandotti, Z. Chen, and X. Zhang, *Phys. Rev. Lett.* **109**, 193901 (2012).
- [22] E. G. Kalnins and W. Miller, *J. Math. Phys.* **17**, 331 (1976).
- [23] J. Durnin, J. J. Miceli, and J. H. Eberly, *Phys. Rev. Lett.* **58**, 1499 (1987).
- [24] J. C. Gutiérrez-Vega, M. D. Iturbe-Castillo, and S. Chávez-Cerda, *Opt. Lett.* **25**, 1493 (2000).
- [25] M. A. Bandres, J. C. Gutiérrez-Vega, and S. Chávez-Cerda, *Opt. Lett.* **29**, 44 (2004).
- [26] J. A. Davis, D. M. Cottrell, J. Campos, M. J. Yzuel, and I. Moreno, *Appl. Opt.* **38**, 5004 (1999).
- [27] G. Agrawal, *Nonlinear Fiber Optics* (Academic, New York, 2012).
- [28] V. P. Lukin, P. A. Konyaev, and V. A. Sennikov, *Appl. Opt.* **51**, C84 (2012).
- [29] A. A. Zozulya and D. Z. Anderson, *Phys. Rev. A* **51**, 1520 (1995).
- [30] F. Ye, D. Mihalache, and B. Hu, *Phys. Rev. A* **79**, 053852 (2009).
- [31] Z. Chen, H. Martin, A. Bezryadina, D. Neshev, Y. S. Kivshar, and D. N. Christodoulides, *J. Opt. Soc. Am. B* **22**, 1395 (2005).
- [32] M. S. Petrović, D. M. Jović, M. R. Belić, and S. Prvanović, *Phys. Rev. A* **76**, 023820 (2007).

Creating aperiodic photonic structures by synthesized Mathieu-Gauss beams

Jadranka M. Vasiljević,¹ Alessandro Zannotti,² Dejan V. Timotijević,^{1,3} Cornelia Denz,² and Dragana M. Jović Savić¹

¹*Institute of Physics, University of Belgrade, P.O. Box 68, 11001 Belgrade, Serbia*

²*Institut für Angewandte Physik and Center for Nonlinear Science (CeNoS),
Westfälische Wilhelms-Universität Münster, 48149 Münster, Germany*

³*Science Program, Texas A&M University at Qatar, P.O. Box 23874 Doha, Qatar*

(Received 16 May 2017; published 17 August 2017)

We demonstrate a kind of aperiodic photonic structure realized using the interference of multiple Mathieu-Gauss beams. Depending on the beam configurations, their mutual distances, angles of rotation, or phase relations we are able to observe different classes of such aperiodic optically induced refractive index structures. Our experimental approach is based on the optical induction in a single parallel writing process.

DOI: [10.1103/PhysRevA.96.023840](https://doi.org/10.1103/PhysRevA.96.023840)

I. INTRODUCTION

Since nondiffracting beams have been introduced in the late 1980s [1,2] as light structures, only recently these structures have drawn considerable attention in various topics such as trapping of colloidal and *in vivo* particles in biophysics [3], atom optics [4], applications of optical lattices in quantum computing [5], as well as quantum optics [6], optical tweezing [7,8], and nonlinear optics [9–11]. Such nondiffracting structures are coming from the well-known classes of simple nondiffracting light beams that are exact solutions of the Helmholtz equation in different coordinate systems [12]: plane waves in Cartesian, Bessel beams in circular cylindrical [2], Mathieu beams in elliptic cylindrical [13], and parabolic beams in parabolic cylindrical coordinates [14].

A simple and robust implementation of optical micro-manipulation technologies—optical tweezers—based on nondiffracting beams, has become a standard tool in biological, medical, and physics research laboratories [15]. Another trend in optical manipulation is the use of synthesized optical beams rather than single beams only; such beams enable a much greater freedom in object manipulation than conventional Gaussian beams [16].

The potential of nondiffracting structures is of significant importance for advances in discrete and nonlinear modern photonics [17–21]. Although the physics of periodic photonic systems are of fundamental importance, deviations from periodicity are of importance as they may result in higher complexity. One such deviation in optics results in the realization of photonic quasicrystals [20,22], the structures that lie between periodic and disordered one. They show sharp diffraction patterns that confirm the existence of wave interference resulting from their long-range order. Recently, a new serial approach for the generation of aperiodic deterministic Fibonacci and Vogel spirals as refractive index structures was presented [23,24]. In particular, the Fourier spectra of tailored aperiodic lattices can be customized to range from discrete to continuous [25], thus featuring unique light propagation as well as localization properties in aperiodic photonic lattices. Of particular interest are also flat-band lattices with a dispersionless energy band composed of entirely degenerate states, so that any excitation of these states yields nondiffracting waves. Such flat band systems have been studied in a number of lattice models including quasi-one-

two-, or three-dimensional settings, diamond ladder, Lieb, or kagome lattices [26–28].

In this paper, we demonstrate a powerful approach for the creation of two-dimensional (2D) aperiodic photonic lattices in a single writing process in parallel. It is based on synthesizing two or more nondiffracting Mathieu-Gauss (MG) beams [29]. By coherently superimposing MG beams with different orders, positions, and relative phases we realize transverse invariant propagating intensity distributions capable of optically inducing corresponding refractive index lattices in photosensitive media. Our approach features the fabrication of versatile aperiodic lattices with controllable properties as well as quasi-one-dimensional structures.

II. CHARACTERIZATION OF SYNTHESIZED MATHIEU-GAUSS BEAMS

For the experimental realization of synthesized MG beams we use the experimental setup shown in Fig. 1. We use a frequency-doubled Nd:YVO₄ laser, expand the laser beam, and illuminate as a plane wave a phase-only spatial light modulator “Holoeye Pluto VIS.” The reflected light field is modulated in both amplitude and phase. This is possible by addressing a precalculated hologram to the SLM containing the information of the complex light field encoded with an additional blazed grating. By applying an appropriate Fourier filter, the tailored complex light field is realized [30,31]. Additionally, the telescope L1-L2 scales down the SLM size by a factor of 10. This extraordinary polarized “structure beam” is used to optically inscribe refractive index modulations in the 15 mm long photorefractive SBN:Ce crystal which is externally biased with an electric dc field of $E_{\text{ext}} = 2000 \text{ V cm}^{-1}$ aligned along the optical $c = x$ axis, perpendicular to the direction of propagation (z axis).

We simulate the nonlinear light propagation in a photonic structure by numerically solving the nonlinear Schrödinger equation:

$$i \partial_z A(\mathbf{r}) + \frac{1}{2} \Delta_{\perp} A(\mathbf{r}) + \frac{1}{2} \Gamma E(|A(\mathbf{r})|^2) A(\mathbf{r}) = 0, \quad (1)$$

where $\Gamma = k_0^2 w_0^2 n_o^4 r_{13,33}$, $k_0 = 2\pi/\lambda$ is the wave number and defined by the wavelength $\lambda = 532 \text{ nm}$, $n_o = 2.325$ is the ordinary, $n_e = 2.358$ is the extraordinary bulk refractive index, $r_{13} = 47 \text{ pm/V}$, $r_{33} = 237 \text{ pm/V}$ are the corresponding

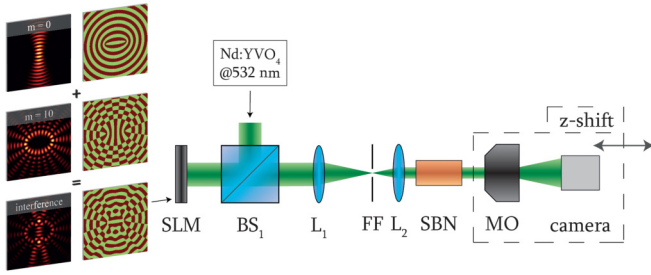


FIG. 1. Experimental setup for the investigation of synthesized MG beams and their optical induction in a photorefractive SBN crystal. BS: beam splitter; FF: Fourier filter; L: lens; MO: microscope objective; SLM: spatial light modulator. Depicted on the left side is a scheme that shows how two single MG beams interfere to create more complex light fields, addressed to the SLM.

electro-optic coefficients, respectively, and w_0 is an arbitrary scaling factor. The electric field $E = E_{\text{ext}} + E_{\text{sc}}$ that builds up inside the SBN crystal is a superposition of an external electric field E_{ext} and an internal space charge field E_{sc} that results due to the incident intensity distribution $I(\mathbf{r}) = |A(\mathbf{r})|^2$. Owing to the biased SBN crystal, we use an anisotropic approximation to calculate the refractive index modulation [32] and solve the potential equation:

$$\Delta\phi_{\text{sc}} + \nabla\phi_{\text{sc}}\nabla \ln(1 + I) = E_{\text{ext}}\partial_x \ln(1 + I), \quad (2)$$

where $E_{\text{sc}} = \partial_x\phi_{\text{sc}}$.

The complex aperiodic beams in this work are based on even Mathieu beams $A_m(\xi, \eta)$ [13], mathematically described as a product of radial c_{em} and angular J_{em} Mathieu function of order m :

$$A_m(\xi, \eta) = C_m(q)J_{\text{em}}(\xi; q)c_{\text{em}}(\eta; q), \quad (3)$$

where $C_m(q)$ is a weighting constant that depends on $q = f^2k_t^2/4$, a parameter of ellipticity which is related to the positions f of the two foci and the transverse wave number $k_t = 2\pi/a$, where a is the characteristic structure size. ξ and η are elliptical coordinates and their relation with spatial coordinates x, y are given with $x + iy = f \cosh(\xi + i\eta)$. Here we use $q = 25$ and $a = 25 \mu\text{m}$. Additionally, the Mathieu beams are apodized with Gaussian beams which yields MG beams [29].

We start our investigations by considering the interference of two even MG beams of different order m_1 and m_2 (Fig. 2), and present their intensity distributions at the input crystal face. For MG beams whose orders have the same parity (even or odd), symmetric synthesized MG structures are observed that propagate unchanged as nondiffracting beams due to identical structure sizes of the individual beams. The intensity distributions are presented for two examples in experiment as well as in numerical simulations in Figs. 2(a) and 2(b). We demonstrate that the superposition of two MG beams of different parity leads to asymmetric intensity distributions [Figs. 2(c) and 2(d)]. In the case of the π out of phase interference, mirror symmetric structures are observed (not shown here). For interfering MG beams of different orders and different parities it is possible to observe symmetric structures only for phase differences of $\pi/2$ that are comparable to synthesized mirror symmetric structures.

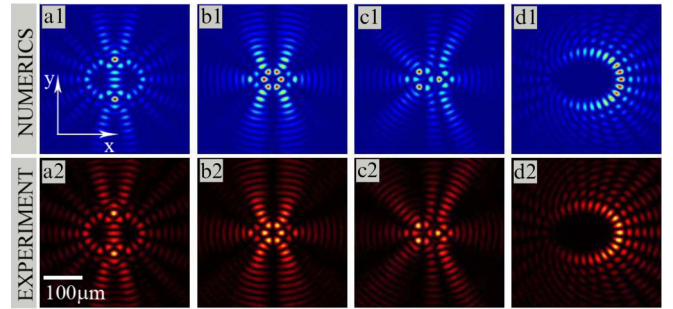


FIG. 2. Interference of two MG beams of different order. Intensity distributions of interfering beams with the same parity: (a) both even: $m_1 = 0, m_2 = 10$; (b) both odd: $m_1 = 1, m_2 = 7$. Intensity distributions of interfering beams with different parity: (c) $m_1 = 2, m_2 = 7$; (d) $m_1 = 13, m_2 = 14$.

Next, we superimpose two even MG beams with the same order, oriented at 90° with respect to each other, considering additionally the in phase and π out of phase configurations. Superimposing MG beams of even parity, we observe distinctive structures for the two different phase configurations [Figs. 3(a), 3(e) and 3(b), 3(f)]. However, using MG beams of odd parity ($m = 5$ or $m = 7$), the same intensity distributions are observed, but mirror symmetric to each other, when changing the phase configurations [Figs. 3(c), 3(g) and 3(d), 3(h)]. This mirror symmetry of superimposed MG beams with odd orders m is related to the intrinsic symmetry of the related Mathieu functions.

Our approach to realize two-dimensional aperiodic lattices finds its origin in synthesizing versatile standard MG beams at different mutual distances. This allows one to continuously increase the degree of aperiodicity. We provide a field

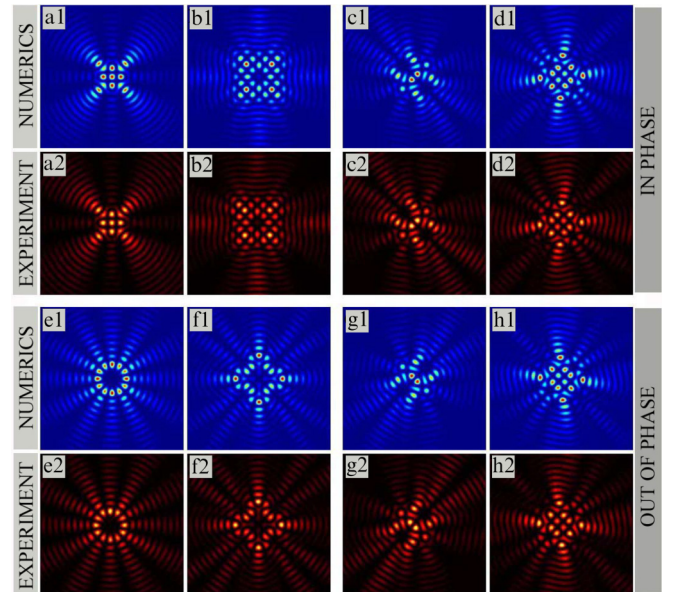


FIG. 3. Transverse interference patterns of two Mathieu-Gauss beams of the same order oriented at 90° with respect to each other: (a),(e) $m_1 = m_2 = 2$, (b),(f) $m_1 = m_2 = 8$ and (c),(g) $m_1 = m_2 = 5$, (d),(h) $m_1 = m_2 = 7$.

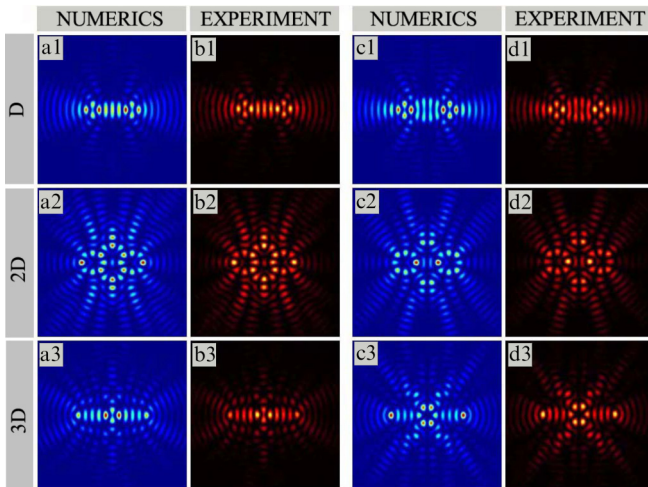


FIG. 4. Interfering MG beams of the same order at different vertical mutual distances: (a),(b) $m = 6$ and (c),(d) $m = 7$. $D = 20 \mu\text{m}$.

distribution that serves as “unit cell” for more complex aperiodic writing light capable of being transferred to tailored refractive index modulations in photosensitive media. A first example that demonstrates the concept (Fig. 4) shows the interference of two even MG beams of the same order. Therefore, we chose MG beams of the order $m = 6$ or $m = 7$ and arrange them at various mutual distances as shown in Figs. 4(a), 4(b) and 4(c), 4(d), respectively. For the following synthesization, we identify the intensity distribution that results for the displacement of $2D = 40 \mu\text{m}$ as most suited.

III. GENERATION OF COMPLEX APERIODIC PHOTONIC STRUCTURES

In order to find conditions for the generation of complex aperiodic photonic structures, we use previously observed synthesized MG beams that provide a unit cell of the photonic lattice. First, we use the example from Fig. 2(b) that has similarities with the unit cell of a periodic lattice created by the interference of six plane waves. By multiplying this structure twice in one row at a distance of $D_x = 80 \mu\text{m}$, we observe a single array [Fig. 5(a)]. Subsequently we multiply the resulting array along the y direction at three different mutual distances $D_y = 80 \mu\text{m}$, $D_y = 88 \mu\text{m}$, and $D_y = 96 \mu\text{m}$. This leads to various aperiodic lattice structures shown in Figs. 5(b)–5(d) that exhibit areas where the initial unit cell is preserving its shape, while additionally novel unit cells emerge whose shape depends on the mutual distances between the multiplied arrays.

Next, configurations are investigated that result from the duplication of the necklace structure from Fig. 3(e). Again, we start with multiplying the structure in one row at different distances. One example is presented in Fig. 5(e) for $D_x = 144 \mu\text{m}$. With such an array, we realize different in two dimensions extended aperiodic structures by changing the mutual distances between the arrays this time additionally in y direction: $D_y = 120 \mu\text{m}$, $D_y = 144 \mu\text{m}$, and $D_y = 152 \mu\text{m}$ [Figs. 5(f)–5(h)]. The initial unit cell is visible in all structures, and it repeats at proper distances, where as well other unit cell

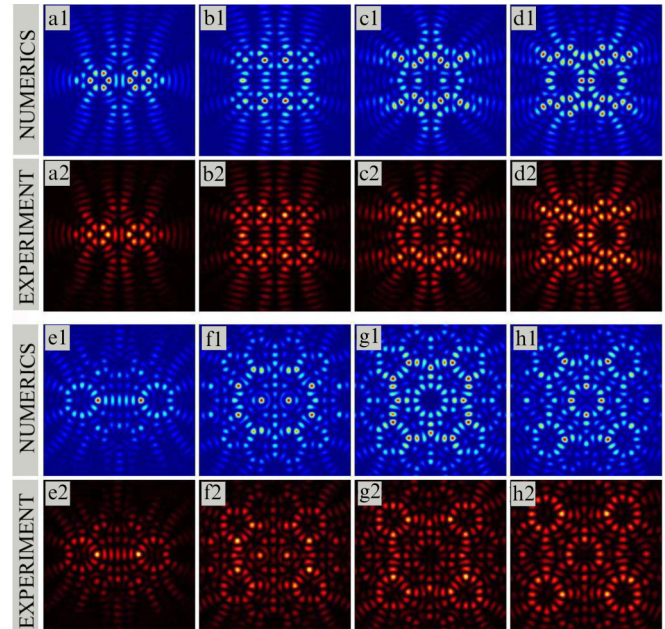


FIG. 5. Generation of aperiodic photonic structures. The first and second rows: multiplying of the structure from Fig. 2(b); the third and fourth rows: multiplying of the structure from Fig. 3(e) at different distances.

structures are visible that can be controlled by changing the distances between initial unit structures used for multiplying.

Figure 6 presents some examples of aperiodic photonic structures, observed using the synthesized MG beams of the sixth and seventh order [Figs. 4(a2) and 4(c2)], as the unit cell. For the synthesized MG beams of the sixth order

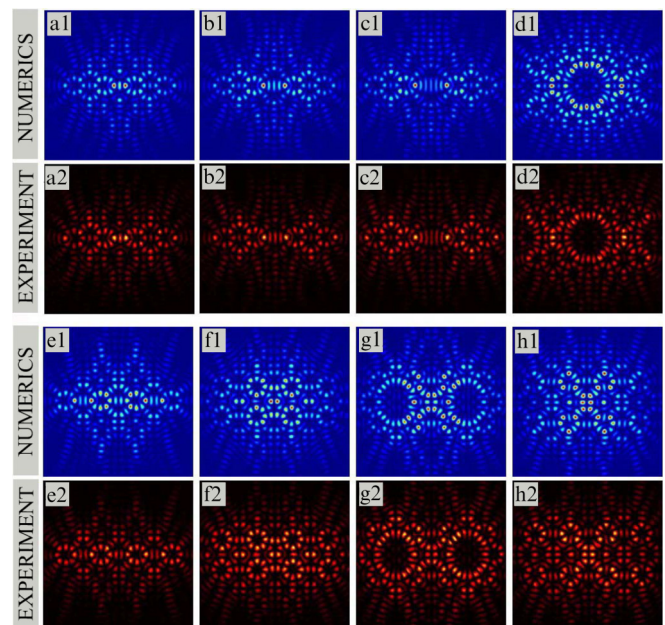


FIG. 6. Aperiodic photonic structures. The first and second row: multiplying of the structure from Fig. 4(a2); the third and fourth row: multiplying of the structure from Fig. 4(c2) at different mutual distances.

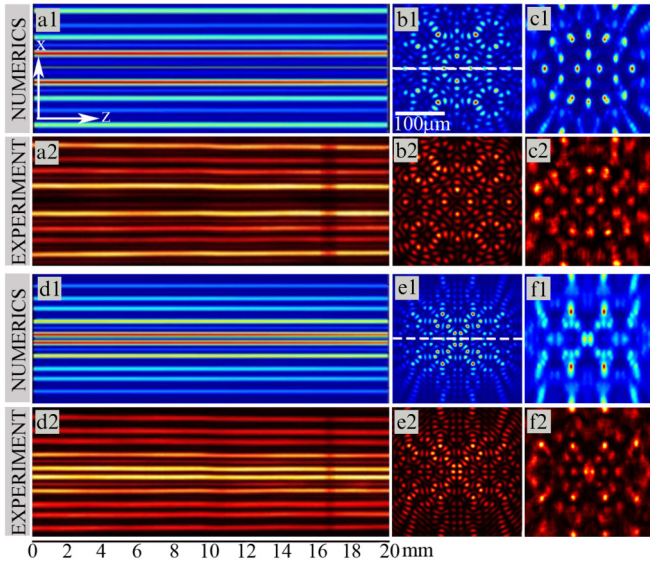


FIG. 7. Waveguiding in aperiodic photonic structures. (a),(b) Lattice beam from Fig. 5(h) and (d),(e) lattice beam from Fig. 6(h) along the longitudinal direction along the propagation, and at the back face of the crystal, respectively. (c),(f) Probe beam at the exit face of the crystal.

(the first and second row), the first three examples present the multiplying of the unit structure along x direction but at different mutual distances: $D_x = 152 \mu\text{m}$ [Fig. 6(a)], $D_x = 176 \mu\text{m}$ [Fig. 6(b)], and $D_x = 192 \mu\text{m}$ [Fig. 6(c)]. As one can see, the shape of the initial structure is preserved, with slightly different interfering patterns between them. The last example [Fig. 6(d)] presents the multiplying of the structure from Fig. 6(b) along y direction for $D_y = 104 \mu\text{m}$.

Synthesized aperiodic MG beams based on seventh order MG beams are presented in the third and fourth row. Figure 6(e) shows the multiplying of the structure from Fig. 4(c2) along the x direction for $D_x = 176 \mu\text{m}$. This structure is further used for multiplying along the y direction at various mutual distances: $D_y = 72 \mu\text{m}$, $D_y = 96 \mu\text{m}$, and $D_y = 104 \mu\text{m}$, and new kinds of aperiodic photonic structures are observed [Figs. 6(f)–6(h)].

We confirm the nondiffracting character of the synthesized MG beams, presented in Figs. 2–6, monitoring their linear propagation through the 20 mm long homogeneous crystal. We exemplarily select the two aperiodic beams demonstrated in Figs. 5(h) and 6(h), and present their linear propagation through the crystal. Figures 7(a) and 7(d) show xz cross sections through the intensity volume that prove

their nondiffracting character. In order to verify that this intensity distribution is capable of realizing aperiodic refractive index modulations, we transfer these ordinary polarized writing beams to aperiodic photonic lattices. The illumination time is 35 s with a moderate laser power of $\approx 30 \mu\text{W}$ and an external electric field of 2000 V/cm. The nonlinear self-interaction is weak and we show the lattice writing beams at the back face of the modulated SBN crystal in Figs. 7(b) and 7(e). Subsequently, we probe the optically induced aperiodic structures with an extraordinarily polarized plane wave. Figures 7(c) and 7(f) conclude these results that clearly demonstrate waveguiding of the initial plane wave in the two-dimensional aperiodic lattice, manifested in a spatially modulated intensity distribution according to the underlying refractive index modulation. Thus the intensity is preferentially guided in areas where the refractive index is increased and spots of high intensity are formed.

The presented method enables the creation of various novel kinds of two-dimensional aperiodic photonic structures in a single optical induction process in parallel. Our approach features the realization of a high versatility of aperiodic lattices that can be tailored in their degree of disorder, ranging from fundamental Mathieu lattices with a high regularity to highly disordered aperiodic structures with quasicontinuous power spectra. It is very flexible owing to the control of the mutual distance between appropriate structures that is easy to realize in experiment, especially compared to previously used optical induction methods [23,24].

IV. CONCLUSIONS

In summary, we have investigated the interference of synthesized MG beams experimentally and numerically. Depending on different configurations, the number of beams, and their mutual distance as well as phase relations, interference effects of two or more spatially displaced or rotated MG beams could be used for optical induction of novel light guiding aperiodic structures in a single parallel writing process. Our experimental results and methods enable further investigations of light propagating in such aperiodic photonic lattices, and could find applications in modern optical information processing.

ACKNOWLEDGMENTS

This work is supported by the German Academic Exchange Service (Project No. 57219089), the Ministry of Education, Science and Technological development, Republic of Serbia (Projects No. OI171036), and the Qatar National Research Fund (NPRP No. 7-665-1-125).

- [1] J. Durnin, *J. Opt. Soc. Am. A* **4**, 651 (1987).
- [2] J. Durnin, J. J. Miceli, and J. H. Eberly, *Phys. Rev. Lett.* **58**, 1499 (1987).
- [3] D. J. Carnegie, D. J. Stevenson, M. Mazilu, F. Gunn-Moore, and K. Dholakia, *Opt. Express* **16**, 10507 (2008).
- [4] D. McGloin, G. C. Spalding, H. Melville, W. Sibbett, and K. Dholakia, *Opt. Express* **11**, 158 (2003).

- [5] R. Raussendorf and H. J. Briegel, *Phys. Rev. Lett.* **86**, 5188 (2001).
- [6] I. Bloch, *Nat. Phys.* **1**, 23 (2005).
- [7] V. Garcés-Chávez, D. McGloin, H. Melville, W. Sibbett, and K. Dholakia, *Nature (London)* **419**, 145 (2002).
- [8] J. Baumgartl, M. Mazilu, and K. Dholakia, *Nat. Photon.* **2**, 675 (2008).

- [9] J. W. Fleischer, M. Segev, N. K. Efremidis, and D. N. Christodoulides, *Nature (London)* **422**, 147 (2003).
- [10] H. Martin, E. D. Eugenieva, Z. Chen, and D. N. Christodoulides, *Phys. Rev. Lett.* **92**, 123902 (2004).
- [11] F. Lederer, G. I. Stegeman, D. N. Christodoulides, G. Assanto, M. Segev, and Y. Silberberg, *Phys. Rep.* **463**, 1 (2008).
- [12] E. G. Kalnins and W. Miller, Jr., *J. Math. Phys.* **17**, 331 (1976).
- [13] J. C. Gutiérrez-Vega, M. D. Iturbe-Castillo, and S. Chávez-Cerda, *Opt. Lett.* **25**, 1493 (2000).
- [14] M. A. Bandres, J. C. Gutiérrez-Vega, and S. Chávez-Cerda, *Opt. Lett.* **29**, 44 (2004).
- [15] M. Woerdemann, C. Alpmann, M. Esseling, and C. Denz, *Laser Photon. Rev.* **7**, 839 (2013).
- [16] C. W. Qiu, D. Palima, A. Novitsky, D. Gao, W. Ding, S. V. Zhukovsky, and J. Gluckstad, *Nanophotonics* **3**, 181 (2014).
- [17] S. Chávez-Cerda, U. Ruiz, V. Arrizón, and H. M. Moya-Cessa, *Opt. Express* **19**, 16448 (2011).
- [18] N. M. Lučić, B. M. Bokić, D. Z. Grujić, D. V. Pantelić, B. M. Jelenković, A. Piper, D. M. Jović, and D. V. Timotijević, *Phys. Rev. A* **88**, 063815 (2013).
- [19] F. Diebel, B. M. Bokić, M. Boguslawski, A. Piper, D. V. Timotijević, D. M. Jović, and C. Denz, *Phys. Rev. A* **90**, 033802 (2014).
- [20] B. Freedman, G. Bartal, M. Segev, R. Lifshitz, D. N. Christodoulides, and J. W. Fleisher, *Nature (London)* **440**, 1166 (2006).
- [21] F. Diebel, B. M. Bokić, D. V. Timotijević, D. M. Jović Savić, and C. Denz, *Opt. Express* **23**, 24351 (2015).
- [22] Z. V. Vardeny, A. Nahata, and A. Agrawal, *Nat. Photon.* **7**, 177 (2013).
- [23] F. Diebel, B. P. Rose, M. Boguslawski, and C. Denz, *Appl. Phys. Lett.* **104**, 191101 (2014).
- [24] M. Boguslawski, N. M. Lučić, F. Diebel, B. D. V. Timotijević, C. Denz, and D. M. Jović Savić, *Optica* **3**, 711 (2016).
- [25] L. D. Negro and S. V. Boriskina, *Laser Photon. Rev.* **6**, 178 (2012).
- [26] D. Leykam, S. Flach, O. Bahat-Treidel, and A. S. Desyatnikov, *Phys. Rev. B* **88**, 224203 (2013).
- [27] J. D. Bodyfelt, D. Leykam, C. Danieli, X. Yu, and S. Flach, *Phys. Rev. Lett.* **113**, 236403 (2014).
- [28] P. P. Beliĉev, G. Gligorić, A. Radosavljević, A. Maluckov, M. Stepić, R. A. Vicencio, and M. Johansson, *Phys. Rev. E* **92**, 052916 (2015).
- [29] C. López-Mariscal, M. A. Bandres, and J. C. Gutiérrez-Vega, *Opt. Eng.* **45**, 068001 (2006).
- [30] J. A. Davis, D. M. Cottrell, J. Campos, M. J. Yzuel, and I. Moreno, *Appl. Opt.* **38**, 5004 (1999).
- [31] E. Otte, C. Schlickriede, C. Alpmann, and C. Denz, *Proc. SPIE* **9379**, 937908 (2015).
- [32] A. A. Zozulya and D. Z. Anderson, *Phys. Rev. A* **51**, 1520 (1995).

Light propagation in quasi-periodic Fibonacci waveguide arrays

N. M. LUČIĆ, D. M. JOVIĆ SAVIĆ,* A. PIPER, D. Ž. GRUJIĆ, J. M. VASILJEVIĆ,
D. V. PANTELIĆ, B. M. JELENKOVIĆ, AND D. V. TIMOTIJEVIĆ

Institute of Physics, University of Belgrade, P.O. Box 68, 11001 Belgrade, Serbia

*Corresponding author: jovic@ipb.ac.rs

Received 26 March 2015; revised 19 May 2015; accepted 3 June 2015; posted 5 June 2015 (Doc. ID 236998); published 26 June 2015

We investigate light propagation along one-dimensional quasi-periodic Fibonacci waveguide array optically induced in Fe:LiNbO₃ crystal. Two Fibonacci elements, A and B, are used as a separation between waveguides. We demonstrate numerically and experimentally that a beam expansion in such arrays is effectively reduced compared to the periodic ones, without changing beam expansion scaling law. The influence of refractive index variation on the beam expansion in such systems is discussed: more pronounced diffraction suppression is observed for a higher refractive index variation. © 2015 Optical Society of America

OCIS codes: (050.5298) Photonic crystals; (190.5330) Photorefractive optics.

<http://dx.doi.org/10.1364/JOSAB.32.001510>

1. INTRODUCTION

The discovery of quasi-crystals in condensed matter by Shechtman *et al.* [1] and their theoretical analysis by Levine and Steinhardt [2] has inspired a new field of research in optics and photonics.

Examples in the field of optics are photonic quasi-crystals with dielectric multilayers forming the Fibonacci sequence as proposed by Kohmoto *et al.* [3], and realized in [4–6], as well as other deterministic aperiodic structures with long-range order [7,8]. Photonic quasi-crystals have peculiar optical properties. Namely, they lie between periodic and disordered structures and exhibit unique and rich symmetries in Fourier space that are not possible within periodic lattices. The large variety of aperiodic structures is very important and could provide significant flexibility and richness when engineering the optical response of devices [9].

The localization of waves is a ubiquitous phenomenon observed in a variety of classical and quantum systems [10–12], including light waves [13–16], Bose–Einstein condensates [17,18], and sound waves [19]. Although stated more than 50 years ago [11], Anderson localization is still one of the most appealing approaches in optical wave manipulation. In this regard, a transverse localization of light in waveguide lattices turns out to be a particularly interesting concept [13,14]. As the transverse expansion properties in periodic photonic lattices [20–23], as well as in disordered ones [14,24–26], have been investigated extensively, the quasi-periodic photonic lattices emerged as a further attractive research field. The light localization in the Aubry–André model of a quasi-periodic lattice is

observed [27], but the transverse expansion in many other models of photonic quasi-crystals [28] is still an open question.

In this paper, we extend these concepts to the beam expansion in quasi-periodic Fibonacci waveguide arrays, considering light propagation along waveguides. We fabricate the array of identical waveguides (identical refractive index profile). The distance between successive waveguides is modulated in the Fibonacci manner. This means that the sequence of separations consists of two elements, A and B, lined in such a way to make a Fibonacci word. We consider how various input beam positions (incident positions) influence diffraction, and compare them with appropriate periodic waveguide arrays. In general, we find the beam expansion is slowed in quasi-periodic Fibonacci waveguide arrays. Increasing the refractive index variation, the effect is more pronounced.

2. EXPERIMENTAL SETUP AND THEORETICAL BACKGROUND

For the experimental realization of the Fibonacci waveguide array we use LiNbO₃ crystal, doped with 0.05% of iron. Dimensions of the crystal are 3 mm × 0.5 mm × 10 mm, with the optical axis along the *z* direction (10 mm). Waveguides are fabricated using an in-house developed laser writing system with a CW laser at 473 nm and a precise two-axis positioning platform. The platform can move the crystal in the *x*–*z* plane. The laser beam propagates along the *y* axis and it is focused by the 50× microscope objective slightly below the upper surface of the crystal. In this way, the laser makes a controllable local change of the refractive index. By moving the sample along the

z direction, a uniform modification of the refractive index profile is achieved [Fig. 1(a)]. The width of the waveguide obtained in this way is approximately $5\ \mu\text{m}$ with a maximum refractive index variation of $\Delta n \sim 1 \times 10^{-4}$, estimated from numerical simulations. The distances between the centers of the adjacent waveguides are $a = 10\ \mu\text{m}$ and $b = 16.18\ \mu\text{m}$, and follow the Fibonacci word rule, with the golden ratio $b/a = (1 + \sqrt{5})/2$ in our case [Fig. 1(c)].

A scheme of the experimental setup is shown in Fig. 1(b). A beam from He:Ne laser, after appropriate preparation, is focused on the front face of the crystal and propagates along the z direction. The beam waist is around $10.5\ \mu\text{m}$ and the power is $10\ \text{nW}$. The light is polarized linearly in the y direction. The crystal is situated in a holder which can be moved in the x direction in small steps. In this way, we can launch the beam into appropriate position in the waveguide array. The intensity pattern appearing at the exit face of the crystal is observed by means of an imaging system which consists of a microscope objective and CCD camera.

To theoretically model light propagation in quasi-periodic Fibonacci waveguide arrays, along the propagation distance z , we consider the paraxial wave equation for the slowly varying electric field amplitude E :

$$i \frac{\partial E}{\partial z} = -\frac{1}{2} \frac{\partial^2 E}{\partial x^2} - V(x)E, \quad (1)$$

where $V(x) = n_s + \Delta n \sum_{i=1}^N e^{-(x-x_i)^2/2\sigma^2}$ is the quasi-periodic refractive index profile of the array, n_s is a bulk material refractive index, and Δn is an optically induced refractive index variation. The two Fibonacci elements, A and B, are used as a separation between the waveguides a and b [see Fig. 1(c)]. An array of N waveguides modeled with Gaussian functions centered at x_i is spaced to follow some Fibonacci word. For example, we experimentally realized a waveguide array that represents the following Fibonacci word: ABAABABAABAABAABA (the first 20 elements) [see

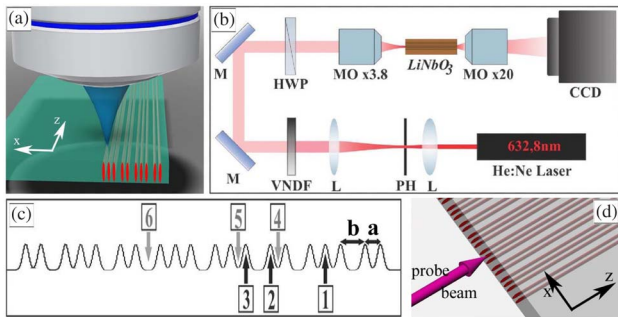


Fig. 1. Setup for an investigation of light propagation in Fibonacci waveguide arrays. (a) Scheme of the laser writing waveguide arrays process in an Fe:LiNbO₃ crystal. (b) Schematic of the experimental setup: He:Ne laser at 632.8 nm; L, lens; PH, pinhole; VNDF, variable neutral density filter; M, mirror; HWP, half-wave plate; MO, microscope objective; CCD, camera. (c) A schematic of a refractive index profile used in numerics ($V(x)$), with two separations between waveguides, a and b . Arrows with numbers show incident beam positions inside waveguides (black) and between waveguides (gray). (d) Schematic geometry of Fibonacci lattice with Gaussian probe beam.

Fig. 1(c)]. For solving our model equation, we use the split-step method with the parameters of our experiment.

3. LIGHT PROPAGATION IN FIBONACCI WAVEGUIDE ARRAYS: EXPERIMENT VERSUS THEORY

We consider beam propagating in Fibonacci waveguide arrays fabricated in our crystal, launched at different incident positions. The propagation characteristics are obtained numerically and experimentally; Fig. 2 summarizes our results. We choose three typical incident positions *inside* waveguides marked by numbers 1, 2, and 3 in Fig. 1(c). Propagations from these positions are represented in the first, second, and third row in Fig. 2. The first column presents intensity distribution along the propagation distance observed numerically, with output profiles in the second column. Experimental results for the same incident positions are presented as intensity distributions at the exit face of the crystal (the forth column) with corresponding profiles in the third column. One can see a very good agreement with numerically obtained profiles.

The main reason for more pronounced diffraction suppression for incident beam positions 1 and 2 [Figs. 2(b) and 2(f)], in comparison with position 3 [Fig. 2(j)], is the separation between incident and neighboring waveguides. While propagating in the medium, the beam displays slowing of beam expansion, compared to the appropriate periodic waveguide arrays [Fig. 4(b)].

Next, we study beam propagating characteristics for incident positions *between* waveguides marked by numbers 4, 5, and 6 in Fig. 1(c). Figure 3 summarizes our numerical and experimental results for these cases. The layout of this figure is the same as in Fig. 2: incident positions 4, 5, and 6 in Fig. 1(c) correspond to the results in the first, second, and third row in Fig. 3, respectively. Beam diffraction for incident positions

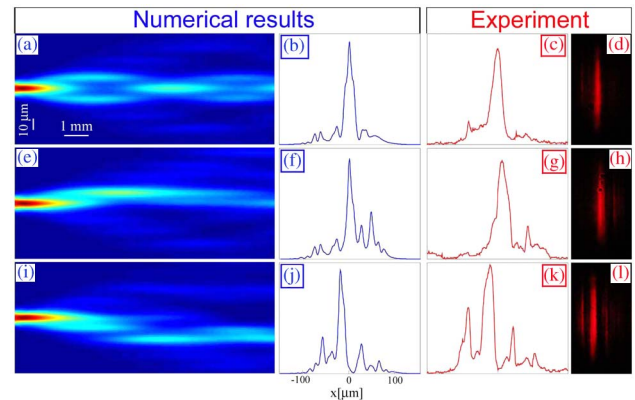


Fig. 2. Light propagation in Fibonacci waveguide arrays. Incident positions of the beam are *inside* certain waveguides, marked with numbers in Fig. 1(c): the first row corresponds to the position 1; the second row corresponds to 2; and the third row corresponds to 3. Intensity distributions of the beam in longitudinal direction during the propagation: (a), (e), and (i) observed numerically. Corresponding intensity profiles at the exit face of the crystal observed numerically: (b), (f), and (j) and experimentally (c), (g), and (k). Experimentally measured intensity distributions at the exit face of the crystal (d), (h), and (l). Physical parameters: the crystal length $L = 1\ \text{cm}$, refractive index variation $\Delta n = 1 \times 10^{-4}$, and Gaussian beam width $10\ \mu\text{m}$.

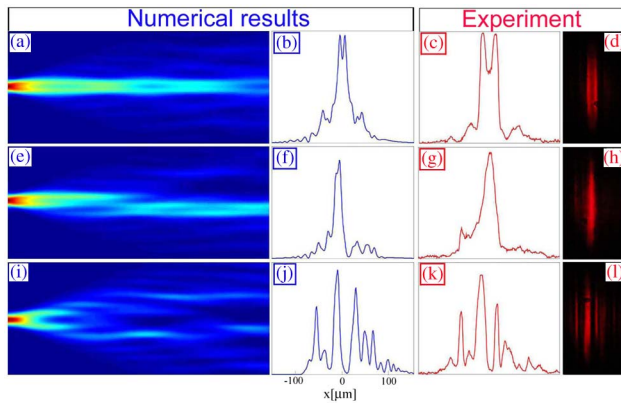


Fig. 3. Light propagation in Fibonacci waveguide arrays with incident positions of the beam *between* certain waveguides, marked with numbers in Fig. 1(c): position 4 corresponds to the first row, 5 to the second row, and 6 to the third row. Intensity distributions of the beam in longitudinal direction during the propagation: (a), (e), and (i) observed numerically. Corresponding intensity profiles at the exit face of the crystal observed numerically (b), (f), and (j) and experimentally (c), (g), and (k). Experimentally measured intensity distributions at the exit face of the crystal (d), (h), and (l). Physical parameters are as in Fig. 2.

between waveguides is more pronounced than for incident positions *inside* waveguides (Fig. 2), but again less pronounced than in periodic waveguide arrays [Fig. 4(b)]. One can see a more pronounced tendency toward diffraction suppression for incident beam position 5 [Fig. 3(g)], compared with 4 [Fig. 3(c)] and 6 [Fig. 3(k)]. We want to stress that these conclusions are relevant only for the distance of propagation in our experiment (1 cm). More general conclusions are drawn in the next chapter, where numerical simulations are performed on longer propagation distances.

4. LIGHT PROPAGATION IN WAVEGUIDE ARRAYS: PERIODIC VERSUS FIBONACCI

We study numerically the beam propagation in Fibonacci waveguide arrays considering longer propagation distances ($L = 10$ cm). To characterize the level of beam expansion, we use the effective beam width $\omega_{\text{eff}} = P^{-1/2}$, where $P = \int |E|^4(x, L) dx / \{ \int |E|^2(x, L) dx \}^2$ is the inverse participation ratio. In such a system, it is useful to perform averaging over different incident beam positions to remove the effects of the local environment, i.e., the influence of the neighboring waveguides. Averaged effective beam width is calculated along the propagation distance, and compared for the Fibonacci waveguide array and three different periodic waveguide arrays. Separations a and b in Fibonacci waveguide arrays are used as periods $d = 16.18 \mu\text{m}$ and $d = 10 \mu\text{m}$ for two periodic waveguide arrays. The third periodic array is produced in such a way that the same number of waveguides as in quasi-periodic is arranged in periodic manner in the same space (in our geometry, its lattice period is $d = 12.38 \mu\text{m}$), aimed as the most appropriate for comparison with Fibonacci waveguide array.

Figure 4(a) presents the averaged effective width (averaged over incident positions) along the propagation distance for Fibonacci lattice and refractive index variation $\Delta n = 1 \times 10^{-4}$,

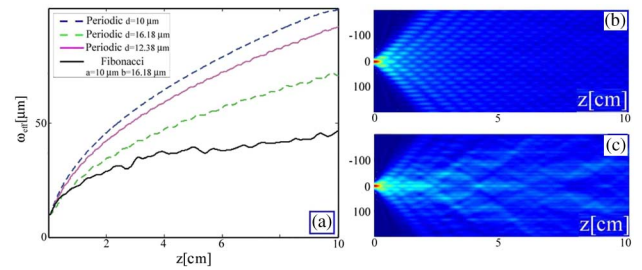


Fig. 4. Comparison between beam diffraction in periodic and quasi-periodic waveguide arrays. (a) Averaged effective beam widths versus the propagation distance, for refractive index variation $\Delta n = 1 \times 10^{-4}$. (b) Field intensity of the beam in longitudinal direction (z) during the propagation for periodic lattice with $d = 12.38 \mu\text{m}$. (c) Averaged field intensity distribution for Fibonacci lattice. Crystal length is $L = 10$ cm.

with the effective beam width for all previously mentioned periodic lattices for the same value of refractive index variation. It should be stressed that the beam width increases more slowly in a Fibonacci lattice compared to the periodic lattices. Clearly, the beam propagation in periodic lattice with $d = 10 \mu\text{m}$ displays the strongest discrete diffraction, followed by other periodic lattices and then quasi-periodic. We also observe that the Fibonacci lattice follows the same beam expansion scaling law [29]. For shorter propagation distances (up to 1.5 cm), beam diffraction in the periodic lattice with $d = 16.18 \mu\text{m}$ is slightly less pronounced than in quasi-periodic because of the weaker coupling between adjacent waveguides in that lattice.

Figure 4(b) presents a typical beam spreading along the propagation distance, for a periodic lattice with $d = 12.38 \mu\text{m}$, simulated for 10 cm of propagation. The averaged intensity distribution for hundreds of different incident positions in a Fibonacci lattice is presented in Fig. 4(c). Compared with the appropriate periodic lattice [Fig. 4(b)], a tendency of Fibonacci lattice to suppress diffraction is evident [Fig. 4(c)].

5. DEPENDENCE OF LIGHT PROPAGATION ON THE REFRACTIVE INDEX VARIATION

At the end, we study the influence of various refractive index variations (Δn) on the beam propagation in Fibonacci waveguide arrays. Again, we calculate the averaged effective width along the propagation distance for each value of Δn . The increase of refractive index variation makes diffraction suppression more pronounced [Fig. 5(a)]: the broadening of the beam becomes almost completely suppressed for longer propagation distances. These curves show a transition from ballistic spreading (normal diffusion) to anomalous diffusion. In addition, a higher refractive index variation changes the anomalous diffusion behavior. The averaged intensity distribution, for hundreds of different incident positions, is presented for $\Delta n = 2 \times 10^{-4}$ in Fig. 5(b), and $\Delta n = 4 \times 10^{-4}$ in Fig. 5(c). These should be compared with the corresponding distribution in Fig. 4(c) for $\Delta n = 1 \times 10^{-4}$. The tendency to suppress diffraction is evident as for a higher refractive index variation; a larger portion of the beam is confined between adjacent waveguides.

Typical averaged intensity distribution profiles in longitudinal direction for propagation lengths of 2, 3, and 4 cm are presented

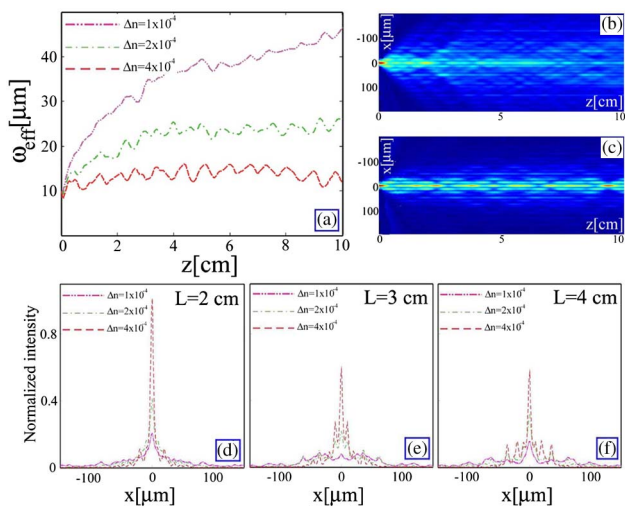


Fig. 5. Light propagation in Fibonacci lattice for a higher refractive index variation. (a) Comparison between propagation in waveguide arrays with different refractive index variation: averaged effective beam widths versus the propagation distance. Averaged field intensity distributions for (b) $\Delta n = 2 \times 10^{-4}$ and (c) $\Delta n = 4 \times 10^{-4}$. Intensity distribution profiles for the same values of Δn at different propagation distances: (d) 2 cm, (e) 3 cm, and (f) 4 cm.

for three values of refractive index variation: $\Delta n = 1 \times 10^{-4}$, $\Delta n = 2 \times 10^{-4}$, and $\Delta n = 4 \times 10^{-4}$ [Figs. 5(d)–5(f)]. Again, one can see a transition toward stronger diffraction suppression with a higher refractive index variation.

6. CONCLUSIONS

In summary, we have observed the beam expansion is slowed down in optically induced Fibonacci waveguide arrays. We have analyzed experimentally and numerically how various incident positions influence propagation characteristics. The experimental results fully agree with the theoretical analysis. Diffraction suppression is observed with Fibonacci waveguide arrays, compared to the appropriate periodic waveguide arrays. We have investigated the influence of refractive index variation on the beam spreading in Fibonacci waveguide arrays. More pronounced diffraction suppression is observed for higher refractive index variations.

Funding. Ministry of Education, Science and Technological Development, Republic of Serbia (OI 171036, OI 171038, III 45016).

REFERENCES

1. D. Shechtman, I. Blech, D. Gratias, and J. W. Cahn, "Metallic phase with long-range orientational order and no translational symmetry," *Phys. Rev. Lett.* **53**, 1951–1953 (1984).
2. D. Levine and P. J. Steinhardt, "Quasicrystals: a new class of ordered structures," *Phys. Rev. Lett.* **53**, 2477–2480 (1984).
3. M. Kohmoto, B. Sutherland, and K. Iguchi, "Localization in optics: quasicrystalline media," *Phys. Rev. Lett.* **58**, 2436–2438 (1987).
4. G. Gumbs and M. K. Ali, "Dynamical maps, Cantor spectra, and localization for Fibonacci and related quasiperiodic lattices," *Phys. Rev. Lett.* **60**, 1081–1084 (1988).

5. W. Gellermann, M. Kohmoto, B. Sutherland, and P. C. Taylor, "Localization of light waves in Fibonacci dielectric multilayers," *Phys. Rev. Lett.* **72**, 633–636 (1994).
6. L. D. Negro, C. J. Oton, Z. Gaburro, L. Pavesi, P. Johnson, A. Lagendijk, R. Righini, M. Colocci, and D. S. Wiersma, "Light transport through the band-edge states of Fibonacci quasicrystals," *Phys. Rev. Lett.* **90**, 055501 (2003).
7. W. Steurer and D. Sutter-Widmer, "Photonic and phononic quasicrystals," *J. Phys. D* **40**, R229–R247 (2007).
8. E. L. Albuquerque and M. G. Cottam, "Theory of elementary excitations in quasiperiodic structures," *Phys. Rep.* **376**, 225–337 (2003).
9. Z. V. Vardeny, A. Nahata, and A. Agrawal, "Optics of photonic quasicrystals," *Nat. Photonics* **7**, 177–187 (2013).
10. P. Sheng, *Scattering and Localization of Classical Waves in Random Media* (World Scientific, 1990).
11. A. Lagendijk, B. Tiggelen, and D. S. Wiersma, "Fifty years of Anderson localization," *Phys. Today* **62**(8), 24–29 (2009).
12. S. S. Abdullaev and F. Kh. Abdullaev, "On the light propagation in the system of tunnel-coupled waveguides," *Sov. J. Radiofizika* **23**, 766 (1980).
13. T. Pertsch, U. Peschel, J. Kobelke, K. Schuster, H. Bartelt, S. Nolte, A. Tünnermann, and F. Lederer, "Nonlinearity and disorder in fiber arrays," *Phys. Rev. Lett.* **93**, 053901 (2004).
14. T. Schwartz, G. Bartal, S. Fishman, and M. Segev, "Transport and Anderson localization in disordered two-dimensional photonic lattices," *Nature* **446**, 52–55 (2007).
15. S. Gentilini, A. Fratalocchi, L. Angelani, G. Ruocco, and C. Conti, "Ultrashort pulse propagation and the Anderson localization," *Opt. Lett.* **34**, 130 (2009).
16. C. Conti and A. Fratalocchi, "Dynamic light diffusion, three-dimensional Anderson localization and lasing in inverted opals," *Nat. Phys.* **4**, 794–798 (2008).
17. G. Roati, C. D'Errico, L. Fallani, M. Fattori, C. Fort, M. Zaccanti, G. Modugno, M. Modugno, and M. Inguscio, "Anderson localization of a non-interacting Bose–Einstein condensate," *Nature* **453**, 895–898 (2008).
18. J. Billy, V. Josse, Z. Zuo, A. Bernard, B. Hambrecht, P. Lugan, D. Clément, L. Sanchez-Palencia, P. Bouyer, and A. Aspect, "Direct observation of Anderson localization of matter waves in a controlled disorder," *Nature* **453**, 891–894 (2008).
19. J. D. Maynard, "Acoustical analogs of condensed-matter problems," *Rev. Mod. Phys.* **73**, 401–417, (2001).
20. H. S. Eisenberg, Y. Silberberg, R. Morandotti, and J. S. Aitchison, "Diffraction management," *Phys. Rev. Lett.* **85**, 1863–1866 (2000).
21. T. Pertsch, T. Zentgraf, U. Peschel, A. Bräuer, and F. Lederer, "Anomalous refraction and diffraction in discrete optical systems," *Phys. Rev. Lett.* **88**, 093901 (2002).
22. D. N. Christodoulides, F. Lederer, and Y. Silberberg, "Discretizing light behavior in linear and nonlinear waveguide lattices," *Nature* **424**, 817–823 (2003).
23. A. Fratalocchi and G. Assanto, "Light propagation through a nonlinear defect: symmetry breaking and controlled soliton emission," *Opt. Lett.* **31**, 1489–1491 (2006).
24. D. M. Jović, Yu. S. Kivshar, C. Denz, and M. R. Belić, "Anderson localization of light near boundaries of disordered photonic lattices," *Phys. Rev. A* **83**, 033813 (2011).
25. D. M. Jović, M. R. Belić, and C. Denz, "Transverse localization of light in nonlinear photonic lattices with dimensionality crossover," *Phys. Rev. A* **84**, 043811 (2011).
26. Y. Lahini, A. Avidan, F. Pozzi, M. Sorel, R. Morandotti, D. N. Christodoulides, and Y. Silberberg, "Anderson localization and nonlinearity in one-dimensional disordered photonic lattices," *Phys. Rev. Lett.* **100**, 013906 (2008).
27. Y. Lahini, R. Pugatch, F. Pozzi, M. Sorel, R. Morandotti, N. Davidson, and Y. Silberberg, "Observation of a localization transition in quasi-periodic photonic lattices," *Phys. Rev. Lett.* **103**, 013901 (2009).
28. E. Maciá, "The role of aperiodic order in science and technology," *Rep. Prog. Phys.* **69**, 397–441 (2006).
29. S. Longhi, "Discrete diffraction and shape-invariant beams in optical waveguide arrays," *Phys. Rev. A* **79**, 033847 (2009).

Certificate of Appreciation

THIS CERTIFICATE IS PRESENTED TO

On behalf of Phronesis LLC, we wish to thank

Dr. Jadranka M. Vasiljević

Institute of Physics, University of Belgrade, Serbia

for his/her phenomenal and worthy oral presentation on
Localization of Light in Mathieu Aperiodic Photonic Lattices
at the
“Webinar on
Lasers, Optics and Photonics”
held during
October 21-22, 2020

Best Regards

iLASERS

Webinar on

LASERS, OPTICS & PHOTONICS

October 21-22, 2020



PHRONESIS LLC

5 Great Valley Pkwy, STE 235 | Malvern PA 19355, USA | Tel: +1 (302) 469-7080
E: contact@phronesisonline.com | W: <https://phronesisonline.com>



WEBINAR ON
iLASERS

Day-2 - October 22, 2020

Keynote Session

10:00-10-45

Title: Surface Morphology, Optical Properties and Exciton Relaxation Processes in Nanoassemblies Based on Semiconductor Quantum Dots and Porphyrins

Eduard Zenkevich, Belarussian National Technical University, Belarus

10:45-10:55 Eye Relaxation Break

Sesions: Quantum Mechanics | Nonlinear Lasers and Nonlinear Optics | Optical Tomography and Optical Metrology

10:55-11-25

Title: Causa Equat Effectum in Quantum Mechanics

Peter Enders, Kazakh National Pedagogical Abai University, Kazakhstan

11:25-11-55

Title: Tertiary Quantization of Quantum Electrodynamics Equations as a Method for Solving Secondary Quantized Equations

Veklenko B.A., Joint Institute for High Temperatures of the Russian Academy of Sciences, Russia

11:55-12:05 Eye Relaxation Break

12:05-12-35

Title: Localization of Light in Mathieu Aperiodic Photonic Lattices

Jadranka M. Vasiljević, Institute of Physics, University of Belgrade, Serbia

12:35-13-05

Title: Fringe Pattern Analysis Using the Fast Fourier Transform and the Morlet Wavelet Transforms

Dahi Ghareab Abdelsalam Ibrahim, National Institute of Standards, Egypt

13:05-13:35

Title: A New Class of Binary Quantum Codes Based on Self-Dual Orientable Embeddings of K_4 , $4s$

Avaz Naghipour, University College of Nabi Akram, Iran

Panel Discussions 13:35-13:50

POSTERS 13:50 ONWARDS (Each Poster for 10 Minutes)

P-01

Title: The Eigenstates of Photon Creation Operator

Huai-Yu Wang, Tsinghua University, China

P-02

Title: Properties of Quantised Space as Source of Nonlocality

Zbigniew Tarnawski, AGH University of Science and Technology, Poland

P-03

Title: Phenomenology of Ultrarelativistic Heavy Ion Collision Using Glauber Model

Sarraj Khan, J.P university, India

LASERS, OPTICS & PHOTONICS

October 21-22, 2020

Localization of Light in Mathieu Aperiodic Photonic Lattices

Jadranka M. Vasiljević

Institute of Physics, University of Belgrade, Serbia

We demonstrate a kind of aperiodic photonic structure realized using the interference of multiple Mathieu beams. Depending on the beam configurations, their mutual distances, angles of rotation, or phase relations we are able to observe different classes of such aperiodic optically induced refractive index structures. Our experimental approach is based on the optical induction in a single parallel writing process.

We study light propagation in a two-dimensional aperiodic photonic lattice realized using the interference of multiple Mathieu beams. We demonstrate experimentally and numerically that such a lattice effectively hinders linear light expansion and leads to light localization. Most promisingly, we show that such an aperiodic lattice supports the nonlinear confinement of light in the form of soliton-like propagation that is robust with respect to changes in a wide range of intensities. The additional level to control the diffraction of light is to add disorder in the aperiodic Mathieu lattice. We realized disordered Mathieu aperiodic lattices and investigate light propagation in them. We observed disorder-enhanced light transport and light localization in disordered aperiodic M.u lattices.

Biography

Dr. Jadranka Vasiljević studied the Faculty of Science at Kragujevac University, Serbia, and graduated as MS in 2014. Since then she joined the research group of Dr. Dragana Jović Savić at the Institute of Physics, University of Belgrade, Serbia. She is part of nonlinear photonics laboratory at the Institute of Physics, University of Belgrade, Serbia. She received her Ph.D. degree in 2020 at the Faculty of Physics at Belgrade University, Serbia. She has published 6 research articles in SCI(E) journals.



Photonics Europe

2018

TECHNICAL PROGRAMME

EXHIBITION GUIDE

Conferences and Courses

22-26 April 2018

Exhibition

24-25 April 2018

Strasbourg Convention & Exhibition Centre
Strasbourg, France

www.spie.org/pe

- Studies on coupling between guided modes and tamm states in one-dimensional photonic crystals**, Sudha Maria Lis S., Shivakiran N. B. Bhaktha, Pratyusha Das, Sakshi Sharma, Indian Institute of Technology Kharagpur (India) [10672-124]
- Enhanced graphene nonlinear response through geometrical plasmon focusing**, José Ramón Martínez Saavedra, ICFO - Institut de Ciències Fotòniques (Spain); F. Javier Garcia de Abajo, ICFO - Institut de Ciències Fotòniques (Spain) and Institució Catalana de Recerca i Estudis Avançats (Spain) [10672-125]
- Waveguide-integrated narrowband transmission filter consisting of two grooves and a ridge cavity**, Evgeni A. Bezus, Leonid L. Doskolovich, Dmitry A. Bykov, Image Processing Systems Institute, Russian Academy of Sciences (Russian Federation) [10672-126]
- Efficient synthesis and optical properties of highly luminescent copper nanoclusters**, Maria Jessabel Talite, National Chiao Tung Univ. (Taiwan); Chi-Tsu Yuan, Chung Yuan Christian Univ. (Taiwan); Wu-Ching Chou, National Chiao Tung Univ. (Taiwan) [10672-127]
- Numerically optimized design for enhanced coupling efficiency of single-photon sources integrated into single-mode waveguides**, Theresa Hoehne, Zuse Institute Berlin (Germany); Peter Schnauber, Sven Rodt, Stephan Reitzenstein, Institut für Festkörperphysik, Technische Univ. Berlin (Germany); Sven Burger, Zuse Institute Berlin (Germany) and JCMwave GmbH (Germany) [10672-128]
- Dielectro-plasmonic tweezers for scalable trapping and hot electrons applications**, Alberto Lauri, Emiliano Cortés, Evangelina Pensa, Imperial College London (United Kingdom); Avijit Barik, Univ. of Minnesota (United States); Aliaksandra Rakovich, Imperial College London (United Kingdom); Sang-Hyun Oh, Univ. of Minnesota (United States); Stefan A. Maier, Imperial College London (United Kingdom) [10672-129]
- Surface wave detection of hypersound in single plasmonic nanoantennas**, Rodrigo Berte, Imperial College London (United Kingdom); Fabricio Della Picca, Lab. de Electronica Cuantica, Univ. de Buenos Aires (Argentina) and El Instituto de Física de Buenos Aires (Argentina) and Consejo Nacional de Investigaciones Científicas y Técnicas (Argentina); Yi Li, Emiliano Cortés, Imperial College London (United Kingdom); Stefan A. Maier, Imperial College London (United Kingdom) and Ludwig-Maximilians-Universität München (Germany); Andrea Bragas, Lab. de Electronica Cuantica, Univ. de Buenos Aires (Argentina) [10672-130]
- Anderson localization of visible light for high-quality on-chip optical cavities**, Oliver Trojak, Tom Crane, Luca Sapienza, Univ. of Southampton (United Kingdom) [10672-131]
- Polarization conversion within ultracompact on-chip all-plasmonic nanocircuits**, Martin Thomaschewski, Yuanqing Yang, Sergey I. Bozhevolnyi, Univ. of Southern Denmark (Denmark) [10672-132]
- Optical sensing with Anderson localized light**, Oliver Trojak, Tom Crane, Luca Sapienza, Univ. of Southampton (United Kingdom) [10672-133]
- Plasmon-exciton interaction in the thin film of inhomogeneous ensemble of silver nanoparticles and cyanine J-aggregates**, Anton A. Starovoytov, Rezida D. Nabiullina, Igor A. Gladskih, ITMO Univ. (Russian Federation) [10672-134]
- Planar waveguide coupler based on tilted Bragg gratings and a discrete cladding mode**, Mathias Weisen, Matthew T. Posner, Optoelectronics Research Ctr. (United Kingdom); James C. Gates, Optoelectronics Research Ctr., Univ. of Southampton (United Kingdom); Corin Gawith, Peter G. R. Smith, Peter Horak, Optoelectronics Research Ctr. (United Kingdom) [10672-135]
- Investigation of bimetallic hollow nanoparticles for colorimetric detection of mercury**, Sangeeta Yadav, VIT Univ. (India); Saumeey Jain, KTH Royal Institute of Technology (Sweden); Jitendra Satija, Ctr. for Nanobiotechnology, VIT Univ. (India) [10672-136]
- Using all dielectric and plasmonic cross grating metasurface for enhancing efficiency of CZTS solar cells**, Omar A. M. Abdelraouf, The American Univ. in Cairo (Egypt) and Ain Shams Univ. (Egypt); Ahmed Shaker, Ain Shams Univ. (Egypt); Nageh K. Allam, The American Univ. in Cairo (Egypt) [10672-137]
- Study of thermo-optical properties of nanofluids of gold and silver nanoparticles functionalized with polyethylene glycol and sodium dodecyl sulfate in water using thermal lens spectroscopy**, Orlando Villegas, Jimmy Castillo, Alberto Fernández, Hector Gutierrez, Univ. Central de Venezuela (Venezuela) [10672-138]
- One-pot synthesis red emission of photoluminescent silane capped gold nanoclusters**, Hsiu-Ying Huang, Chi-Tsu Yuan, Chung Yuan Christian Univ. (Taiwan) [10672-139]
- Nanofabrication on unconventional platforms: implications for novel opto-electronic functionalities, design, and enhanced performance**, Jagdish Anakkavoor Krishnaswamy, Kavita Garg, Sandeep B.S., Kumar M.P., Praveen C. Ramamurthy, Debiprosad Roy Mahapatra, Indian Institute of Science (India) [10672-140]
- The glutathione-capped gold nanoclusters based on doping zinc ion with aggregation-induced emission enhancement**, Kun-Blin Cai, Li-Yun Chang, Chi-Tsu Yuan, Hsiu-Ying Huang, Chung Yuan Christian Univ. (Taiwan) [10672-141]
- Near-field localization of Au nano-objects: PEEM and group theory description**, Sarra Mitiche, Sylvie Marguet, Fabrice Charra, Ludovic Douillard, CEA-Ctr. de SACLAY (France) [10672-142]
- Nanostructured layer of InP on GaP surface**, Tinatin Laperashvili, Orest Kvitsiani, Institute of Cybernetics (Georgia); Davit Laperashvili, Georgian Technical Univ. (Georgia) [10672-143]
- Integration of carbon nanotubes in slot photonic crystal cavities**, Elena Durán-Valdeiglesias, Ctr. de Nanociencias et de Nanotechnologies (France); Thi Hong Cam Hoang, Ctr. de Nanociencias et de Nanotechnologies (France) and Institute of Materials Science (Viet Nam); Carlos Alonso-Ramos, Samuel Serna, Ctr. de Nanociencias et de Nanotechnologies (France); Weiwei Zhang, Ctr. de Nanociencias et de Nanotechnologies (France) and Univ. of Southampton (United Kingdom); Xavier Le Roux, Ctr. de Nanociencias et de Nanotechnologies (France); Matteo Balestrieri, CEA-Ctr. de SACLAY (France) and Commissariat à l'Énergie Atomique (France) and Nanosciences et Innovation pour les Matériaux, la Biomédecine et l'Énergie (France); Francesco Biccari, Anna Vinattieri, Lab. Europeo di Spettroscopia Non-Lineari, Univ. degli Studi di Firenze (Italy); Delphine Marris-Morini, Ctr. de Nanociencias et de Nanotechnologies (France); Arianna Filoramo, CEA-Ctr. de SACLAY (France) and Commissariat à l'Énergie Atomique (France) and Nanosciences et Innovation pour les Matériaux, la Biomédecine et l'Énergie (France); Massimo Gurioli, Lab. Europeo di Spettroscopia Non-Lineari, Univ. degli Studi di Firenze (Italy); Eric Cassan, Ctr. de Nanociencias et de Nanotechnologies (France) [10672-144]
- Optical coupling of a Mie-resonant silicon nanoparticle to a waveguide revealed by third harmonic generation spectroscopy**, Kirill I. Okhlopkov, Alexander A. Ezhov, Pavel A. Shafirin, M.V. Lomonosov Moscow State Univ. (Russian Federation); Nikolay A. Orlikovskiy, Bauman Moscow State Technical Univ. (Russian Federation); Maxim R. Shcherbakov, M.V. Lomonosov Moscow State Univ. (Russian Federation) and Cornell Univ. (United States); Andrey A. Fedyanin, M.V. Lomonosov Moscow State Univ. (Russian Federation) [10672-145]
- Distance dependence of carrier transfer via tunneling processes from graphene quantum dots to InGaN quantum well**, Tzu-Neng Lin, Svetta Reina Merden S. Santiago, Ji-Lin Shen, Chung Yuan Christian Univ. (Taiwan) [10672-146]
- Propagation of surface helicons in a semiconductor**, Valentin A. Tolkachev, Chelyabinsk State Univ. (Russian Federation); Igor V. Bychkov, Dmitry A. Kuzmin, Chelyabinsk State Univ. (Russian Federation) and South Ural State Univ. (Russian Federation); Vladimir G. Shavrov, Kotelnikov Institute of Radio Engineering and Electronics of Russian Academy of Sciences (Russian Federation); Olga Kharitnova, Chelyabinsk State Univ. (Russian Federation) [10672-147]
- Chirality and discrete diffraction in nonlinear Mathieu lattices**, Marius Rimmler, Alessandro Zannotti, Westfälische Wilhelms-Universität Münster (Germany); **Jadranka Vasiljevic**, Dejan V. Timotijevic, Dragana M. Jović Savić, Univ. of Belgrade (Serbia); Cornelia Denz, Westfälische Wilhelms-Universität Münster (Germany) [10672-148]
- Helium ion beam fabrication of nanofiber Bragg cavities**, Andreas W. Schell, ICFO - Institut de Ciències Fotòniques (Spain); Hideaki Takashima, Hirogona Maruya, Atsushi Fukuda, Kyoto Univ. (Japan) [10672-149]
- Tailored orbital and spin energy flow structures for advanced optical trapping**, Eileen Otte, Eric Asché, Ramon Runde, Cornelia Denz V, Westfälische Wilhelms-Universität Münster (Germany) [10672-150]
- Compact Bloch surface waves devices based on multimode interference effect**, Kirill Safronov, Ksenia A. Abrashitova, Dmitry N. Gulkin, Natalia Kokareva, Ilya Antropov, Vladimir O. Bessonov, Andrey A. Fedyanin, M.V. Lomonosov Moscow State Univ. (Russian Federation) [10672-151]
- Temperature-dependent photoluminescence in nitrogen-doped graphene quantum dots**, Svetta Reina Merden S. Santiago, Tzu-Neng Lin, Ji-Lin Shen, Chung Yuan Christian Univ. (Taiwan) [10672-152]
- A software for the simulation of light scattering by many particles in planarly layered media**, Amos Egel, Dominik Theobald, Guillaume Gornard, Uli Lemmer, Karlsruhe Institut für Technologie (Germany) [10672-153]
- GaP-on-insulator as a platform for nonlinear photonics**, Simon Hönl, Katharina Schneider, IBM Research - Zürich (Switzerland); Pol Welter, IBM Research - Zurich (Switzerland) and ETH Zurich (Switzerland); Yannick Baumgartner, Herwig Hahn, Lukas Czornomaz, IBM Research - Zürich (Switzerland); Dalziel J. Wilson, IBM Research - Zurich (Switzerland) and École Polytechnique Fédérale de Lausanne (Switzerland) [10672-154]
- Microwave surface plasmon-polariton resonances in VO₂ during metal-insulator phase transition**, Dmitry A. Kuzmin, Igor V. Bychkov, Chelyabinsk State Univ. (Russian Federation) and South Ural State Univ. (Russian Federation); Alexander P. Kamantsev, Victor V. Koledov, Dmitry S. Kuchin, Alexey V. Mashirov, Vladimir G. Shavrov, Kotelnikov Institute of Radio Engineering and Electronics of Russian Academy of Sciences (Russian Federation) [10672-155]

Chirality and discrete diffraction in nonlinear Mathieu lattices

M. Rimmler¹, A. Zannotti¹, J. M. Vasiljevic², D. V. Timotijevic^{2,3}, D. M. Jovic Savic², and C. Denz¹

¹*Institute of Applied Physics and Center for Nonlinear Science (CeNoS), University of Münster, 48149 Münster, Germany*

²*Institute of Physics, University of Belgrade, P.O. Box 68, 11001 Belgrade, Serbia*

³*Science Program, Texas A&M University at Qatar, P.O. Box 23874 Doha, Qatar*

Non-diffracting beams are highly relevant in optics and atom physics, particularly because their transverse intensity distributions propagate unchanged for hundreds of diffraction lengths. Thus, they feature applications in free-space wireless communications, optical interconnections, long-distance laser machining, and surgery. Four different fundamental families of propagation invariant light fields exist. They distinguish in the underlying real space coordinate system: Discrete, Bessel, Weber, and Mathieu non-diffracting beams. Latter ones obey the Helmholtz equation in elliptic cylindrical coordinates and are therefore best suited to address physical effects in elliptical coordinates.

Mathieu beams are classified according to their symmetry properties as even and odd. Their transverse discrete intensity distributions in elliptical or hyperbolic geometries can be shaped by their order and an ellipticity parameter. These real-valued beams have only discrete spatial phase distributions. In contrast, so called elliptical and helical Mathieu beams are obtained as complex superpositions of appropriate even and odd Mathieu beams, thus showing outstanding continuously modulated spatial phase distributions that act as orbital angular momenta, associated with a transverse energy flow.

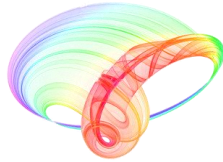
In our contribution we investigate and control the nonlinear optical induction of photonic Mathieu lattices in photosensitive media. As flexible material we chose a photorefractive SBN crystal, showing a non-local, anisotropic nonlinearity.

Focusing on elliptic Mathieu beams, during linear propagation their transverse energy redistribution along elliptic paths is compensated in each point, enabling for an invariant transverse intensity distribution. However, this energy flow withstands a direct observation. We demonstrate that their nonlinear self-action in SBN breaks this sensitive equilibrium. Consequently, a new type of rotating beam formation arises with high intensity filaments corresponding to the energy flow in an enforced preferential direction. This process is beneficially applied to realize chiral twisted photonic refractive index structures with a tunable ellipticity.

Further, we present our studies on the nonlinear dynamics of discrete Mathieu beams in SBN, showing examples of appropriate fundamental even Mathieu beams in order to realize one- and two-dimensional transverse lattices. The nonlinear optical induction process leads to the formation of discrete refractive index lattices and a self-interaction of the writing Mathieu beams with the realized photonic structure, capable of altering the writing beams' propagation similar to the well-known linear discrete diffraction. Controlling the strength of the nonlinearity allows tailoring the degree of diffraction. Moreover, probing the lattice linearly with Gaussian beams and tunable incident angles reveals the signature of discrete and anomalous diffraction. This allows to control the strength of diffraction, such that under certain tilts, the probing beams may cross the lattice diffractionless.

Our investigations both represent individual contributions towards the realization of advanced complex waveguiding in photorefractive crystals.

Book of abstracts



PHOTONICA2019

The Seventh International School and Conference on
Photonics, 26 August – 30 August 2019, Belgrade, Serbia

& Machine Learning with Photonics Symposium
(ML-Photonica 2019)



& ESUO Regional Workshop



& COST action CA16221



Editors: Milica Matijević, Marko Krstić and Petra Beličev

Belgrade, 2019

ABSTRACTS OF TUTORIAL, KEYNOTE, INVITED LECTURES,
PROGRESS REPORTS AND CONTRIBUTED PAPERS

of

The Seventh International School and Conference on Photonics
PHOTONICA2019, 26 August – 30 August 2019, Belgrade, Serbia

and

Machine Learning with Photonics Symposium

and

ESUO Regional Workshop

Editors

Milica Matijević, Marko Krstić and Petra Beličev

Technical Assistance

Danka Stojanović and Goran Gligorić

Publisher

Vinča Institute of Nuclear Sciences

Mike Petrovića Alasa 12-14, P.O. Box 522

11000 Belgrade, Serbia

Printed by

Serbian Academy of Sciences and Arts

Number of copies

300

ISBN 978-86-7306-153-5

QO.6 Transient properties of electromagnetically induced transparency in spherical quantum dot with hydrogen impurity	75
<i>Lj. Stevanović, J. Zimmermann, N. Filipović, V. Pavlović</i>	
QO.7 Pulse propagation through rectangular quantum dots under conditions of electromagnetically induced transparency	76
<i>V. Pavlović, Ž. Lazjić, Lj. Stevanović, N. Filipović</i>	
QO.8 Ground state and collective modes of dipolar BECs	77
<i>D. Vudragović, V. Veljić, I. Vasić, A. Balaž</i>	
QO.9 Field-Induced Narrowing and Broadening of a Magnetic Resonance in a Bichromatic Microwave Field.....	78
<i>W. Gawlik, M. Mrózek, A. M. Wojciechowski, A. G. Buzzykin, E. Yu. Perlin</i>	

2. Nonlinear optics

NO.1 Comparison of mid-infrared nonlinear crystals efficiency.....	80
<i>A. A. Ionin, I. O. Kinyaevskiy, A. M. Sagitova</i>	
NO.2 Waveguiding in Mathieu photonic lattices	81
<i>J. M. Vasiljević, A. Zannotti, D. V. Timotijević, C. Deniz, D. M. Jović Savić</i>	
NO.3 Strain of MoS2 mapped with second harmonic generation microscopy	82
<i>M. Spasenović, A. J. Krmpot, M. D. Rabasović, N. Vujičić, V. Jadriško, D. Čapeta, M. Kralj</i>	
NO.4 CO laser sum frequencies spectrum tuning by ZnGeP ₂ crystal temperature tuning.....	83
<i>A. A. Ionin, I. O. Kinyaevskiy, Yu. M. Klimachev, A. Yu. Kozlov, A. M. Sagitova, Yu. M. Andreev</i>	
NO.5 An analysis for fiber optical parametric amplifier in presence of attenuation and random dispersion fluctuations.....	84
<i>M. S. Kovacevic, K. K. Y. Wong, A. Djordjević</i>	
NO.6 Amplitude squeezing by four wave mixing in hot potassium vapor	85
<i>M. M. Ćurčić, B. M. Jelenković</i>	
NO.7 Evolution of laser pulse propagation in Four Wave Mixing atomic medium.....	86
<i>D. Arsenović, Ž. Nikitović, B. Zlatković, I. Radojičić, M. Ćurčić, A. J. Krmpot, B. Jelenković</i>	
NO.8 Double-periodic solutions and Talbot carpets of extended nonlinear Schrödinger equations	87
<i>S. N. Nikolić, O. A. Ashour, N. B. Aleksić, Y. Zhang, M. B. Belić, S. A. Chin</i>	
NO.9 Numerical study of the supercontinuum generation in the telecommunications windows in photonic crystal fiber	88
<i>M. Veljković, A. Mancić, D. Milović, A. Maluckov</i>	

Waveguiding in Mathieu photonic lattices

J. M. Vasiljević¹, A. Zannotti², D. V. Timotijević¹, C. Denz² and D. M. Jović Savić¹

¹*Institute of Physics, University of Belgrade, P.O. Box 68, 11001 Belgrade, Serbia*

²*Institute of Applied Physics and Center for Nonlinear Science (CeNoS),*

Westfälische Wilhelms-Universität Münster, 48149 Münster, Germany

e-mail: jadranka@ipb.ac.rs

Nondiffracting beams are highly applicable in optics, photonics and atom physics, peculiar because their transverse intensity distributions propagate unchanged for hundreds of diffraction lengths and allow creating 1D and 2D photonic lattices in photosensitive media [1]. Among the variety of different nondiffracting beams [2-5], Mathieu beams solve the Helmholtz equation in elliptic cylindrical coordinates [4, 6-7]. Mathieu beams are classified according to their symmetry properties as even and odd and their transverse discrete intensity distributions can be shaped by their order and an ellipticity parameter. These real-valued beams are characterized by only discrete spatial phase distributions. By complex superposition of appropriate even and odd Mathieu beams, elliptical Mathieu beams are obtained, showing remarkable continuously modulated spatial phase distributions that possess orbital angular momenta, associated with transverse energy flow.

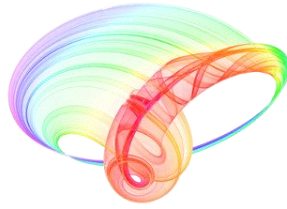
We exploit Mathieu beams as lattice-writing light to fabricate discrete waveguide structures and investigate their nonlinear self-action in these structures, leading to morphing discrete diffraction. We investigate Mathieu beams of different orders in a photorefractive SBN crystal, experimentally and numerically. We link linear discrete diffraction with nonlinear self-effects and demonstrate a gradual transition from one to two dimensions [8]. The self-action of a zero-order Mathieu beam in a nonlinear medium shows characteristics similar to discrete diffraction in one-dimensional waveguide arrays. Mathieu beams of higher orders show discrete diffraction along curved paths, showing the fingerprint of respective two-dimensional photonic lattices.

Linear propagation of elliptic Mathieu beams enables a nondiffracting transverse intensity distribution with transverse energy redistribution along elliptic paths compensated in each point. In contrast, their nonlinear self-action in SBN breaks this sensitive equilibrium. We demonstrated a new type of rotating beam formation arises with high-intensity filaments corresponding to the energy flow in an enforced preferential direction [9]. This process is beneficially applied to realize chiral twisted photonic refractive index structures with a tunable ellipticity.

REFERENCES

- [1] Z. Bouchal, Czech. J. Phys. 53, 537 (2003).
- [2] J. Durnin, J. Opt. Soc. Am. A 4, 651 (1987).
- [3] J. Durnin, J. J. Miceli, J. H. Eberly, Phys. Rev. Lett. 58, 1499 (1987).
- [4] J. C. Gutiérrez-Vega, M. D. Iturbe-Castillo, S. Chávez-Cerda, Opt. Lett. 25, 1493 (2000).
- [5] M. A. Bandres, J. C. Gutiérrez-Vega, Chávez-Cerda, Opt. Lett. 29, 44 (2004).
- [6] J. C. Gutiérrez-Vega et al., Opt. Commun. 195, 35 (2001).
- [7] J. C. Gutiérrez-Vega, R. M. Rodríguez-Dagnino, Am. J. Phys. 71, 233 (2003).
- [8] A. Zannotti et al., Adv. Optical Mater. 6, 1701355 (2018).
- [9] A. Zannotti et al., Opt. Lett. 44, 1592 (2019).

Book of abstracts



PHOTONICA2017

The Sixth International School and Conference on Photonics

& COST actions: MP1406 and MP1402



&H2020-MSCA-RISE-2015 CARDIALLY workshop



28 August – 1 September 2017

Belgrade, Serbia

Editors

Marina Lekić and Aleksandar Krmpot

Institute of Physics Belgrade, Serbia

Belgrade, 2017

ABSTRACTS OF TUTORIAL, KEYNOTE, INVITED LECTURES,
PROGRESS REPORTS AND CONTRIBUTED PAPERS

of

The Sixth International School and Conference on Photonics
PHOTONICA2017

28 August – 1 September 2017
Belgrade Serbia

Editors

Marina Lekić and Aleksandar Krmpot

Technical assistance

Marko Nikolić and Danica Pavlović

Publisher

Institute of Physics Belgrade
Pregrevica 118
11080 Belgrade, Serbia

Printed by

Serbian Academy of Sciences and Arts

Number of copies

300

ISBN 978-86-82441-46-5

Q.O.11	Electromagnetically induced transparency in degenerate 3-level ladder-type system.....	58
	<i>Lj. Stevanović, N. Filipović and V. Pavlović</i>	
Q.O.12	Husimi function for time-frequency analysis in optical, microwave and plasmonics applications.....	59
	<i>Milena D Davidović, Miloš D Davidović, Ljubica D Davidović, Vladimir A Andreev, Dragomir M Davidović</i>	
 2. Nonlinear optics		
N.O.1	Quasi-stable rotating solitons supported by a single spiral waveguide.....	60
	<i>Aleksandra I. Strinić, Milan S. Petrović, Najdan B. Aleksić and Milivoj R. Belić</i>	
N.O.2	Routing of optical beams by asymmetric defects in (non)linear waveguide arrays.....	61
	<i>M. Stojanović Krasić, S. Jovanović, A. Mančić and M. Stepić</i>	
N.O.3	Four wave mixing in potassium vapor with off-resonant double lambda system.....	62
	<i>D. Arsenović, M. M. Ćurčić, B. Zlatković, A. J. Krmpot, I. S. Radojičić, T. Khalifa and B. M. Jelenković</i>	
N.O.4	Towards the fully developed statistical approach of vector rogue waves.....	63
	<i>A. Mančić, A. Maluckov, F. Baronio, Lj. Hadzievski, S. Wabnitz</i>	
N.O.5	Signatures of non-quenched disorder in the wave pattern's spreading in flat band geometries.....	64
	<i>G. Gligorić, A. Maluckov</i>	
N.O.6	Molecules in a bicircular strong laser field.....	65
	<i>D. Habibović, A. Čerkić, M. Busuladžić, A. Gazibegović-Busuladžić, S. Odžak, E. Hasović, and D. B. Milošević</i>	
N.O.7	Enhanced second harmonic generation in lithium niobate photonic crystal cavities.....	66
	<i>Reinhard Geiss, Séverine Diziain, Michael Steinert and Thomas Pertsch</i>	
N.O.8	Solitons generated by self-organization in bismuth germanium oxide single crystals during the interaction with laser beam.....	67
	<i>V. Skarka, M. Lekić, A. Kovačević, B. Zarkov, and N. Z. Romčević</i>	
N.O.9	Broad-band femtosecond pulses, λ^3 type diffraction and X-waves. Evolution and management.....	68
	<i>V. Slavchev, A. Dakova, D. Dakova, K. Kovachev and L. Kovachev</i>	
N.O.10	Sum frequency conversion of compact Q-switched cryogenic slab RF discharge CO laser radiation in nonlinear ZnGeP ₂ crystal.....	69
	<i>A. Ionin, I. Kinyaevskiy, Yu. Klimachev, Yu. Kochetkov, A. Kozlov, L.V. Seleznev, D. Sinitsyn, D. Zemtsov</i>	
N.O.11	Realizing aperiodic photonic lattices by synthesized Mathieu-Gauss beams.....	70
	<i>J. M. Vasiljević, Alessandro Zannotti, D. V. Timotijević, Cornelia Denz, D. M. Jović Savić</i>	
N.O.12	Measurement of powerful ultrashort UV pulse parameters.....	71
	<i>A.A. Ionin, D.V. Mokrousova, D.A. Piterimov, L.V. Seleznev, A.V. Shutov, E.S. Sunchugasheva, N.N. Ustinovskii, V.D. Zvorykin</i>	
N.O.13	Polarization properties of vector solitons in optical fibers.....	72
	<i>A. Dakova, L. Kovachev, D. Dakova, D. Georgieva and V. Slavchev</i>	
N.O.14	Optical-Terahertz Solitons.....	73
	<i>A.N. Bugay and S.V. Sazonov</i>	
N.O.15	Vortices and topological structures in photorefractive materials.....	74
	<i>M. Ćubrović and M. Petrović</i>	
N.O.16	Exact traveling and solitary wave solutions to the generalized Gross-Pitaevskii equation with cylindrical potential.....	75
	<i>Nikola Z. Petrović</i>	
N.O.17	Nonlinear Fourier analysis of a mode-locked laser.....	76

Realizing aperiodic photonic lattices by synthesized Mathieu-Gauss beams

J. M. Vasiljević¹, Alessandro Zannotti², D. V. Timotijević^{1,3}, Cornelia Denz², D. M. Jović Savić¹

¹*Institute of Physics, University of Belgrade, P.O. Box 68, 11001 Belgrade, Serbia*

²*Institute of Applied Physics and Center for Nonlinear Science (CeNoS), Westfälische Wilhelms-Universität Münster, 48149 Münster, Germany*

³*Science Program, Texas A&M University at Qatar, P.O. Box 23874 Doha, Qatar*
e-mail: jadranka@ipb.ac.rs

Over the years, non-diffracting wave configurations have drawn considerable attention, particularly in the areas of optics, atom physics, biophysics, as well as optical tweezing [1], and nonlinear optics [2, 3]. The interest in such optical waves is due to the fact that, their transverse intensity distributions propagate unchanged for hundreds of diffraction lengths. The potential of non-diffracting structures is of significant importance for advances in discrete and nonlinear modern photonics [4, 5]. One prominent class of non-diffracting waves is given by Mathieu beams, which appear as translationally invariant solution of the Helmholtz equation in elliptic cylindrical coordinates.

Synthesizing two or more non-diffracting Mathieu-Gauss (MG) beams, we demonstrate a powerful new approach for the creation of two-dimensional (2D) aperiodic photonic lattices, in a single writing process in parallel. Depending on the beam configurations of coherently superimposed MG beams, their mutual distances, angles of rotation or phase relations we are able to realize transverse invariant propagating intensity distributions capable to optically induce corresponding refractive index lattices in photosensitive media. Our approach features the fabrication of versatile aperiodic lattices with controllable properties as well as quasi one-dimensional structures. Our results and methods enable further investigations of light propagating in such aperiodic photonic lattices, and could find applications in modern optical information processing.

REFERENCES

- [1] V. Garcés-Chávez, D. McGloin, H. Melville, W. Sibbett, and K. Dholakia, *Nature* 419, 145 (2002).
- [2] J.W. Fleischer, M. Segev, N. K. Efremidis, and D. N. Christodoulides, *Nature* 422, 147 (2003).
- [3] H. Martin, E. D. Eugenieva, and Z. Chen, *Phys. Rev. Lett.* 92, 123902 (2004).
- [4] F. Diebel, B. M. Bokić, M. Boguslawski, A. Piper, D. V. Timotijević, D. M. Jović, and C. Denz, *Phys. Rev. A* 90, 033802 (2014).
- [5] F. Diebel, B. M. Bokić, D. V. Timotijević, D. M. Jović Savić, and C. Denz, *Opt. Express* 23, 24351 (2015).

PHOTONICA2015.

V International School and Conference on Photonics
& COST actions: MP1204 and BM1205
& the Second international workshop "Control of light and
matter waves propagation and localization in photonic
lattices"
www.vin.bg.ac.rs/photonica_2015

Book of Abstracts



Editors

Suzana Petrović, Goran Gligorić and Milutin Stepić

Belgrade, 2015.

Book of abstracts



PHOTONICA2015

the Fifth international school and conference on
photonics

& COST actions: MP1204 and BM1205

& the Second international workshop "Control of light and matter
waves propagation and localization in photonic lattices"

24 August – 28 August 2015

Belgrade, Serbia

Editors

Suzana Petrović, Goran Gligorić and Milutin Stepić

Vinča Institute of Nuclear Sciences, Belgrade, Serbia

Belgrade, 2015

ABSTRACTS OF TUTORIAL, KEYNOTE AND INVITED
LECTURES AND CONTRIBUTED PAPERS

of

the Fifth international school and conference on photonics
PHOTONICA2015

and

COST actions MP1204 and BM1205

and

the Second international workshop
"Control of light and matter waves propagation and localization in
photonic lattices"

24 August – 28 August 2015

Belgrade Serbia

Editors

Suzana Petrović, Goran Gligorić, Milutin Stepić

Technical assistance

Petra Beličev, Marijana Petković

Publisher

Vinča Institute of Nuclear Sciences
Mike Petrovića Alasa 12-14, P.O. Box 522
11001 Belgrade, Serbia

Printed by

Serbian Academy of Sciences and Arts

Number of copies

300

ISBN 978-86-7306-131-3

O.NO.5	Self-focusing and plasma generation of linear polarized laser pulse in optical schemes with preferential directions	62
	<i>A. Ionin, D. Mokrousova, L. Seleznev, D. Sinitsyn, E. Sunchugasheva, N. Fokina</i>	
O.NO.6	Observation of flat band properties in photonic lattices	64
	<i>R. Vicencio</i>	
O.NO.7	Charge Flipping Vortices in DNLS trimer and hexamer	65
	<i>P. Jason, M. Johansson</i>	
P.NO.1	Formation of optically induced photonic waveguides in a bulk of lithium niobate with a pyroelectric response	65
	<i>A. Perin, V. Shandarov</i>	
P.NO.2	Optical properties of spherical quantum dot with on-center hydrogen impurity in magnetic field	67
	<i>Lj. Stevanović, N. Filipović, V. Pavlović</i>	
P.NO.3	On localized modes in nonlinear binary kagome ribbons	68
	<i>P. Beličev, G. Gligorić, A. Radosavljević, A. Maluckov, M. Stepić, R. Vicencio, M. Johansson</i>	
P.NO.4	Interference structures in nonlinear processes in strong infrared laser fields	69
	<i>D. Habibović, S. Odžak, M. Busuladžić, E. Hasović, A. Gazibegović-Busuladžić, A. Čerkić, D. B. Milošević</i>	
P.NO.5	Light propagation through the composite linear photonic lattice containing two nonlinear defects	70
	<i>M. Stojanović-Krasić, A. Mančić, S. Kuzmanović, S. Đorić Veljković, M. Stepić</i>	
P.NO.6	On high power dynamically stable vortices in multicore optical fibers	71
	<i>A. Radosavljević, A. Daničić, J. Petrović, A. Maluckov, Lj. Hadžievski, A. Rubenchik, S. Turitsyn</i>	
P.NO.7	The nonlinear optical properties and electronic transitions of thienylpyrroles-containing chromophores: A DFT study	72
	<i>D. Avci, Ö. Tamer, A. Başoğlu, Y. Atalay</i>	
P.NO.8	Stable temporal dissipative solitons in resonant gases confined in PBG fibers	73
	<i>M. Facão, M. Carvalho, S. Rodrigues, M. Ferreira</i>	
P.NO.9	Light propagation in deterministic aperiodic Fibonacci waveguide arrays	74
	<i>J. Vasiljević, N. Lučić, D. Timotijević, A. Piper, D. Grujić, D. Pantelić, B. Jelenković, D. Jović Savić</i>	
P.NO.10	Counterpropagating optical solitons in PT symmetric photonic lattices	75
	<i>M. Petrović, A. Strinić, M. Belić</i>	
P.NO.11	Quench Dynamics for Trapped Dipolar Fermi Gases	76
	<i>V. Veljić, A. Balaž, A. Pelster</i>	
P.NO.12	Trapped Bose-Einstein Condensates with Strong Disorder	76
	<i>V. Lončar, A. Balaž, A. Pelster</i>	
P.NO.13	Faraday Waves in Dipolar Bose-Einstein Condensates	77
	<i>D. Vudragović, A. Balaž</i>	
P.NO.14	Linear modulational stability analysis of Ginzburg-Landau dissipative vortices	78
	<i>N. Aleksić, V. Skarka, M. Belić</i>	
P.NO.15	Spectral Method for Numerical Solution of the Nonlocal Nonlinear Schrödinger Equation on the GPU	78
	<i>B. Aleksic, M. Belić</i>	

We have also found a PBG fiber and a gas configuration whose characteristics permit the propagation of such stable solitons. Nevertheless, the linear gain, that is possible because the gas is only confined in the hollow core but not in the cladding holes, brings background instability.

Here, we systematically address the configurations of gases confined in PBG fibers that are more suitable for stable dissipative solitons, studying the dependence of sign and magnitude of the equation parameters with the experimental conditions. Moreover, we will obtain a propagation equation in fourth order which introduces a delayed Raman scattering term. This new term creates a new branch of solutions that exist and are stable in a limited range of the parameter space for which there is linear loss, so that, the background is stable.

REFERENCES

- [1] T. Hong, Phys. Rev. Lett. 90, 183901 (2003).
- [2] C. Hang, V. V. Konotop, Phys. Rev. A 81, 053849 (2010).
- [3] Y. Wu, L. Deng, Phys. Rev. Lett. 93, 143904 (2004).
- [4] J. Xu, G. Huang, Opt. Exp. 2, 5149 (2013).
- [5] Y. Zhang et al., Phys. Rev. A 82, 053837 (2010).
- [6] Z. Wu et al., Opt. Exp. 23, 8430 (2015).
- [7] M. Facão et al., Phys. Rev. A 91, 013828 (2015).

Light propagation in deterministic aperiodic Fibonacci waveguide arrays

J. M. Vasiljević, N. M. Lučić, D. V. Timotijević, A. Piper, D. Ž. Grujić,
D. V. Pantelić, B. M. Jelenković and D. M. Jović Savić
Institute of Physics, University of Belgrade, P.O. Box 68, 11001 Belgrade, Serbia
e-mail: jadranka@ipb.ac.rs

During the 1980s quasi-crystallographic structures in solid state physics fundamentally amazed the scientific community [1], and inspired a new field of research in optics and photonics. Owing to the analogy of photonic lattices to solid state systems, the first optical experiments were implemented analyzing aperiodic media [2]. Irregular photonic lattices are of great interest as these structures offer proper band gaps where propagation is forbidden while translation invariance and thus the general scheme of Bloch wave propagation within periodic arrangements are broken. Asking for aperiodic structures rapidly the nomenclature of Fibonacci grating came up for this often is referred to as the embodiment of irregularity [3,4]. Generally spoken, the research field of aperiodic lattices is a fertile topic [5] as these structures offer the possibility of light localization in deterministic disordered structures that are settled between periodic and disordered systems [6]. Light localization in quasi-periodic photonic lattices is observed in Aubry André model and also realized experimentally in AlGaAs substrate [7].

We extend these concepts to quasi-periodic Fibonacci waveguide arrays, considering light propagation along waveguides. We fabricate the array of identical waveguides (identical refractive index profile) in Fe:LiNbO₃ crystal. The distance between successive waveguides is modulated in Fibonacci manner. This means that the sequence of separations consists of two elements, A and B, lined in such a way to make Fibonacci word. We have analyzed experimentally and numerically how various incident beam positions influence propagation and localization characteristics and compare it with appropriate periodic waveguide arrays. In general, we find the beam expansion is slowed down in quasi-periodic Fibonacci waveguide arrays, and localization properties in such lattice are closer to a random than periodic lattice. However, with a modification of the refractive index variation, the localization effects are observed for shorter propagation distances by increasing refractive index variation.

REFERENCES

- [1] D. Shechtman et al., Phys. Rev. Lett. 53, 1951 (1984).
- [2] D. Levine, P. J. Steinhardt, Phys. Rev. Lett. 53, 2477 (1984).
- [3] G. Gumbs, M. K. Ali, Phys. Rev. Lett. 60, 1081 (1988).
- [4] E. L. Albuquerque, M. G. Cottam, Phys. Rep. 376, 225 (2003).
- [5] Z. V. Vardeny, A. Nahata, A. Agrawal, Nat. Photon. 7, 177 (2013).
- [6] A. Lagendijk, B. van Tiggelen, D. S. Wiersma, Phys. Today 62, 24 (2009).
- [7] Y. Lahini et al., Phys. Rev. Lett 103, 013901 (2009).

Counterpropagating optical solitons in PT symmetric photonic lattices

M. S. Petrović^{1,2}, A. I. Strinić^{2,3} and M. R. Belić²

¹ *Institute of Physics, PO Box 57, 11001 Belgrade, Serbia*

² *Texas A&M University at Qatar, PO Box 23874, Doha, Qatar*

³ *Institute of Physics, University of Belgrade, PO Box 68, 11080 Belgrade, Serbia*

e-mail: petrovic@ipb.ac.rs

We construct solitonic solutions for the system of two optical beams propagating in opposite directions [1, 2] in parity-time (PT) symmetric [3, 4] photonic lattices by using modified Petviashvili method [5]. Our system support PT symmetric fundamental solitons, as well as solitary vortices. We propagate them and investigate their basic characteristics. We report power transfer between counterpropagating beams and symmetry breaking (or split-up) transition.

REFERENCES

- [1] M. Petrovic et al., Phys. Rev. Lett. 95, 053901 (2005).
- [2] M. S. Petrovic et al., Laser Photonics Rev. 5, 214 (2011).
- [3] C. M. Bender, S. Boettcher, Phys. Rev. Lett. 80, 5243 (1998).
- [4] C. M. Bender, Rep. Prog. Phys. 70, 947 (2007).
- [5] V. I. Petviashvili, Fiz. Plazmy 2, 469 (1976) [Sov. J. Plasma Phys. 2, 257 (1976)].

UNIVERSITY OF BELGRADE
FACULTY OF PHYSICS

Jadranka M. Vasiljević

**Propagation, localization, and control of light in
Mathieu lattices**

Doctoral Dissertation

Belgrade, September 2020

UNIVERZITET U BEOGRADU

FIZIČKI FAKULTET

Jadranka M. Vasiljević

**Prostiranje, lokalizacija i kontrola svetlosti u
Matjeovim rešetkama**

doktorska disertacija

Beograd, septembar 2020

Komisija za odbranu teze

Mentor:

- dr Dragana M. Jović Savić , naučni savetnik,
Institut za fiziku, Univerzitet u Beogradu

Komentor:

- dr Dejan V. Timotijević , naučni savetnik,
Institut za fiziku, Univerzitet u Beogradu

Članovi komisije:

- dr Dejan V. Timotijević , naučni savetnik,
Institut za fiziku, Univerzitet u Beogradu
- Prof. dr Milorad Kuraica, redovni profesor, Fizički fakultet,
Univerzitet u Beogradu
- Prof. dr Djordje Spasojević, redovni profesor, Fizički fakultet,
Univerzitet u Beogradu
- Prof. dr Dragica Knežević, vanredni profesor,
Prirodno Matematički Fakultet, Univerzitet u Kragujevcu

Datum odbrane:

SPISAK RADOVA KORIŠĆENIH U DISERTACIJI:

- J. M. Vasiljević, A. Zannotti, D. V. TimotijeVić, C. Denz, and D. M. Jović Savić, Phys. ReV. A 96, 023840, 2017.
- J. M. Vasiljević, A. Zannotti, D. V. Timotijević, C. Denz, and D. M. Jović Savić, Phys. Rev. A 97, 033848, 2018.
- A. Zannotti, J. M. Vasiljević, D. V. Timotijević, D. M. Jović Savić and C. Denz, Adv. Optical Mater. 97, 1701355, 2018.
- A. Zannotti, J. M. Vasiljević, D. V. Timotijević, D. M. Jović Savić and C. Denz, Optics Letters 44(7), 1592, 2019.

RADOVI KOJI NISU U VEZI SA DISERTACIJOM:

- N. M. Lučić, D. M. Jović Savić, A. Piper, D. Ž. Grujić, J. M. Vasiljević, D. V. Pantelić, B. M. Jelenković, and D. V. Timotijević, Journal of the Optical Society of America B 32(7), 1510 (2015).

Abstract

The main topic of this thesis is the examination of the propagation and control of light in Mathieu photonic lattices. The main directions of research are based on the formation of photonic lattices using single Mathieu beams or superposition of multiple Mathieu beams in a photorefractive crystal, then the propagation of light in photonic lattices thus formed, and the examination of the nonlinear propagation of single or elliptic Mathieu beams in a nonlinear photorefractive crystal.

The thesis is divided into seven chapters, and the content of the individual chapters is given in the following text.

The introductory chapter provides an overview of the results in the field of nonlinear photonics related to one of realizations of photonic crystals, photonic lattices. An overview of the known research and the achievements in the field of nonlinear optics and their contribution to other related fields are represented as well as future direction for research.

In the next chapter the photonic lattices are described, as well as achievements related to the investigation inside this thesis. The optical induction technique for the realization of photonic lattices is explained specifically by using propagation invariant light fields, i.e. nondiffracting beams.

In the third chapter nondiffracting beams are introduced with emphasis on the large group of Mathieu beams. Different families of Mathieu beams are shown: single even and odd Mathieu beams, elliptic and hyperbolic Mathieu beams. These beams will be used in this thesis to generate different photonic lattices in photorefractive media by optical induction.

The following chapter contains the description of the experimental method used for the research presented in this thesis to generate photonic lattices using Mathieu beams in a photorefractive strontium barium niobate crystal (SBN). Additionally, the light propagation in such generated Mathieu photonic lattices is described. This chapter contains the experimental explanation of photorefractive effect and refractive index modulation in photorefractive crystals as the main effect for optical induction of photonic lattices inside SBN crystal.

In the next chapter a numerical model for the examination of the propagation of the Mathieu light field, inside a photorefractive SBN crystal is described. Single Mathieu beams are used for experimental realization of photonic Mathieu lattices as well as interference of Mathieu beams, which produced numerous aperiodic lattices. A numerical model for the study of light propagation in photonic lattices created by nondiffracting Mathieu beams is also described.

In the next chapter, the results of the experimental and theoretical investigation are presented. This chapter is divided into three separate sections. In the first section, the nonlinear self-interaction of a single Mathieu beams in SBN crystal is investigated, numerically and experimentally. New effect, 1D and 2D nonlinear discrete diffraction are demonstrated as well as nonlinear Mathieu lattices. The nonlinear self-interaction of the elliptical Mathieu beams in the SBN crystal is examined and their utilization for the realization of dynamical structures which rotates in direction predicted with energy flow, i.e. Poynting vector. Such rotating dynamic structures are suited for the realization of chiral waveguides with the possibility of controlling the chirality and number of the waveguides. The second section of this chapter contains an examination of the propagation of an elliptical vortex beam in photonic lattices created by single Mathieu beams in SBN crystal. The conditions for the formation of

stable vortex states such as elliptical vortex necklaces, how the order or ellipticity of Mathieu beam, size and topological charge of the elliptical vortex beam influence the stability of vortex states. The third section an approach for the realization of two-dimensional aperiodic lattices using the interference of several Mathieu beams is presented. Therefore, the propagation of a narrow probe beam is examined in such a formed lattice. It is investigated how the local environment will affect the diffraction of the probe beam in the lattice as well as the conditions for the formation of localized states in such lattices. The propagation of light in aperiodic lattices is compared with propagation in appropriate periodic lattices. The periodic square lattice with a period equal to the characteristic structured size of Mathieu beam is used.

The last chapter summarizes the results of the research and their potential application in other related fields. Due to the examination of nonlinear propagation of Mathieu beams in the photorefractive SBN crystal new effect, nonlinear discrete diffraction is revealed. Examination of elliptical Mathieu beams significantly contributed to the realization of chiral two-dimensional photonic lattices with adjustable properties via the optical induction technique facilitated by the elliptical Mathieu beams. The conditions during which Mathieu beams remain robust in the crystal are shown, as well as the various photonic lattices created by Mathieu beams, with waveguides located along straight and curved paths (circle, ellipse or hyperbola), nonlinear Mathieu lattices, chiral lattices, as same as different aperiodic lattices created via interference of Mathieu beams. In Mathieu lattices, the propagation of elliptic vortex is examined and various stable states such as elliptical vortex necklaces are found, as well as the conditions under which they remain stable. In aperiodic Mathieu lattices propagation of narrow Gaussian beam is examined the same as parameters for realization of strong localized states like spatial solitons or Anderson localization.

Key words: Mathieu beams, nonlinear photorefractive crystal, aperiodic photonic lattices, nonlinear photonic lattices, chiral photonic lattice, nonlinear morphing discrete diffraction, energy flow, vortices, vortex necklaces, solitons.

Scientific field: Physics

Research area: Nonlinear photonics

Rezime

Tema ove teze je ispitivanje prostiranja i kontrole svetlosti u Matjeovim rešetkama. Osnovni pravci istrživanja usmereni su ka formiranju fotonskih rešetki korišćenjem pojedinačnih Matjeovih zraka ili superpozicije više Matjeovih zraka u fotorefraktivnom kristalu, zatim ka prostiranju svetlosti u tako formiranim fotonskim rešetkama kao i ispitivanju nelinearnog prostiranja pojedinačnih ili eliptičnih Matjeovih zraka u nelinearnom fotorefraktivnom kristalu.

Rad je podeljen u sedam poglavlja, a sadržaj pojedinačnih poglavlja dat je u daljem tekstu.

U uvodnom poglavlju dat je pregled dosadašnjih rezultata u oblasti nelinearne fotonike povezanih sa fotonskim kristalima odnosno fotonskim rešetkama kao jedne od realizacija fotonskih kristala. Dat je pregled istraživanja, i osvrt na dostignuća u oblasti nelinearne optike i njihov doprinos u drugim srodnim oblastima kao i pravci za buduća istraživanja.

U sledećem poglavlju opisane su fotonske rešetke kao i neke od važnijih dostignuća u toj oblasti povezana sa istraživanjem u ovoj tezi. Objašnjena je tehnika optičke indukcije za formiranje fotonskih rešetki korišćenjem zraka nepromenljivih tokom propagacije tj. nedifragujućih zraka.

U trećem poglavlju opisani su nedifragujući zraci, a posebno jedna obimna grupa Matjeovih zraka. Prikazane su različite grupe Matjeovih zraka: pojedinačni parni i neparni Matjeovi zraci, Eliptični i Hiperbolični Matjeovi zraci, koje će se u ovoj tezi koristiti za izradu različitih fotonskih rešetki.

U sledećem poglavlju opisana je experimentalna metoda korišćena u toku istraživanja, čiji rezultati su prikazana u ovoj tezi, za formiranja fotonskih rešetki pomoću Matjeovih zraka u fotorefraktivnom kristalu stroncijum barijum niobatu (SBN). Takodje je opisana i metoda za ispitivanje prostiranja svetlosti u tako formiranim Matjeovim rešetkama. Ovo poglavlje sadrži eksperimentalno objašnjenje fotorefraktivnog efekta i modulacije indeksa prelamanja u fotorefraktivnom kristalu kao glavnih efekata pri upisivanju fotonske rešetke.

U narednom poglavlju opisan je numerički model kojim se opisuje prostiranje Matjeovog svetlosnog polja u fotorefraktivnom SBN kristalu, koji se koristi i za kreiranje Matjeovih rešetki. Matjeove rešetke kreirane su korišćenjem pojedinačnih Matjeovih zraka ili prethodne interferencije više Matjeovih zraka koji stvaraju brojne aperioidične rešetke. Potom je opisan numerički model za izučavanje linearnog i nelinearnog prostiranja svetlosti u fotonskim rešetkama kreiranim pomoću nedifragujućih Matjeovih zraka.

U narednom poglavlju prikazani su rezultati ekperimentalnog i teorijskog istraživanja. Ovo poglavlje je podeljeno na tri zasebne celine. U prvoj celini ispitivana je nelinearna samo-interakcija pojedinačnog Matjeovog zraka u SBN kristalu, numerički i eksperimentalno. Pokazan je novi efekat, 1D and 2D nelinearna diskretna difrakcija kao i nelinearne Matjeove rešetke. Ispitana je nelinearna samo-interakcija eliptičnih Matjeovih zraka u SBN kristalu kao i njihova upotreba za realizaciju dinamičkog struktura koje rotiraju u tokom protiranja u pravcu protoka energije, koji je određen Pointingovim vektorom. Takve rotirajuće dinamičke strukture pogodne su za izradu iskrivljenih talasovoda sa mogućnošću kontrolisanja zakrivljenosti i broja talasovoda. Druga celina ovog poglavlja sadrži ispitivanje prostiranja eliptičnog vorteksnog zraka u fotonskim rešetkama kreiranih pomoću pojedinačnih Matjeovih zraka. Ispitivani su uslovi za formiranje stabilnih vorteksnih stanja kao što su vorteksne ogrlice, kako red ili eliptičnost Matjeovog zraka ili širana i toplološko naelktrisanje eliptičnog

vorteksa utiču na stabilnost vorteksnih stanja. U trećoj celini je prikazan pristup za generisanje novih dvodimenzionalnih aperiodičnih rešetki pomoću interferencije više Matjeovih zraka. U tako formiranim rešetkama ispitivano je prostiranje uskog probnog zraka. Ispitivano je kako lokalno okruženje utiče na difrakciju probnog zraka u rešetci kao i uslova za formiranje lokalizovanih stanja u takvim rešetkama. Prostiranje svetlosti u aperiodičnim rešetkama poredjeno je sa prostiranjem svetlosti u odgovarajućoj periodičnoj rešetki. Korišćena je periodična kvadratna rešetka sa periodom jednakim karakterističnoj veličini Matjeovog zraka korišćenog za izradu aperiodične rešetke.

U poslednjem poglavlju sumirani su rezultati istraživanja i njihova potencijalna primena u drugim srodnim oblastima. Prilikom ispitivanja nelinearnog prostiranja Matjeovih zraka u fotorefraktivnom SBN kristalu otkriven je novi efekat, nelinearna diskretna difrakcija. Ispitivanje eliptičnih Matjeovih zraka omogućio je značajan doprinos za realizaciju hiralnih dvodimenzionalnih fotonskih rešetki sa podesivim osobinama pomoću optički indukovane tehnike olakšane korišćenjem eliptičnih Matjeovih zraka. Pokazani su uslovi tokom kojih Matjeovi zrak ostaje robustan u kristalu kao i različite fotonske rešetke kreirane pomoću Matjeovih zraka sa talasovodima raspoređenim duž prave ili krive linije (krug, elipsa ili hiperbola), nelinearne Matjeove rešetke, hiralne Matjeove rešetke, kao i brojne aperiodične rešetke kreirane interferencijom Matjeovih zraka. U Matjevima rešetkama ispitivano je prostiranje eliptičnog vorteksa u kojima su pokazana stabilna vorteksna stanja kao što su eliptične vorteksne ogrlice kao i uslovi pod kojima ostaju stabilne. U aperiodičnim Matjeovim rešetkama ispitana je propagacija uskog Gausjanskog zraka i parametri za nastanak jako lokalizovanih stanja kao što su prostorni solitoni ili Andersonove lokalizacije .

Ključne reči: Matjeovi zraci, nelinearni fotorefraktivni kristal, aperiodične fotonske rešetke, nelinearne fotonske rešetke, zakrivljene fotonske rešetke, nelinearna diskretna difrakcija, protok energije, vorteksi, vorteksne ogrlice, solitoni.

Naučna oblast: Fizika

Uža naučna oblast: Nelinearna fotonika

Zahvalnica

Rezultati rada koje obhvata ova doktorskoj disertaciji pod naslovom "Prostiranje, lokalizacija i kontrola i svetosti u Matjeovim rešetkama" izvedeni su na Institutu za fiziku u Beogradu pod mentorstvom naučnih savetnika, Dr Dragane M. Jović Savić i Dr Dejana V. Timotijević.

Zahvaljujem Dragani i Dejanu za smernice i podršku u svim aspektima doktorata i pomoći pri svim problemima i preprekama. Uveli su me u uzbudljivo istraživačko polje nelinearne optike i preneli dragoceno znanje koje ću nastaviti da primenjujem tokom svoje dalje naučne karijere. Kao moji mentori, značajno su doprineli da moje doktorske studije postanu pozitivno iskustvo.

Tokom rada na ovoj tezi bila sam zaposlena u Laboratoriji za nelinearnu fotoniku na Instituta za fiziku u Beograd. Imala sam priliku da budem deo bilateralnog projekta Republike Srbije i Republike Nemačke. Takodje bih želela da se zahvalim svim koautorima koji su doprineli istraživanju prikazanom u ovoj tezi, Dr Korneliji Dens i dr Alesandru Zanotiju. Kako su moje kolege sa posla iz različitih oblasti, mogla sam da čujem o širokom spektru istraživačkih tema i da radim u podsticajnom okruženju.

Ovaj rad finansijski je podržalo Ministarstvo prosvete, nauke i tehnološkog razvoja Republike Srbije kroz grant Institutu za fiziku Beograd i kroz projekte OII71036, kao i medjunarodni projekat između Republike Srbije i Nemačke službe za akademsku razmenu (Projekat 57219089) tokom koje sam posetila Institut za primenjenu fiziku Univerziteta u Minsteru, Nemačka.

Zahvalnost dugujem i članovima komisije na efikasnom i brzom pregledanju rada.

Na kraju, želela bih da se zahvalim svojoj porodici i prijateljima na podršci i ohrabrenju tokom proteklih godina.

Acknowledgments

The work presented in this thesis (Propagation, localization, and control of light in Mathieu lattices) was carried out at the Institute of Physics Belgrade under the supervision of Dr. Dragana M. Jović Savić and Dr. Dejan V. Timotijević.

I am indebted to Dragana and Dejan for guidance and support in all aspects of my PhD studies and help whenever I had a question or encountered an obstacle. They introduced me to the exciting research field of nonlinear optics and passed on valuable knowledge that I will continue to use throughout my future scientific career. As my supervisors, they significantly contributed to making my PhD studies a positive experience.

During the work on this thesis, I was employed at the Nonlinear Photonics Laboratory of the Institute of Physics Belgrade. I had many opportunities to participate in international collaboration between Republic of Serbia and Republic of Germany. I would also like to acknowledge all my other coauthors who contributed to the research presented in this thesis, Dr. Cornelia Denz and, Dr. Alessandro Zannotti. I thank them for fruitful collaboration. As my colleagues from work are from different fields, I could hear about a wide variety of research topics and work in a stimulating environment.

This work was financially supported by the Ministry of Education, Science, and Technological Development of the Republic of Serbia through the grant to the Institute of Physics Belgrade, through Projects OII71036, and the international project between the Republic of Serbia and the German Academic Exchange Service (Project 57219089) during which I visited the Institute of Applied Physics, University of Münster, Germany.

I also owe gratitude to the members of the commission for the efficient and fast review of the work.

Finally, I would like to thank my family and friends for their support and encouragement during the past years.

Contents

1	Introduction	1
2	Photonic lattices	4
2.1	Photonic lattices and the optical induction technique	6
3	Nondiffracting beams	7
3.1	Mathieu functions	8
3.2	Mathieu nondiffracting beams	10
4	Experimental methods for photonic lattices generation and light propagation in photonic lattices	15
4.1	Photorefractive effect	15
4.1.1	The linear electro-optic effect	17
4.2	Properties of photorefractive SBN crystal	17
4.3	Experimental realization of photonic lattices	20
4.4	Experimental realization of light propagation in photonic lattices	21
5	Numerical tools for photonic lattices generation and light propagation in photonic lattices	23
5.1	Basic equation of light propagation in nonlinear photorefractive media	23
5.2	Propagation of light in photonic lattices	26
5.3	The symmetrized split-step beam propagation method and calculation of Potential equation	27
6	Results and discussion	29
6.1	Nonlinear self-action of Mathieu beams in SBN crystal and Mathieu photonic lattices	29
6.1.1	Switching discrete diffraction in nonlinear Mathieu lattices	29

6.1.2	The self-action of elliptical Mathieu beams in nonlinear media	34
6.2	Elliptical vortex necklaces in Mathieu lattices	39
6.3	Creation of aperiodic photonic lattices and investigation of light propagation in the aperiodic Mathieu lattice	45
6.3.1	Creating aperiodic photonic structures by synthesized Mathieu-Gauss beams	45
6.3.2	Light propagation in aperiodic photonic lattices created by synthesized Mathieu-Gauss beams	52
6.3.3	Localization of light in disordered aperiodic Mathieu lattices	56
7	Conclusion	59
	References	62

List of Figures

2.1	Discrete diffraction in (A) 1D arrays of evanescently coupled optical waveguides [3] (B) 2D periodic photonic lattices [29].	5
3.1	Intensity distributions of (A) Bessel, (B) Mathieu and (C) Parabolic nondiffracting beams.	8
3.2	Elliptic coordinate system. Curves $\xi = \text{constant}$ are confocal ellipses, curves $\eta =$ constant are orthogonal hyperbolas; $0 \leq \eta < 2\pi$, $0 \leq \xi < \infty$. For limit $f \rightarrow 0$ polar coordinates are review.	9
3.3	Intensity and phase distribution of <i>even Mathieu beams</i> of different order m , with same parameter of ellipticity $q = 25$, and characteristic structure size $a = 25\mu\text{m}$	10
3.4	Intensity and phase distribution of <i>odd Mathieu beams</i> of different order m , with same parameter of ellipticity q , and same characteristic structure size $a = 25\mu\text{m}$	11
3.5	Intensity and phase distribution of even Mathieu beam of order $m = 8$, with character- istic structure size $a = 25\mu\text{m}$ and different parameter of ellipticity q	11
3.6	Intensity and phase distribution of even Mathieu beam of order $m = 4$, with parameter of ellipticity $q = 25$ and different characteristic structure size a	12
3.7	Intensity and phase distribution of <i>elliptic Mathieu beams</i> of different order m , with same parameter of ellipticity q , and same characteristic structure size $a=25\mu\text{m}$	13
3.8	Intensity and phase distribution of <i>Hyperbolic Mathieu beams</i> of different order m , with same parameter of ellipticity q , and same characteristic structure size $a=25\mu\text{m}$. .	13
4.1	Illustration of photorefractive effect.	16
4.2	Geometry of SBN crystal and axis orientation.	19
4.3	Experimental setup for realization of photonic lattices in SBN crystal: SLM - spatial light modulator, BS - beam splitter, L - lens, FF - Fourier filter, MO - macroscopic objective.	20
4.4	Experimental setup for light propagation in optically induced photonic lattices in SBN crystal: SLM - spatial light modulator, BS - beam splitter, L - lens, FF - Fourier filter, MO - macroscopic objective.	22
5.1	Schematic for the computation of one step propagation via Symmetrized SSBM. . . .	28

6.1	Experimental properties of a zeroth-order even Mathieu beam. (A1) Transverse intensity and (A2) phase distribution in 15mm long SBN crystal. (A3) Cross section through the volume at the orientation indicate with dashed line in (A1).	30
6.2	Dimensional crossover based on increasing beam order of the Mathieu beam. Transverse intensity distributions of: (A) zeroth-order, (B) sixth-order, (C) eleventh-order and (D) fifteenth-order Mathieu beams.	30
6.3	Nonlinear discrete diffraction of zeroth-order Mathieu beam in dependence of the strength of the nonlinearity controlled by beam power P . First column presents simulated cross section through the volume at the orientation indicate with dashed line in (B1) for increasing beam powers. Second and third column presents simulated and experimentally observed intensity distributions at the back face of SBN 15mm long crystal. $P_0 = 10\mu\text{W}$	31
6.4	Switching discrete diffraction on curved paths based on the self-action of sixth-order even Mathieu beam: (A) simulated and (B) experimentally observed transverse intensity distributions at the crystal's back face. (C) Intensity profiles along the hyperbolic waveguide layers indicated in (B). $P_0 = 10\mu\text{W}$	32
6.5	Switching discrete diffraction on curved paths based on the self-action of eleventh-order even Mathieu beam: first row simulated and second experimentally observed transverse intensity distributions at the crystal's back face. $P_0 = 20\mu\text{W}$	33
6.6	Narrow Gaussian probe beam in Mathieu lattice potentials from: (A) Fig. 6.3 (A1); (B) Fig. 6.4 (A1) central waveguides; and (C) Fig. 6.4 (A1) purple waveguide layer.	33
6.7	The elliptic Mathieu beam characterized by the Poynting vector (indicated by arrows). (A1), (A2) numerically calculated intensity and phase, and (B1), (B2) intensity and phase experimentally observed of the elliptic Mathieu beam order $m = 10$, $q = 25$ and $a = 25\mu\text{m}$. (C) Numerical simulation of the 3D intensity distribution of initial ellipse of the elliptic Mathieu beam inside 20mm long SBN crystal.	35
6.8	Nonlinear self-action of elliptic Mathieu beam with increasing beam powers. The transverse intensity distributions of elliptic Mathieu beams ($a = 15\mu\text{m}$) at the back face of the SBN crystal, nonlinearly inscribed with increasing beam powers. (Top) numerical simulations (calculated Poynting vector indicated by arrows) compared with the (bottom) experimental results. $P_0 \approx 20\mu\text{W}$	36
6.9	Numerical simulation of the 3D intensity volume inside 20mm long SBN crystal. Fabrication of photonic structure (A) from Fig. 6.8 (A3) and (B) from Fig. 6.10 (A3).	37
6.10	Nonlinear self-action with increasing structure sizes a . Numerically calculated (top) and experimentally measured (bottom) transverse intensity distributions at the back face of the SBN crystal after nonlinear self-interacting propagation of elliptic Mathieu beams ($P \approx 20\mu\text{W}$), for beams with different structure sizes a . Arrows indicate the Poynting vector.	38
6.11	Characteristic of Mathieu lattice and elliptic vortex. (A) Intensity distribution for Mathieu lattice of order $m = 8$, ellipticity $q = 15$ and structure size $a = 90\mu\text{m}$ in the front face of the SBN crystal. (B), (C) Intensity and phase distributions of elliptic vortex in the front face of the SBN crystal.	39

6.12	Elliptical necklaces in Mathieu lattices with different ellipticity parameter q and topological charge $C_T = 1$. The input vortex beam is shown with the layout of the lattice beams indicated by open circles (the first column). The corresponding intensity distributions are shown at the exit crystal face in numerical results (second column) and experiment (third column). Numerical lattice intensity $I_{latt} = 0.3$, and input vortex intensity $I = 0.005$; the experimental lattice power $P_{latt} = 20\mu\text{W}$ and input vortex power $P = 8\mu\text{W}$	40
6.13	Stable elliptical necklaces in Mathieu lattices of different order m with ellipticity parameter $q = 0$ and topological charge $C_T = 1$: (A) $m = 9$, (B) $m = 10$, (C) $m = 11$, (D) $m = 12$	41
6.14	Multiple elliptical necklaces in Mathieu lattices of order $m = 8$ with ellipticity parameter $q = 0$ and topological charge $C_T = 1$: (A) The input vortex beam is shown with the layout of the lattice beams indicated by open circles. Numerically observed (B) phase and, (C) intensity distributions at the back face of the crystal. Numerical lattice intensity $I_{latt} = 0.3$, and input vortex intensity $I = 0.005$	41
6.15	Single- and multiple-charged elliptical necklaces. (A1) - (D1) Numerically observed intensity and (A2) - (D2) phase distributions. (A3) - (D3) experimentally observed intensity distributions at the back face of the crystal. The lattice ellipticity $q = 15$ and other parameters are as in Fig. 6.15.	42
6.16	Phase singularity separation. (A) Phase singularity separation versus C_T for various lattice ellipticity after 15mm propagation distance. (B) Phase singularity separation versus propagation distance for various C_T for $q = 15$ (Fig. 6.15). Separations are measured between the two singularities for lattice ellipticity as a Euclidean distance.	43
6.17	Dipole states in Mathieu lattices of various ellipticity (A) $q = 0$, (B) $q = 10$, and (C) $q = 15$. Intensity and phase distributions are presented after 10cm propagation. (D) Normalized z component of the angular momentum along the propagation distance. Other parameters are as in Fig. 6.12.	43
6.18	Nonlinear vortex propagation in Mathieu lattices. (A1), (B1) intensity distributions, (A2), (B2) corresponding phase distributions at the exit face of crystal obtained from numerical simulations, (A3), (B3) intensity distributions at the exit face of crystal experimentally obtained. Input vortex intensities in numerical simulation are (A1) $I=0.01$ and (B1) $I = 0.1$, with appropriate input vortex power in experiment (A3) $P = 20\mu\text{W}$ and (B3) $P = 30\mu\text{W}$	44
6.19	Interference of two MG beams of different order. Transverse intensity distribution obtained by interfering MG beams with the same parity: (A) both even $m_1 = 0$ and $m_2 = 10$; (B) both odd $m_1 = 1$ and $m_2 = 7$, or different parity: (C) $m_1 = 2$ and $m_2 = 7$ (D) $m_1 = 13$ and $m_2 = 14$	46
6.20	Interference of two MG beams of different order and phase configurations. Transverse intensity distribution of superimposing beams with the same parity: (A) $m_2 = 7$, $m_1 = 2$, π out of phase; (B) $m_2 = 2$, $m_1 = 7$, $\pi/2$ out of phase; (C) $m_2 = 13$, $m_1 = 14$, π out of phase; (D) $m_2 = 13$, $m_1 = 14$, $\pi/2$ out of phase.	46
6.21	Transverse interference patterns of two MG beams of the same order m , in-phase and oriented at 90° with respect to each other: even parity (A) $m = 2$; (B) $m = 8$; and odd parity (C) $m = 5$; (D) $m = 7$	47

6.22	Transverse interference patterns of two MG beams of the same order m oriented at 90° with respect to each other in π out of phase configurations: even parity (A) $m = 2$; (B) $m = 8$; and odd parity (C) $m = 5$; (D) $m = 7$	47
6.23	Interference of MG beams with same order at different mutual distances along x -axis: (A), (B) $m = 6$ and (C), (D) $m = 7$. First row: interference at mutual distance $D = 20\mu\text{m}$, second: doubled distance $2D$, and third: triple distance $3D$	48
6.24	Realization of aperiodic photonic lattices by multiplying the structure (A)-(D) from Fig. 6.19 (B) and (E)-(H) Fig. 6.22 (A) at various distances.	49
6.25	Various aperiodic photonic structures realized by multiplying (A) - (D) the structure from Fig. 6.23 (A2) and (E) - (H) the structure from Figs. 6.23 (C2) at different mutual distances.	50
6.26	Waveguiding in aperiodic photonic structures. As writing beam is used structure from: (A), (B): Fig. 6.24 (H); (D), (E): Fig. 6.25 (H). Intensity distribution of probe beam at the exit face of the crystal (C), (F).	51
6.27	Transverse intensity distribution of periodic and aperiodic lattices. (A) Aperiodic lattice created via MG beams, (B) typical unit cell, where the yellow arrows indicate the probe beam excitation sites. (C) Periodic square lattice with period d equal to the characteristic structure size $a = 2\pi/k_\perp$ of used MG beams, $d = a = 25\mu\text{m}$	52
6.28	Discrete diffraction and lattice solitons in an aperiodic photonic lattice. Numerically and experimentally observed transverse intensity distributions at the crystal's back face in linear regime (the first row) and two nonlinear regimes: (the second row) numerical probe beam intensity of $I = I_0 = 0.7$ and appropriate experimental beam power of $P_0 = 50\mu\text{W}$ and (the third row) numerical probe beam intensity of $2I_0$ and experimental beam power of $2P_0$	53
6.29	Averaged intensity distributions at the lattice output, for 100 different probe beam excitation sites, in (A) linear and (B), (C) nonlinear cases. (D1) and (D2) present averaged intensity profiles, taken along the horizontal and vertical transverse direction (indicated with the white lines in (A)), respectively. Parameters are as in Fig. 6.28.	54
6.30	Comparison between beam spreading in linear and two nonlinear regimes inside the aperiodic lattice and an appropriate periodic square lattice. Numerical simulation of averaged effective width (averaged over 100 excitation positions) along the propagation distance. ω_{in} is the initial effective width. Parameters are as in Fig. 6.28.	55
6.31	The transition from aperiodic Mathieu lattice to disorder lattices.	56
6.32	Numerical simulated averaged intensity distributions at the lattice output, for 60 different probe beam excitation sites and different disorder strength (A) - (F). (G) Averaged effective width along the propagation distance for different disorder strength. Lattice maximum intensity $I_{\text{latt}} = 0.5$	57
6.33	Numerical simulated results of averaged effective beam width of probe beam versus disorder strength after 2cm for different maximum lattice intensities.	58

Chapter 1

Introduction

Research in the field of photonics involves the overlap of three basic scientific disciplines that are leading in today's technological development: electronics, optics, and material physics. The results of such research are applicable in many fields, and during the years the scope and level of research and investment in this area are explosively increasing. The physics of semiconductors had the main role in information and communication technologies, but the advances are accomplished during the past decade by using a new class of materials - **photonic crystals** [1]. They are optical materials with a periodically modulated refractive index. According to the refractive index variations and period in space, there are one-dimensional (1D), and Bragg reflectors, dielectric mirrors, thin films, dielectric Fabry-Perot filters, etc.) are some of examples, two-dimensional (2D) e.g. commercially used holey fibers, and three-dimensional (3D) (Yablonovite, wood-pile, or opal geometry structures, etc.) photonic crystals. They have been used to control light propagation and emission. Because of their periodic nature, photonic crystals form allowed and forbidden photonic bands, the same as electronic bands in semiconductors. It is shown that light in photonic crystals propagates like an electron in semiconductors with periodic potential. Thus, photonic crystals can be considered analogs of semiconductor materials. Besides, photonic crystals are noticed in nature in different forms. But their artificial realization started from Lord Rayleigh, permit investigation of light propagation phenomena promising useful applications in other fields.

Photonic lattices are one of the realizations of photonic crystals, they represent optical waveguides with periodic changes in the refractive index of the medium, with low refractive index contrast. The studies about the photonic lattices are modeled by the paraxial equation formally identical to the Schrödinger equation, which describes crystal lattices of solid-state physics. In photonic lattices propagation coordinate z is equivalent to the time coordinate in the Schrödinger equation. Periodical refractive index change, provides photonic band gaps in photonic lattices. They are recognized as electronic band gaps of crystal lattices of solid-state physics where the periodic potential of the atoms leads to forbidden regions in the transmission spectrum. The photonic band gaps show forbidden regions for electromagnetic wave propagate.

An important feature of photonic lattices is the ability to manipulate light propagation in the direction of periodicity. In photonic lattices, phenomena analogous to phenomena from solid-state physics such as Bloch oscillations, Zener tunneling, Anderson localization, etc. are found. To increase the control opportunities of electromagnetic wave nonlinear optical materials e.g. nonlinear photorefractive crystals are used. In such materials light-matter interaction is established, allowing light to influence the optical properties of materials and thus the light itself. Due to the nonlinearity and periodic change of the refractive index in the photonic lattices, a competition of linear and nonlinear phenomena occurs and self-trapping lights, the appearance of spatial, or lattices solitons, modulation instabilities, etc. are observed in photonic lattices.

The optical induction technique allows the realization of different photonic lattices inside a photosensitive material. Photonic lattices, characterized by refractive index modulation in a certain direction opposite to translational invariance through the direction of propagation are frequently realized in different photorefractive crystals. **Nondiffracting beams** due to their propagation invariant transverse intensity distributions have been utilized in the realization of photonic lattices by optical induction technique. Their transverse spatial frequency components lie on a circle in the corresponding Fourier plane, to demonstrate their nondiffracting character [2]. They are exact solutions of the Helmholtz equation in different coordinate systems. Depending on the underlying real space coordinate system, mostly, four families of nondiffracting beams are used for optical induction of photonic lattices: in Cartesian coordinate system discrete nondiffracting beams (plane wave interference patterns i.e. discrete beams), in cylindrical coordinates Bessel beams, in elliptic cylindrical coordinate system Mathieu beams, and in parabolic cylindrical coordinates system parabolic beams. Besides nondiffracting character, they possess other peculiar characteristics like robustness and self-healing, and they had been used in different fields such as atomic optics, optical tweezers, nonlinear optics, etc.

Until now, different researches about photonic lattices as well as control and manipulation of light in photonic lattices are done. In periodic photonic lattices, it is shown that control of light propagation is determined by bandgap properties [3]. The discrete diffraction behavior of the evanescently coupled waveguide arrays (1D periodic waveguide arrays) was examined first. In weakly guiding waveguides the light was readily confined at discrete sites, or light would be exchanged through waveguides via coupling during propagation. When only one waveguide is initially excited by light, diffraction is different from that occurring in continuous systems, the most of the light energy is carried out along two major lobes far from the center excited waveguide. This diffraction pattern today is known as discrete diffraction [4]. Also, discrete diffraction is observed in two-dimensional photonic lattices [5]. The optical solitons in waveguide arrays are explained as a balance between nonlinearity of waveguides and discrete diffraction effects arising from linear coupling among adjacent waveguides [6, 7]. Light is nonlinearly confined in a few waveguides and it can propagate diffractionless. Optical discrete solitons in two-dimensional nonlinear waveguide lattices were observed in photorefractive crystals [5, 8].

Research in the field of photonics has been extended from the periodic lattices and the propagation of light in them to the study of disordered photonic structures [9, 10] and deterministic aperiodic structures, which are at the transition between periodic and disordered structures [11]. Disorder in photonic systems creates weak or strong localization of light, known as Anderson localization and coherent backscattering [12, 13, 14]. **Deterministic aperiodic structures**, discovered 1984, are the structures with fifth-order symmetry, which was considered nonexistent in crystals, and a long-range order that was considered nonexistent in amorphous bodies [15]. When quasicrystals are found in solid-state physics, many new research fields are open in optics and photonics [16, 17, 18]. Quasicrystals are unique structures that can be viewed as extensions of the periodic crystal concept in which translational symmetry is replaced by long-range order. Sharp diffraction patterns confirm the existence of wave interference as a consequence of long-range order [19]. They do not have translational symmetry, so it is not possible to define a unit cell. However, due to the long-range order, phenomena characteristic for periodic structures, such as Bragg diffraction, are observed in quasicrystals. They can be formed by a substitution paving rule based on two or more building blocks. The most famous example of these structures is the Penrose lattice, and over time various other schemes have been developed to form new kinds of quasicrystals (Fibonacci, Thue-Morse, Rudin-Shapiro, etc.).

Light control is crucial for many scientific fields from classical nonlinear optics to plasma physics, Bose-Einstein condensate, solid-state physics, and recently in information technology. The leading trend is the search for optical analogs for electronically integrated circuits that enable routing, control, and processing of optical signals. Deterministic aperiodic photonic structures are appropriate for the control and manipulation of light and future utilization in optical devices. Control and manipulation of light in such specially designed structures is an active topic of research in optic and photonics.

The realization of various aperiodic structures and their further investigation are some of the main motivations for research in this thesis. The versatility of aperiodic structures is very important and provides considerable flexibility and richness in modeling the optical response. Propagation of light in such structures is still an exciting area for researchers and essential for the application of future devices. Nondiffracting Mathieu beams are outstanding candidates for the creation of new aperiodic photonic lattices. The interference of Mathieu beams in a different spatial disposition one to another provides an approach realization of aperiodic patterns and their optical induction in photosensitive media to induce aperiodic lattice. Moreover, further examination of light propagation in these aperiodic lattices in the linear and nonlinear regimes is one of the main topics in this thesis.

Straight waveguides were the first and simplest step for the examination of light propagation. Further, waveguides with bending in the longitudinal direction, periodically oscillating waveguides, or chiral waveguides have been realized and manipulation of light propagation was examined in some of them [20, 21, 22]. Two-dimensional twisted lattices still are a challenge in experimental realization and this is a very appealing area of research. They require compound experimental setup, longer experimental realization time, or expensive equipment. The realization of chiral structures using the optical induction technique and Mathieu beams is the motivation for research in this thesis. Elliptical Mathieu beams would be investigated in different nonlinear regimes to inspect if they can create stable or dynamic structures. The realization of 2D twisted dynamic structures inside nonlinear photorefractive crystal via elliptical Mathieu beams would be a substantial contribution to the simplify realization of chiral lattices by optical induction.

Chapter 2

Photonic lattices

Photonic crystals exist in nature, however, they can be realized artificial. Resulting in previous research their properties are a great replacement for semiconductors. Researchers around the world investigate the propagation of electromagnetic waves in photonic crystals as well as the potential application of photonic crystals in technological development. Photonic crystal fibers. i.e holey fibers and photonic lattices are some of the realizations of photonic crystals. Holey fibers are applied in many areas like fiber-optic communications, fiber lasers, nonlinear devices, etc., therefore, already present in our everyday life.

Photonic lattices are artificial structures with periodical refractive index modulation, with low contrast of refractive index compared to photonic crystals. 1D photonic waveguides are periodic in one transversal direction and invariant through the longitudinal direction, 2D photonic lattices are characterized by periodical modulation in both transversal directions and invariant through the longitudinal direction, while 3D photonic lattices have periodically modulation in whole three dimensions. Propagation of light differs in photonic lattices then in homogeneous media, so they are powerful tools to manipulate light propagation. Many new phenomena, like discrete diffraction, lattice and gap solitons, harmonic generation, stimulated scattering etc. are allowed in them.

According to many examinations about photonic lattices, which possess Brillouin zones, allowed and forbidden bands, and so on, it is observed analogous between light propagation in photonic lattices and motion of electrons in semiconductors [23]. Electromagnetic wave propagates in photonic lattices the same as electron in crystal lattices of solid-state physics. Many experimental studies of photonic lattices are done to prove and other phenomena predicted by quantum mechanics like Bloch oscillations [24], Zener tunneling [25] and Anderson localization [13]. Investigation of light propagation in photonic lattices is explained by the paraxial equation which is the analog of the quantum-mechanical Schrödinger equation but time coordinate is replaced with propagation coordinate z [26].

In the past, various periodic photonic structures have been exploited to control the propagation properties of electromagnetic waves. 1D arrays of evanescently coupled optical waveguides are created with an equal distance between waveguides, with all characteristics of a photonic crystal structure (Brillouin zones, band structure, etc.) [27]. In such systems (Fig. 2.1 (A1)), light couples between waveguides through tunneling, showing its diffraction characteristics. When low-intensity light is injected into one or a few neighboring waveguides, it couples to more and more further waveguides, broadening its spatial distribution. This is a new physical effect in comparison to diffraction in homogeneous media. In the linear regime, light diffracts from inner excited waveguide to outer waveguides. This characteristic diffraction pattern is known as *discrete diffraction* and the same effect is observed in both 1D and 2D periodic photonic lattices as shown in Fig. 2.1 [7, 27, 28].

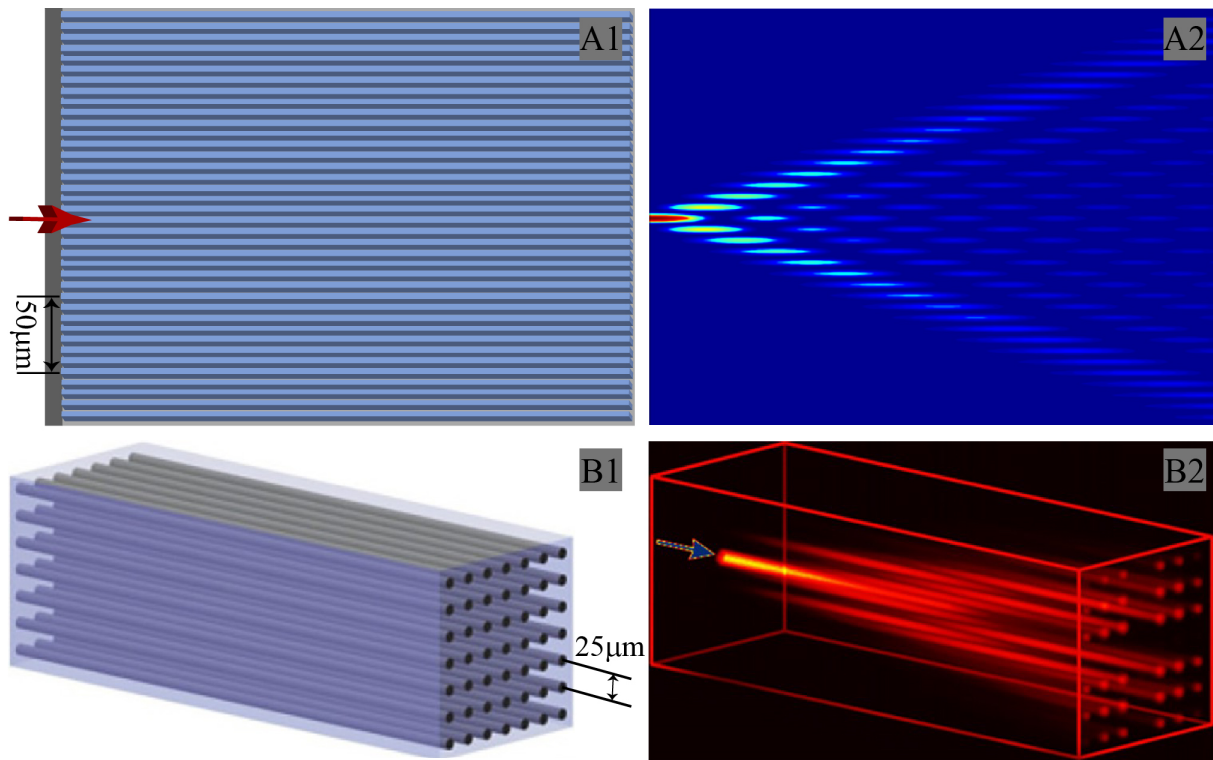


Figure 2.1: Discrete diffraction in (A) 1D arrays of evanescently coupled optical waveguides [3] (B) 2D periodic photonic lattices [29].

Nonlinear optic, as an active research area includes fundamental studies of light-matter interactions to numerous optical applications. The high-intensity light of the probe beam produces nonlinear responses of light in photosensitive material. When high-intensity light excites into one or a few neighboring waveguides light diffraction is confined with the nonlinearity of media and *spatial* and *lattice solitons* were achieved in 1D and 2D periodic photonic lattices [3, 30, 31].

Propagation of light in periodic lattices results in many fascinating effects but using disorder lattices and photonic quasi-crystals, which are in between periodic and disorder structures, the new fields of research are opened. In the last decade's examination of **disorder photonic lattices** acquire the attention. Since the first experimental observation of Anderson localization, new investigations about the Anderson localization in disorder systems were revealed like Anderson localization of light near boundaries of disorder lattices or dimensionality switching and with the continuous transformation of the lattice structure from one-dimensional to two-dimensional were done [9, 32, 33, 34, 35].

Examination of light propagation in photonic quasi-crystals, and **deterministic aperiodic structures** like Penrose quasicrystals, Fibonacci arrays, Thue-Morse, Rudin-Shapiro sequences, Vogel lattice etc. [16, 19, 36, 11], extensively increase. Localization of light is observed in some of them. The quasi-crystals with the increasing disorder as well as light propagation in them were examined. In such structures, light localization is observed, while enhancing wave transport was established. However, new approaches for the realization of different aperiodic lattices and light expansion in them is still an open question in optics. Such researches would provide fundamental explanations of light transport in aperiodic lattices.

2.1 Photonic lattices and the optical induction technique

There are several methods used for the experimental realization of photonic lattices, like waveguides detached in semiconductors [37], lithography, lattices optically induced in photosensitive media [8], laser-written arrays in silica [38] etc.

The optical induction technique is significant because allows an arbitrary structuring of photorefractive materials and fast and simple erase of such structures with white light. By this technique, it is possible to generate different photonic lattices: periodic, aperiodic, or disordered for fundamental investigations of wave propagation in such structures. The basic idea of the optical induction technique is to modulate the refractive index of nonlinear material by external illumination (photorefractive effect). By spatial light modulator, the linearly polarized light wave (lattice beam) is spatially modulated. Thus, refractive index modulation into the biased photosensitive crystal is induced and photonic lattices is generated into the crystal. Such photonic lattices are suited for study of additional probe beam propagation.

Some of the photorefractive materials, such as strontium barium niobate crystal SBN crystal, show a strong polarization anisotropy, where the strength of the nonlinearity is dependent on a light wave polarization (equivalently the corresponding electro-optic coefficient) [39]. Ordinary polarized light wave in SBN propagates in an effectively linear regime, does not show any self-action, but induces the required refractive index modulation i.e. photonic lattices. An extraordinary polarized light wave, in general, used as a probe beam, feels different nonlinear response of such crystal in the dependency of the beam power (nonlinearity strength). For low-intensity, probe beam feels low nonlinearity strength, while if the intensity of the probe beam is sufficiently increased, it modifies the refractive index and propagates nonlinearly through crystal. Photonic lattices, optically induced in SBN crystal, are used for studying linear and nonlinear propagation effects in dependency on the probe beam power.

In order to achieve desired 1D or 2D photonic structures using the optical induction technique, the transversally periodic intensity distribution, invariant along the propagation directions are used. *Nondiffracting beams* are convenient for the realization of photonic lattices by optical induction technique due to their transverse-invariant propagation. They can conveyance their intensity distribution to the complete length of the photorefractive crystals. Nondiffracting beams are used for optically induction of different periodic structures (strip, square, diamond, hexagonal, etc. patterns), a new class of photonic structures like Bessel, Mathieu, or Weber lattices, quasi-periodic Penrose lattice, or deterministic aperiodic structures like Vogel or Fibonacci lattices, etc. Also, three-dimensional periodical lattices and helical structures are produced by using nondiffracting beams and reconfigurable optical induction method [40, 41]. Mathieu beams are one of the nondiffracting beams with diversity intensity distribution. So far such beams are only in few realization of photonic lattices. In this thesis, Mathieu beams would be examined for optical induction of different photonic lattices.

Chapter 3

Nondiffracting beams

Nondiffracting beams are monochromatic optical fields with propagation-invariant transverse intensity distributions. The term nondiffracting beam was introduced by Durnin in 1987 for the propagation in vacuum [42]. They were examined as exact solutions of the homogeneous Helmholtz equation in different coordinate systems [42, 43, 44]. Nondiffracting beams were obtained in the system of the cylindrical coordinates under the limitation that their complex amplitude is separable as the product of the functions which depend on the transverse coordinates and propagation coordinate [42]. The transverse amplitude profile of such beams was mathematically described by the Bessel functions and they are named Bessel beams. Later, different kinds of nondiffracting beams were introduced [45, 46] and their properties and applications are examined.

Nondiffracting beams with finite energy are reviled bounded or by the homogeneously transmitting aperture of finite dimensions or by the Gaussian aperture, known as **pseudo-nondiffracting beams**. Numerically and experimentally investigations show that the nondiffracting and pseudo-nondiffracting beams own the sharp δ -like angular spectrum, represented by a circle in the Fourier plane, which proves their propagation-invariant character [47]. Propagation-invariant characteristics of such beams make them useful in optical micromanipulation [48], nonlinear optics [8, 3], wireless communication, etc.

Beside completely eliminated diffraction of the such beams, additional properties, helpful for potential applications are detected. One highly valuable property is the robustness of the nondiffracting beams [49, 50]. It was shown that the nondiffracting beam shows the resistance of the against amplitude and phase distortions, also they are able to regenerate its intensity profile to the original form in the free propagation behind the nontransparent obstacle [51], verified by the simple experiment [47]. Nondiffracting beams also possess a self-reconstruction ability (The Talbot effect and self-imaging) [52]. Efficient methods of generating nondiffracting beams require the use of the computer-generated holograms [53], the axicon [54] or the programmable spatial light modulators [55].

Two-dimensional scalar time-independent Helmholtz equation:

$$\nabla_t^2 U(x, y) + k_t^2 U(x, y) = 0 \quad (3.0.1)$$

is separable in 11 coordinate systems but admits separation into the transverse and longitudinal parts only in four coordinate systems: **Cartesian**, **circular cylindrical**, **elliptical cylindrical**, and **parabolic cylindrical** coordinates [2]. Each of these coordinate systems gives rise to a certain type of nondiffracting beam such as **discrete** (plane wave and superposition of plane waves), **Bessel**, **Mathieu**, and **Parabolic beams**, respectively.

Periodic intensity patterns are generated as a superposition of the plane waves. Plane waves whose transverse Fourier components are located on the same ring determined by their wave vectors,

create stationary intensity distribution along the propagation direction. One dimensional periodic intensity distribution would be achieved if two plane waves have interfered, also two-dimensional periodic (square, hexagonal, etc.) intensity can be created by the superposition of multiple plane waves [40, 56, 8]. Moreover, quasiperiodic pattern e.g. Penrose lattice is generated with the superposition of five plane waves [19, 57, 58, 59].

By transforming and solving the Helmholtz EQ. (3.0.1) in circular cylindrical coordinates Bessel beams are obtained and their transverse intensity distributions are characterized by concentric rings [42]. Fig. 3.1 (A) depicts a zero-order Bessel beam. In recent studies, Bessel beams were applied to induce periodic lattices, and even 2D Fibonacci lattices [60].

Mathieu beams are solutions of the Helmholtz equation in the elliptical coordinates system [45]. Their transverse intensity distribution consists of discrete spots along elliptic or hyperbolic paths. The numerically calculated transverse intensity distribution for the fourth-order Mathieu beam is shown in Fig. 3.1 (B).

Parabolic beams are the fourth family of nondiffracting beams. They are the solution of the Helmholtz equation in the parabolic cylindrical coordinate system [46]. In Fig. 3.1 (C) transverse intensity distribution of the Parabolic beam with continuous parameter $a = 0$ is depicted.

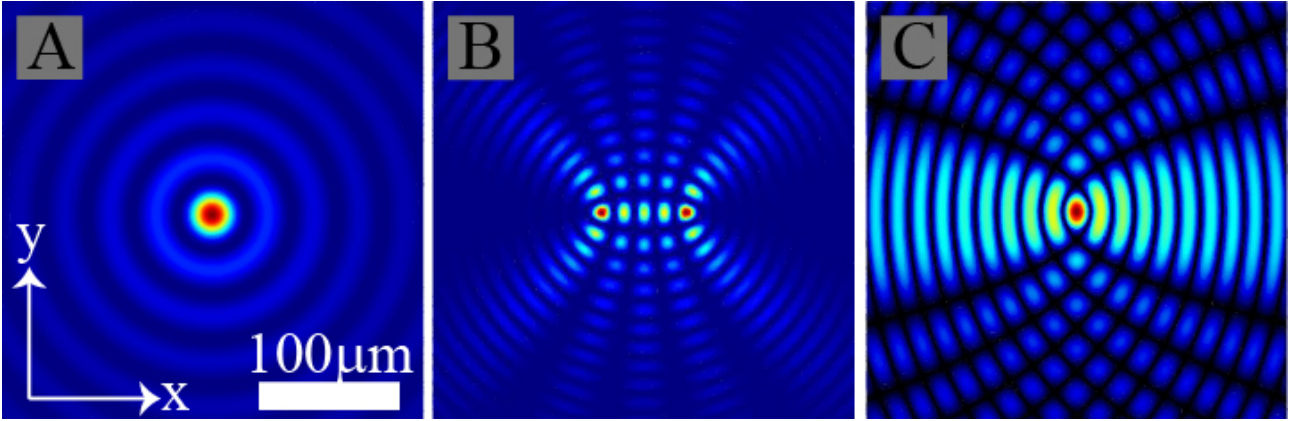


Figure 3.1: Intensity distributions of (A) Bessel, (B) Mathieu and (C) Parabolic nondiffracting beams.

3.1 Mathieu functions

Plenty of scientific and engineering problems lead to differential equations of the Mathieu type. Solutions of these equations are known as Mathieu functions. First, they are analyzed by Mathieu in 1868 [61]. Later these functions were further investigated in numerous investigations like the motion of an electron in a one-dimensional potential [62], wave propagation in periodic structure [63], analysis of vibrating modes in the elliptical membrane [64], or used for the formulation of invariant optical fields [45].

Mathieu equations originate from the separation of Helmholtz equation in elliptical cylindrical coordinates. By transformation rectangular coordinates (x, y) to elliptical cylindrical coordinates (ξ, η) by coordinate transformation

$$x + iy = f \cosh(\xi + i\eta) \quad (3.1.2)$$

$(x = f \cosh(\xi) \cos(\eta), y = f \sinh(\xi) \sin(\eta))$ with corresponding Laplacian transformation EQ. (3.0.1)

is transformed to the *two-dimensional Helmholtz equation in elliptic coordinates*

$$\left[\partial_{\xi}^2 + \partial_{\eta}^2 + \frac{f^2 k_t^2}{2} \cos(2\xi) - \cos(2\eta) \right] U(\xi, \eta) = 0. \quad (3.1.3)$$

The solutions of EQ. (3.1.3) are separable as the product of the functions which depend on the elliptical cylindrical coordinates (ξ, η) as $U(\xi, \eta) = R(\xi)A(\eta)$. The functions $R(\xi)$ and $A(\eta)$ must satisfy the equations

$$\left[d_{\xi}^2 + (a - 2q \cosh(2\xi)) \right] R(\xi) = 0, \quad (3.1.4)$$

$$\left[d_{\eta}^2 + (a - 2q \cos(2\eta)) \right] A(\eta) = 0. \quad (3.1.5)$$

where q is a dimensionless parameter related to the transverse propagation constant k_t as $q = \frac{f^2 k_t^2}{4}$, where f is semi-focal distance and a is the separation constant arising from the separation of variables method.

In physics and engineering literature EQs. (3.1.4) and (3.1.5) are known as *the Radial Mathieu Equation*, and *the Angular Mathieu Equation*, respectively. Their solutions are **the Radial Mathieu Functions** and **the Angular Mathieu Functions**. This nomenclature originates from the similarity between elliptical (ξ, η) and polar coordinates: the elliptic variable η has a domain $0 \leq \eta < 2\pi$ and plays a similar role to a polar angle, whereas the variable ξ , with domain $0 \leq \xi < \infty$ behaves as a radial variable (Fig. 3.2).

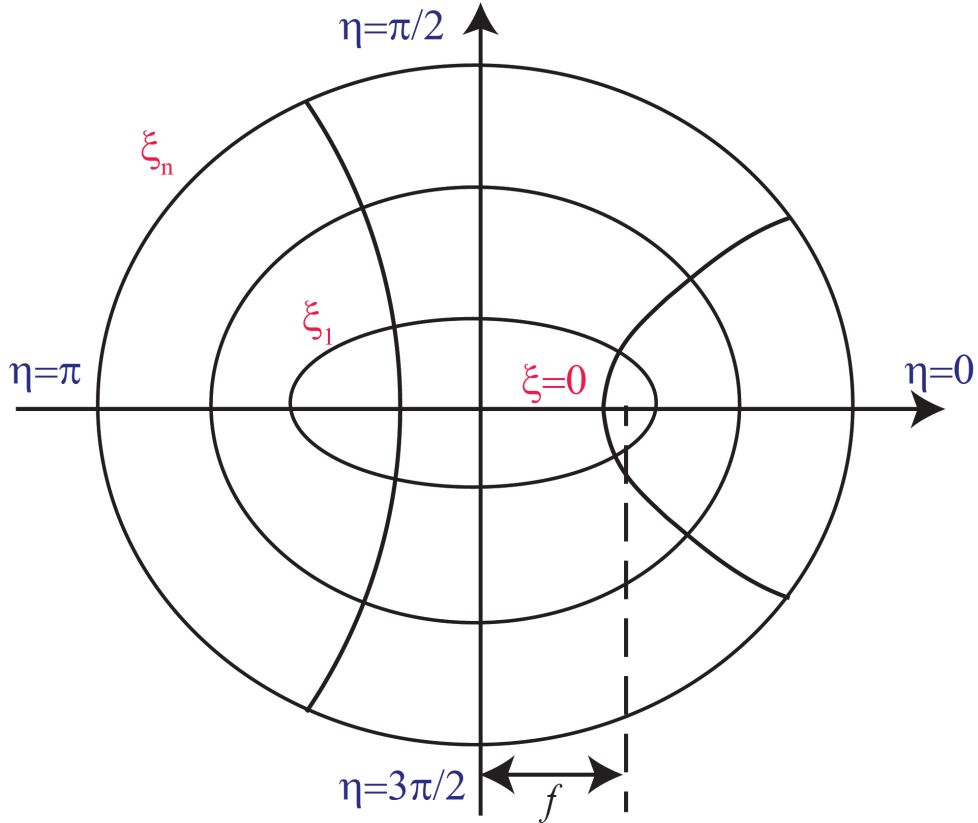


Figure 3.2: Elliptic coordinate system. Curves $\xi = \text{constant}$ are confocal ellipses, curves $\eta = \text{constant}$ are orthogonal hyperbolas; $0 \leq \eta < 2\pi$, $0 \leq \xi < \infty$. For limit $f \rightarrow 0$ polar coordinates are review.

In this thesis, Mathieu functions are used to create an enormous family of Mathieu nondiffracting beams.

3.2 Mathieu nondiffracting beams

Among diverse families of nondiffracting beams, Mathieu beams may be interpreted as a generalized beam class, which interpolate between Cartesian and spherical coordinates [45, 46, 65, 66]. Their transverse spatial intensity distributions can form paths on ellipses or hyperbola. Mathieu functions are used for mathematical observation of Mathieu beams.

Single Mathieu beams of order m are mathematically described by a product of Radial and Angular Mathieu functions of order m , introduced in the previous section. Single Mathieu beams have two parity: *even* (e) and *odd* (o) represented as [67]

$$M_m^e(\xi, \eta) = C_m(q) J_{em}(\xi; q) c_{em}(\eta; q), \quad (3.2.6)$$

$$M_m^o(\xi, \eta) = S_m(q) J_{om}(\xi; q) s_{em}(\eta; q). \quad (3.2.7)$$

where $C_m(q)$ and $S_m(q)$ are weighting constants, depend on *parameter of ellipticity* $q = \frac{f^2 k_t^2}{4}$ related with position f of the two foci and transverse wave number $k_t = 2\pi/a$, where a is *characteristic beams size*. J_{em} and J_{om} are even and odd Radial Mathieu functions of order m , and ellipticity q . c_{em} and s_{em} are even and odd Angular Mathieu functions of order m , and ellipticity q .

Order of even Mathieu beams starts from zero, in contrast, odd Mathieu beams starts from order one. In Figs. 3.3 and 3.4 there are shown even and odd Mathieu beams of different order m , with the same parameter of ellipticity $q = 25$, and characteristic structure size $a = 25\mu\text{m}$. As the order of Mathieu beams increases, intensity distributions become more complex, because they are separated in compound sites arranged over different paths straight or curved lines.

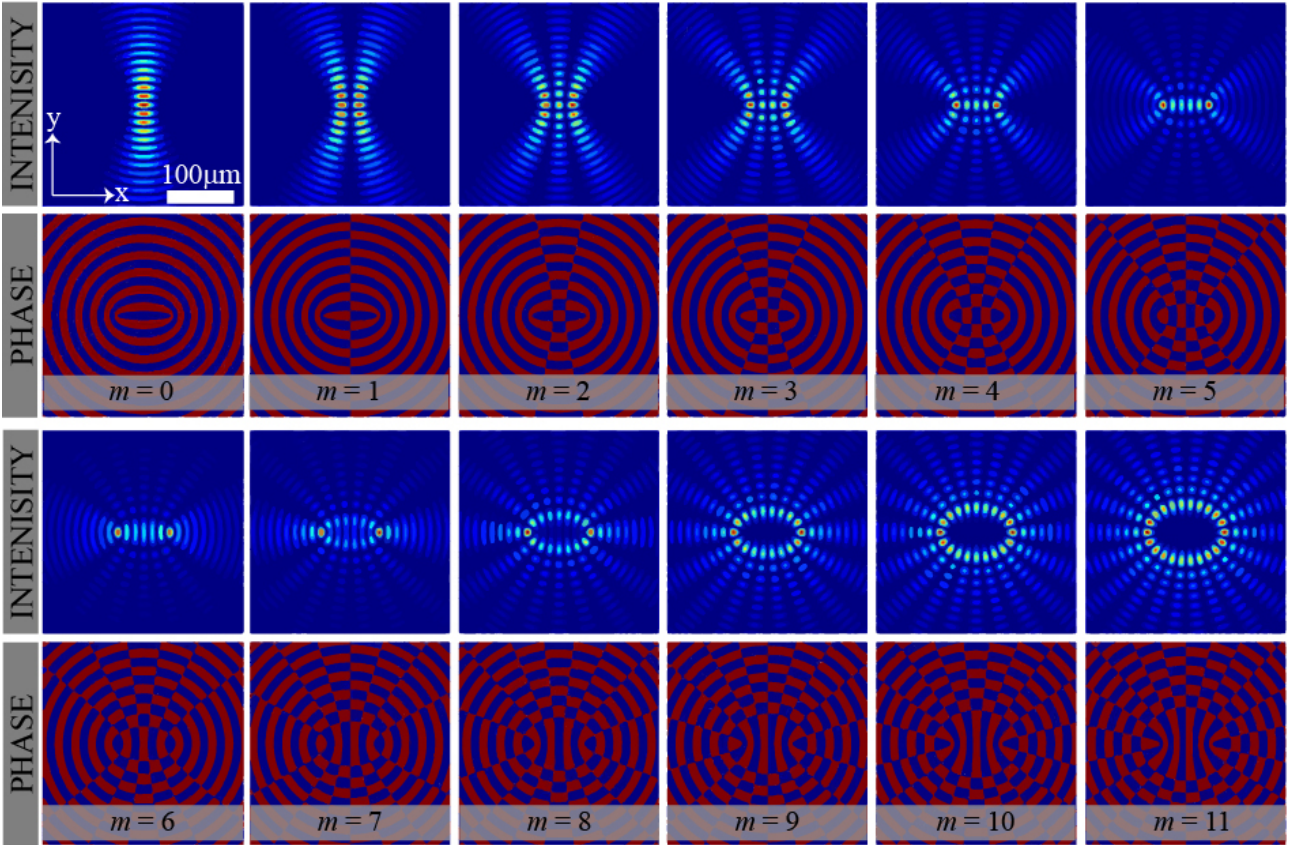


Figure 3.3: Intensity and phase distribution of *even Mathieu beams* of different order m , with same parameter of ellipticity $q = 25$, and characteristic structure size $a = 25\mu\text{m}$.

Mathieu beams rely on the elliptic cylindrical coordinate system, which is reflected in their transverse intensity and phase distributions. From phase distributions shown in Figs. 3.3 and 3.4, separate regions of different phases values on the ellipses and hyperbolas with joint foci are noticeable, therefore the elliptical character of Mathieu beams displayed.

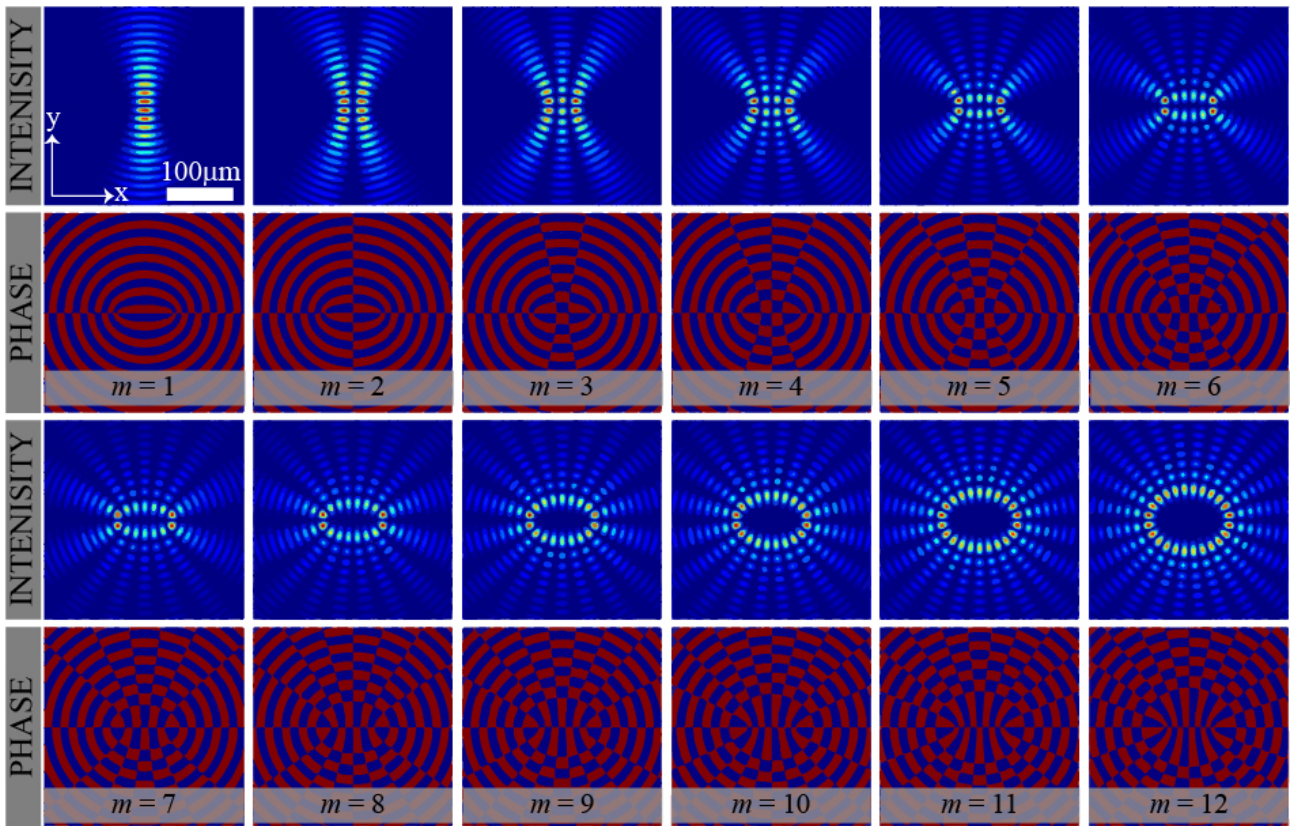


Figure 3.4: Intensity and phase distribution of *odd Mathieu beams* of different order m , with same parameter of ellipticity q , and same characteristic structure size $a = 25\mu\text{m}$.

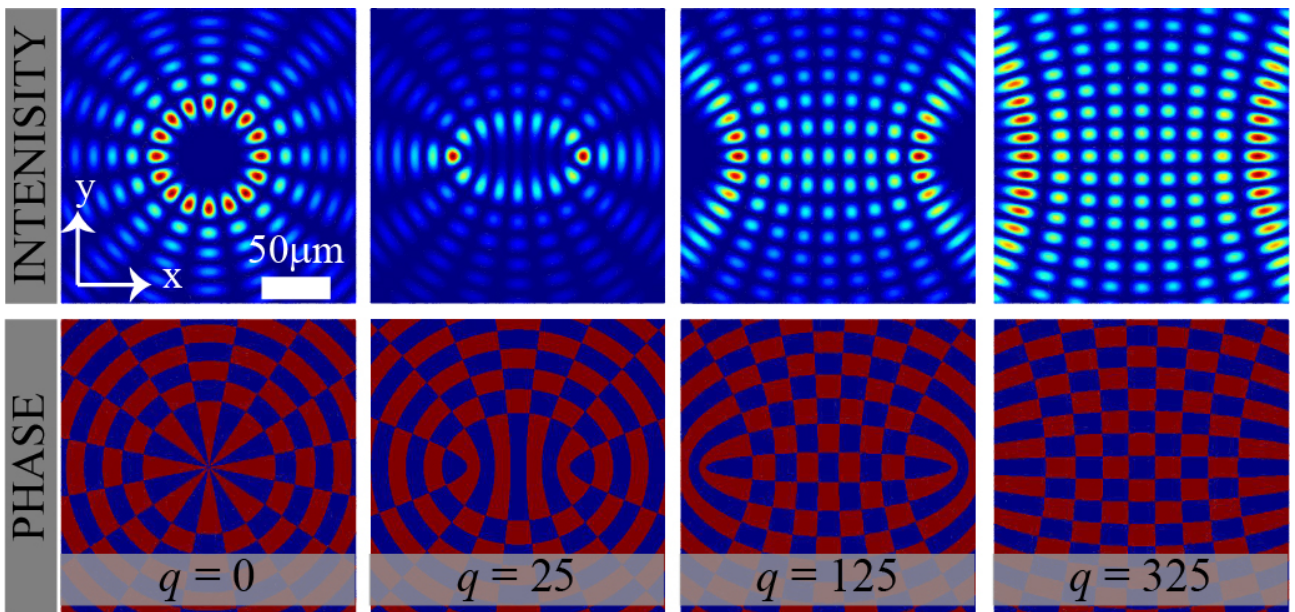


Figure 3.5: Intensity and phase distribution of even Mathieu beam of order $m = 8$, with characteristic structure size $a = 25\mu\text{m}$ and different parameter of ellipticity q .

Parameter of ellipticity changes the shape of Mathieu beam. The shape of even Mathieu beam of order $m = 8$ and structure size $a = 25\mu\text{m}$ is examined according to increasing different values of ellipticity $q = [0, 25, 125, 325]$ as depicted in Fig. 3.5 while characteristic structure size a influence on the size of Mathieu beams.

Next, the influence of beams size a is examined. Even Mathieu beam of order $m = 4$ and ellipticity $q = 25$ for different structure sizes $a = [6.25, 12.5, 25, 50]\mu\text{m}$ are depicted in Fig. 3.6. While the characteristic size of Mathieu beams increases, the distance between the sites increases too.

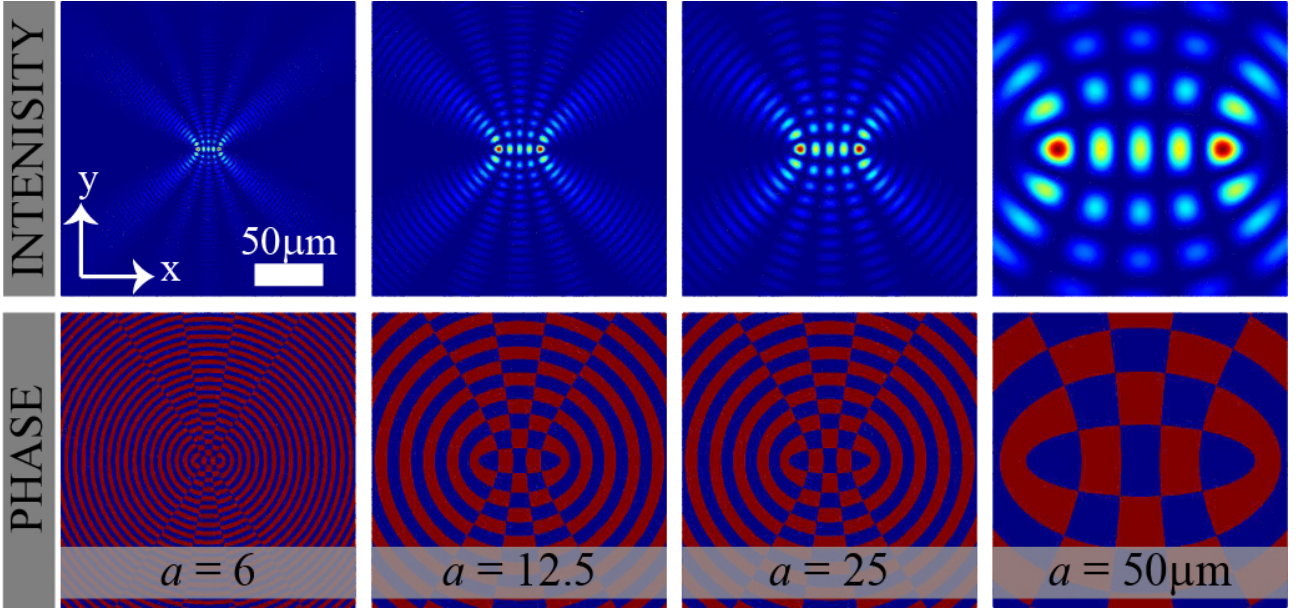


Figure 3.6: Intensity and phase distribution of even Mathieu beam of order $m = 4$, with parameter of ellipticity $q = 25$ and different characteristic structure size a .

A complex superposition of even and odd Mathieu beams of the same order m represents *elliptic Mathieu (ELM) beams* which intensity and phase distribution are shown in Fig. 3.7. For a monochromatic, scalar elliptic Mathieu beam of order m , the light field is given by

$$ELM(\xi, \eta) = M_m^e + iM_m^o. \quad (3.2.8)$$

The transversal intensity distributions of elliptic Mathieu beams are distinguished by a series concentric ellipses, while the phase distributions are continuously modulated along ellipses.

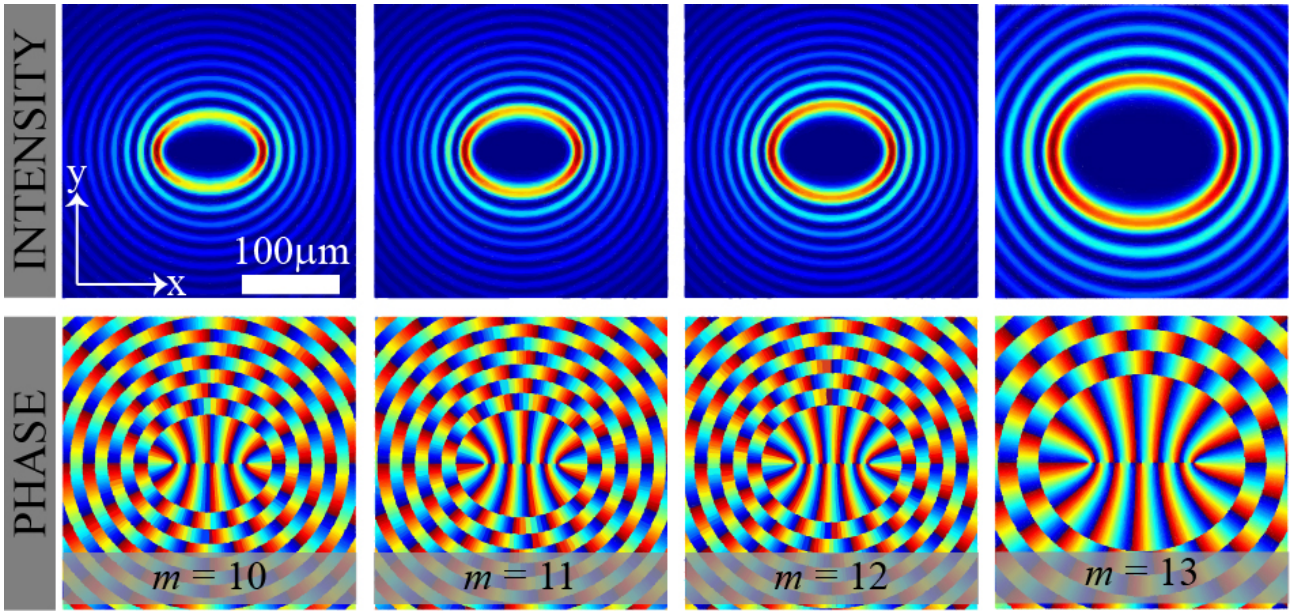


Figure 3.7: Intensity and phase distribution of *elliptic Mathieu beams* of different order m , with same parameter of ellipticity q , and same characteristic structure size $a=25\mu m$.

A complex superposition of even Mathieu beams of order m and odd Mathieu beams of the order $(m + 1)$ represents *hyperbolic Mathieu beams* which intensity and phase distribution are shown in Fig. 3.8.

$$HyM(\xi, \eta) = M_m^e + iM_{m+1}^o \quad (3.2.9)$$

The transversal intensity distributions of Hyperbolic Mathieu beams are distinguished by a series of hyperbolas, while the phase distributions are continuously modulated along hyperbolas.

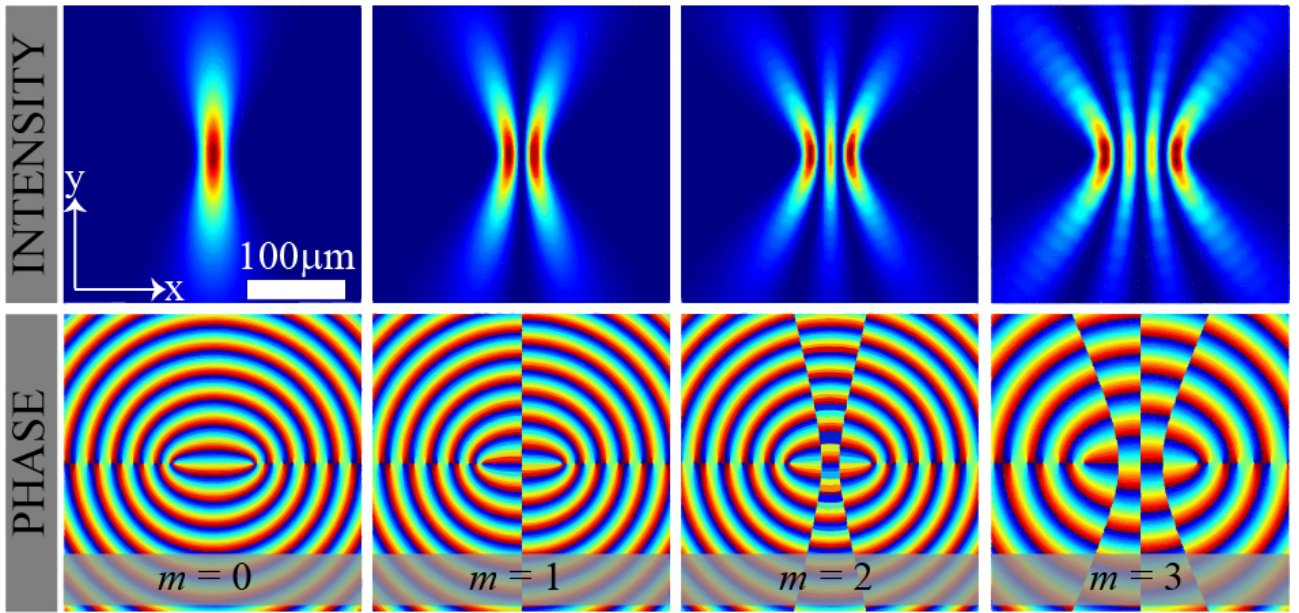


Figure 3.8: Intensity and phase distribution of *Hyperbolic Mathieu beams* of different order m , with same parameter of ellipticity q , and same characteristic structure size $a=25\mu m$.

Scalar even and odd Mathieu beams exhibit only real-valued field distributions, therefore their transverse Poynting vector vanishes. In contrast, the elliptic Mathieu beams are complex spatial modulated beams, owing to the occurrence as a complex superposition of even and odd Mathieu beam of the same order, showing outstanding continuously modulated spatial phase distributions, i.e., orbital angular momentum [66, 68, 69]. Thus, for these beams a transverse energy flow is present, described by their Poynting vector.

Chapter 4

Experimental methods for photonic lattices generation and light propagation in photonic lattices

In this thesis, nondiffracting Mathieu beams are used as light fields for optical induction of refractive index modulations in 15mm or 20mm long photorefractive SBN crystal. Moreover, linear and nonlinear propagation of single Mathieu beams and elliptical Mathieu beams is investigated in such crystal.

This chapter presents mechanisms of photorefractive effect and refractive index modulation in photorefractive SBN crystal. Two experimental realizations are illustrated, one for experimental realization of photonic Mathieu lattices by optical induction, and the other for experimental investigation linear and nonlinear light propagation of the probe beam (plane wave, Gaussian or elliptical vortex) in such photonic lattices optically induced in a nonlinear photorefractive SBN crystal.

4.1 Photorefractive effect

Photorefractive optics is a field of nonlinear optics important in scientific research as well as in technological applications. This field of physics studies the phenomena associated with the propagation of laser beams in nonlinear photorefractive materials. Photorefractive materials have been known for 40 years. Mostly, these are translucent and anisotropic ferroelectric crystals pure or with certain impurities whose energy states are in between the valence and the conduction band. Impurities are select to be acceptors or donors for the crystal. When the photorefractive crystal is illuminated with the light of the appropriate wavelength some of the electrons or holes from donors or acceptors are photoionized and they elevate from the valence to the conduction zone (Fig. 4.1). Free electrons and holes are generated in illuminated areas. Diffusion or drift can affect the movement of charges in the conduction zone.

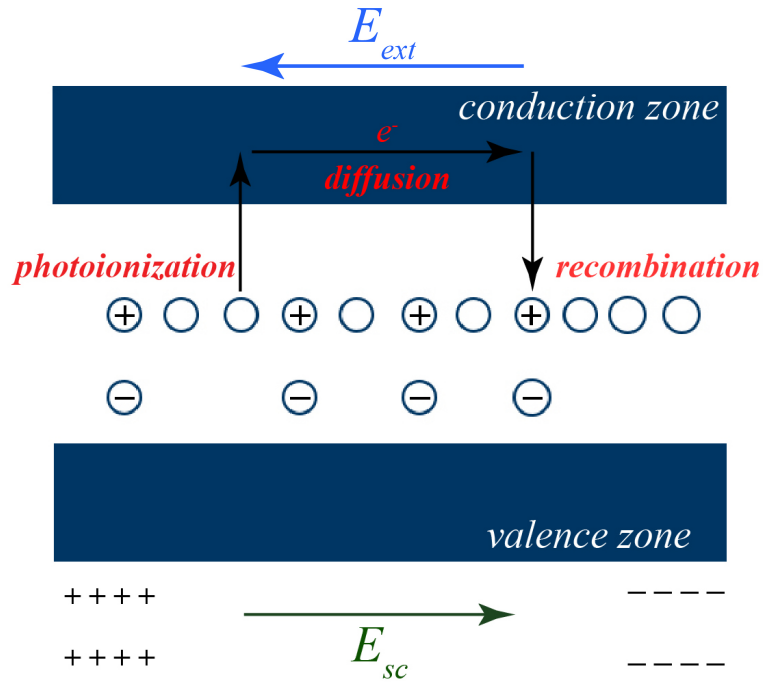


Figure 4.1: Illustration of photorefractive effect.

In diffusion, mechanism charges are recombined with empty donors or traps. Static space-charge field E_{sc} is build up by such recombination process, This space charge field creates the refractive index modulation via the linear electro-optic effect (the Pockels effect). The strength of the refractive index modulation depends on the illumination intensity and the intrinsic parameters of the crystal.

The second mechanism for index modulation is the drift. Opposite to the diffusion, the drift occurs only if an external electric field is applied to the crystal. Excited electrons and holes are accelerated by the external field and move until the force created with the external field is compensated by the internal field, which is created by the resulting inhomogeneous charge distribution. Electrons are more drifted then holes. Drift distance of electrons depends on the external field. In general, a combination of both effects exists with an external field, but in this thesis, drift effect is much stronger than diffusion, hence the effects of diffusion mechanism would be neglected is some examinations.

The photorefractive effect has several distinctive properties: dependence of doped element, it is the highly sensitive effect (observed at low light intensities), slow effect (depend on the light intensity, doped element mobility, and external field intensity). In some photorefractive materials, the refractive index modulation is highly persistent in the dark. Also, the refractive index modulation is erasable by homogenous illumination like LED light or high temperature, without crystals damaged.

The photorefractive effect is found in several classes of electro-optic materials such as barium titanate ($BaTiO_3$), lithium niobate ($LiNbO_3$), zinc telluride ($ZnTe$), potassium niobate ($KNbO_3$), strontium barium niobate (SBN), organic photorefractive materials, certain photopolymers, and some multiple quantum well structures. Such crystals are used for frequency filtering in the field of mobile communications, as electro-optic modulators, in nonlinear photonics, etc. In photorefractive crystals, holograms [70] or photonic lattices [39, 8] are formed.

4.1.1 The linear electro-optic effect

The photorefractive effect depends on the linear electro-optic effect i.e. Pockels effect as mentioned in the previous section. This effect describes the change of the refractive index of a material induced by the presence of a static electric field E_{sc} [71, 72, 73]. This is a second-order nonlinear effect related to second-order nonlinear susceptibility. The refractive index change is described by the impermeability tensor $\hat{\eta}$ i.e. the inverse of the dielectric permittivity tensor $\hat{\epsilon}$ as

$$\Delta\hat{\eta}_{i,j} = \Delta\hat{\epsilon}^{-1} = \Delta \left(\frac{1}{n_0^2} \right)_{i,j} = \sum_{k=1}^3 r_{i,j,k} E_k^{sc} \quad (4.1.1)$$

where, $r_{i,j,k}$ is the linear electro-optic tensor, E_k^{sc} is the applied electric field and $k, i, j = 1, 2, 3$ (or x, y, z). The dielectric permittivity tensor $\hat{\epsilon}$ is a symmetric tensor of rank 2 (matrix 3 x 3)

$$\hat{\epsilon} = \epsilon_0 n_0^2 = \epsilon_0 \begin{bmatrix} (n_0^o)^2 & 0 & 0 \\ 0 & (n_0^o)^2 & 0 \\ 0 & 0 & (n_0^e)^2 \end{bmatrix}, \quad (4.1.2)$$

$$\hat{\eta} n_0^2 = 1 \quad (4.1.3)$$

where n_0^o, n_0^e are unperturbed refractive indices of ordinary and extraordinary polarization, respectively. The linear electro-optic tensor $r_{i,j,k}$ is third-rank tensor, which 27 components can be reduced to 18 independent, because $\hat{\epsilon}$ and $\hat{\eta}$ are symmetric so indices i and j may be interchanged $r_{i,j,k} = r_{j,i,k}$. In this manner, new notation for linear electro-optic tensor is introduced

$$r_{1k} = r_{11k}, \quad (4.1.4)$$

$$r_{2k} = r_{22k}, \quad (4.1.5)$$

$$r_{3k} = r_{33k}, \quad (4.1.6)$$

$$r_{4k} = r_{23k} = r_{32k}, \quad (4.1.7)$$

$$r_{5k} = r_{13k} = r_{31k}, \quad (4.1.8)$$

$$r_{6k} = r_{12k} = r_{21k}. \quad (4.1.9)$$

Some of these components are equal to zero or identical in many of the photorefractive crystals in dependency on the crystal point group symmetry.

4.2 Properties of photorefractive SBN crystal

In optics different photonic lattices have been optically induced in photorefractive media and use for further investigation of light propagation. In photorefractive SBN crystal, due to his properties, refractive index changes are controlled locally by an external electric field, thereby allowing the realization of adaptive waveguides and complex photonic structures by light.

SBN crystal ($Sb_x Ba_{1-x} Nb_2 O_6$, $0.25 \leq x \leq 0.75$) communally pure and doped with Ce, Cr, Co, Fe is an excellent optical and photorefractive material frequently used in electro-optics, acousto-optics or photorefractive nonlinear optics. Pure SBN crystals are used in optical information storage and investigations of relaxor phase transitions. Megumi et al. were the first who discovered a noticeable

improvement of the photorefractive properties when doping SBN with cerium [70]. SBN crystal was doped by adding different amounts of CeO₂ to the melt. The nowadays growing technique (Modified Stepanov technique [74]) provides outstanding optical quality crystals with a definite cross-section and linear dimensions up to 100 mm. This unique crystal growing technique allows fabrication of high-quality SBN crystal with particularly large electro-optic, thermo-optic, pyro-electric and piezo-electric coefficients, and excellent optical quality. The possibility of inducing reversible refraction index modulation by inhomogeneous illumination (photorefractive effect) is the most important characteristic of SBN crystal. Such crystal possesses huge flexibility, provided since inscribed structures can easily be erased with homogeneous white light illumination.

SBN is a birefringent, uniaxial and anisotropic material with crystallographic symmetry $4mm$. For SBN crystal dominant effect that leads to a refractive index modulation is linear electro-optic effect, where refractive index modulation is related to the linear electro-optic coefficients. Due to the point group symmetry of $4mm$ the only non-vanishing electro-optic coefficients for SBN are r_{13} , r_{33} , and r_{42} , where especially $r_{13}, r_{42} \ll r_{33}$:

$$r_{i,j,k} = \begin{bmatrix} 0 & 0 & r_{13} \\ 0 & 0 & r_{13} \\ 0 & 0 & r_{33} \\ 0 & r_{42} & 0 \\ r_{42} & 0 & 0 \\ 0 & 0 & 0 \end{bmatrix}. \quad (4.2.10)$$

Due to this new relation for the change of impermeability tensor EQ. (4.1.1) in SBN crystal is define as

$$\Delta\hat{\eta} = \Delta \left(\frac{1}{n_0^2} \right) = \begin{bmatrix} r_{13}E_z^{sc} & 0 & r_{42}E_x^{sc} \\ 0 & r_{13}E_z^{sc} & r_{42}E_y^{sc} \\ r_{42}E_z^{sc} & r_{42}E_y^{sc} & r_{33}E_z^{sc} \end{bmatrix}. \quad (4.2.11)$$

Biased on EQ. (4.2.11), the refractive index change is defined as $\Delta n^2 = -n^2(\Delta\hat{\eta})n^2$ or

$$\Delta n^2 = - \begin{bmatrix} (n_0^o)^4 r_{13} E_z^{sc} & 0 & (n_0^o)^2 (n_0^e)^2 r_{42} E_x^{sc} \\ 0 & (n_0^o)^4 r_{13} E_z^{sc} & (n_0^o)^2 (n_0^e)^2 r_{42} E_y^{sc} \\ (n_0^o)^2 (n_0^e)^2 r_{42} E_z^{sc} & (n_0^o)^2 (n_0^e)^2 r_{42} E_y^{sc} & (n_0^o)^4 r_{33} E_z^{sc} \end{bmatrix}. \quad (4.2.12)$$

The refractive index can be separate on part without light n_0^2 i.e. refractive index of SBN crystal and part with refractive index change Δn induces by light. Expression for Δn is obtained by the approximation $n^2 = n_0^2 + \Delta n^2 = (n_0 + \Delta n)^2 = n_0^2 + 2n_0 \Delta n + \mathcal{O}[\Delta n]^2$. Since $\Delta n^2 \ll n$ quadratic term Δn^2 , can be neglected and refractive index change is obtained

$$\Delta n \approx -\frac{1}{2} \begin{bmatrix} (n_0^o)^3 r_{13} E_z^{sc} & 0 & (n_0^o)(n_0^e)^2 r_{42} E_x^{sc} \\ 0 & (n_0^o)^3 r_{13} E_z^{sc} & (n_0^o)(n_0^e)^2 r_{42} E_y^{sc} \\ (n_0^o)^2 (n_0^e) r_{42} E_z^{sc} & (n_0^o)^2 (n_0^e) r_{42} E_y^{sc} & (n_0^o)^3 r_{33} E_z^{sc} \end{bmatrix}. \quad (4.2.13)$$

For SBN crystal, the optical c -axis coincides with the x -axis (Fig. (4.2)), same the direction the electric field $\mathbf{E}_{sc} = E_{sc} \cdot \mathbf{e}_x$. SBN crystal shows strong polarization anisotropy so the index change for a light that is ordinary (normal to c -axis) polarized is much smaller than for extraordinary polarized light. According to EQ. (4.2.13), the following expressions for the refractive index change induced by of ordinary and extraordinary light are

$$\Delta n^o \approx -\frac{1}{2}n_0^{o2}r_{13}E_{sc}, \quad (4.2.14)$$

$$\Delta n^e \approx -\frac{1}{2}n_0^{e2}r_{33}E_{sc}. \quad (4.2.15)$$

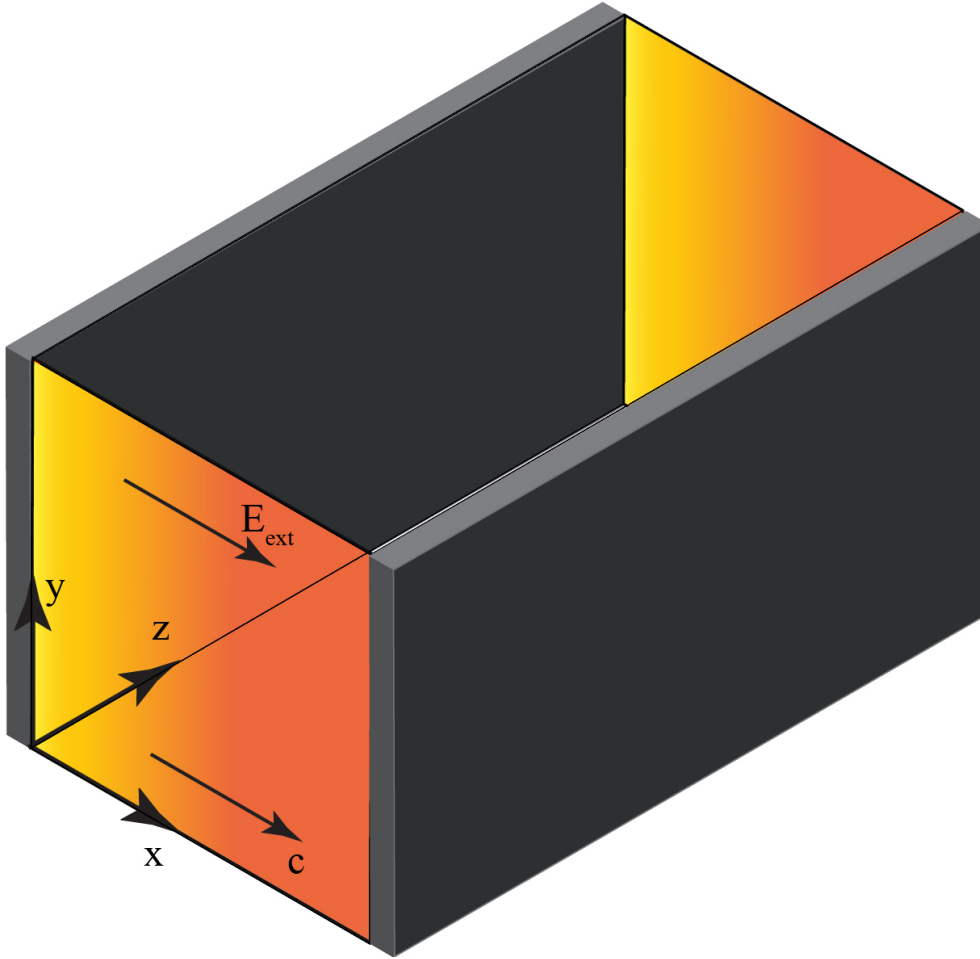


Figure 4.2: Geometry of SBN crystal and axis orientation.

SBN ($Sb_{0.6}Ba_{0.4}Nb_2O_6$) crystal doped with 0.002 wt. % CeO_2 , with typical geometrical dimensions of $5 \times 5 \times 15mm^3$ or $5 \times 5 \times 20mm^3$ is used in this thesis for experimental realizations as well as in numerical simulations. Such crystal is characterized with unperturbed refractive indices $n_0^o = 2.325$ and $n_0^e = 2.358$ and corresponding the electro-optic coefficients $r_{13} = 47.1$ pm/V and $r_{33} = 237.0$ pm/V for ordinary and extraordinary polarization, respectively [75].

4.3 Experimental realization of photonic lattices

Photonic lattices can be created by modulating the refractive index of the medium, which includes direct laser writing, optical lithography, or drilling techniques. A very practical method is *the optical induction technique* in photorefractive material that produces permanent, reversible photonic structures represented by the intensity profile of a nondiffracting light field. It has an advantage over other techniques because it is simply possible to write and erase structures without permanently damaging the crystal. Photorefractive SBN crystal is a suitable material to optically induce photonic lattice. The basic conception of the optical induction technique in SBN crystal is to modulate the refractive index by external illumination (photorefractive effect). According to recalculated modulation illumination, different refractive index modulations are acquired. This technique was used for generation of periodic lattices [8], aperiodic lattices [60, 76], random lattices [9] or dielectric structures by artificially designed refractive index modulation, i.e. helical twisted photonic lattices [41].

Figure 4.3 presents the experimental setup for the optical induction of photonic lattices in SBN crystal. As a light source is used the frequency-doubled Nd: YVO₄ (neodymium-doped yttrium orthovanadate) laser which gives continuously light with a wavelength $\lambda = 532\text{nm}$. The laser beam is expanded and collimated to illuminate spatial light modulator (SLM) as a plane wave (Fig. 4.3). SLM (Holoeye Pluto VIS) is a phase-only modulator that has full HD $1920 \times 1080 \text{ px}^2$ displays, with a pixel size of $8 \times 8 \mu\text{m}^2$ and dimensions of $11.25 \times 8.64 \text{ mm}^2$, created from Liquid Crystal on Silicon. By SLM the reflected light field is modulated in both amplitude and phase [77]. Different paraxial scalar light fields are used for refractive index modulation by addressing a precalculated hologram to the SLM containing the information of the complex light field encoded with an additional blazed grating. The telescope L₁ - L₂ scales down the SLM size by a factor of 10 and by applying an appropriate Fourier filter inside this telescope the tailored complex light field is realized [77, 78]. The SBN crystal shown in Fig. 4.2 is installed in the experimental setup with its optical *c*-axis perpendicular to the direction of propagation, declared to be the *z*-axis. The SBN crystal is placed in the beam path, therefore the modulation is envisioned at the front face of the crystal.

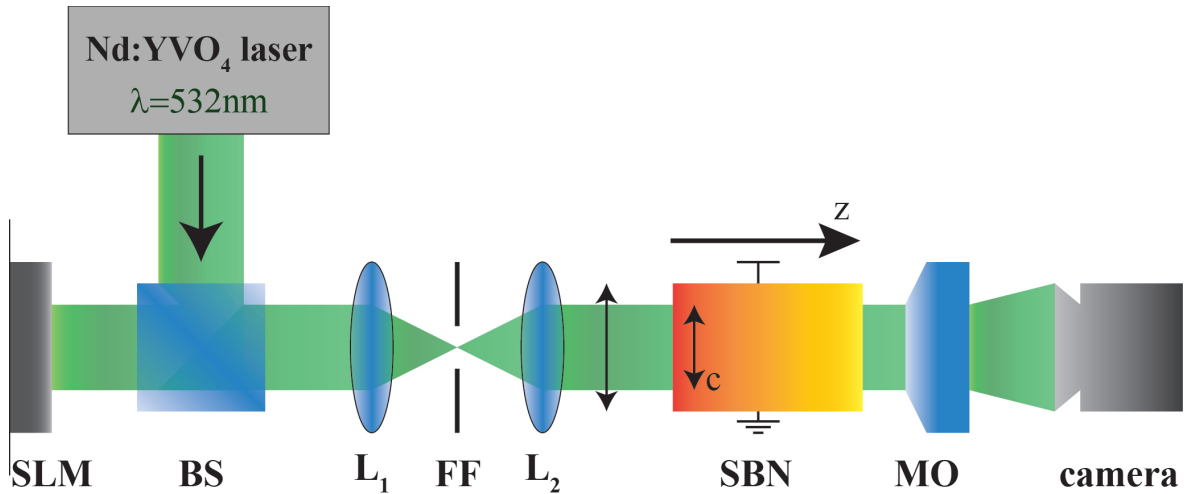


Figure 4.3: Experimental setup for realization of photonic lattices in SBN crystal: SLM - spatial light modulator, BS - beam splitter, L - lens, FF - Fourier filter, MO - macroscopic objective.

The crystal is externally biased with an electric dc field of E_{ext} aligned along the optical $c = x$ -axis, perpendicular to the direction of propagation (z -axis) via electrodes as depicted in Fig. 4.2. The ordinary polarized light linearly polarized in the y -direction, address the electro-optic coefficient

r_{13} on SBN crystal. Such structure beams are used for experimental examination of linear propagation or optical induction of photonic lattices via Mathieu beams. The extraordinary polarized light linearly polarized in the x -direction, addressing the electro-optic coefficient r_{33} of SBN crystal controls the nonlinear response of SBN crystal. Due to this the extraordinary polarized beam is used for experimental examination of nonlinear propagation of Mathieu beams in SBN crystal. Typically, the strength of the electric field is $E_{ext} = 0.8 - 2$ kV/cm. By this redistribution of charge is fast and distinguished refractive index modulations in the order of $\Delta n_{max} = 10^{-4}$ are achieved.

Behind the SBN crystal, an imaging system with a microscope objective (MO) and the camera is placed. The imaging system is mobile in the z -direction. The back face of the photorefractive crystal is imaged by a microscope objective onto the camera. Because the refractive index of the material is spatially modulated the light distribution inside the SBN crystal can not be imaged from experimental realization. Numerical simulations are used to predict the experimental realization. When experimental and numerical results have a good agreement, numerical simulations are used to present light distributions inside the crystal.

4.4 Experimental realization of light propagation in photonic lattices

For the investigation of light propagation in photonic lattices, the optical induction technique has been extended in the photorefractive SBN crystal by using ordinary polarized writing beam for lattice induction and extraordinary for probe beam [39], because SBN crystal feels different nonlinearity strength according to light polarization depending on the electro-optic coefficient r_{ij} . Ordinary polarized light with appropriate electro-optic coefficient r_{13} propagates in almost linear regime, while extraordinary polarized light with higher electro-optic coefficient $r_{33} \gg r_{13}$ feels stronger nonlinearity.

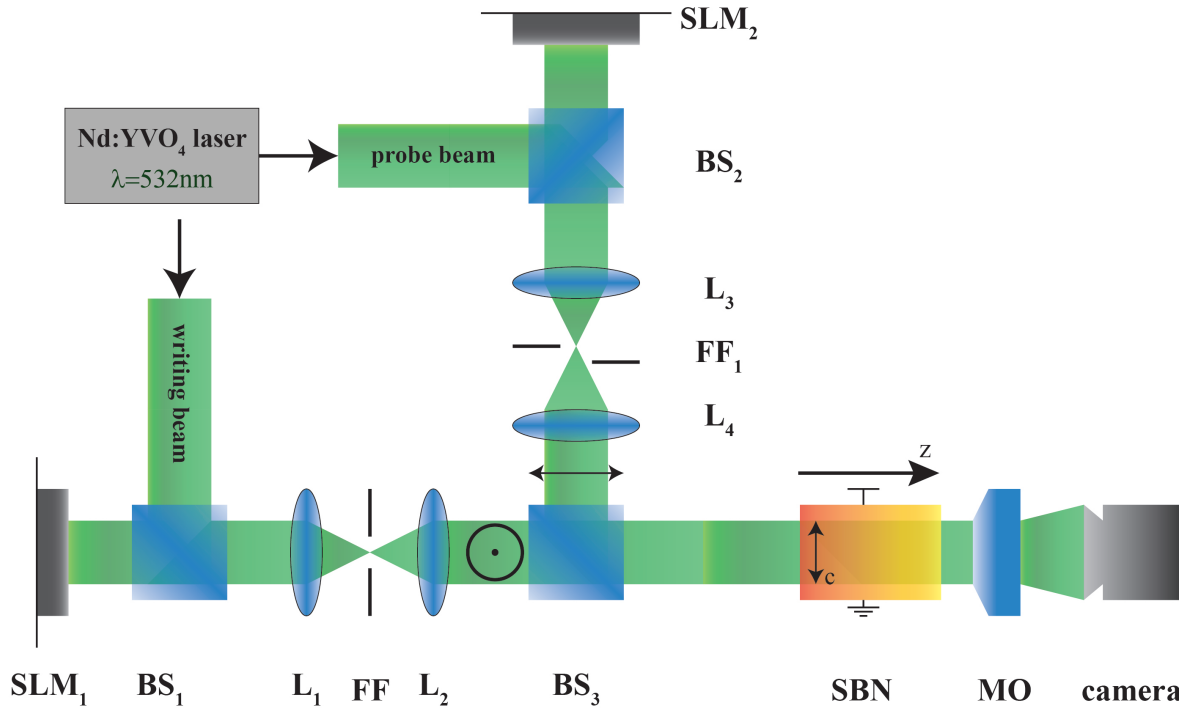


Figure 4.4: Experimental setup for light propagation in optically induced photonic lattices in SBN crystal: SLM - spatial light modulator, BS - beam splitter, L - lens, FF - Fourier filter, MO - macroscopic objective.

The experimental setup for the investigation of light propagation in photonic lattices is shown in Fig. 4.4. The new setup is more complex than the previous one. The same laser source is used. The continuous laser beam is split via beam splitter into two separate beams: the ordinary polarized writing beam and the extraordinary polarized probing beam. The writing beam is used for optical induction of refractive index modulations in a photorefractive SBN crystal in the same way as in the previous section. Both beams are spatially tailored in intensity and phase by two phase-only SLMs. For this purpose, pre-encoded holograms are addressed to the SLMs Holoeye Pluto and Heo and their diffraction patterns are bandpass filtered in Fourier space (FF1 & FF2). Both SLMs have full HD resolution displays, with a pixel size of $8 \times 8 \mu\text{m}^2$ and dimensions of $11.25 \times 8.64 \text{mm}^2$. By telescopes (L1 - L2 and L3 - L4) the SLMs size is scaled down and both spatially tailored light beams are superimposed with beam splitter BS_3 to send modulated light to the front face of the SBN crystal.

SBN crystal is externally biased with an electric field aligned along the optical $c = x$ -axis, perpendicular to the direction of propagation, the z -axis parallel to the long axis of the crystal presented in Fig. (4.2). Probing the artificial photonic structure is done with the extraordinary polarized probe beam that addresses the stronger electro-optic coefficient r_{33} responsible for the nonlinear response. Strength of nonlinearity is determined by applied external field E_{ext} and laser power P . Typically, the strength of the electric field is $E_{ext} = 0.8 - 2 \text{ kV/cm}$ and distinguished refractive index modulations is in the order of $\Delta n_{max} = 10^{-4}$.

An imaging system made of a microscope objective and camera detects transverse intensity distributions at the back of the crystal. Intensity distributions of the probe beam or writing beam could be recorded. While the intensity distribution of the probe beam at the back face of the crystal is recording the writing beam and external field are turned off and vice versa.

Chapter 5

Numerical tools for photonic lattices generation and light propagation in photonic lattices

In this chapter, the numerical model for the examination of Mathieu light beams propagation and creation of Mathieu lattices in photorefractive SBN crystal is presented. Afterwards, the numerical model for investigation of light propagation in such created photonic lattices by using Mathieu beams is introduced.

Such numerical methods are used to simulate earlier presented experiments. But in experiments exist some limits like the length of the crystal, inability to record the crystal volume, hence numerical simulations are a good opportunity to present requirements that are not feasible in experimental realization.

5.1 Basic equation of light propagation in nonlinear photorefractive media

In the purpose of examination in this thesis, investigation of light propagation in nonlinear photorefractive media starts from the Maxwell's equations in regions containing no free charges or currents, $\rho = 0$ and $\mathbf{j} = 0$:

$$\frac{\partial \mathbf{D}}{\partial t} = \nabla \times \mathbf{H}, \quad (5.1.1)$$

$$\frac{\partial \mathbf{B}}{\partial t} = -\nabla \times \mathbf{E}, \quad (5.1.2)$$

$$\nabla \cdot \mathbf{B} = 0, \quad (5.1.3)$$

$$\nabla \cdot \mathbf{D} = 0. \quad (5.1.4)$$

where \mathbf{D} is the electric displacement, \mathbf{B} is the magnetic induction, \mathbf{E} is the electric field, and \mathbf{H} is the magnetic field. They are related by following equations:

$$\mathbf{D} = \varepsilon_0 \cdot \mathbf{E} + \mathbf{P}, \quad (5.1.5)$$

$$\mathbf{B} = \mu_0 \cdot \mathbf{H} \quad (5.1.6)$$

where ϵ_0 , and μ_0 denotes the permittivity and permeability of free space, and \mathbf{P} the induced polarization of the material. By mathematical calculation *the wave equation of electric filed* is obtained

$$\nabla \times \nabla \times \mathbf{E} + \frac{1}{c^2} \frac{\partial^2 \mathbf{E}}{\partial t^2} = -\frac{1}{\epsilon_0 c^2} \frac{\partial^2 \mathbf{P}}{\partial t^2} \quad (5.1.7)$$

where $c = \frac{1}{\sqrt{\mu_0 \epsilon_0}}$ is the sped of light in vacuum.

For nonlinear photorefractive media, polarization of light is dependent on the electric field as $\mathbf{P} = \epsilon_0 \chi_{eff} \mathbf{E}$, where $\chi_{eff}(I = |E|^2)$ is effective intensity dependent susceptibility. According to this the electric displacement and effective refractive index are define as $\mathbf{D} = \epsilon_0(1 + \chi_{eff})\mathbf{E}$, $n(I) = \sqrt{1 + \chi_{eff}}$. The wave equation (5.1.7) can be rewrite according to the relation $\nabla \times \nabla \times \mathbf{E} = \nabla(\nabla \cdot \mathbf{E}) - \nabla^2 \mathbf{E}$ as

$$\nabla(\nabla \cdot \mathbf{E}) - \nabla^2 \mathbf{E} = -\frac{n^2(I)}{c^2} \frac{\partial^2 \mathbf{E}}{\partial t^2}. \quad (5.1.8)$$

Term $\nabla^2 \mathbf{E}$ is small for most cases of interest and can be neglected, thus, *the Helmholtz equation* is obtained

$$-\nabla^2 \mathbf{E} + \frac{n^2(I)}{c^2} \frac{\partial^2 \mathbf{E}}{\partial t^2} = 0. \quad (5.1.9)$$

Propagation of light in photorefractive media induce refractive index change, according to that refractive index $n^2(I) = n_0^2 + \Delta n^2(I)$ is divided into two parts: the part without light n_0^2 (refractive index of the crystal) and part with refractive index change Δn induces by light. Through this thesis, the propagation of the light field is in the z -direction, examined with linearly polarized light, thus, electric field is specified via

$$\mathbf{E}(r, t) = U(\mathbf{r}) e^{(k_z \cdot z - \omega t)} \mathbf{e}_x \quad (5.1.10)$$

with longitudinal wavevector $k_z = n_0 k_0$, $k_0 = \frac{\omega}{c}$, and $\mathbf{r} = \{x, y, z\}$.

In the standard *paraxial approximation*, the wave envelope slowly varying in the z -direction in contrast with the fast oscillating part of the wave in the z -direction, $|k_z \partial_z U| \gg |\partial_z^2 U|$. A significance of paraxial approximation is to permit that the double partial z derivative of the envelope can be neglected $|\partial_z^2 U| \approx 0$. EQ. (5.1.10) is substituted in EQ. (5.1.9) with respect of paraxial approximation, resulting in *two-dimensional nonlinear paraxial Schrödinger equation* (NPE)

$$i \frac{\partial U(\mathbf{r})}{\partial z} + \frac{1}{2k_z} \nabla_{\perp}^2 U(\mathbf{r}) + \frac{k_z}{2n_0^2} \Delta n^2(I) U(\mathbf{r}) = 0 \quad (5.1.11)$$

with $\nabla_{\perp}^2 = \left(\frac{\partial}{\partial x^2} + \frac{\partial}{\partial y^2} \right)$. The EQ. (5.1.11) describes paraxial light wave propagation ($k_x^2 + k_y^2 \ll k_z^2$) and includes nonlinear response of media. Light propagates in the z -direction, linearly polarized, parallel to the optical c -axis of the crystal, with slowly varying wave envelope $U(\mathbf{r})$ in the z -direction on a scale much more longer then the wavelength $\lambda = 2\pi/k$.

By NPE (EQ. (5.1.11)) linear and nonlinear light propagation phenomena in photorefractive media can be described. In photorefractive material, main effect for refractive index modulation is the linear electro-optic effect in combination with charge transport mechanisms and requires an external electric field. The presence of a dc field leads to the change in the dielectric permittivity, thus light induced refractive index change Δn in dependence of the electro-optic coefficient r_{ijk} and the electric field E (EQ. (4.2.13)). The band transport model describes the dynamics of the charge

carriers inside the crystal [79]. The electron movement in the conduction zone is affected by different process: drift due to the electric field \mathbf{E} and diffusion, with diffusion constant $D = \frac{k_b T}{e}$ where T is the absolute temperature, k_b Boltzmann constant, and e the elementary charge of electron. Therefore, it is crucial to know how the space-charge field generated by the incident light looks like. When an external electric field is applied in one transverse dimension the distinct anisotropic properties of biased photorefractive crystals have to be used. Zozulya and Anderson first introduced such a model [80]. For the anisotropic model, the general potential equation is defined as

$$\Delta\phi_{sc} + \nabla \ln(1 + I)\nabla\phi_{sc} = E_{ext} \frac{\partial}{\partial x} \ln(1 + I) - D [\Delta \ln(1 + I) + (\nabla \ln(1 + I))^2]. \quad (5.1.12)$$

In 2D case the potential equation has no analytical solution, therefore it has to be solved numerically. Afterward, the resulting potential can be used to calculate the total electric field and the refractive index modulation dependent on initial intensity distribution.

In some cases of this thesis, the diffusion effect is taken into account particularly when the strong nonlinearities are applied along the direction of the optical c -axis. Due to the diffusion shift, asymmetry in intensity distribution is noticed along the optical c -axis of the crystal. But in some examination in this thesis diffusion effect is neglected $D = 0$. Therefore, the potential equation is simplified

$$\Delta\phi_{sc} + \nabla \ln(1 + I)\nabla\phi_{sc} = E_{ext} \frac{\partial}{\partial x} \ln(1 + I), \quad (5.1.13)$$

and the space-charge field is express in terms of its electrostatic potential $E_{sc} = \partial_x \phi_{sc}$. Due to this, the total electric field $E(I) = E_{ext} + E_{sc}(I)$ that builds up inside the photorefractive crystal is the sum of the external light field E_{ext} and internal space charge field E_{sc} which depends on the initial light intensity $I = |U|^2$. The potential equation carries all information about the photorefractive nonlinearity i.e. the dependency $E_{sc}(I)$. Photorefractive nonlinearity is saturable due to bounded space charge field E_{sc} with applied external field E_{ext} . Also, it is nonlocal, refractive index change depends in each point on the intensity distribution in the whole transverse plane. Self-focusing nonlinearity is determined with $E_{ext} > 0$, in contrast to defocusing nonlinearity where $E_{ext} < 0$. Linear and nonlinear light propagation effects in photorefractive SBN crystal throughout this thesis are explained by the basic propagation model which includes joined propagation (EQ. (5.1.11)) and potential (EQ. (5.1.12) or EQ. (5.1.13)) equations.

This model is used for examination of linear and nonlinear propagation of paraxial light beam with initial intensity distribution defined by Mathieu beam (single or elliptic Mathieu beam) in nonlinear photorefractive SBN crystal. The strength of nonlinearity is varied by the strength of the external electric field E_{ext} (typically $E_{ext} = 0.8 - 2$ kV/cm) or intensity I of certain Mathieu beam. This model allows simulation of experimental realization of Mathieu lattices in photorefractive SBN crystal, biased by the external electric field E_{ext} along the crystal's optical c -axis (as shown in Fig. 4.2). As a writing beam for lattice is used ordinary polarized Mathieu beam. According to this writing beam propagates in linear regime inside the crystal, and due to refractive index modulation creating 1D or 2D Mathieu photonic lattices.

In some cases, the two-dimensional nonlinear paraxial Schrödinger equation can be solved analytically, but according to the requirements in this thesis, comprehensive numerical model have to be implemented to solve this equation and model the light propagation in nonlinear media. One of the methods to numerically solve propagation (EQ. (5.1.11)) and potential (EQ. (5.1.12) or (5.1.13)) equations is a *symmetrized split step propagation method* [81]. First, the model equations are rewrite in dimensionless form, introducing the dimensionless variables: $X = x/x_0$, $Y = y/x_0$, $Z = z/k_z x_0^2$ and $\Phi_{sc} = \phi_{sc}/x_0 E_{ext}$, (x_0 is a transverse scaling factor)

$$i\frac{\partial U}{\partial Z} + \frac{1}{2k_z}[\nabla_{\perp}^2 + V(I)]U = 0, \quad (5.1.14)$$

$$\Delta\Phi_{sc} + \nabla \ln(1 + I)\nabla\Phi_{sc} = \frac{\partial}{\partial x} \ln(1 + I)$$

with $\nabla_{\perp}^2 = \left(\frac{\partial}{\partial X^2} + \frac{\partial}{\partial Y^2}\right)$, where $V(I) = \frac{k_z^2 x_0^2}{n_0^2} \Delta n^2(I) = -k_z^2 (n_0^{e,o})^4 r_{ij} E_{sc}$ is potential optically induced in nonlinear photorefractive crystal ($n_0^{e,o}$ - ordinary or extraordinary refractive index with corresponding linear electro-optic coefficient r_{13} or r_{33} , respectively).

5.2 Propagation of light in photonic lattices

To propagation of light in optically induced photonic lattice into photorefractive SBN crystal is examined by *the nonlinear Schrödinger equation* for an initial paraxial scalar light field $U(\mathbf{r})$ with longitudinal wavevector k_z

$$i\frac{\partial U(\mathbf{r})}{\partial Z} + \frac{1}{2k_z}[\nabla_{\perp}^2 + V(I)]U(\mathbf{r}) = 0. \quad (5.2.15)$$

Nonlinear potential depends on the incident light intensity, defined by photorefractive nonlinearity a $V(I) = \frac{k_z^2 x_0^2}{n_0^2} \Delta n^2(I) = -k_z^2 (n_0^{o,e})^4 r_{13,33} E_{sc}$, where n_0^o and n_0^e are ordinary and extraordinary refractive index with corresponding linear electro-optic coefficient r_{13} and r_{33} , respectively. The laser wavelength λ related with the wavenumber $k = \frac{2\pi}{\lambda} = \sqrt{k_t^2 + k_z^2}$, k_t is the transverse wavenumber. The electric field build inside the SBN crystal $E = E_{ext} + E_{sc}$ is dependent on the external light field E_{ext} and the internal space charge field E_{sc} , which is a result of the incident intensity distribution $I(\mathbf{r}) = |U(\mathbf{r})|^2$. The refractive index modulation $\Delta n^2(I)$ according to the anisotropic approximation is calculation via solving potential equation ($E_{sc} = \partial_x \phi_{sc}$) where diffraction effect is neglected

$$\Delta\phi_{sc} + \nabla \ln(1 + I + I_{latt})\nabla\phi_{sc} = E_{ext} \frac{\partial}{\partial x} \ln(1 + I + I_{latt}), \quad (5.2.16)$$

and I_{latt} denotes the lattice intensity distribution. Propagation (5.2.15) and potential (5.2.16) equations are related and for their numerically solution is used symmetrized split-step beam propagation method [81]. Again, the model equations are rewrites in dimensionless form, introducing the dimensionless variables: $X = x/x_0$, $Y = y/x_0$, $Z = z/k_z x_0^2$ and $\Phi_{sc} = \phi_{sc}/x_0 E_{ext}$, (x_0 is a transverse scaling factor)

$$i\frac{\partial U}{\partial Z} + \frac{1}{2k_z}[\nabla_{\perp}^2 + V(I)]U = 0, \quad (5.2.17)$$

$$\Delta\Phi_{sc} + \nabla \ln(1 + I + I_{latt})\nabla\Phi_{sc} = \frac{\partial}{\partial x} \ln(1 + I + I_{latt})$$

This model is used for examination of linear and nonlinear effects of probe beam propagation (plane wave, elliptic optical vortex, or Gaussian beam) in different Mathieu photonic lattices. One possibility is to use a single Mathieu beam to create photonic lattices. Furthermore, numerous aperiodic lattices are formed via the interference of Mathieu beams.

5.3 The symmetrized split-step beam propagation method and calculation of Potential equation

In past, various numerical methods are revealed to calculate NPE. Due to the problem a convenient numerical method is chosen. The symmetrized split-step beam propagation method (Symmetrized SSBM) or the symmetrized split-step Fourier method is one technique for numerical solving NPE and potential equations. Symmetrized SSBM has been revealed as a rather fast and reliable method, appropriate for problems inside this thesis.

Primarily, NPE and potential equation are written in dimensionless form like EQ. (5.1.14) or EQ. (5.2.17). The dimensionless NPE is separated in terms of dispersion and nonlinearity. To use Symmetrized SSBM for solving NPE dispersion and nonlinearity terms are decoupled for a small propagation distance, ΔZ . Operators \hat{D} and \hat{N} are written to correspond to the dispersion and nonlinearity terms, respectively. Operator form of NPE is

$$\frac{\partial U(r_{\perp}, Z)}{\partial Z} = i(\hat{D} + \hat{N})U(r_{\perp}, Z) \quad (5.3.18)$$

with dispersion $\hat{D} = \frac{1}{k_z} \nabla_{\perp}^2$ and nonlinear operator $\hat{N} = V(I)$.

Whole propagation length is divided into small spatial steps, with step size ΔZ . To avoid errors proper choice of step size and optimal computational window in the transverse plane (X, Y) are required. Propagation in one step, from Z to $Z + \Delta Z$, is calculated in alternating steps in which either diffraction effect or nonlinear effect are considered. A formal solution of equation EQ. (5.3.18) for the propagation from Z to $Z + \Delta Z$ is given as

$$U(r_{\perp}, Z + \Delta Z) = e^{\Delta Z(\hat{D} + \hat{N})}U(r_{\perp}, Z), \quad (5.3.19)$$

where $r_{\perp} = (X, Y)$ yields transverse coordinates.

The numerical model is derived by applying the Baker-Hausdorff formula for noncommutative operators \hat{D} and \hat{N} [82]. For Symmetrized SSBM, first is computed diffraction effect over the half step size, $\frac{\Delta Z}{2}$, then is computed nonlinearity effect at the step midpoint for the whole step, and in the end diffraction effect is computed over $\frac{\Delta Z}{2}$.

Diffraction is obtained by using a pseudospectral method, which includes the Fast Fourier Transform (FFT) and the nonlinear effect is neglected. FFT of the envelope at the propagation distance Z facilitates computation of the differential operator by $\nabla_{\perp}^2 = -(k_x^2 + k_y^2)$. An inverse Fourier transform then gives the diffracted field envelope at the propagation distance $Z + \Delta Z$.

The nonlinear correction depends on incident intensity distribution. To implement nonlinear correction over the whole step ΔZ first the potential equation is calculated in over propagation step by an iterative procedure in order to potential dependence on initial intensity, afterwards propagation of the light field is calculated for the whole step including potential.

To compute the propagation four Fourier Transforms are used in one step via Symmetrized SSBM. The computation of one step of the propagation can be summarized as (schema represented in Fig. 5.1)

$$U(r_{\perp}, j\Delta z) = \mathcal{F}^{-1} \left[\exp\left(\frac{\Delta z}{2} \hat{D}(i\omega)\right) \mathcal{F} \left[\exp\left(\int_z^{z+\Delta z} \hat{N}(z') dz\right) \right. \right. \\ \left. \left. \mathcal{F}^{-1} \left[\exp\left(\frac{\Delta z}{2} \hat{D}(i\omega)\right) \mathcal{F} [U(r_{\perp}, (j-1)\Delta z)] \right] \right] \right]$$

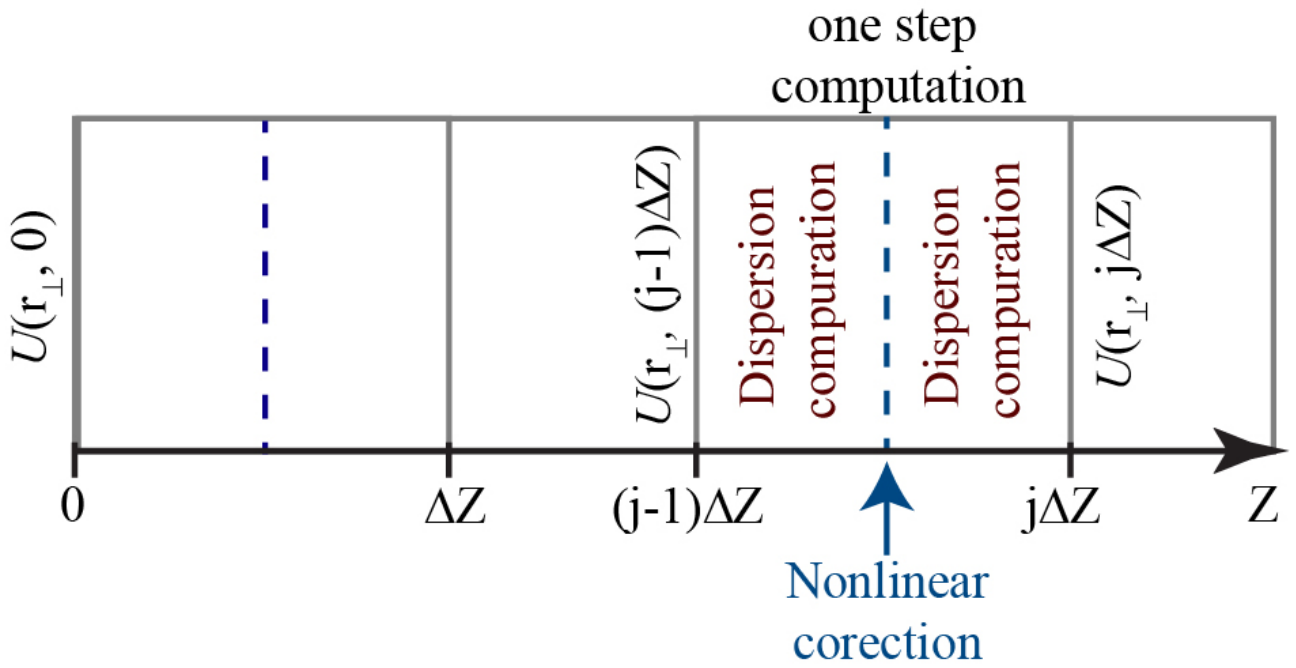


Figure 5.1: Schematic for the computation of one step propagation via Symmetrized SSBM.

Nonlinear paraxial and potential equations are coupled in problems involved in this thesis. The potential equation provides information about the photorefractive nonlinearity during propagation, determined by initial intensity distribution, $E_{sc}(I)$. For numerical simulation of such equations model, the iterative calculation procedure is applied. In every iteration step, the Symmetrized SSBM is applied with determined refractive index modulation and light field distribution at the initial position. Hence, this is an initial value problem, which makes it computationally efficient.

Chapter 6

Results and discussion

6.1 Nonlinear self-action of Mathieu beams in SBN crystal and Mathieu photonic lattices

In this section nonlinear self-action of single and elliptic Mathieu beams in photorefractive SBN crystal is explored with increasing nonlinearity strength. They would be exploited as writing light for fabricating discrete nonlinear photonic waveguide structures or dynamical chiral photonic structures with a tunable chirality.

6.1.1 Switching discrete diffraction in nonlinear Mathieu lattices

Mathieu beams, as nondiffracting beams, have the propagation-invariant intensity distributions in a vacuum. However, the question is does they remain nondiffracting in the nonlinear photosensitive medium? Thus, linear and nonlinear propagation of single Mathieu beams would be investigated experimentally and numerically in the photorefractive SBN crystal. The experimental setup for this investigation is depicted in Fig. 4.3.

In the beginning, the free-space propagation of even Mathieu Beam of order zero, with ellipticity $q = 25$ and characteristic structure size $a = 25\mu\text{m}$ is examined. The transverse intensity distribution is shown in Fig. 6.1 (A1) has the quasi 1D discrete intensity distribution, with corresponding phase distribution Fig. 6.1 (A2). In free-space it propagates invariant over a 6.36mm, which corresponds to 15mm in the homogenous SBN crystal as shown in Fig. 6.1 (A3). The same conclusions are worthy of higher-order Mathieu beams.

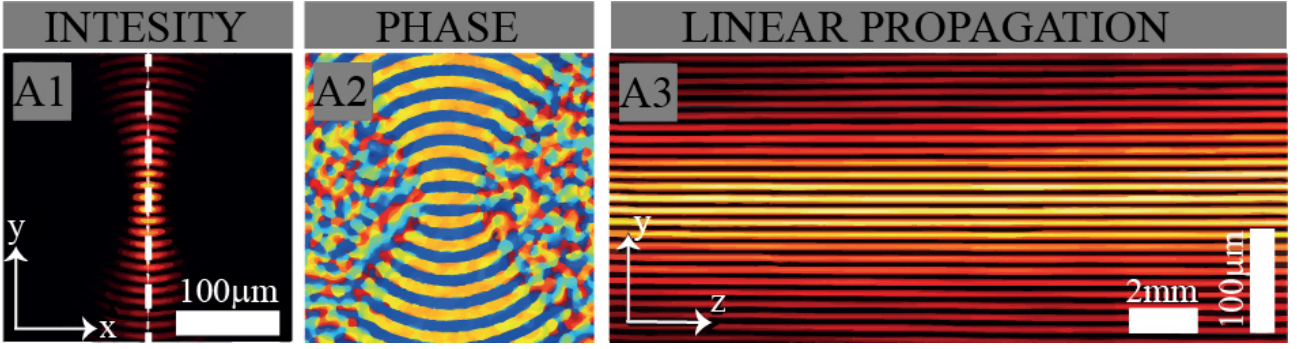


Figure 6.1: Experimental properties of a zeroth-order even Mathieu beam. (A1) Transverse intensity and (A2) phase distribution in 15mm long SBN crystal. (A3) Cross section through the volume at the orientation indicate with dashed line in (A1).

Fig. 6.2 (A) shows that the zeroth-order Mathieu beam has one path which corresponds to 1D discrete intensity distribution. Hence, the zeroth-order Mathieu beam is appropriate for the examination of nonlinear self-action in the 1D path. If the Mathieu beam order is incremented the number of paths increases as shown in Figs. 6.2 (B), (C), (D), but now straight and curved paths are noticeable. The transverse intensity distribution of higher-order Mathie beams consist of multiple paths, which can serve as 2D photonic lattices. Thus, the dimensional crossover from 1D to 2D photonic lattices is apparent from the zeroth-order Mathieu beam to fifteenth-order Mathieu beams. The higher order Mathieu beams are appropriate for an examination of nonlinear self-action in curved 2D paths. One interesting property of higher-order Mathieu beams is that while the order increase inner paths are straight with equidistant intensity spots. By changing order or ellipticity, different distances between spots are achievable. Due to this, higher-order Mathieu beams are convenient for facile realization of periodic patterns, reducing realization time.

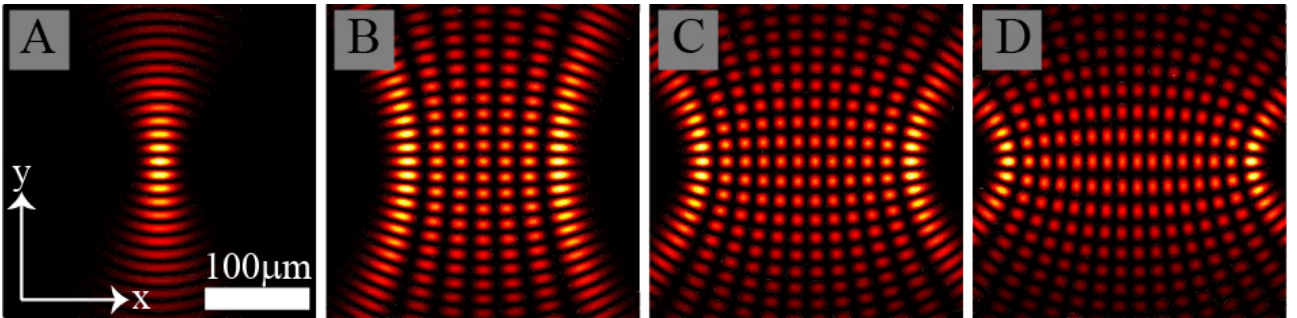


Figure 6.2: Dimensional crossover based on increasing beam order of the Mathieu beam. Transverse intensity distributions of: (A) zeroth-order, (B) sixth-order, (C) eleventh-order and (D) fifteenth-order Mathieu beams.

Mathieu beams are suited for the investigation of switching diffraction in self-induced waveguides, experimentally and numerically. The lattice-fabricating zeroth-order Mathieu beam depicts in Fig.6.1 shows nonlinear discrete diffraction as a result of self-action in dependence of the beam power P that influences the strength of the nonlinearity, shown in Fig. 6.3. In the first column (Figs. 6.3 (A1) - (A3)) are represented simulated yz cross-sections through the intensity volume, in the second one (Figs. 6.3 (B1) - (B3)) the simulated transverse intensity distributions, while in the third one (Figs. 6.3 (C1) - (C3)) the experimentally obtained transverse intensity distributions at the back face of the SBN crystal.

For lowest power $P = P_0 = 10\mu\text{W}$ the waveguides are well fabricated as presented in the

first row of Fig. 6.3. The noticed discrete diffraction of Mathieu beam is like as broad Gaussian beam propagation in 1D periodic waveguide arrays [27]. For doubled beam powers $P = 2P_0$ and $P = 4P_0$ spreading of the highest intensities are observed away from the center and towards the outer parts along the y -axis as shown in Figs. 6.3 ((A2) - (C2)) and (A3) - (C3)). Considering that the initial zeroth-order Mathieu beam has its maximum in the origin and the envelope of the 1D intensity distribution is along the y -axis the refractive index modulation and thus the self-action of the writing beam is strongest in the center. For high beam power of $4P_0$ thermal diffusive effects are increased along the optical c axis, parallel to the x -axis, noticeable along the x -axis as the shift in intensity in (B3) and (C3). According to this investigation, the new effect is founded, named **1D nonlinear discrete diffraction** or **morphing discrete diffraction**. This effect is a nonlinear pandan of linear discrete diffraction in 1D waveguide arrays.

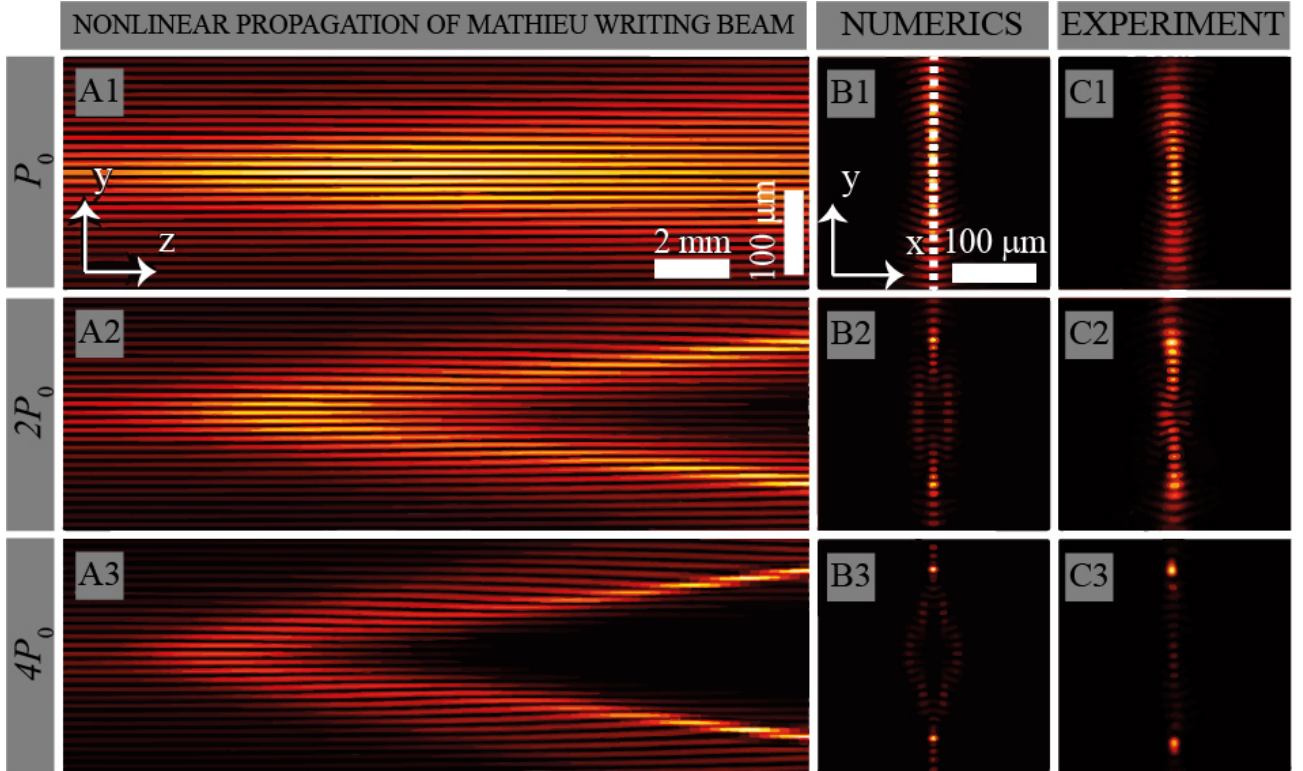


Figure 6.3: Nonlinear discrete diffraction of zeroth-order Mathieu beam in dependence of the strength of the nonlinearity controlled by beam power P . First column presents simulated cross section through the volume at the orientation indicate with dashed line in (B1) for increasing beam powers. Second and third column presents simulated and experimentally observed intensity distributions at the back face of SBN 15mm long crystal. $P_0 = 10\mu\text{W}$.

Also, higher order Mathieu beams with ellipticity $q = 325$ and characteristic structure size $a = 25\mu\text{m}$ were investigated with increasing beam powers P . Figure 6.4 shows the result of nonlinear self-action of sixth-order Mathieu beam. First row (A) shows simulated and second row (B) experimentally observed transverse intensity distributions at the back face of the 15mm long SBN crystal in the according to a successive doubling of the initial beam power $P_0 = 10\mu\text{W}$. Intensity profiles along each hyperbolic layer depicted in (B) are shown in treed row (C).

For the lowest power $P = P_0$, the highest intensities, located in the center of an initial sixth-order Mathieu beam, are redistributed towards the outer parts in the y -direction, which confirms by the intensity profile along the green line Figs. 6.4 (B1) and (C1). Only central hyperbolic arms of the Mathieu lattice feel the lowest nonlinearity, also visible on the intensity profile along further hyperbolic layers. When nonlinearity strength is incremented by doubling the power $P = 2P_0$

and $P = 4P_0$, even further hyperbolic arms of the Mathieu lattice are affected. Central intensities spread outwards along 2D curves (Figs. 6.4 ((A2), (B2)) and ((A3), (B3))), confirmed and by intensity profiles (Figs. 6.4 ((C2), (C2))). Thermal diffusion additionally introduces the shift in the x -direction, intensities merging due to modulation instabilities influence the intensity redistribution and both experimental and numerical results are asymmetric. Still the pure effect of **2D nonlinear discrete diffraction** along hyperbolic paths is in general recognizable. When the diffusive term in potential equation is neglected, numerically simulated intensity distribution would be symmetric (not shown).

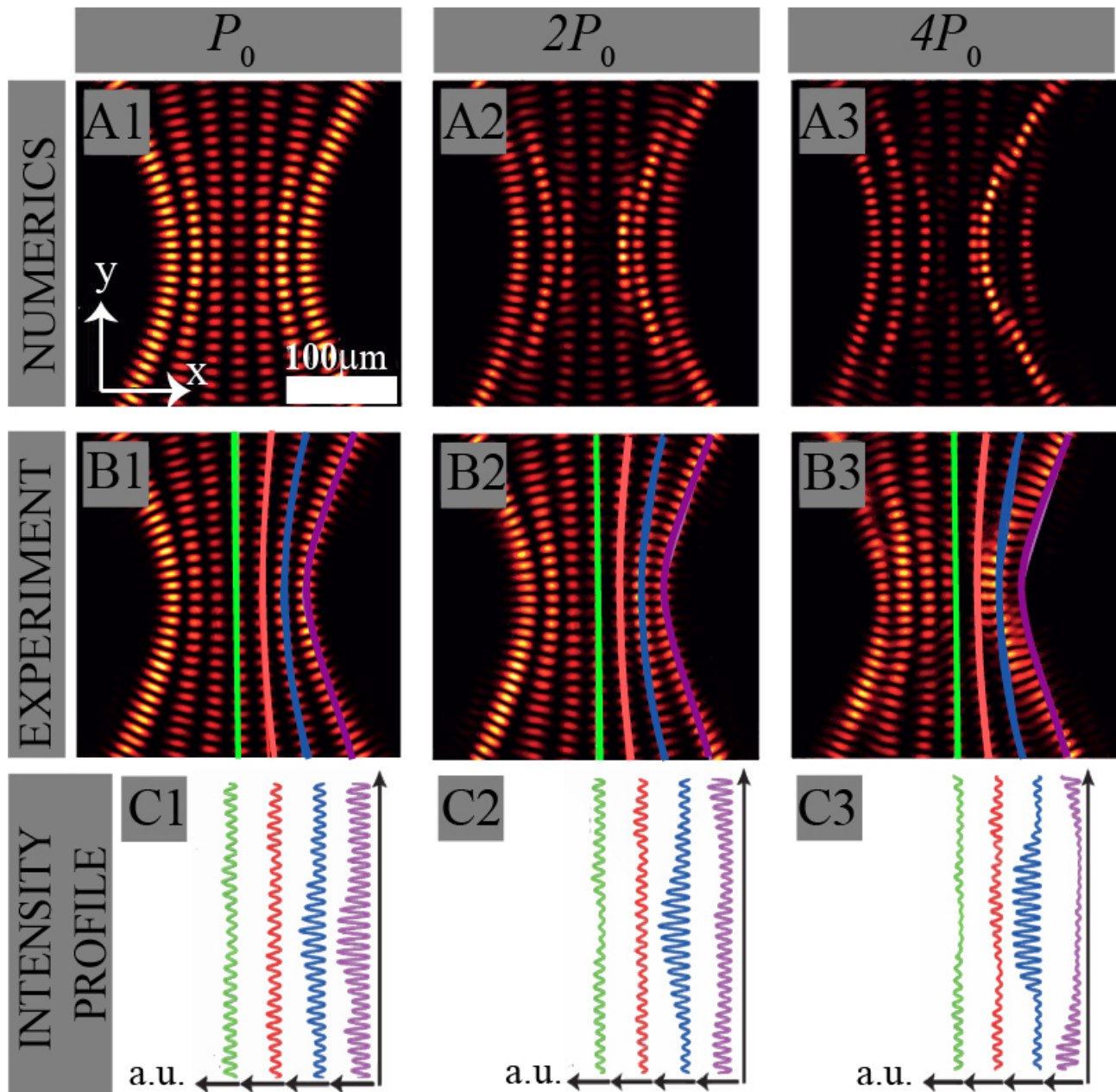


Figure 6.4: Switching discrete diffraction on curved paths based on the self-action of sixth-order even Mathieu beam: (A) simulated and (B) experimentally observed transverse intensity distributions at the crystal's back face. (C) Intensity profiles along the hyperbolic waveguide layers indicated in (B). $P_0 = 10\mu\text{W}$.

Figure 6.5 shows the result of nonlinear self-action of the eleventh-order Mathieu beam. The first row shows simulated and second row experimentally observed transverse intensity distributions

at the back face of the 15mm long SBN crystal in the dependency of a successive increase of the initial beam power $P_0 = 20\mu\text{W}$. For the lowest power, the only central arm of eleventh-order Mathieu beam is slightly affected by nonlinearity and the highest intensity located in the center is diffracted to out parts in the y -direction (Figs. 6.5 (A1), (A2)). But, with power increasing additional hyperbolic arms are affected and central intensities are spreading outwards along 2D curves, depicted in Fig. 6.5 (B1), (B2), (C1), (C2). For higher power thermal diffusion shift in x -direction appears, creating modulation instabilities, merging of the intensities visible as asymmetric intensity distributions.

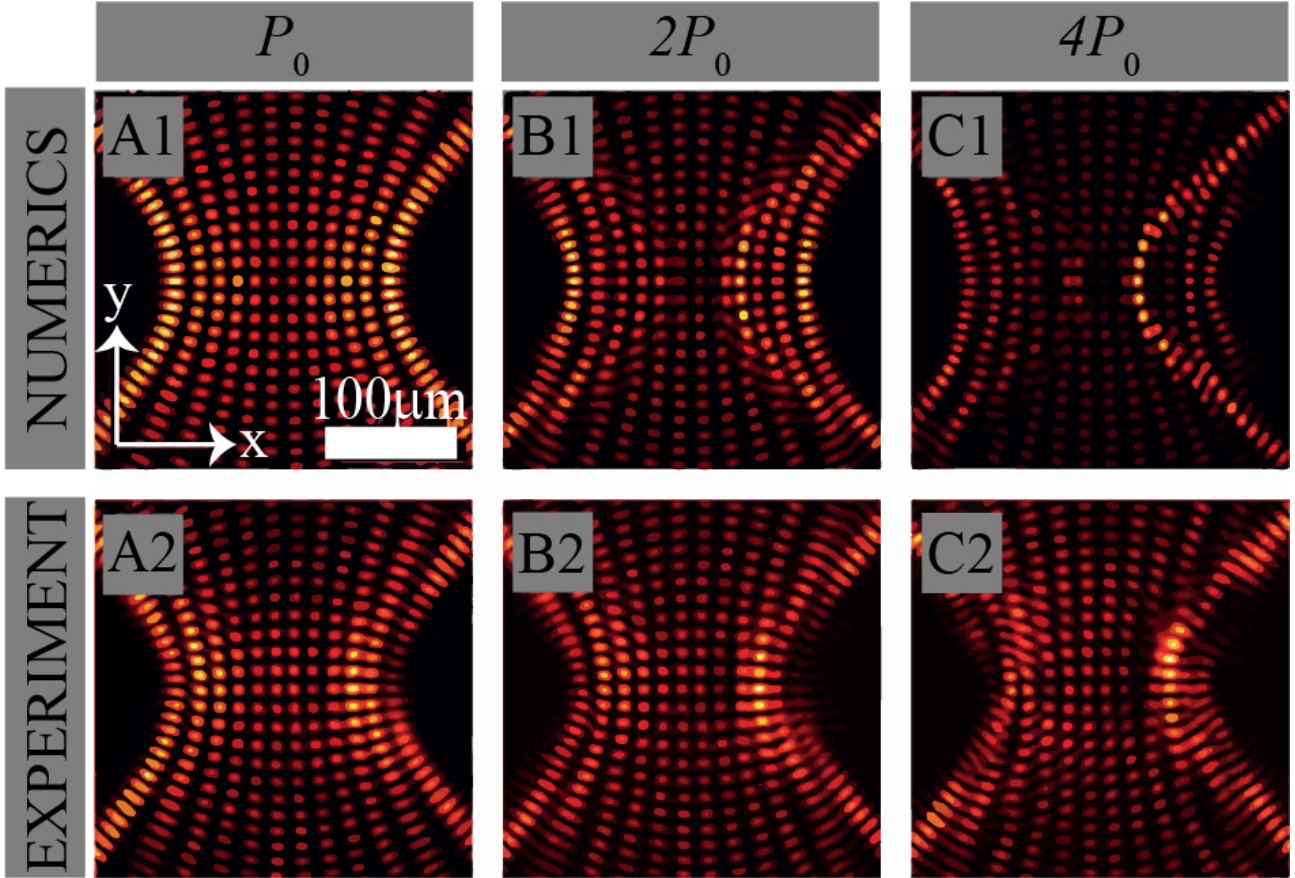


Figure 6.5: Switching discrete diffraction on curved paths based on the self-action of eleventh-order even Mathieu beam: first row simulated and second experimentally observed transverse intensity distributions at the crystal's back face. $P_0 = 20\mu\text{W}$.

Once more, intensity distributions that reflect linear discrete diffraction are observed but in the nonlinear regime and the outward-directed intensity transport in the nonlinear lattices follows mainly along with each hyperbolic layer of the higher order Mathieu beam. In this examination **switching discrete diffraction along curved 2D paths** is realized.

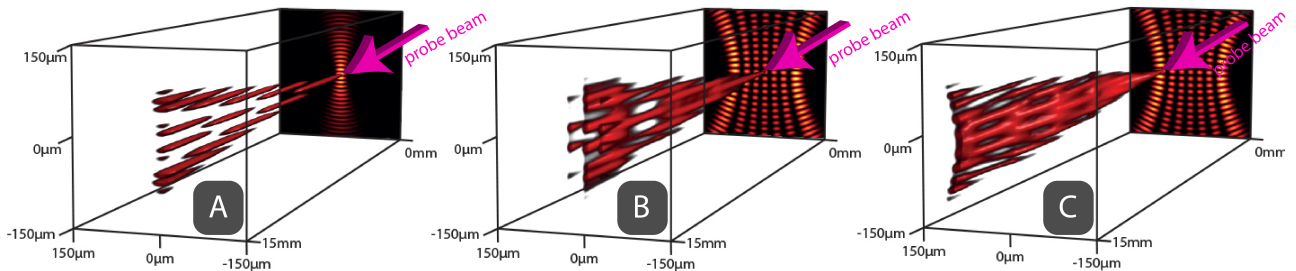


Figure 6.6: Narrow Gaussian probe beam in Mathieu lattice potentials from: (A) Fig. 6.3 (A1); (B) Fig. 6.4 (A1) central waveguides; and (C) Fig. 6.4 (A1) purple waveguide layer.

Linear propagation of narrow Gaussian beams in Mathieu lattices presented in the previous paragraphs are numerically simulated and presented in Fig. 6.6. Discrete Mathieu lattices by themselves imprint the intensity distribution on probing light beam that is typical for discrete diffraction. Figure 6.6 (A) images the intensity distribution of such a Gaussian probe beam inside the Mathieu lattice shown in Fig. 6.3 (A1). The initial plane in Fig. 6.6 marks the lattice. The perpendicularly launched probe beam flows from one waveguide to another, generating diffraction characteristics as in 1D waveguide arrays. Next, the probe beam is launched in the central spot of the central arm of the 2D lattice shown in Fig. 6.4 (A1). The intensity distribution of the probe beam inside the lattice is depicted in Fig. 6.6 (B) showing that probe beam diffraction characteristics as discrete diffraction in 2D lattices. In the end, probe beam is launched in a central spot of an outer hyperbolic layer imaged in Fig. 6.4 (A1). The intensity distribution of the probe beam inside the lattice is depicted in Fig. 6.6 (C), demonstrating 1D discrete diffraction along the hyperbolic waveguide layer.

This subsection presents nonlinear self-action in Mathieu beams leading to switching discrete diffraction. Mathieu beams of different orders are investigated in nonlinear photorefractive SBN crystal, numerical and experimentally. First, linear discrete diffraction is connected with nonlinear self-effects in the quasi one-dimensional lattice. Then the same effect is observed in the two-dimensional lattice with a gradual transition from one to two dimensions. The term switching diffraction is used to explain nonlinear behavior similar to discrete diffraction, phenomena characteristic for linear propagation of light in periodic arrays or lattices.

6.1.2 The self-action of elliptical Mathieu beams in nonlinear media

The self-action of elliptical Mathieu beams in nonlinear 20mm long SBN crystal is investigated experimentally and numerically as well as their orbital angular momentum. Single scalar even and odd Mathieu beams exhibit only real-values field distribution and their transverse Poynting vector therefore vanishes. Elliptic Mathieu beams are the complex superposition of even and odd Mathieu beam mathematically described with EQ. (3.2.8). In contrast to single Mathieu, their intensity distributions are distinguished by a series of concentric ellipses, while the phase distributions are continuously modulated along that ellipses and they possess transverse energy flow [69].

Generally, the energy flow of light is determined by both, its spin angular momentum and its orbital angular momentum (OAM), which is described by the Poynting vector [83]. For linear propagation of continuously modulated nondiffracting beams in homogeneous media, the energy flow is hidden because the transverse intensity distribution stays invariant and the energy flow is continuously redistributed. Linearly polarized, the transverse light field has the transverse time-averaged Poynting vector $\langle S \rangle$ determined by the spatial OAM distribution and given by [84]

$$\langle S \rangle = \frac{i\omega\epsilon_0}{2}(Ely^*\nabla Ely - Ely\nabla Ely^*), \quad (6.1.1)$$

where $\omega = ck$ is the angular-frequency that connects the speed of light c with the wave number $k = 2\pi/\lambda$, defined by the wavelength λ . ϵ_0 is the vacuum permittivity, and Ely denotes elliptic Mathieu beam. Here is considered only the transverse (x, y) component of the Poynting vector.

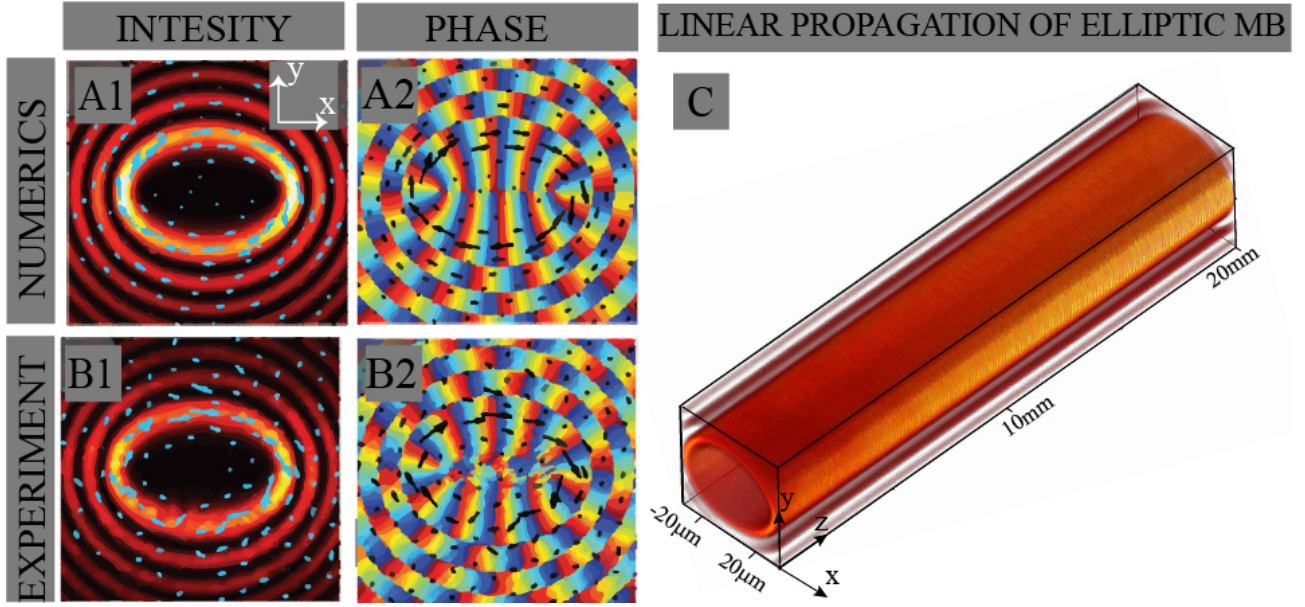


Figure 6.7: The elliptic Mathieu beam characterized by the Poynting vector (indicated by arrows). (A1), (A2) numerically calculated intensity and phase, and (B1), (B2) intensity and phase experimentally observed of the elliptic Mathieu beam order $m = 10$, $q = 25$ and $a = 25\mu\text{m}$. (C) Numerical simulation of the 3D intensity distribution of initial ellipse of the elliptic Mathieu beam inside 20mm long SBN crystal.

Figure 6.7 depicts the intensity and phase distribution of an elliptic Mathieu beam of order $m = 10$ with an ellipticity $q = 25$ and characteristic structure size $a = 25\mu\text{m}$ at the initial plane of the crystal ((A), (B)). Numerical and experimental transverse Poynting vectors are calculated with EQ. (6.1.1), and corresponding Pointing vectors are indicated in Fig. 6.7 with overlying arrows. Also, Fig. 6.7 (C) presents numerically simulated visualization intensity distribution of the such Mathieu beam through the 2mm long crystal.

In numerical simulations, the electric field, $\psi = Ely$ is calculated and by using relation $\psi = Ie^{i\phi}$, intensity (I) and phase (ϕ) distributions are obtained as shown in the first row in Fig. 6.7 (A1), (A2)). Such calculated electric field is used for numerical Poynting vector calculation of the elliptic Mathieu beams according to EQ. (6.1.1). In contrast, in the experimental realization, only the transverse intensity (I) and phase (ϕ) distributions are accessible (Fig. 6.7 (B1, B2)). Using relation $\psi = Ie^{i\phi}$ the experimentally electric field is obtained and used for calculation od experimental Poynting vector of the elliptic Mathieu beam toward to EQ. (6.1.1).

Linear propagation of elliptic Mathieu beams in homogeneous media has balanced intensity re-distribution (Fig. 6.7 (C)). In the following, elliptic Mathieu beams are examined in nonlinear regimes. The results are demonstrated for the elliptic Mathieu beam of order $m = 10$ (Fig. 6.7) but the same conclusions would be demonstrated for different parameters of elliptic Mathieu beams. Nonlinear propagation of elliptic Mathieu beams in SBN crystal is investigated with the experimental setup shown in Fig. 4.3, and corresponding transverse intensity distributions from the back face of the SBN crystal are imaged. Experimental results are compared with matching numerical simulations.

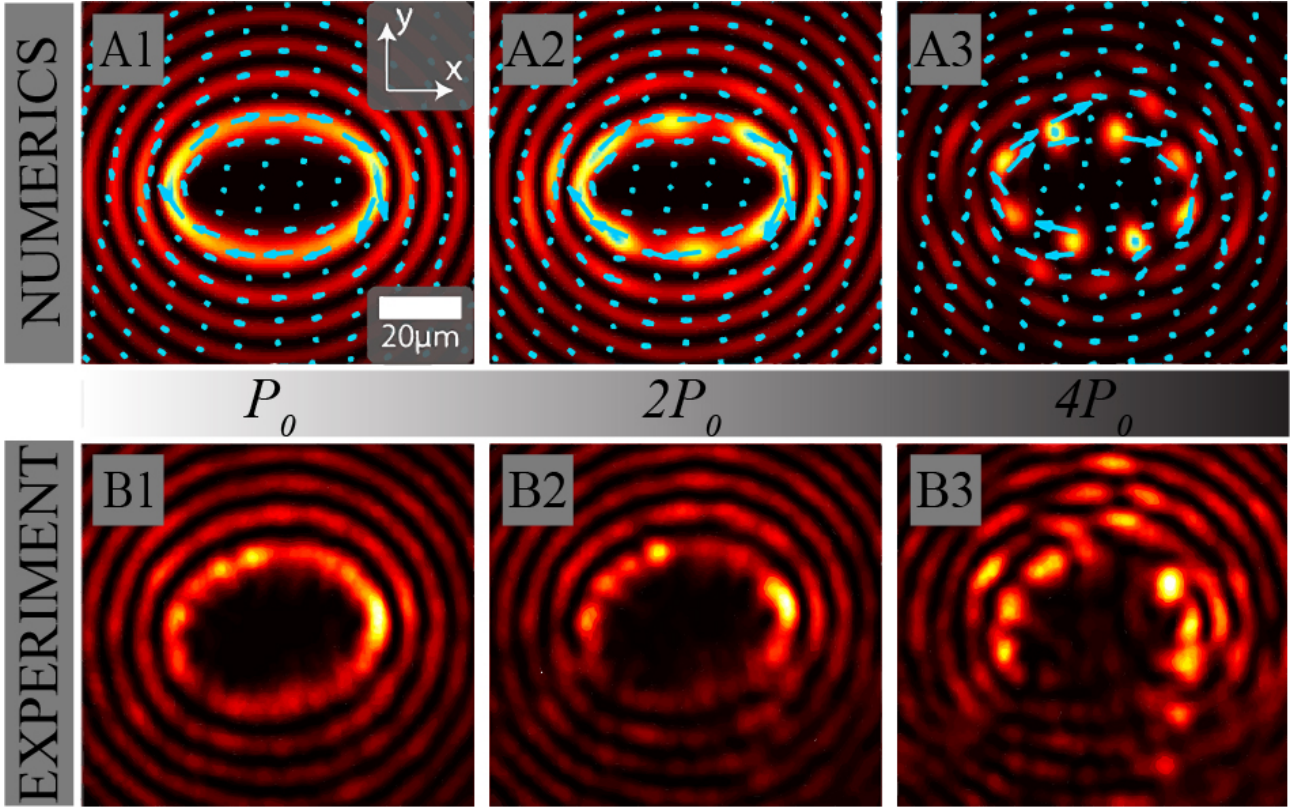


Figure 6.8: Nonlinear self-action of elliptic Mathieu beam with increasing beam powers. The transverse intensity distributions of elliptic Mathieu beams ($a = 15\mu\text{m}$) at the back face of the SBN crystal, nonlinearly inscribed with increasing beam powers. (Top) numerical simulations (calculated Poynting vector indicated by arrows) compared with the (bottom) experimental results. $P_0 \approx 20\mu\text{W}$

The investigation starts with the nonlinear self-action of the elliptic Mathieu beam with a structure size of $a = 15\mu\text{m}$ in the SBN crystal. Refractive index modulation is optically induced with elliptic Mathieu beam as a writing beam. Such induced refractive index depth estimates in the order of 10^{-4} , both experimentally and numerically. The initial beam power $P_0 \approx 20\mu\text{W}$ is increased twice, by doubling in two steps, both in numerical simulations and experiments. The results are shown in Fig. 6.8, where the first row represents the transverse intensity distributions at the back face of the SBN crystal from numerical simulations while the second row shows corresponding experimental results. For a demonstration of energy flow of elliptic Mathieu beam in SBN crystal, only the numerical calculated Poynting vector is observed and they are indicated with arrows in Figs. 6.8.

At the front face of the crystal, the Poynting vector is along the initial ellipse (Fig. 6.7). For low power $P = P_0$ the Poynting vector stays directed along the initial ellipse even at the back face of the crystal after nonlinear self-action as depicted in Fig. 6.8 (A1). Numerically and experimentally observed intensity distributions at the back face shows a high agreement. It is shown that elliptic Mathieu beam propagates almost linearly for low power and output intensity distribution is almost unchanged, so the beam is still nondiffracting.

Nonlinear self-interaction is gradually increased by doubling the power of $P = 2P_0$, due to that the intensity distribution is changed and the breaking of the energy flow is demonstrated. Beforehand smoothly ellipse is modulated in the form of occurring accumulations of intensity, and the writing beam thus can not be considered as nondiffracting Mathieu beam. For the highest beam power of $4P_0$, the ellipse is broken in separated spots of high intensity. These high spots intensity rotate in the direction indicated by the Poynting vector (Fig. 6.8 (A3)). The number of spots depends on the

order m of the elliptic Mathieu beams, but the strength of nonlinearity or the propagation distance also changes the number of high intensity spots.

The spots that emerged at the back face of crystal are a consequence of modulation instabilities on an ellipse [85]. The anisotropic medium and the modulation of the intensity distribution, which mostly occurs along the intrinsic ellipse, establish the refractive index modulation in the direction of the optical $c = x$ -axis. The energy flow, along the intrinsic ellipse, is directed perpendicular to the optical axis where the refractive index modulation is weak, while the flow parallel to the c -axis is hindered because the refractive index modulation is strong. The conglomerations of high-intensity appear in particular at the trough of the high refractive index thus enough intensity is accumulated to create solitary strands of increased refractive index. These solitary strands of the increased refractive index form a twisted photonic structure inside the photorefractive crystal.

Experimental intensity distribution shows asymmetry due to the thermal diffusion effect along the optical c -axis. But, the numerical intensity distributions are simulated with neglected diffusion part in potential equation (EG. (5.1.12)).

Numerical simulations are used for illustration of how the main intensity, distributed on an ellipse in the front face, propagate through the nonlinear 20mm long SBN crystal. In Fig. 6.9 (A) is presented the 3D distribution of the main intensity inside the crystal for the photonic structure depicted in Fig. 6.8 (A3). It is visible that after some propagation distance the main intensity is separated into high intensity spots, which rotates in the direction determined by energy flow, thereby, rotating refractive index strands are forming.

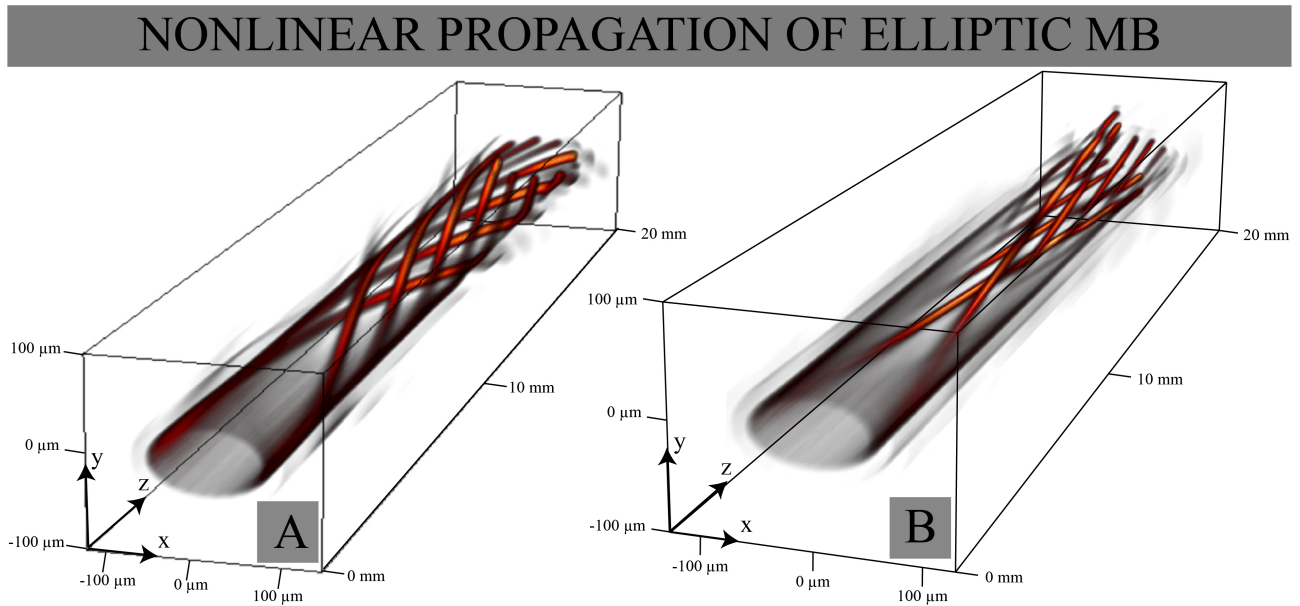


Figure 6.9: Numerical simulation of the 3D intensity volume inside 20mm long SBN crystal. Fabrication of photonic structure (A) from Fig. 6.8 (A3) and (B) from Fig. 6.10 (A3).

The investigation is dedicated to how characteristic structure size $a = 2\pi/k_t$ of elliptic Mathieu beam influence on intensity filamentations in the nonlinear medium. Figure 6.10 shows the influence of increasing characteristic beam sizes $a = [15, 20, 25] \mu\text{m}$ to the nonlinear propagation for constant beam power of $P_0 \approx 20\mu\text{W}$, experimentally and numerically. Arrows again indicate the numerically calculated Poynting vector. For $a = 15\mu\text{m}$ (Fig.6.10 (A1)) conglomerations of intensity is not visible, but for $a = 20\mu\text{m}$ filamentation occurs as depict in Fig.6.10 (A2). This filamentation is similar to one occur for $a = 15\mu\text{m}$ with the higher power P in between $2P_0$ and $4P_0$ depicted in Figure 6.8.

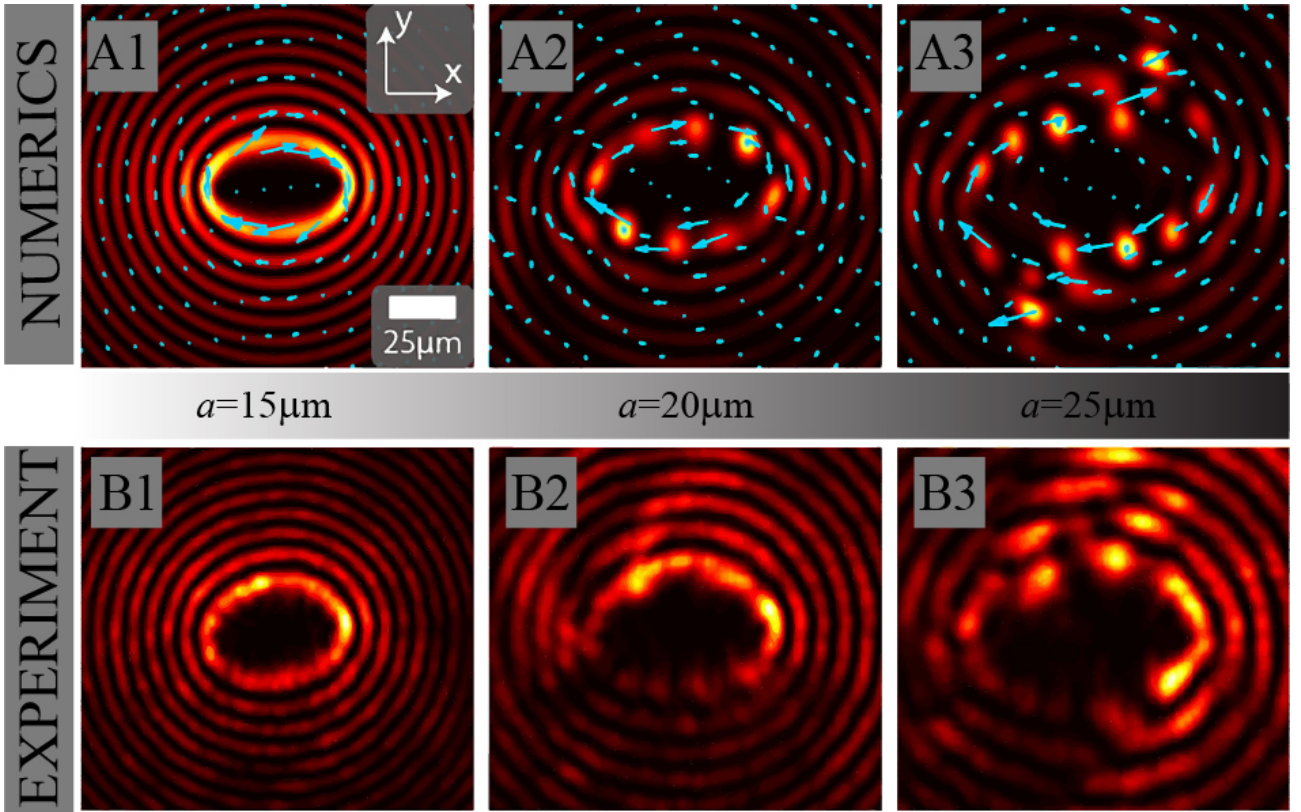


Figure 6.10: Nonlinear self-action with increasing structure sizes a . Numerically calculated (top) and experimentally measured (bottom) transverse intensity distributions at the back face of the SBN crystal after nonlinear self-interacting propagation of elliptic Mathieu beams ($P \approx 20 \mu\text{W}$), for beams with different structure sizes a . Arrows indicate the Poynting vector.

For structure size $a = 25\mu\text{m}$ the self-action is strong and tends to become stronger for larger structure sizes a . In contrast to previous cases, the intensity spreads to ellipses located more outside due to increasing modulation instabilities and more spots with high intensity are observed. Consequently, the Poynting vector directs outward for the outer high-intensity spots (Fig.6.10 (A3)). Experimental results are asymmetric due to the thermal diffusion effect, which is neglected in numerical calculation.

For this structure size 3D distribution of the main intensity inside the crystal is presented in Fig. 6.9 (B). After some propagation distance, the main and next intensities are separated into high intensity spots, which rotates in the direction determined by energy flow generating rotating refractive index strands. It is demonstrated that by increasing the structure size a of elliptic Mathieu beams, the local slope of the helix of the emerging rotating strands of higher refractive index is decreased.

Figure 6.9 presents the numerical visualization of rotating high-intensity filaments, i.e. 2D twisted waveguides through the crystal due to the nonlinear self-interaction of elliptic Mathieu beams. An enhanced degree of branching could be observed in the dependency of beam size a of elliptic Mathieu beam. By changing beam size a and power P it is possible to manage the number of rotating strands and their slope. This illustrates optically induced chiral Mathieu photonic lattice where the rotation of waveguides is directed by the direction of the energy flow of elliptic Mathieu beams, with the opportunity to change the period of rotation as well as the radius of waveguides. Further investigations could potentially show advanced light-matter interactions, e.g., when probing these diverse chiral structures with chiral light.

This section represents an approach to identify and visualize the energy flow of light based

on the symmetry breaking by nonlinear light-matter interaction of OAM carrying beams. Elliptic Mathieu beams with outstanding continuously modulated OAM distributions are used for the purpose. It is revealed that the nonlinear self-action of elliptic Mathieu beams managed the formation of high-intensity filaments, which rotated in the direction determined by the energy flow. It is examined how the strength of the nonlinearity and the structure size of the Mathieu beams influence the emerging photonic structure. Twisted refractive index formations, which could act as chiral waveguides, are observed in the limited regime with proper parameters of the nonlinearity and structure size. Hence, by this approach, it is provided a new method for the realization of the chiral photonic lattices with longitudinally increasing "helix slopes", and additionally tailored transverse ellipticities.

6.2 Elliptical vortex necklaces in Mathieu lattices

In this section, linear and nonlinear excitation of two-dimensional Mathieu photonic lattices induces in photorefractive SBN crystal is investigated experimentally and numerically. Elliptical vortex beam is used as probe beam. First, a single Mathieu beam is used to fabricate Mathieu lattices and the propagation of elliptic vortices is examined in them. The main goal of this examination is to provide the conditions for the existence of spatially localized vortex states.

The optical vortex possesses a phase singularity and a rotational flow around the singular point in a given direction can be applied in many physical systems [86]. Different single Mathieu beams are used as writing light for the optical induction of Mathieu lattices with different shapes. Certain Mathieu lattices optically induced in nonlinear SBN crystal are an exemplary two-dimensional photonic structure for the examination of the propagation of elliptical vortex beams.

The experimental setup for this investigation is depicted in Fig. 4.4. The experiment is realized in photorefractive SBN crystal with a geometrical dimension $5 \times 5 \times 15 \text{mm}^3$. Nd: YVO₄ laser is used as the light source. Crystal is externally biased with an electric field $E_{ext} = 1600 \text{ V/cm}$ aligned along the optical $c = x$ -axis, perpendicular to the direction of propagation (z -axis). As for writing beam, even Mathieu beams of order $m = 8$, characteristic beam size $a = 90 \mu\text{m}$, and various ellipticity parameters q is used, and the elliptic vortex is used as the probe beam, shown in Fig. 6.11.

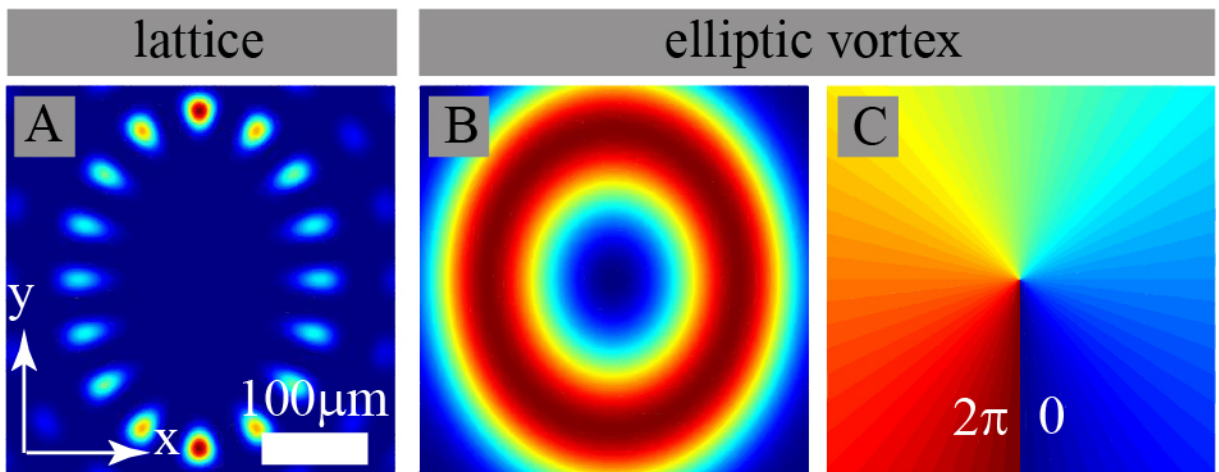


Figure 6.11: Characteristic of Mathieu lattice and elliptic vortex. (A) Intensity distribution for Mathieu lattice of order $m = 8$, ellipticity $q = 15$ and structure size $a = 90 \mu\text{m}$ in the front face of the SBN crystal. (B), (C) Intensity and phase distributions of elliptic vortex in the front face of the SBN crystal.

This investigation starts by considering the Mathieu lattices optically induced with even Mathieu beam of order $m = 8$, with increasing ellipticity parameter q . The ellipticity parameter q is gradually increased allowing change of the photonic structure shape from a circle to an ellipse. The presence of the lattice during vortex propagation induces separation of confinement elliptic vortex in filaments around the location of the incident vortex ring and the surrounding lattice sites.

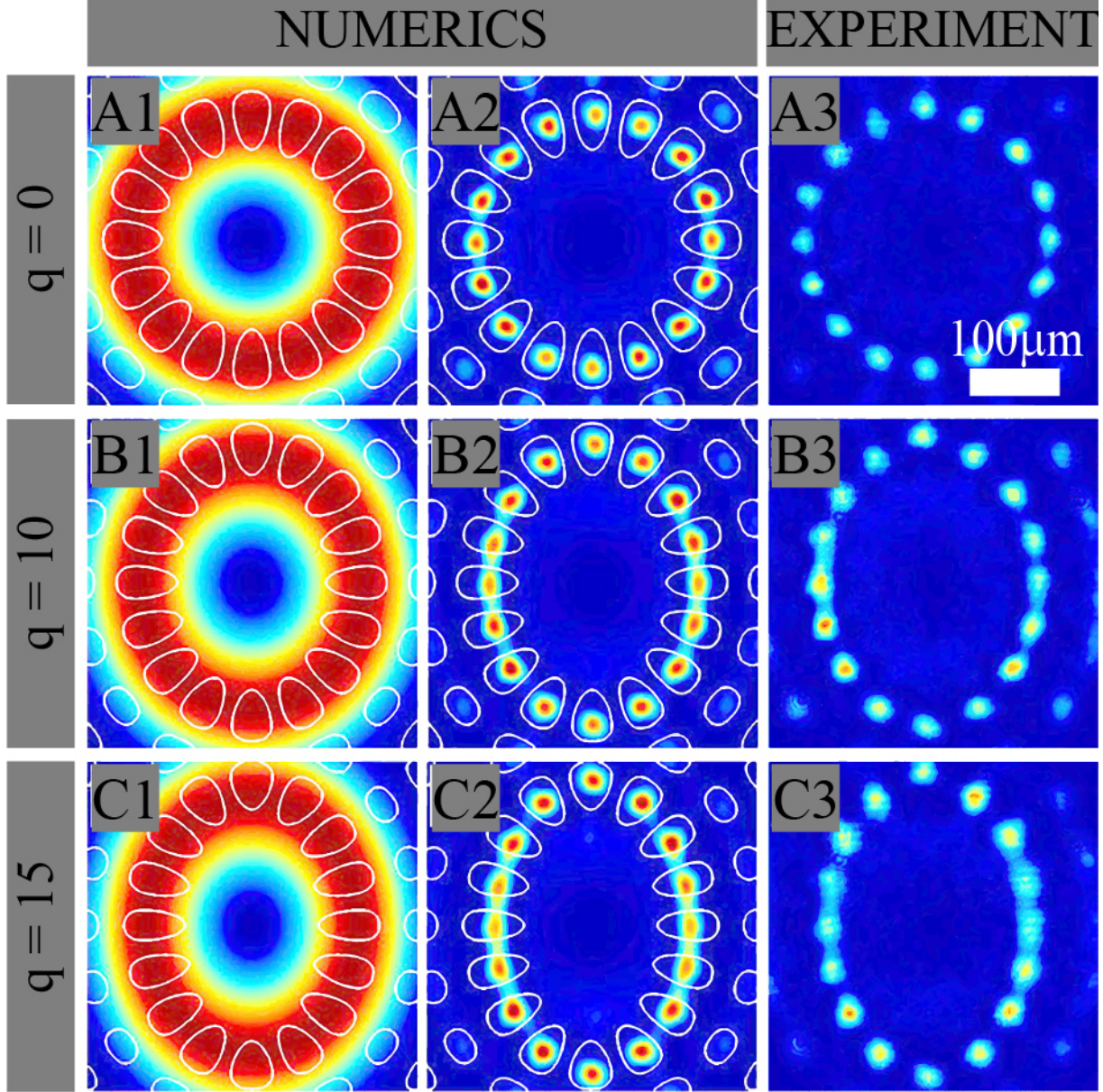


Figure 6.12: Elliptical necklaces in Mathieu lattices with different ellipticity parameter q and topological charge $C_T = 1$. The input vortex beam is shown with the layout of the lattice beams indicated by open circles (the first column). The corresponding intensity distributions are shown at the exit crystal face in numerical results (second column) and experiment (third column). Numerical lattice intensity $I_{latt} = 0.3$, and input vortex intensity $I = 0.005$; the experimental lattice power $P_{latt} = 20 \mu\text{W}$ and input vortex power $P = 8 \mu\text{W}$.

Figure 6.12 summarizes results for three different values for ellipticity parameter q of Mathieu lattices. The input vortex beam with topological charge $C_T = 1$ varies to cover the sites on the inner lattice ring. The first two columns show results from numerical simulations while in the third one experimentally observed results are presented. In the case with no ellipticity ($q = 0$), a stable necklace

beam is observed for a quasi-linear case (very low nonlinearity) (Fig. 6.12 (A)). Next, the lattice ellipticity is increased while other parameters are unchanged. Again elliptical necklaces are obtained but necklace "pearls" are slightly close to each other, determined by shape and distribution of the lattice sites in that lattice area. These vortex states are stable during propagation inside the 15mm long crystal.

When beam order ($m > 8$) is increased, elliptical necklaces with a larger number of pearls are observed. These structures are stable along with propagation for the length of the crystal and topological charge $C_T = 1$. Figure 6.13 presents the intensity distributions of elliptical necklaces in Mathieu lattices of order $m = [9, 10, 11, 12]$ at the exit crystal face from numerical simulations. If the broader vortex beam covers more rings of the Mathieu lattices multiple necklaces are observed but they are not stable during propagation (Fig. 6.14).

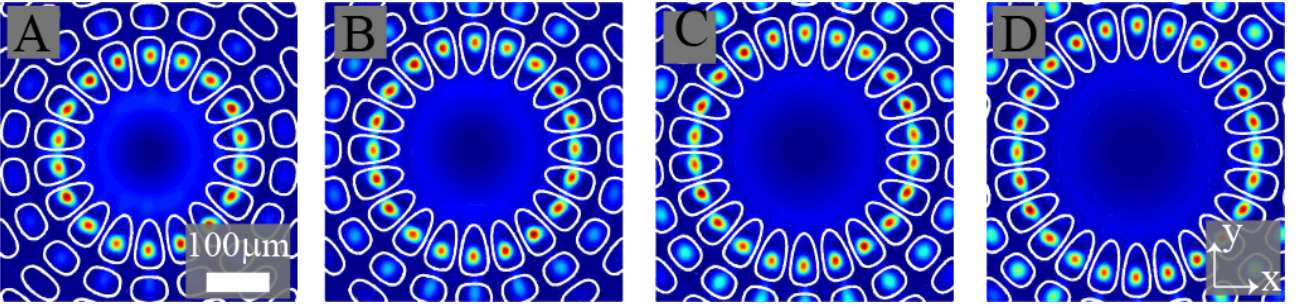


Figure 6.13: Stable elliptical necklaces in Mathieu lattices of different order m with ellipticity parameter $q = 0$ and topological charge $C_T = 1$: (A) $m = 9$, (B) $m = 10$, (C) $m = 11$, (D) $m = 12$.

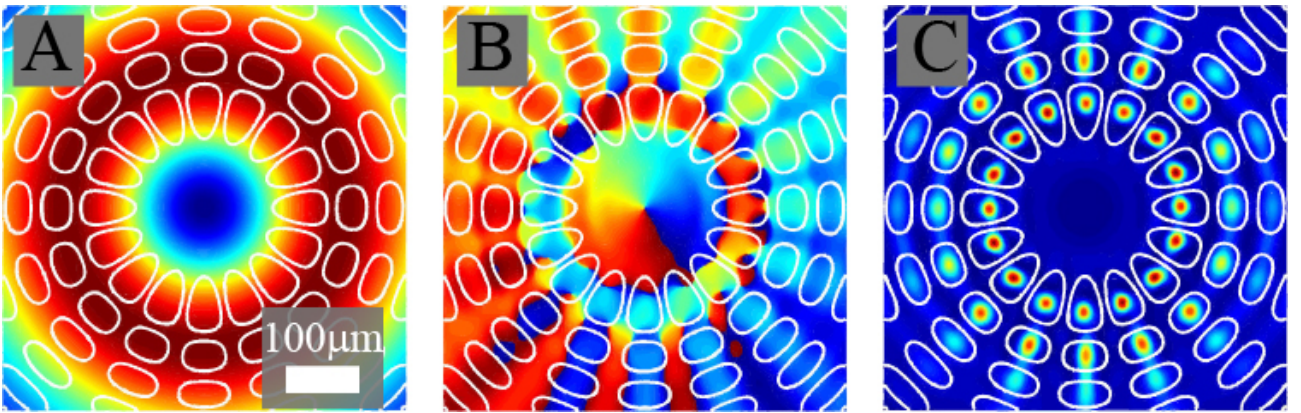


Figure 6.14: Multiple elliptical necklaces in Mathieu lattices of order $m = 8$ with ellipticity parameter $q = 0$ and topological charge $C_T = 1$: (A) The input vortex beam is shown with the layout of the lattice beams indicated by open circles. Numerically observed (B) phase and, (C) intensity distributions at the back face of the crystal. Numerical lattice intensity $I_{latt} = 0.3$, and input vortex intensity $I = 0.005$.

In further, higher-order vortex beams are investigated in Mathieu lattices with $q = 15$. As the probe beam is used the same vortex beam but with different topological charge C_T . The results are depicted in Fig. 6.15. While C_T increment, energy flow inside the inner lattice ring causes an increase in asymmetry. But from the overall phase distribution, it is noticeable that the central area still preserves the expected vortex state. The phase on the inner lattice ring still corresponds to the input C_T , but it is circularly shifted with respect to the central vortex area. Phase distributions along the propagation are shifted along the inner lattice ring, as well as in the central part of the phase distributions.

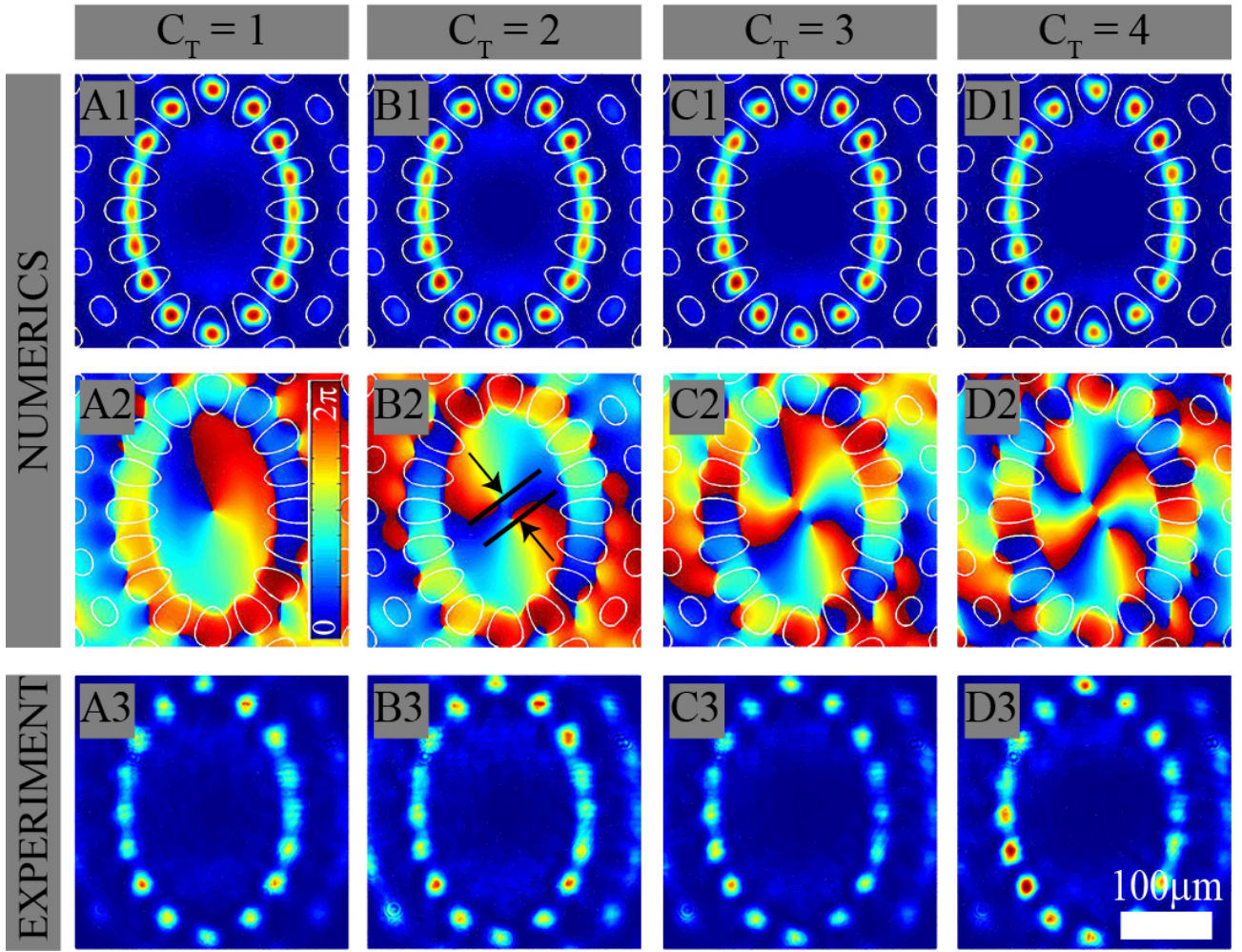


Figure 6.15: Single- and multiple-charged elliptical necklaces. (A1) - (D1) Numerically observed intensity and (A2) - (D2) phase distributions. (A3) - (D3) experimentally observed intensity distributions at the back face of the crystal. The lattice ellipticity $q = 15$ and other parameters are as in Fig. 6.15.

In contrast to the conventional multiple-charged vortex where the embedded phase singularity is multiply folded, the elliptical necklaces show an unfolded behavior in the phase distribution. For higher-order elliptical vortices, a spatial separation of several single-charged phase singularities is observed [87]. Phase singularities separation has the finite distance and depends on the lattice ellipticity, or the topological charge of input vortex C_T . The Euclidean distance between the two furthest singularities, as indicated in Fig. 6.15 (B2), are calculated for different lattice ellipticity and the results are presented in Fig. 6.16 (A). For higher ellipticities, q higher values of separations distance are observed. When C_T increase, phase singularity separation distances also increases for all ellipticities. Phase singularity separation distances are also calculated during propagation, for higher $C_T = 2, 3, 4$ and $q = 15$ (Fig. 6.16 (B)). As propagation distance increase higher values of separations are observed for higher C_T .

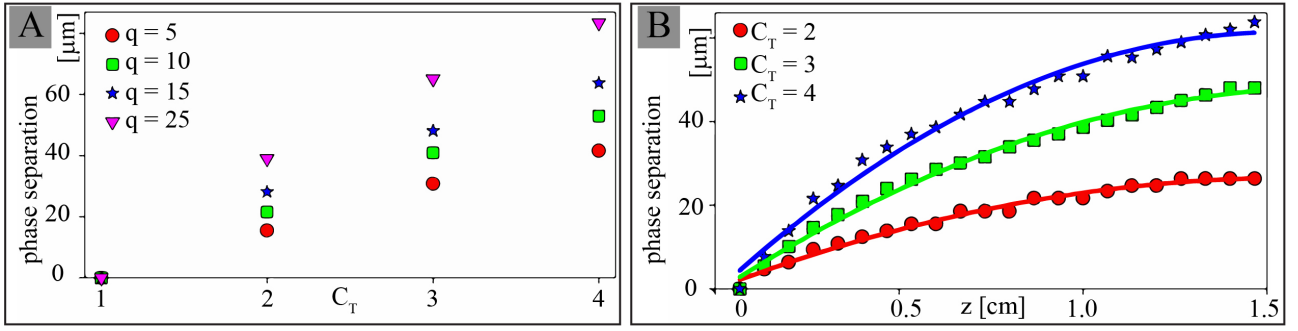


Figure 6.16: Phase singularity separation. (A) Phase singularity separation versus C_T for various lattice ellipticity after 15mm propagation distance. (B) Phase singularity separation versus propagation distance for various C_T for $q = 15$ (Fig. 6.15). Separations are measured between the two singularities for lattice ellipticity as a Euclidean distance.

The elliptical necklaces are obtained in the quasi-linear regime. Their stability is investigated for propagation distances longer than crystal size via numerical simulations. It is established that elliptical necklaces are stable for propagation length of few crystal sizes, but they transform to oscillating dipole states after 10cm propagation length, as shown in Fig. 6.17 (A)-(C). Their central part of phase distribution remains unchanged, in contrast along the inner lattice ring where initial phase distribution is completely broken. Higher-order vortex states shown in Fig. 6.15 (B)-(D) are slightly asymmetric and stable only for short propagation distance comparable with crystal size.

The standard definition for the (normalized) z component of the orbital angular momentum (AM) gave as [88]

$$L_z = -\frac{i}{2} \int \int dxdy A^*(x, y)(x\partial_y - y\partial_x)A(x, y) + cc. \quad (6.2.2)$$

is used to calculate the orbital AM of necklace beams $A(x, y)$ during propagation. Figure 6.17 (D) presents the mean orbital AM, L_z per transverse plane dependent on the propagation distance z of the necklace states along the propagation distance for different ellipticity parameters q . For higher lattice ellipticity, AM transfer is less in compression for lower ellipticities where the neighboring lobes exchange more power during the propagation (depicted with a red plot in Fig. 6.17 (D)).

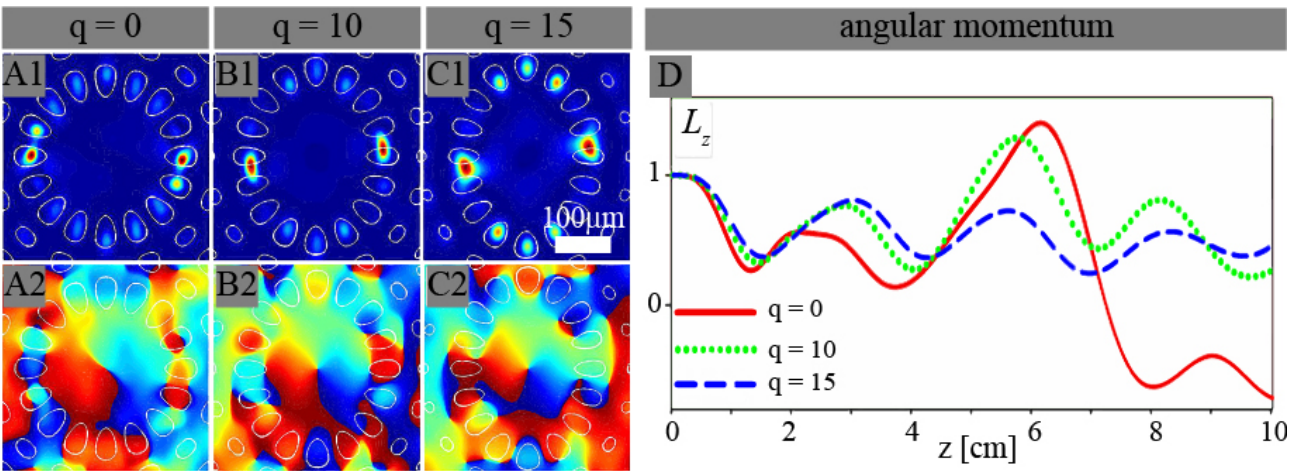


Figure 6.17: Dipole states in Mathieu lattices of various ellipticity (A) $q = 0$, (B) $q = 10$, and (C) $q = 15$. Intensity and phase distributions are presented after 10cm propagation. (D) Normalized z component of the angular momentum along the propagation distance. Other parameters are as in Fig. 6.12.

In the end vortex stability with increasing nonlinearity is investigated. Experimental and numerical results are presented in Fig. 6.18 for vortex states with $C_T = 1$ and lattice ellipticity $q = 15$ for 15mm long crystal. With lower powers, neighboring lobes exchange some power, the elliptical necklace is damaged, and regular oscillations along the propagation are found [Fig. 6.18 (A)]. For higher beam power, irregular oscillations are observed, even more noticeable for longer propagation distances [Fig. 6.18 (B)]. From phase distribution, it is visible that only the central part stays unchanged, in contrast to the inner lattice ring.

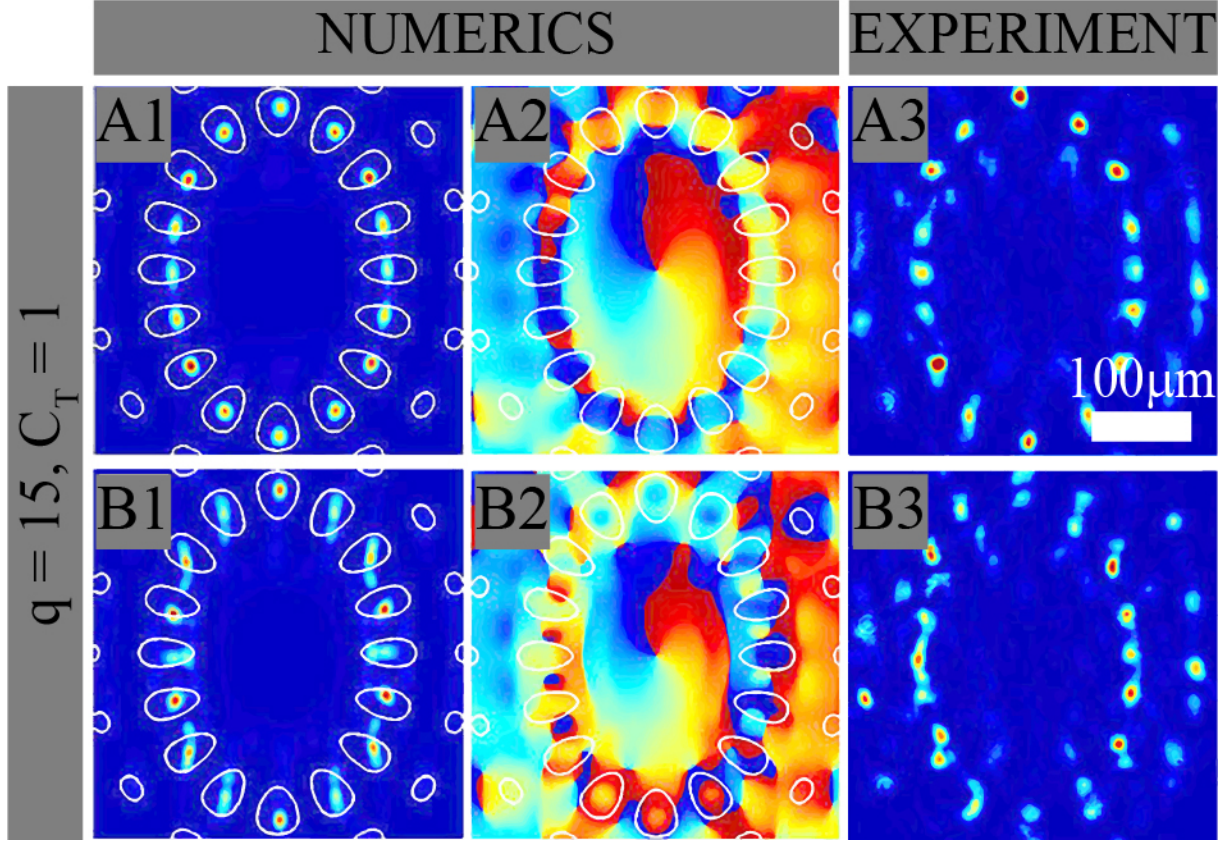


Figure 6.18: Nonlinear vortex propagation in Mathieu lattices. (A1), (B1) intensity distributions, (A2), (B2) corresponding phase distributions at the exit face of crystal obtained from numerical simulations, (A3), (B3) intensity distributions at the exit face of crystal experimentally obtained. Input vortex intensities in numerical simulation are (A1) $I=0.01$ and (B1) $I = 0.1$, with appropriate input vortex power in experiment (A3) $P = 20\mu\text{W}$ and (B3) $P = 30\mu\text{W}$.

In this section, experimental and numerical investigation of the elliptical vortex inside the optically induced Mathieu lattices in 15mm long SBN crystal is presented. Stable elliptical necklaces are obtained, control of the shape and size of the elliptical necklace was analyzed, as well as the number of pearls in them by changing order of the Mathieu lattices and their ellipticities. For higher-order vortices, it has been noticed separation of phase singularity, which is calculated. It is demonstrated that separation increase with increasing C_T , ellipticity or propagation distance. The conditions for stable elliptical necklaces were found and their orbital AM is measured. Oscillating dipole states or dynamic instabilities were observed for longer propagation distances, higher beam power, and higher-order vortices. These results enable further investigations of vortex beam control in photonic lattices optically induced by other than Mathieu beams and they have potential applications in the field of optical micromanipulation to guide, trap, and sort objects.

6.3 Creation of aperiodic photonic lattices and investigation of light propagation in the aperiodic Mathieu lattice

In this section, would be considered an influential approach for the creation of the two-dimensional (2D) aperiodic photonic lattices in a SBN crystal by using Mathieu nondiffracting beams as well as the linear and nonlinear propagation of light in such formed lattices.

6.3.1 Creating aperiodic photonic structures by synthesized Mathieu-Gauss beams

Even Mathieu beams have different intensity distributions as shown in Fig. 3.3, hence it is possible to create different 2D photonic lattices only by changing the order m , or ellipticity q of a single Mathieu beam. Such photonic lattices are well-suited systems for control and manipulation of light propagation. However, in this section 2D aperiodic photonic lattices are created by synthesizing two or more even Mathieu beams. Even Mathieu beams with the same ellipticity $q = 25$ and characteristic beams size $a = 25\mu\text{m}$ are used. Additionally, the Mathieu beams are apodized with Gaussian beams which yield to finite energy pseudo-nondiffracting beams, *Mathieu - Gauss beams* (MG) [89].

Three different ideas presented in this section for the creation of various *complex aperiodic Mathieu beams* would be used for optically-induced photonic lattices. These results will open new future research especially in the field of light propagation in such aperiodic photonic lattices and potential application in the realization of optical devices.

The interference of two even MG beams of a different order m_1 and m_2 is investigated and their transversal intensity distribution is reproduced from numerical simulations and experiment in Fig.6.19. When MG beams with the same orders parity in phase configuration (m_1, m_2 - both even or both odd) interfere the observed structures are symmetric according to y -axis. Two examples for $m_1 = 0, m_2 = 10$ and $m_1 = 1, m_2 = 7$ are shown in Figs. 6.19 (A) and 6.19 (B), respectively. But, if the interfering MG beams have different orders parity and in phase configuration ($m_1 = 2, m_2 = 7$ and $m_1 = 13, m_2 = 14$) asymmetric intensity distributions are realized and depicted in Figs. 6.19 (C) and 6.19 (D), respectively.

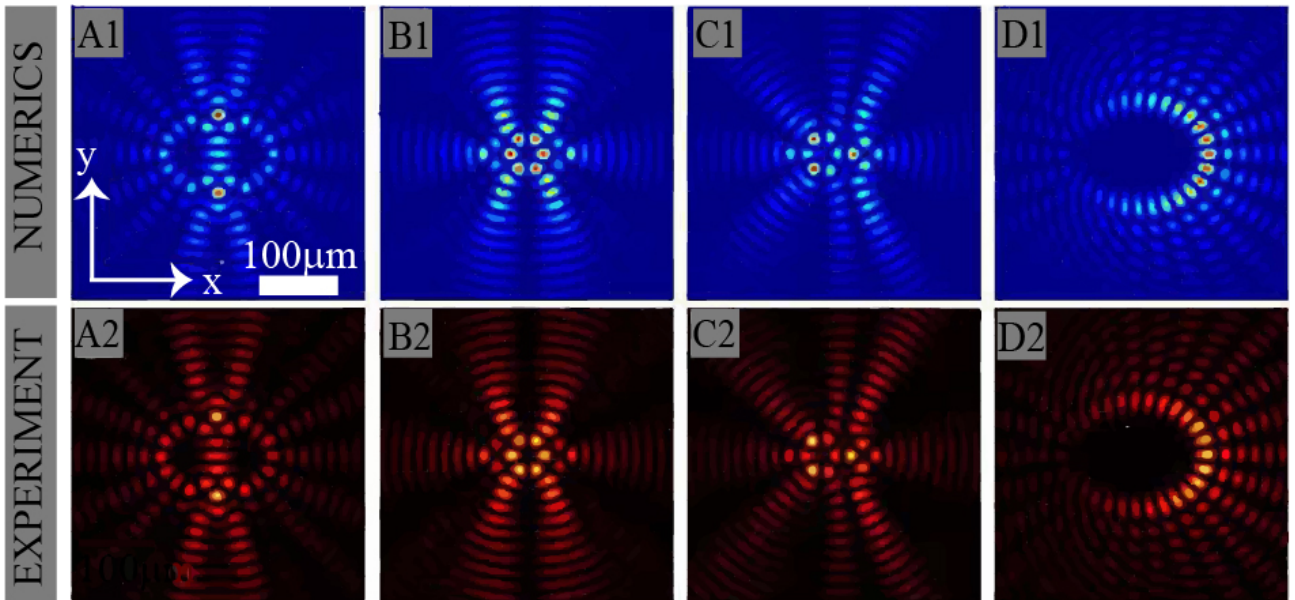


Figure 6.19: Interference of two MG beams of different order. Transverse intensity distribution obtained by interfering MG beams with the same parity: (A) both even $m_1 = 0$ and $m_2 = 10$; (B) both odd $m_1 = 1$ and $m_2 = 7$, or different parity: (C) $m_1 = 2$ and $m_2 = 7$ (D) $m_1 = 13$ and $m_2 = 14$.

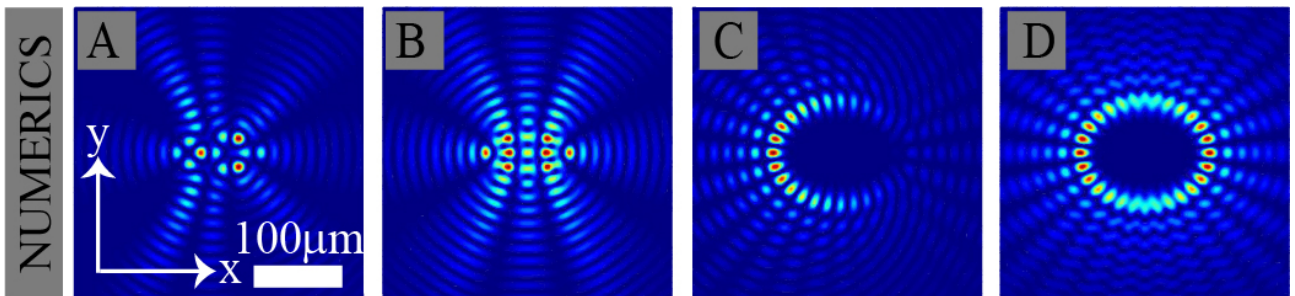


Figure 6.20: Interference of two MG beams of different order and phase configurations. Transverse intensity distribution of superimposing beams with the same parity: (A) $m_2 = 7$, $m_1 = 2$, π out of phase; (B) $m_2 = 2$, $m_1 = 7$, $\pi/2$ out of phase; (C) $m_2 = 13$, $m_1 = 14$, π out of phase; (D) $m_2 = 13$, $m_1 = 14$, $\pi/2$ out of phase.

In the previous cases, both interfering beams are in phase. In the case of the π out of phase interference, mirror-symmetric structures are revealed (Fig. 6.20 (A), (C)). It is possible to observe symmetric structures by interfering MG beams of different orders parties only if they have phase differences of $\pi/2$ (Fig. 6.20 (B), (D)). The comparable structures could be produced by synthesizing mirror-symmetric structures.

In second approach two even MG beams with the same order m , but oriented at 90° with respect to each other are superimposed, considering additionally the in-phase and π out of phase configurations and results are depicted in Figs. 6.21 and 6.22, respectively. First, two MG beams of even order parity m are superimposed and results for $m = 2$ and $m = 8$ are presented in Figs. 6.21 (A), (B) and Figs. 6.22 (A), (B) for in-phase and π out of phase configurations, respectively. Afterward, MG beams of odd order parity ($m = 5$ or $m = 7$) are used and results are depicted in Figs. 6.21 (C), (D) for in-phase configurations and in Figs. 6.22 (C), (D) for π out of phase configurations.

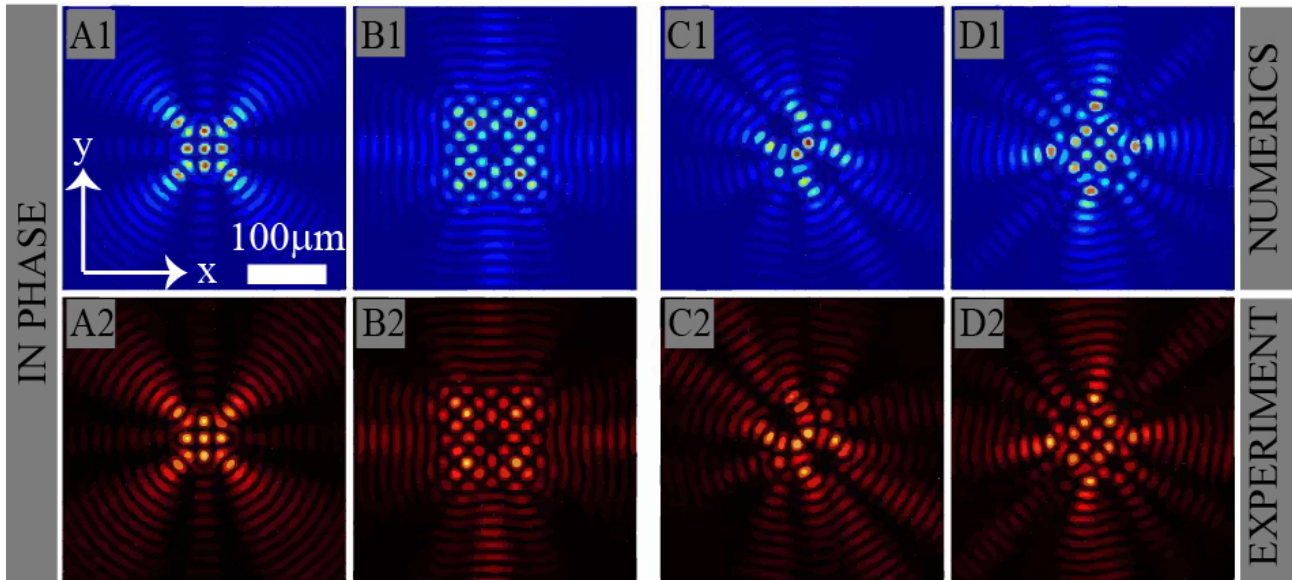


Figure 6.21: Transverse interference patterns of two MG beams of the same order m , in-phase and oriented at 90° with respect to each other: even parity (A) $m = 2$; (B) $m = 8$; and odd parity (C) $m = 5$; (D) $m = 7$.

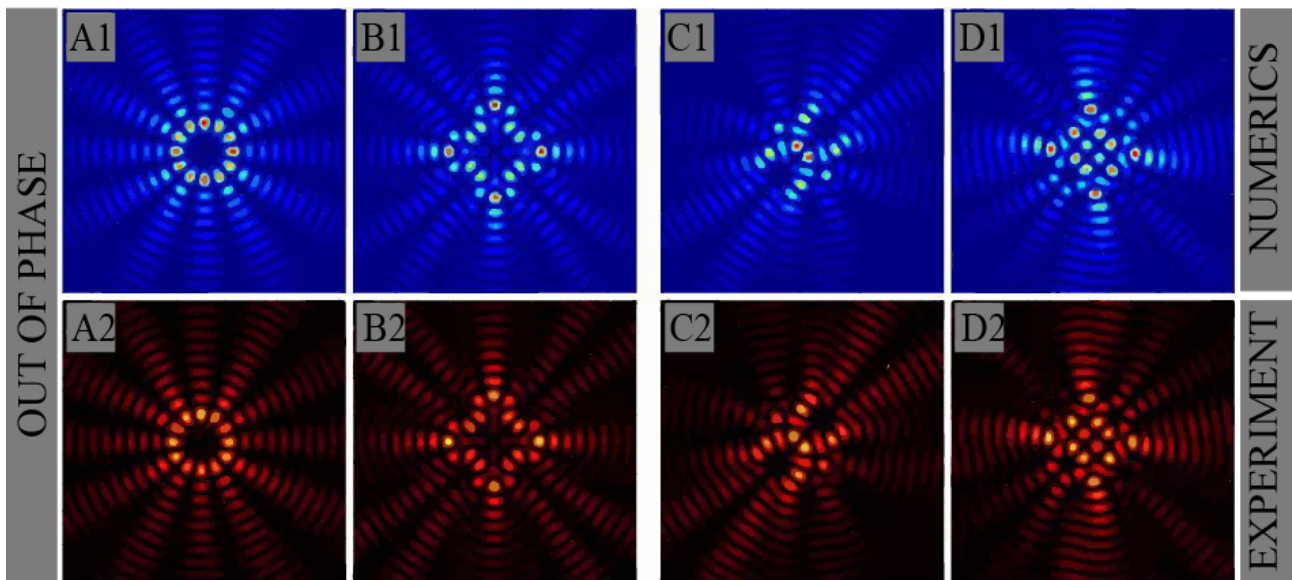


Figure 6.22: Transverse interference patterns of two MG beams of the same order m oriented at 90° with respect to each other in π out of phase configurations: even parity (A) $m = 2$; (B) $m = 8$; and odd parity (C) $m = 5$; (D) $m = 7$.

All results are variable according to phase configurations. It is noticeable that for interference of MG beams with even order parity distinguish structures are observed for two different phase con-

figurations, while for MG beams with odd order parity the same intensity distributions are observed but mirror-symmetric to each other. This mirror symmetry of superimposed MG beams with odd orders m is related to the intrinsic symmetry of the related Mathieu functions.

The next approach for the realization of 2D complex aperiodic structures is established on the superposition of MG beams at different mutual distances. The most opportunities for the realization of different patterns are provided by this approach. Figure 6.23 shows the interference of two even MG beams of the same order, $m = 6$ or $m = 7$ arrange along x -axis at various mutual distances D , $2D$ and $3D$, where $D = 20\mu\text{m}$.

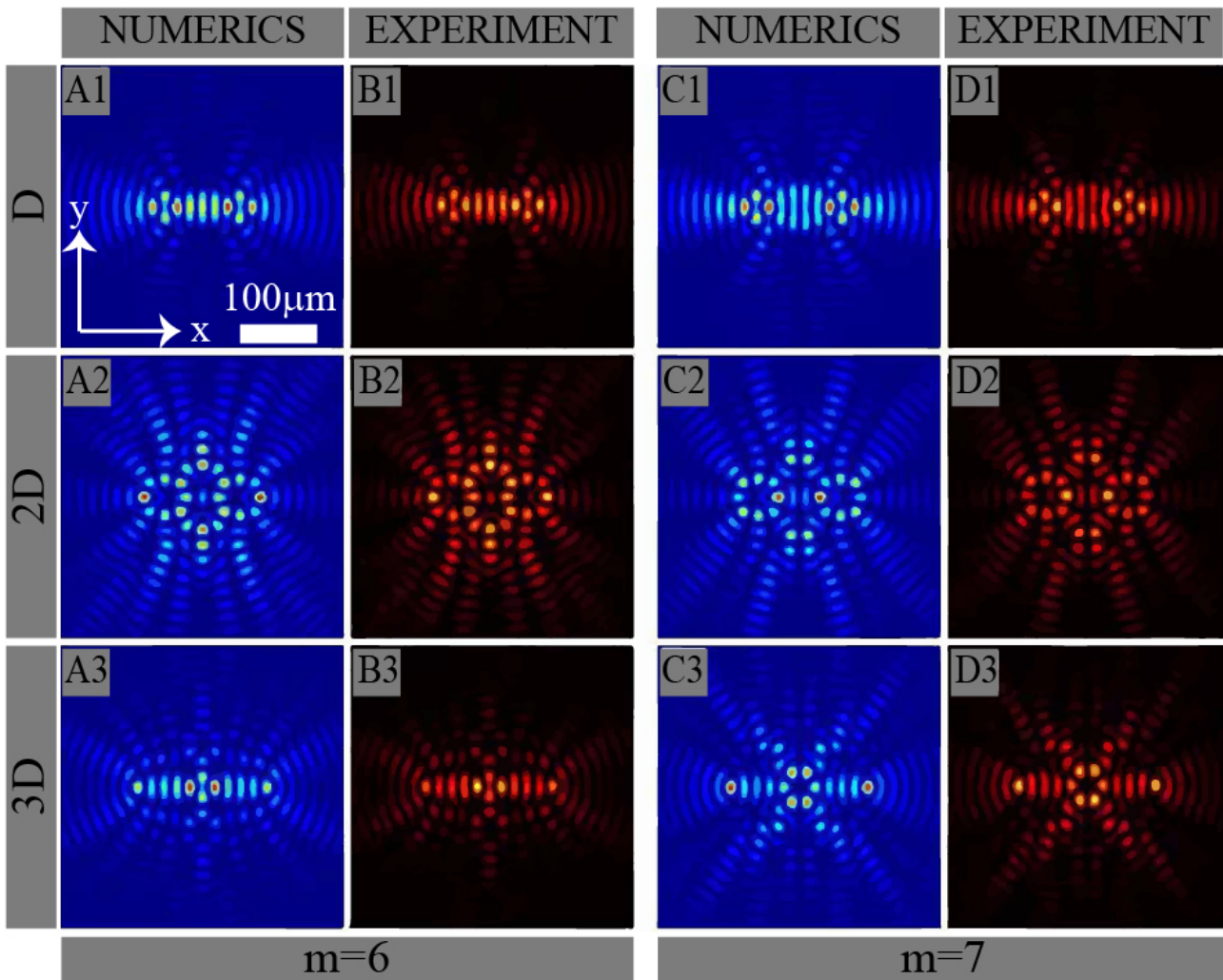


Figure 6.23: Interference of MG beams with same order at different mutual distances along x -axis: (A), (B) $m = 6$ and (C), (D) $m = 7$. First row: interference at mutual distance $D = 20\mu\text{m}$, second: doubled distance $2D$, and third: triple distance $3D$.

In order to generate different complex aperiodic photonic structures via Mathieu beams, the previous approach of synthesizing multiple MG beams at different mutual distances is used. By using previous approaches, new field distributions are provided and they serve as a "unit cell" for more complex aperiodic beams. Such complex aperiodic beams could be used as writing light capable of being transferred to tailored refractive index modulations in photosensitive media i.e. photonic lattices. The unit cell would be multiplied in x or y direction which allows continuously increase the degree of aperiodicity.

In continuation new aperiodic photonic structures would be produced. First, pattern from Fig. 6.19 (B) is used as unit cell and multiply twice in x -direction at the distance of $D_x = 80\mu\text{m}$. The single array is observed and presented in Fig. ?? (A). Afterward, the resulting array is multiplied along the y -direction at three different mutual distances $D_y = 80\mu\text{m}$, $D_y = 88\mu\text{m}$, and $D_y = 96\mu\text{m}$. Various aperiodic lattice structures are observed as shown in Figs. ?? (B) - (D). Those examples exhibit areas where the initial unit cell is preserving its shape, but additionally novel unit cells appear in depends on the mutual distances between the multiplied arrays.

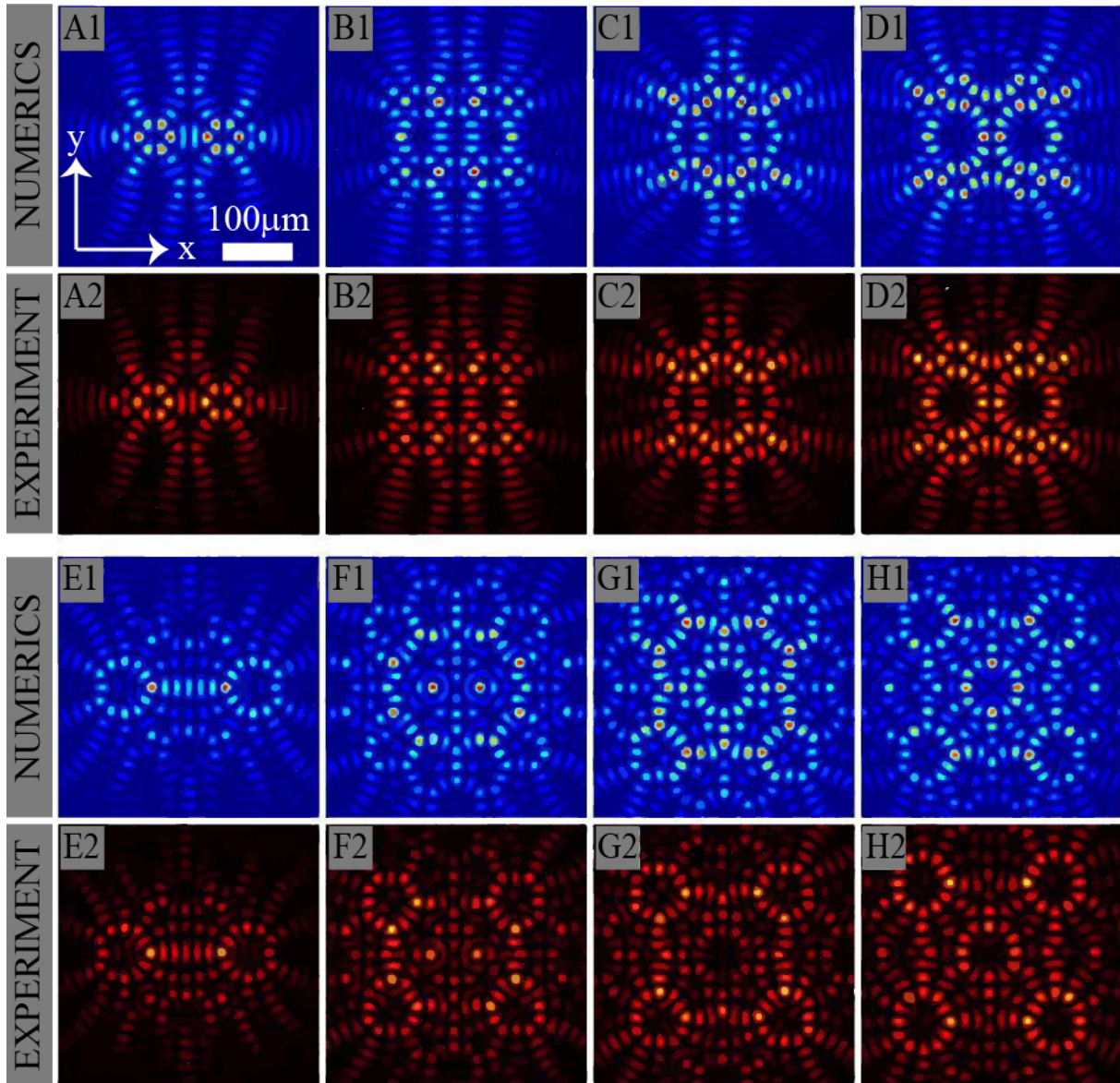


Figure 6.24: Realization of aperiodic photonic lattices by multiplying the structure (A)-(D) from Fig. 6.19 (B) and (E)-(H) Fig. 6.22 (A) at various distances.

Next, the necklace structure from Fig. 6.22 (A) is investigated as unit cell. The unite cell is multiplied in x -direction at different distances. One example is presented in Fig. 6.24 (E), for $D_x = 144\mu\text{m}$. Such observed structure is multiplied in y -direction to create a complex aperiodic structure by changing the mutual distances between them: $D_y = [120, 144, 152]\mu\text{m}$ (Figs. 6.24 (F) - (H)). Initial unit cell and additional ones, which can be control by changing the distances between initial unit cell used for multiplying, are observed.

Figure 6.25 presents novel 2D aperiodic photonic structures crated via Mathieu beams. The

unit cell depicted in Fig. 6.23 (A2) is multiplied along x -axis at different mutual distances: $D_x = [152, 176, 192] \mu\text{m}$ and equivalent results are shown in Figs. 6.25 (A) - (C), respectively. By this, the initial structure shape is preserved but with slightly different interfering patterns between them. Then the structure from Fig. 6.25 (D) is multiplied along y -direction for $D_y = 104\mu\text{m}$, and a new 2D complex structure is observed.

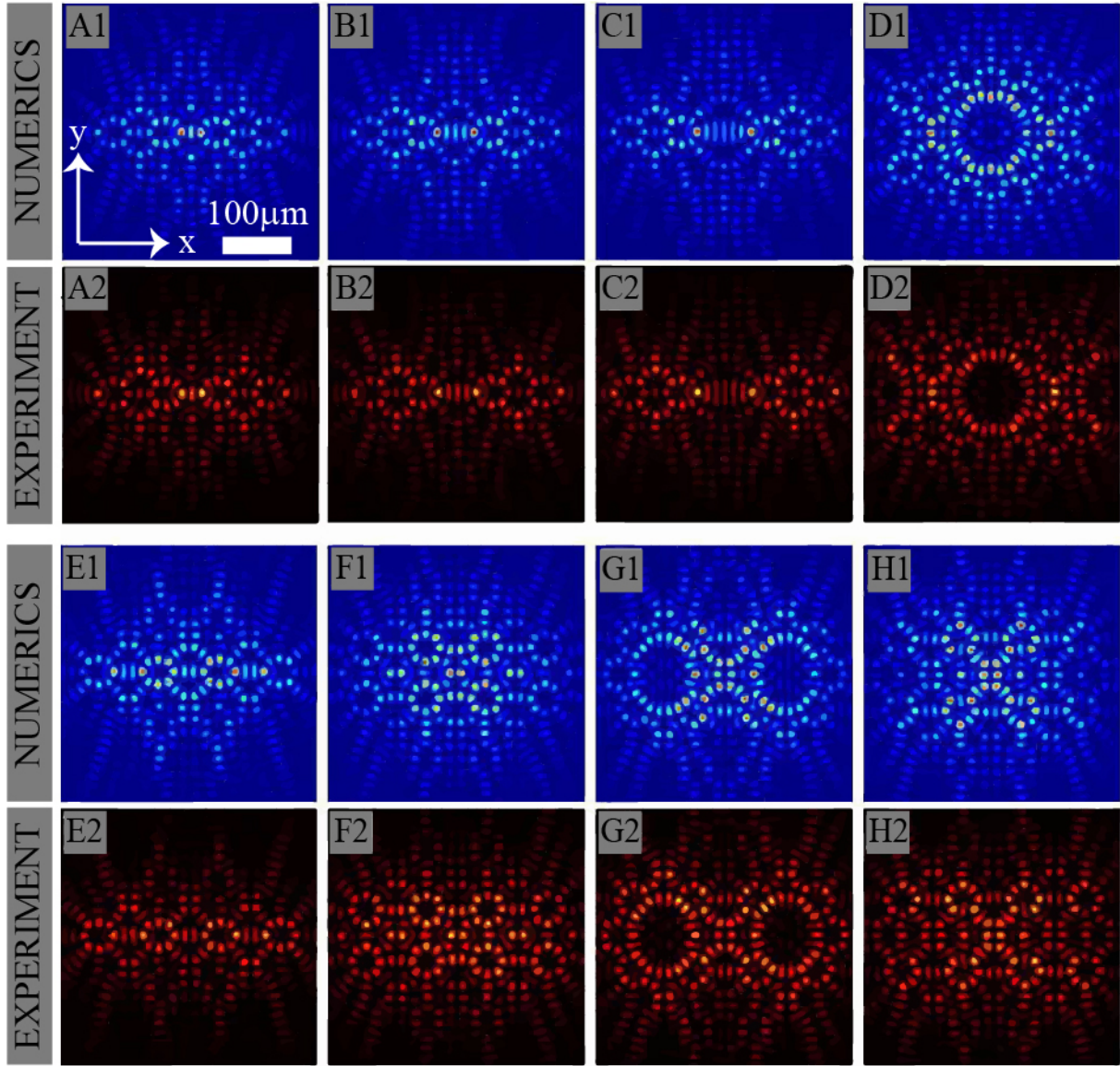


Figure 6.25: Various aperiodic photonic structures realized by multiplying (A) - (D) the structure from Fig. 6.23 (A2) and (E) - (H) the structure from Figs. 6.23 (C2) at different mutual distances.

Figure 6.25 presents novel 2D aperiodic photonic structures, with the structure from Figs. 6.23 (C2) as unit cell. Such structure is multiplied in x -axis for distance $D_x = 176\mu\text{m}$ and result is shown in Fig. 6.25 (E). Observed structure is multiplied along the y -direction at various mutual distances: $D_y = 72\mu\text{m}$, $D_y = 96\mu\text{m}$, and $D_y = 104\mu\text{m}$, and additional shapes of 2D aperiodic photonic structures are observe, as shown in Figs. 6.25 (F) - (H).

Such formed complex aperiodic structures would be used as writing light to create 2D photonic lattices in photosensitive SBN crystal and examine light propagation in them (next subsection). Therefore, their nondiffracting character has to be confirmed in SBN crystal. Two aperiodic structures, presented in Figs. 6.24 (H) and 6.25 (H), are investigated during linear propagation through the 20mm long crystal. Figures 6.26 (A) and (D) depict xz cross-sections through the intensity volume at the orientation indicated with the white line in Figs. 6.26 (B) and (E), respectively. This xz cross-section proves that the complex beams propagate invariant through the SBN crystal. Experimental setup presented in Fig. 4.3 is used for optical induction of aperiodic photonic lattices by ordinary polarized writing beams. The illumination time is 35s with a moderate laser power of $P \approx 30\mu\text{W}$ and an external electric field of $E_{ext} = 2000 \text{ V/cm}$. Due to weak nonlinear self-action, lattice writing beams inscribe stationary photonic lattices in crystal. Numerically and experimentally intensity distribution at the back face of the crystal are represented in Figs. 6.26 (B) and (E).

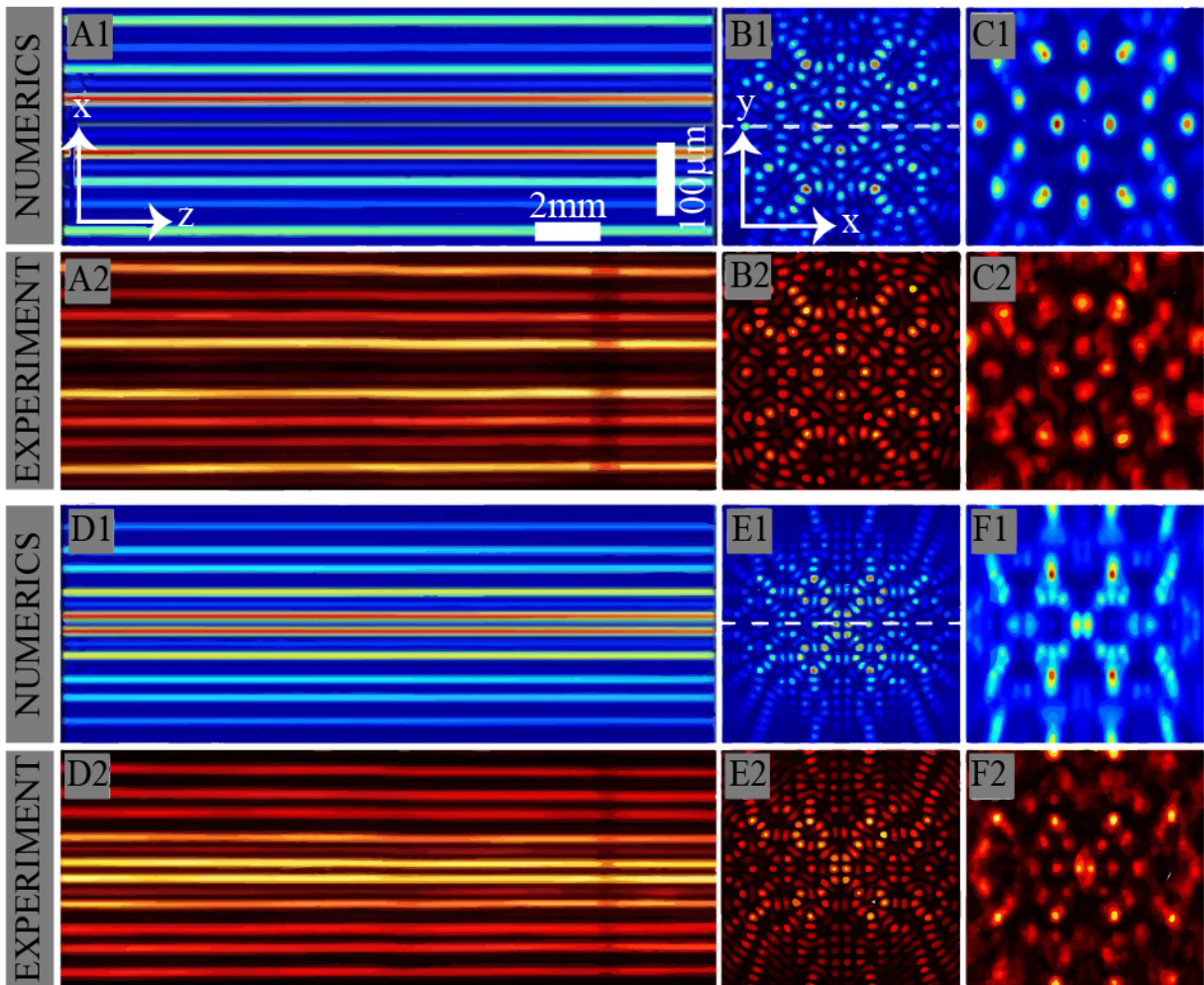


Figure 6.26: Waveguiding in aperiodic photonic structures. As writing beam is used structure from: (A), (B): Fig. 6.24 (H); (D), (E): Fig. 6.25 (H). Intensity distribution of probe beam at the exit face of the crystal (C), (F).

In addition, the optically induced 2D aperiodic lattices were probed with an extraordinarily polarized plane wave to demonstrate waveguiding using the experimental setup shown in Fig. 4.4. Figures 6.26 (C) and (F) demonstrate waveguiding of the initial plane wave in the 2D aperiodic lattices, manifested in a spatially modulated intensity distribution according to the underlying refractive index modulation. As expected, the intensity is preferentially guided in areas where the refractive index is increased and high intensity spots are formed.

In this research, an approaches for realization of numerous new aperiodic patterns by coherently superimposing Mathieu-Gauss beams with different orders, positions, and relative phases is presented. The various 2D aperiodic photonic Mathieu lattices are created by the optical induction technique in SBN crystal. This research is extend, with light propagation study in such aperiodic photonic lattices.

6.3.2 Light propagation in aperiodic photonic lattices created by synthesized Mathieu-Gauss beams

In this section, the effects of light propagation in the aperiodic photonic lattices created by synthesized MG beams in a SBN crystal are investigated experimentally and numerically. The influence of various input beam positions on light diffraction is investigated in linear and nonlinear regimes.

Figure 4.4 shows the experimental setup to fabricate and probe MG beam based photonic lattices. Photonic structure is probed with extraordinarily polarized Gaussian probe beams to feel stronger nonlinearity effect. Figs. 6.27 (A) and (B) present an aperiodic lattice and the characteristic lattice unit cell. The probe beam is launched into a single site inside aperiodic lattice unit cell and experiences lateral transport within the lattice as it propagates along its axis. Thus, the probe beam propagation resulting in a diffraction pattern in dependence of the local structure, which is in contrast to a simple periodic lattice where probe beam expansion is the same for each initial site excitation. In an aperiodic lattice different local environments exist, hence the transport behavior is expected to vary significantly from site to site. Three excitation positions with different local environment are chosen as depicted in Fig 6.27 (B).

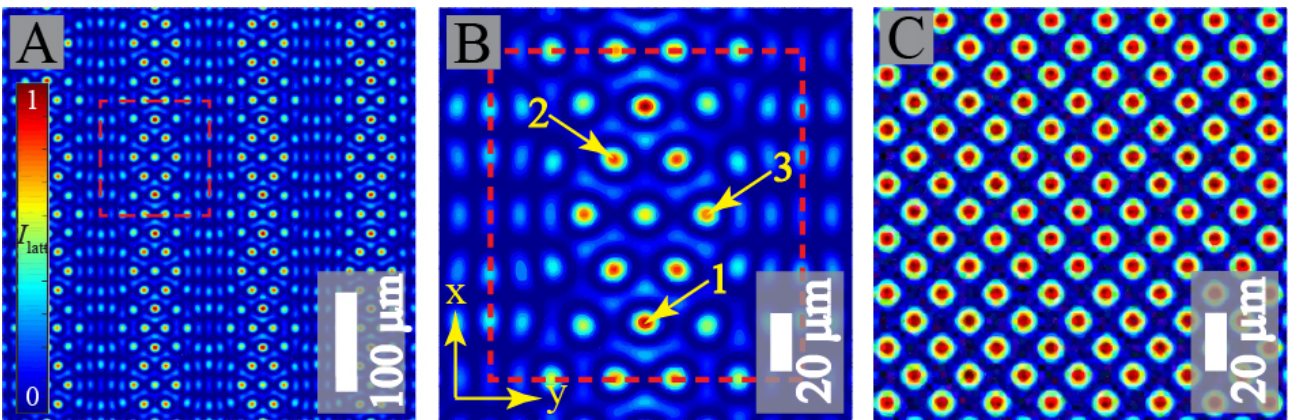


Figure 6.27: Transverse intensity distribution of periodic and aperiodic lattices. (A) Aperiodic lattice created via MG beams, (B) typical unit cell, where the yellow arrows indicate the probe beam excitation sites. (C) Periodic square lattice with period d equal to the characteristic structure size $a = 2\pi/k_{\perp}$ of used MG beams, $d = a = 25 \mu\text{m}$.

First, the linear propagation of light is investigated in such lattice. The lattice is fabricated with the external electric field of $E_{ext} = 2000$ V/cm and laser power of $P_0 = 50\mu W$, which corresponds to a simulated lattice intensity of $I_{latt} = I_0 = 0.7$. After the lattice writing beam and the external electric field E_{ext} are switched off, the Gaussian probe beam with a FWHM of $w_0 = 8\mu m$ and low power of a few $I = 10\mu W$ illuminates one site into the lattice to display linear propagation.

Figure 6.28 presents the intensity distributions of the probe beam after propagating through the lattice inside 20mm long SBN crystal for three distinguish excitation sites marked by numbers 1, 2, and 3 in Fig. 6.27 (B). The first row in Fig. 6.28 shows transverse intensity distributions for those three probing, obtained at the back face of the 20mm long SBN crystal. The propagation through the lattice differs in dependency on which local lattice site is excited. Therefore, the discrete diffraction profiles at the lattice output differ from each other.

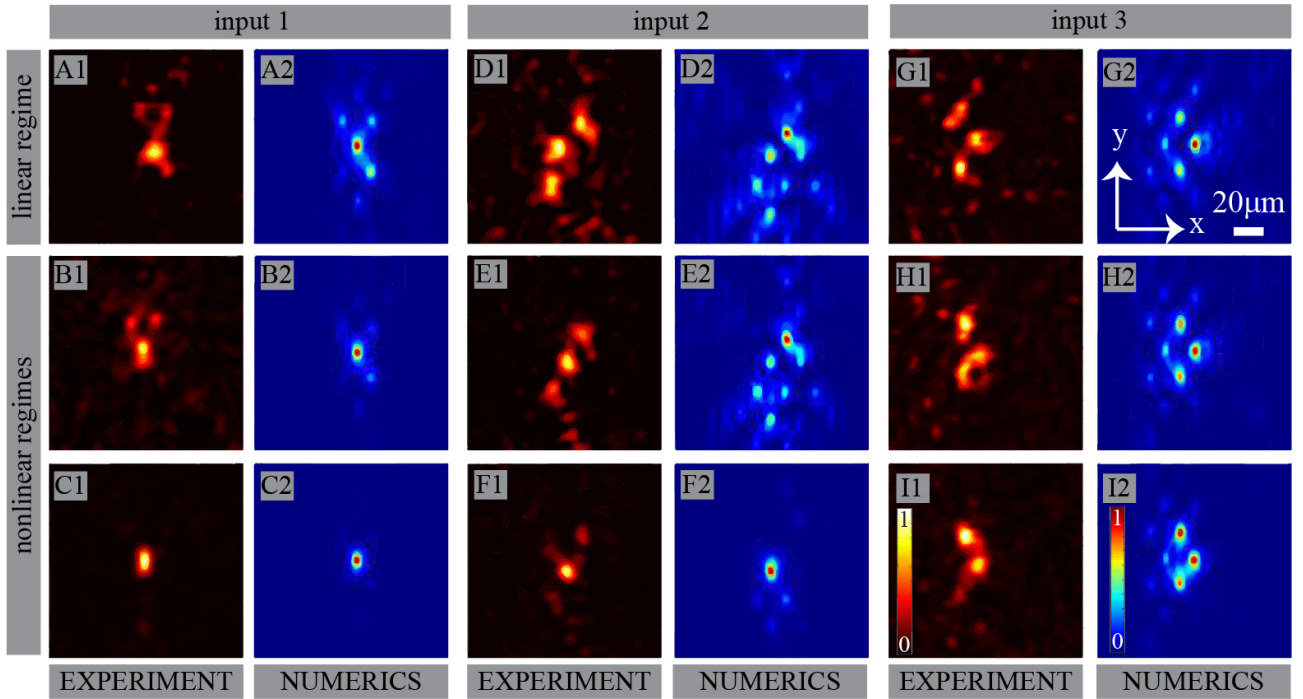


Figure 6.28: Discrete diffraction and lattice solitons in an aperiodic photonic lattice. Numerically and experimentally observed transverse intensity distributions at the crystal's back face in linear regime (the first row) and two nonlinear regimes: (the second row) numerical probe beam intensity of $I = I_0 = 0.7$ and appropriate experimental beam power of $P_0 = 50\mu W$ and (the third row) numerical probe beam intensity of $2I_0$ and experimental beam power of $2P_0$.

Further, numerous experiments and numerical calculations are performed to observe nonlinear localization of the discrete diffraction pattern. Consequently, the intensity of the probe beam is incremented to increase nonlinearity strength. The second row of Fig. 6.28 shows the transverse intensity distribution of the probe beam when propagating through the commonly fabricated lattice with a beam power of $P_0 = 50\mu W$ or $I = I_0 = 0.7$. Next, the strength of the nonlinearity is increased by doubling the beam power $2P_0$ in the experiment and simulation, and the results are presented in the third row of Fig. 6.28.

For the input position 1 and sufficiently high beam powers a *spatial soliton* in the aperiodic lattice are observed (Figs. 6.27 (C1), (C2)), while the other input positions 2 & 3 do not support this localized state (Figs. 6.27 (E), (F), (H), (I)) for the same beam power. Robustness of such spatial soliton is examined numerically by changing the intensities of the probe beams while keeping all

other parameters fixed, and it was found that such solitons remain unchanged up to 3 times higher beam power. The stability of spatial soliton is studied numerically in dependence of the propagation distance and stable output intensity distribution is obtained up to 10cm (not shown).

For the investigation of localization properties of the aperiodic Mathieu lattice in general, independent of the concrete excitation site, the light propagation in the lattice is numerically simulated for 100 different probe beam excitation positions and their expansion is averaged. The probe beam is moved with equidistant spacing across the unit cell depicted in Fig. 6.27 (B). Figure 6.29 presents results for the identical intensities as in Fig. 6.28. The gradual transition from suppressed discrete diffraction to nonlinear localization is noticed. While nonlinearity increases, the output averaged transverse intensity profiles in Fig. 6.29 (A), (B), (C) narrow. But, due to the diverse contributions that are averaged (on- and off-lattice sites are included), their profiles shown in (D) do not show the soliton shape as typically known from spatial bright solitons in the bulk.

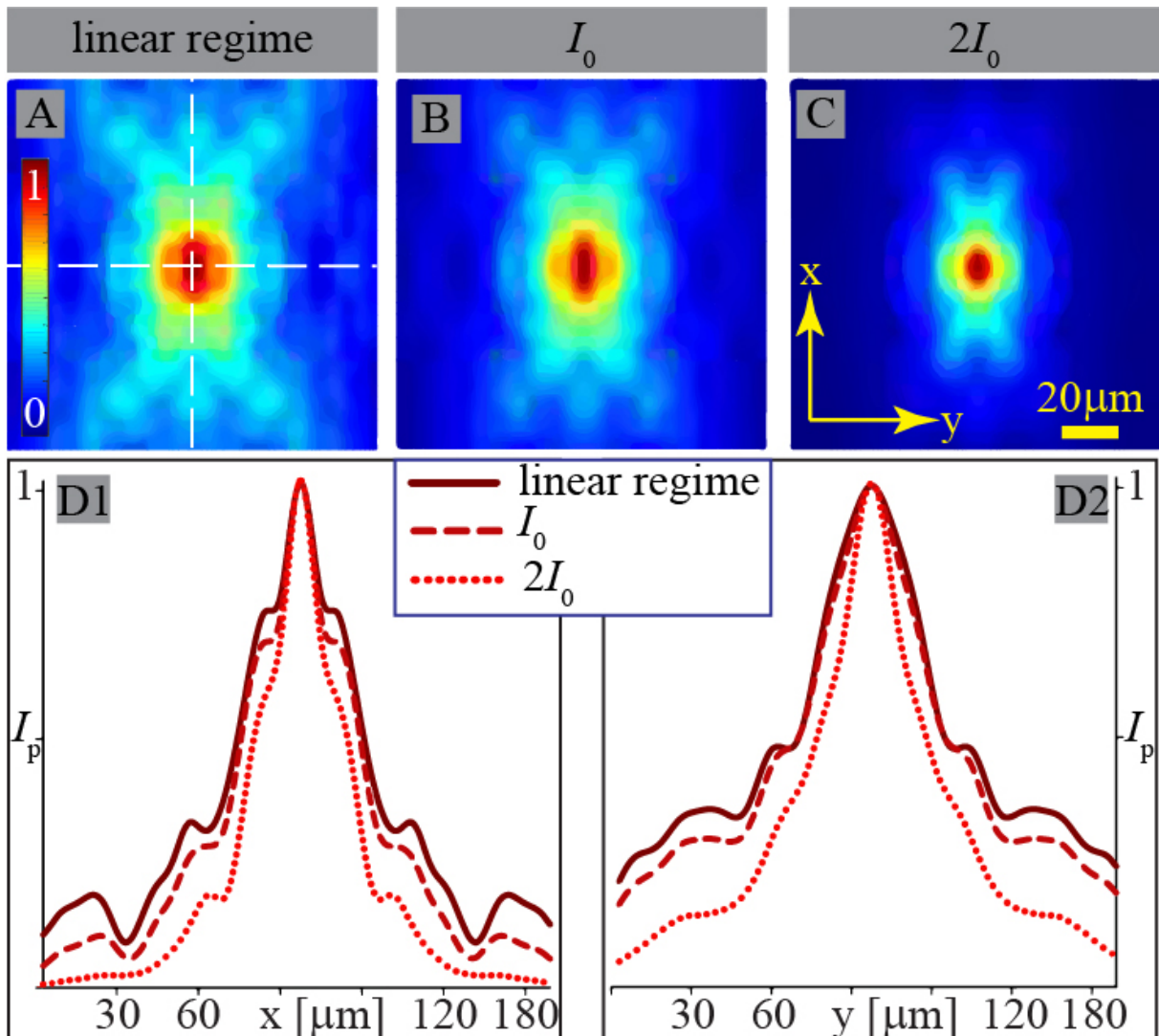


Figure 6.29: Averaged intensity distributions at the lattice output, for 100 different probe beam excitation sites, in (A) linear and (B), (C) nonlinear cases. (D1) and (D2) present averaged intensity profiles, taken along the horizontal and vertical transverse direction (indicated with the white lines in (A)), respectively. Parameters are as in Fig. 6.28.

The effective beam width $\omega_{\text{eff}} = \text{PR}(z)^{-1/2}$, is calculated to characterize the amount of beam expansion, where

$$\text{PR}(z) = \frac{\int |A(x, y, z)|^4 dx dy}{(\int |A(x, y, z)|^2 dx dy)^2} \quad (6.3.3)$$

is the inverse participation ratio [9]. For aperiodic lattices, it is useful to calculate effective width over different incident beam positions and to present averaging effective width in order to remove the effects of the local environment. The averaged effective beam width is calculated along with the propagation distance. A statistical analysis of the effective beam width for the cases demonstrated in Fig. 6.29 is performed. Figure 6.30 shows these results. Hence, it is noticeable that beam expansion during propagation is more hindered while the input beam power increase.

The propagation of light in Mathieu aperiodic lattice is compared with the propagation of light in periodic square lattice. The square lattice is created with period d equal to the characteristic structure size $a = 2\pi/k_{\perp}$ of MG beams used to create the aperiodic lattice, $d = a = 25 \mu\text{m}$ (Fig. 6.27 (C)) (angular spectrum of aperiodic lattice and square lattice lie on same ring). It is demonstrated that light is less localized in the periodic square lattice than in the aperiodic lattice created by synthesizing MG beams.

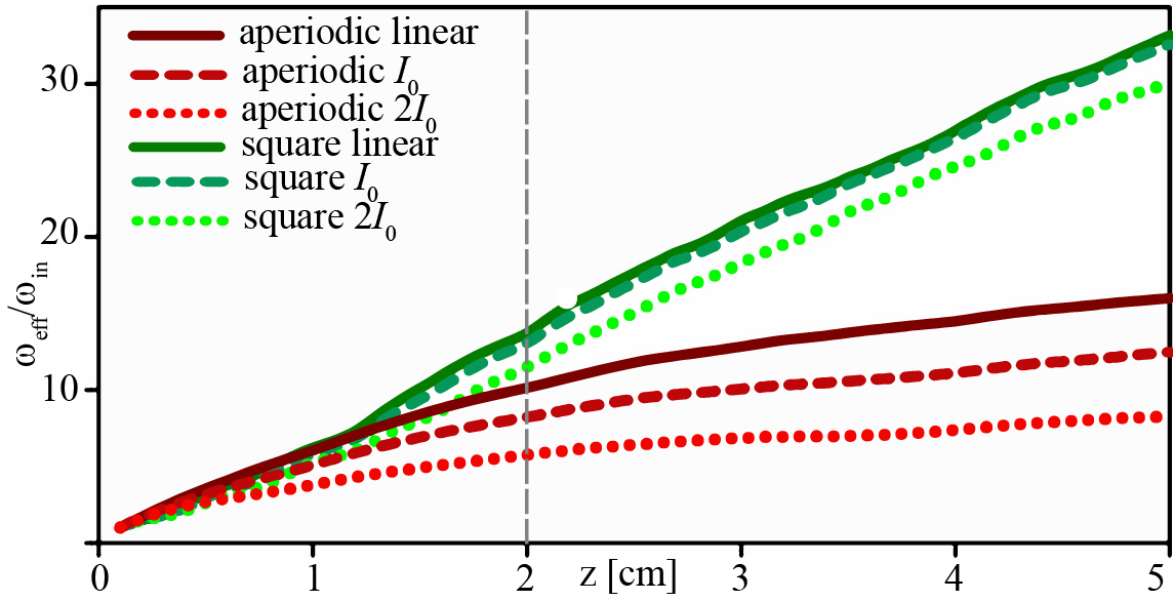


Figure 6.30: Comparison between beam spreading in linear and two nonlinear regimes inside the aperiodic lattice and an appropriate periodic square lattice. Numerical simulation of averaged effective width (averaged over 100 excitation positions) along the propagation distance. ω_{in} is the initial effective width. Parameters are as in Fig. 6.28.

6.3.3 Localization of light in disordered aperiodic Mathieu lattices

In this section there were introduced new kind of aperiodic lattices realized by synthesizing MG beams, and demonstrated enhanced localization of light with increasing input beam power. In further studies of light localization such aperiodic lattices realized by synthesizing MG beams are used for realization of new lattices with both aperiodic lattice and disorder. Transverse localization of light in solid-state physic is demonstrated in random media without nonlinearity, today known as Anderson localization. Realizing that the Anderson localization is a wave phenomenon relying on interference, these concepts were extended to optics and photonics. In past decades Anderson localization is studied in photonic lattices, both numerically and experimentally in one- and two-dimensional systems with the disorder. After the first experimental transverse localization in the two-dimensional periodic lattice with the disorder (a periodic structure superimposed with the disorder) [9] many studies followed in a different one- and two-dimensional photonic lattices, periodic, quasicrystals, etc. A narrow probe beam is launched in disorder photonic lattices and his linear propagation was examined through the lattices with increasing disorder level. These studies are demonstrating the transition from the diffraction of light to Anderson localization when the disorder level is increased. Aperiodic lattices, located between periodic and disorder lattices, are suitable for an investigation of light localization and light transport properties in such lattices containing disorder.

For the investigation of light localization, a propagation invariant optical systems are required. Aperiodic lattices realized by synthesizing MG beams are propagation invariant. One transverse intensity distribution of such lattice is shown in Fig. (6.31) (A). The realization of propagation invariant two-dimensional disordered pattern has to be provided. The spectra of propagation invariant beams are located on circles in the transverse Fourier space. By choosing a constant amplitude but random phases, as indicated in Fig. (6.31) (B), the random granular intensity distribution is realized in the real-space transverse plane. Their mean grain size a is adjustable as it is connected to the radius of the Fourier space circle $k = 2\pi/a$, here directly related with characteristic structure size a of MG beam used for the realization of aperiodic lattices. Now, when propagation invariant aperiodic lattices and disorder patterns are obtained, new two-dimensional photonic lattices with random fluctuation can be realized according to relation $Lattice = (1 - nu) AP + p D$, where AP denotes aperiodic lattice, nu disorder strength and DP is disorder pattern. Disorder strength is controllable same as maximum lattice intensity. Intensity distribution of new lattice with 30% of disorder with maximum lattice intensity $I_{latt} = 0.5$ observed by this approach is represented in Fig. (6.31) (C).

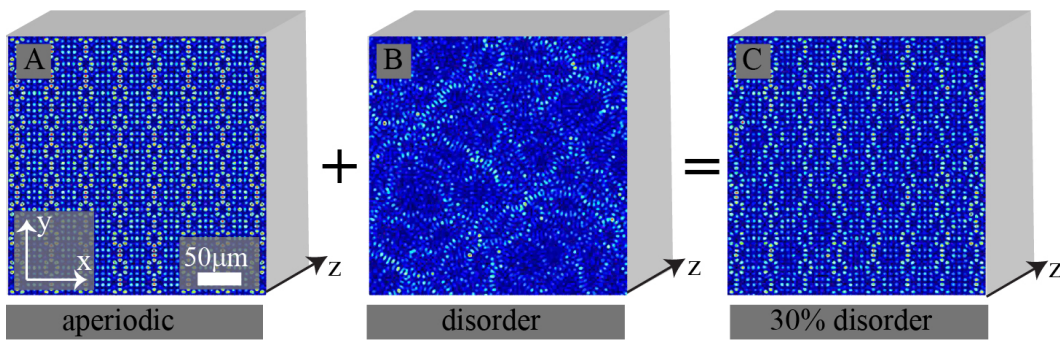


Figure 6.31: The transition from aperiodic Mathieu lattice to disorder lattices.

First, linear light propagation properties are studied in such lattice depending on the disorder strength. The Gaussian probe beam with a FWHM of $w_0 = 8 \mu\text{m}$ is launched into a single site inside lattice. As shown previously for the investigation of localization properties of the aperiodic Mathieu lattice in general, independent of the concrete excitation site, the light propagation in the lattice is

numerically simulated for numerous different probe beam excitation positions and their expansion is averaged. Likewise, to obtain transverse localization of light in random lattices, averaging over multiple different probe beam excitation positions or different spatial realization of the disorder has to be performed.

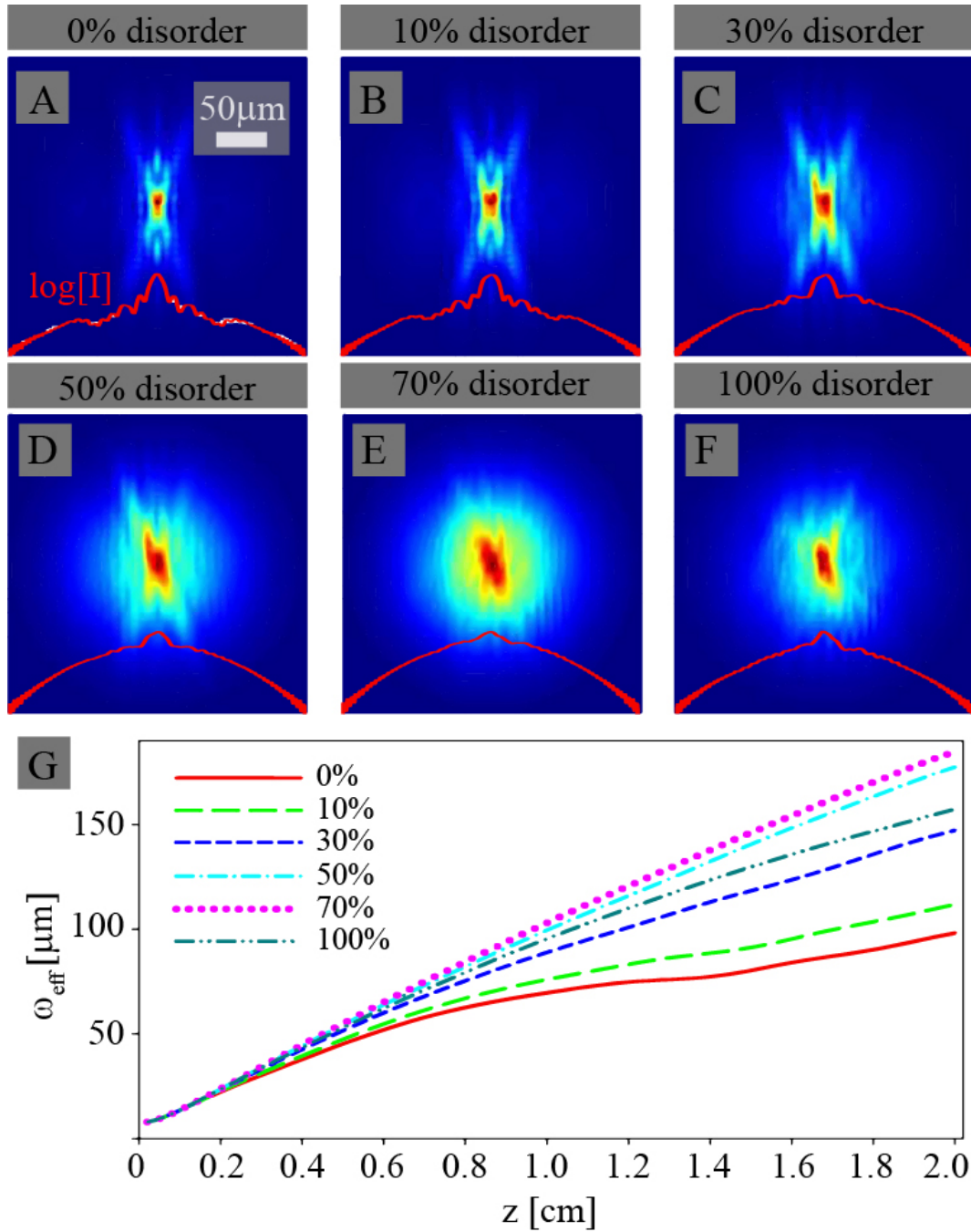


Figure 6.32: Numerical simulated averaged intensity distributions at the lattice output, for 60 different probe beam excitation sites and different disorder strength (A) - (F). (G) Averaged effective width along the propagation distance for different disorder strength. Lattice maximum intensity $I_{\text{latt}} = 0.5$.

Aperiodic lattice is between the periodic and disordered one, hence, it was necessary to perform analysis for different incident beam positions in order to remove the effects of the local environment. For such statistical analysis, the participation ration determined by equation (6.3.3) is used as a measure of localization, i.e. the effective beam width is calculated and averaged for 60 different probe beam excitation positions of the probe beam. Figure (6.32) presents numerical simulated averaged

intensity distributions for 60 different probe beam excitation positions of the probe beam after linear propagating through the lattice with increasing percent of disorder in 20mm long SBN crystal. The effective beam width is calculated to characterize the amount of beam diffraction, i.e. light transport. Figure (6.32) (G) displays the averaged effective beam width of 60 different probe beam excitation positions along with the propagation distance for different disorder strength. The averaged effective beam width in the aperiodic lattice with any percent of disorder (Fig. (6.32) (B-F)) is greater than in the averaged effective beam width without disorder (Fig. (6.32) (A)). This indicates that the light diffracts more along the propagation distance if a disordered fluctuation exists, and this demonstrates enhanced light transport caused by a disorder in the aperiodic lattice realized by synthesizing MG beams. In contrast, the averaged effective beam width in the lattice with higher disorder strength ($>70\%$) is smaller than for lower percent of the disorder indicating that light is more localized for higher disorder strength. According to the logarithm of the intensity profile, it is noticed that for higher disorder strength Anderson localization of light is obtained.

Next, the averaged effective beam width over 60 different excitation positions of the probe beam after 2cm propagation distance is calculated for different percents of disorder and for various maximum lattice intensities, and results are shown in Fig. (6.33). It is obvious if the maximum lattice intensity is weak, diffraction, and localization of light are less noticeable as disorder strength increases. In contrast, for higher lattice intensities, diffraction and localization of light are more pronounced while disorder increases.

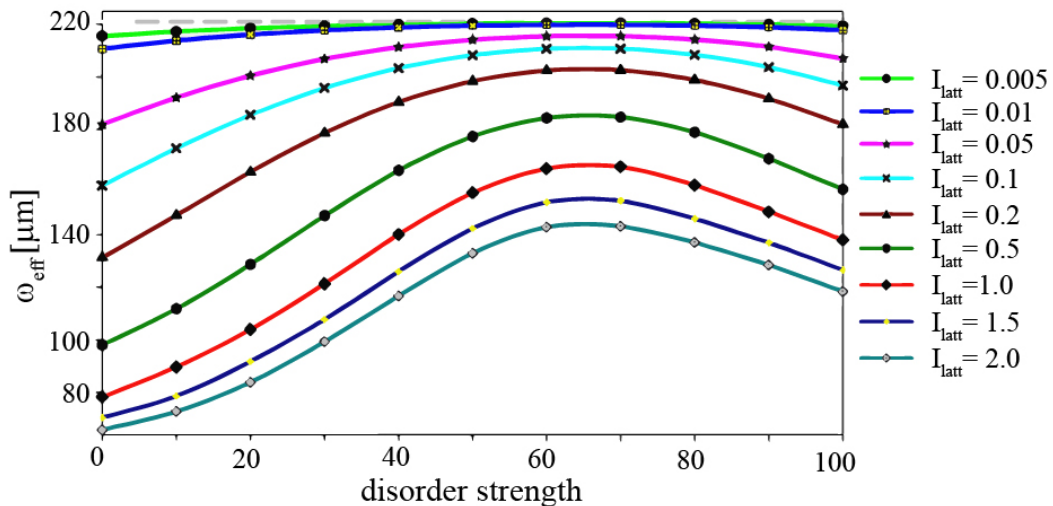


Figure 6.33: Numerical simulated results of averaged effective beam width of probe beam versus disorder strength after 2cm for different maximum lattice intensities.

This section presents new aperiodic lattices realized by MG beams, as well as experimental and numerical investigation of linear and nonlinear propagation of the Gaussian probe beam in them. It is observed that Mathieu beams, due to their different intensity distribution shapes create versatility aperiodic structures. This research endorses the realization of aperiodic lattices with the versatility in aperiodic which provides considerable flexibility and richness in light propagation modeling. It is observed that the excitation of the probe beam in dependency of the input beam position in aperiodic Mathieu lattice creates different diffraction of light. By comparing light propagation in such lattice and appropriate periodic lattice light it is demonstrated that in aperiodic latticed light is more localized. Moreover, an approach for the realization of disorder Mathieu aperiodic lattices is introduced. Mathieu aperiodic lattices in this section are used for examination of light localization. Localization of light in them is obtained with increasing nonlinearity of probe beams or disorder strength of used disordered Mathieu lattice.

Chapter 7

Conclusion

Photonic lattices offer great potential for controlling and manipulating light propagation, therefore, they become an important research area of modern optics during the last decades. Many researches from this field are applicable in the development of other areas, particularly in information and communication technologies. Moreover, when the photonic lattices are inscribed in some nonlinear material, a combination of photonic lattice properties and nonlinearity provides a unique opportunity to achieve ultimate control over linear and nonlinear light propagation. Optical induction in the photorefractive medium provides a successful experimental realization of photonic lattices. Due to the fast and easy reconfiguration of refractive index modulations with optical induction technique easy fabrication of different photonic lattices is provided. Through this thesis different optically induction photonic lattices are realized and fundamental studies of wave propagation in such deterministic aperiodic photonic lattices are examined.

Nondiffracting Mathieu beams facilitate the realization of various photonic lattices in photorefractive crystal via optical induction, even using single or elliptical Mathieu beams, as well as the superposition of multiple Mathieu beams. By this plentiful family of nondiffracting beams, photonic lattices with the configurable shape are realized in this thesis. Single Mathieu beams with manageable ellipticity q , and characteristic structure size a provides realization of both 1D and 2D photonic lattices. Photonic waveguides are realized along different paths like straight layer, circle, ellipse, or even hyperbola only by using Mathieu beams. Also, higher-order Mathieu beams make progress in the realization of the periodic lattice with a manageable period between waveguides.

The realization of discrete aperiodic lattices and propagation of light in them is an unfasten area for research. Mathieu beams, due to diversity of intensity distribution, are great candidates for the creation of various discrete aperiodic lattices. In these thesis, several approaches for the realization of aperiodic lattices using the interference of Mathieu beams in different relations one to another are involved. Thus, different aperiodic photonic lattices are presented light propagation is investigated. Due to different environments in such lattices control of light propagation is possible in both linear or nonlinear regimes. Conditions for light localization are examined. Strong light localization such as robust spatial soliton formation with respect to intensity changes and propagation length is demonstrated in the nonlinear regimes in such lattices. Aperiodic lattices created by synthesizing Mathieu beams hinders the beam expansion during propagation compared to periodic lattices. These results open new directions to exploit light propagating in a broad range of aperiodic photonic lattices and may have applications in capacity-enhanced optical information processing.

The study of the nonlinear propagation of single Mathieu beams of different orders provides nonlinearity strength range in which Mathieu beams preserve nondiffracting character during propagation. Hence, in these range realization of nonlinear Mathieu lattices are feasible. In such nonlinear

lattices, a narrow Gaussian beam propagates the same as in 1D or 2D periodic lattices creating well-known discrete diffraction intensity distribution during the propagation. The potential of using Mathieu beams for the realization of such nonlinear lattices is due to the opportunity to arrange waveguides in the straight array as same as in the hyperbolic array. Therefore, in such nonlinear waveguides 1D discrete diffraction along the straight and hyperbolic waveguide layer is demonstrated.

Research of nonlinear propagation of elliptical Mathieu beams reveals that for very low nonlinearities elliptical Mathieu beams remain nondiffracting beams. Opposite, for higher nonlinearities, the intensity distribution is modulated in the form of high-intensities filament, and the elliptical Mathieu beams are no longer nondiffracting. It is demonstrated that during propagation, these high-intensity modulations along inner ellipse are rotating in the direction determined by energy flow i.e. Poynting vector. The filamentation is investigated in dependence of nonlinearity strength, stricter size, and order of Mathieu beam. Due to this, it is demonstrated that the number of filaments and the velocity of rotation filaments can be increased by increasing these parameters. By elliptical Mathieu beams, dynamical rotation structures are achieved inside SBN crystal.

According to the previous study about elliptical Mathieu beams, 2D chiral waveguides with manageable properties, as well as the possibilities to change the number of chiral waveguides or their slope are demonstrated. It is established that the strength of nonlinearity, order, and characteristic structure size of used Mathieu beams increase the number of chiral waveguides, while the characteristic structure size strongly influences the slope of waveguides. This is an improvement for the realization of 2D chiral photonic lattices with manageable properties. In past realization, chiral lattices are experimentally realized demanding a long realization time because every waveguide is separably inscribed into the crystal using complex experimental setups. By using elliptical Mathieu beams, chiral lattices can be fast and easily realized in photosensitive media by optical induction techniques. Such lattices open new fields for research of light propagation.

Due to investigation in this thesis new phenomena, nonlinear discrete diffraction, or morphing discrete diffraction are demonstrated by using Mathieu beams in nonlinear SBN crystal. 1D nonlinear discrete diffraction is specified by nonlinear propagation of zero-order Mathieu beam inside photorefractive media. When the order of the Mathieu beam increases also the number of spots over straight or hyperbolic layers increases, allowing dimensional cross over from one- to two-dimensional structures. Several higher-order Mathieu beams were investigated during nonlinear propagation in photorefractive media, and consequently, 2D nonlinear discrete diffraction is demonstrated.

Control of light propagation in Mathieu lattices is examined, such as the propagation of elliptical vortex in appropriate Mathieu lattices. It is demonstrated that elliptical vortex propagated in Mathieu lattices creating the stable elliptical vortex necklaces during propagation, oscillating dipoles, dynamic instabilities. The stability of vortex necklaces is examined for different Mathieu beam orders and ellipticities, different sizes, and topological charge of the elliptical vortex, over long propagation distances, and strength of nonlinearity. It is revealed that higher beam order provides more pearls in elliptical vortex necklaces, as well as the size of the elliptical vortex, while the ellipticity changes the distance between the pearls, while higher orders topological charges harm the stability of elliptical vortex necklaces. Higher orders topological charges visible influence on the phase distributions, creating phase separation which increases while the ellipticity, topological charge, and propagation distance increase. For longer propagation distances elliptical necklaces are stable for propagation length of few crystal sizes, but for further propagation distances, the oscillating dipole states are realized. According to nonlinearity strength, elliptical necklaces are stable only for low nonlinearities. In contrast, for higher nonlinearities, elliptical necklaces are damaged. This research supports the future examination of the elliptical vortex in different suitable lattices realized with optical induction technique. Such research leads to the potential application of elliptical vortex beams in optical tweezers, quantum information processing, or optical manipulation and trapping.

In this thesis different photonic lattices are featured, accomplished with Mathieu nondiffracting beams as well as manipulation of light transport in different Mathieu lattices. In particular, different Mathieu aperiodic lattices created in this thesis can be extended to studies of other deterministic aperiodic photonic lattices optically induced by other than Mathieu beams. Further examination of various aperiodic lattices would contribute to a fundamental understanding of light transport characteristics in these artificially designed structures. Such examination opens and new applications of aperiodic lattices to control of light or future devices realizations.

Bibliography

- [1] J. D. Joannopoulos, S. G. Johnson, J. N. Winn, and R. D. Meade, *Photonic Crystals: Molding the Flow of Light*, 2nd ed. (Princeton University, 1995).
- [2] Z. Bouchal, Czechoslovak Journal of Physics, 53, 537 (2003).
- [3] F. Lederer, G. I. Stegeman, D. N. Christodoulides, G. Assanto, M. Segev, Y. Silberberg, Phys. Rep. 463, 1 (2008).
- [4] S. Somekh, E. Garmire, A. Yariv, H.L. Garvin, R.G. Hunsperger, Appl. Phys. Lett. 22, 46 (1973).
- [5] J.W. Fleischer, T. Carmon, M. Segev, N.K. Efremidis, D.N. Christodoulides, Phys. Rev. Lett. 90, 023902 (2003).
- [6] D.N. Christodoulides, R.I. Joseph, Opt. Lett. 13, 794 (1988).
- [7] H.S. Eisenberg, Y. Silberberg, R. Morandotti, A.R. Boyd, J.S. Aitchison, Phys. Rev. Lett. 81, 3383 (1998).
- [8] J.W. Fleischer, M. Segev, N.K. Efremidis, D.N. Christodoulides, Nature 422, 147 (2003).
- [9] T. Schwartz, G. Bartal, S. Fishman, and M. Segev, Nature 446, 52 (2007).
- [10] D. S. Wiersma, Nat. Photon. 7, 188, (2013).
- [11] L. Dal Negro and S. V. Boriskina, Laser Photonics Reviews 6 (2), 178 (2012).
- [12] P. W. Anderson, Phys. Rev. 109, 1492 (1958).
- [13] A. Lagendijk, B. van Tiggelen, and D. S. Wiersma, Phys. Today 62, 24 (2009).
- [14] M. Segev, Y. Silberberg, and D. N. Christodoulides, Nature Photon. 7, 197 (2013).
- [15] D. Shechtman, I. Blech, D. Gratias, and J.W. Cahn, Phys. Rev. Lett. 53, 1951 (1984).
- [16] Z. V. Vardeny, A. Nahata, and A. Agrawal, Nat. Photon. 7, 177 (2013).
- [17] W. Steurer and S. Deloudi, *Crystallography of Quasicrystals - Concepts, Methods and Structures*, Springer Series in Material Science 126 (Springer Verlag, Berlin, 2009).
- [18] M. Senechal, *Quasicrystals and geometry* (Cambridge Univ. Press, Cambridge), 199).
- [19] B. Freedman, G. Bartal, M. Segev, R. Lifshitz, D. N. Christodoulides, and J. W. Fleisher, Nature 440, 1166 (2006).

- [20] R. Morandotti, U. Peschel, J.S. Aitchison, H.S. Eisenberg, Y. Silberberg, Phys. Rev. Lett. 83, 4756 (1999).
- [21] I. L. Garanovich, A. A. Sukhorukov, Y. S. Kivshar, Cent. Eur. J. Phys. 6(3), 593 (2008).
- [22] M. C. Rechtsman, J. M. Zeuner, Y. Plotnik, Y. Lumer, D. Podolsk, F. Dreisow, S. Nolte, M. Segev, and A. Szameit, Nature 496, 196 (2013).
- [23] I. L. Garanovich, S. Longhi, A. A. Sukhorukov, Y. S. Kivshar, Physics Reports 518, 1 (2012).
- [24] T. Pertsch, P. Dannberg, W. Elflein, A. Brauer, F. Lederer, Phys. Rev. Lett. 83, 4752 (1999).
- [25] H. Trompeter, W. Krolikowski, D.N. Neshev, A.S. Desyatnikov, A.A. Sukhorukov, Y.S. Kivshar, T. Pertsch, U. Peschel, F. Lederer, Phys. Rev. Lett. 96, 053903 (2006).
- [26] S. Longhi, Laser Photonics Rev. 3, 243 (2009).
- [27] T. Pertsch, T. Zentgraf, U. Peschel, A. Brauer, and F. Lederer, Phys Rev. Lett. 88, 093901 (2002).
- [28] T. Pertsch, U. Peschel, F. Lederer, J. Burghoff, M. Will, S. Nolte, and A. Tünnermann, Opt. Lett. 29, 468 (2004).
- [29] A. Szameit, and S. Nolte, J. Phys. B: At. Mol. Opt. Phys. 43, 163001 (2010).
- [30] Y. S. Kivshar, G. P. Agrawal, *Optical Solitons: From Fibers to Photonic Crystals*, Academic Press, San Diego, 2003.
- [31] D.N. Christodoulides, F. Lederer, Y. Silberberg, Nature 424, 817 (2003).
- [32] D. M. Jović, Yu. S. Kivshar, C. Denz, and M. R. Belić Phys. Rev. A 84, 043811 (2011).
- [33] A. Szameit, Y. V. Kartashov, F. Dreisow, M. Heinrich, T. Petrisch, S. Nolte, A. Tünnermann, V. A. Vysloukh, F. Lederer, and L. Torner, Phys. Rev. Lett. 102, 063902 (2009).
- [34] D. M. Jović, M. R. Belić, and C. Denz, Phys. Rev. A 84, 043811 (2011).
- [35] Y. Lahini, A. Avidan, F. Pozzi, M. Sorel, R. Morandotti, D. N. Christodoulides, and Y. Silberberg, Phys. Rev. Lett. 100, 013906 (2008).
- [36] N. M. Lučić, D. M. Jović Savić, A. Piper, D. Ž. Grujić, J. M. Vasiljević, D. V. Pantelić, B. M. Jelenković, and D. V. Timotijević, Journal of the Optical Society of America B 32(7), 1510 (2015).
- [37] P. Millar, J.S. Aitchison, J.U. Kang, G.I. Stegeman, A. Villeneuve, G.T. Kennedy, W. Sibbett, J. Opt. Soc. Am. B 14, 3224 (1997).
- [38] S. Nolte, M. Will, J. Burghoff, A. Tuennermann, Appl. Phys. A 77, 109 (2003).
- [39] N. K. Efremidis, S. Sears, D. N. Christodoulides, J. W. Fleischer and M. Segev, Phys. Rev. E 66, 046602, 2002.
- [40] J. Becker, J. Xavier, M. Boguslawski, P. Rose, J. Joseph, and Cornelia Denz, Proc. of SPIE vol. 7712 77123A 1-6 (2010).
- [41] A. Zannotti, F. Diabel, M. Boguslawski and C. Denz, Adv. Opt. Mater. 5, 1600629 (2017).

- [42] J. Durnin, *J. Opt. Soc. Am. A* 4, 651 (1987).
- [43] P. Zhang, Y. Hu, T. Li, D. Cannan, X. Yin, R. Morandotti, Z. Chen, and X. Zhang, *Phys. Rev. Lett.* 109, 193901 (2012).
- [44] E. G. Kalnins and W. Miller, *J. Math. Phys.* 17, 331 (1976).
- [45] J. C. Gutiérrez-Vega, M. D. Iturbe-Castillo, and S. Chávez-Cerda, *Opt. Lett.* 25, 1493 (2000).
- [46] M. A. Bandres, J. C. Gutiérrez-Vega, and S. Chávez-Cerda, *Opt. Lett.* 29, 44 (2004).
- [47] Z. Bouchal, J. Wagner, M. Chlup, *Optics Communications* 151,207 (1998).
- [48] J. Baumgartl, M. Mazilu, and K. Dholakia, *Nature Photon* 2, 675 (2008).
- [49] J. Broky, G. A. Siviloglou, A. Dogariu, and D. N. Christodoulides, *Optics Express* 16(17), 12880 (2008).
- [50] S. Vyas, Y. Kozawa, and S. Sato, *J. Opt. Soc. Am. A* 28, 837 (2011).
- [51] S. Sogomonian, S. Klewitz, S. Herminghaus, *Optics Communications* 139, 313(1997).
- [52] S. Chávez-Cerda, M. A. Meneses-Nava, and J. M. Hickmann, *Optics Letters* 23(24), 1871 (1998).
- [53] A. Vasara, J. Turunen, and A. T. Friberg, *J. Opt. Soc. Am. A* 6, 1748 (1989).
- [54] G. Scott, N. McArdle, *Optical Engineering* 31(12), 2640 (1992).
- [55] N. Chattrapiban, E. A. Rogers, D. Cofield, W. T. Hill, III, and R. Roy, *Opt. Lett.* 28, 2183 (2003).
- [56] P. Rose, B. Terhalle, J. Imbrock, C. Denz, *J. Phys. D: Appl. Phys.*, 41, 224004 (2008).
- [57] Y. S. Chan, C. T. Chan, Z. Y. Liu, *Phys. Rev. Lett.*, 80, 956 (1998).
- [58] E. Zoorob, M. D. Charlton, G. J. Parker, J. J. Baumberg, M. C. Netti, *Nature*, 404, 740 (2000).
- [59] M. Bayindir, E. Cubukcu, I. Bulu, E. Ozbay, *Phys. Rev. B*, 63, 161104 (2001).
- [60] M. Boguslawski, N. M. Lučić, F. Diebel, D. V. Timotijević, C. Denz, and D. M. Jović Savić, *Optica* 3(7), 711 (2016).
- [61] E. Mathieu, *Journal de Mathématiques Pures et Appliquées* 13, 137-203 (1868).
- [62] T. R. Carver, *American Journal of Physics* 39, 1225 (1971).
- [63] R. C. Cross, *Am. J. Phys.* 53, 563 (1985).
- [64] J. Gutiérrez-Vega, S. Chávez-Cerda, and Ramón Rodríguez-Dagnino *Rev. Mex. Fis.* 45(6), 613 (1999).
- [65] C. L. López-Mariscal, M. A. Bandres, J. C. Gutiérrez-Vega, Chávez-Cerda, *Opt. Express* 13, 2364 (2005).
- [66] J. C. Gutiérrez-Vega, M. D. Iturbe-Castillo, G. A. Ramírez, E. Tepichín, R. M. Rodríguez-Dagnino, S. Chávez-Cerda, G. H. C. New, *Opt. Commun.* 195, 35 (2001).

- [67] J. C. Gutiérrez-Vega, R. M. Rodríguez-Dagnino, M. A. Meneses-Nava, S. Chávez-Cerda, *Am. J. Phys.* 71, 233 (2003).
- [68] C. López-Mariscal, J. C. Gutiérrez-Vega, G. Milne, K. Dholakia, *Opt. Express* 14, 4182 (2006).
- [69] C. Alpmann, R. Bowman, M. Woerdemann, M. Padgett, C. Denz, *Opt. Express* 18, 26084 (2010).
- [70] K. Megumi, H. Kozuka, M. Kobayashi, Y. Furuhashi: *Appl. Phys. Lett.* 30, 631 (1977).
- [71] R. W. Boyd, *Nonlinear optics*, Elsevier Inc. 2008.
- [72] P. Yeh, *Introduction to Photorefractive Nonlinear Optics*, John Wiley and Sons, Inc., New York, Chichester, Brisbane, Toronto, Singapore, (1993).
- [73] B. E. A. Saleh, M. C. Teich, *Fundamentals of Photonics*, John Wiley and Sons, Inc Hoboken, New Jersey, Canada, 2nd edition (2007).
- [74] L. I. Ivleva, N.V. Bogodaev, N. M. Polozkov, V. V. Osiko, *Optical Materials* 4(2-3), 168 (1995).
- [75] D. Kip, S. Aulkemeyer, K. Buse, F. Mersch, R. Pankrath, E. Krätzig, *Phys. Stat. Sol. A*, 154, K5 (1996).
- [76] J. M. Vasiljević, A. Zannotti, D.V. Timotijević, C. Denz, and D. M. Jović Savić, *Phys. Rev. A* 96, 023840, 2017.
- [77] J. A. Davis, D. M. Cottrell, J. Campos, M. J. Yzuel, I. Moreno, *Applied Optics*, 38, 5004 (1999).
- [78] E. Otte, C. Schlickriede, C. Alpmann, and C. Denz, *Proc. SPIE* 9379, 937908 (2015).
- [79] N. V. Kukhtarev, V. B. Markov, S. G. Odoulov, M. S. Soskin, V. L. Vinetskii, *Ferroelectrics* 22, 961 (1979).
- [80] A. A. Zozulya and D. Z. Anderson, *Phys. Rev. A* 51, 1520 (1995).
- [81] G. P. Agrawal, *Nonlinear Fiber Optics* 5th edition, Academic Press (2012).
- [82] G. H. Weiss, A.A. Maradudin, *J. Math. Phys.* 3, 771 (1962).
- [83] M. Born, E. Wolf, *Principles of Optics*, 7th ed., Cambridge University Press, Cambridge, UK 1999.
- [84] L. Allen, M. Padgett, M. Babiker, *Prog. Opt.* 39, 291 (1999).
- [85] C. Denz, M. Schwab, C. Weillnau, *Transverse-Pattern Formation in Photorefractive Optics*, 1st ed., Springer-Verlag, Berlin, Heidelberg, New York 2003.
- [86] L. M. Pismen, *Vortices in Nonlinear Fields* (Clarendon, Oxford, 1999).
- [87] F. Ye, D. Mihalache, B. Hu, *Phys. Rev. A*, 79, 053852 (2009).
- [88] Z. Chen, H. Martin, A. Bezryadina, D. Neshev, Y. S. Kivshar, and D. N. Christodoulides, *J. Opt. Soc. Am. B* 22, 1395 (2005).
- [89] C. López-Mariscal, M. A. Bandres, and J. C. Gutiérrez-Vega, *Optical Engineering* 456, 068001 (2006).

Biografija

Jadranka Vasiljević rođena je u Kraljevu 27. maja 1990. godine. Osnovne akademske studije završila je 2013. godine na Prirodno-matematičkom fakultetu Univerziteta u Kragujevcu, smer Fizika, sa prosečnom ocenom 9,51.

Iste godine upisala je master akademske studije na Prirodno - matematičkom fakultetu Univerziteta u Kragujevcu, smer Fizika, koje je završila 2014. godine sa prosečnom ocenom 9,5. Završni rad pod nazivom: "*Prostiranje i lokalizacija svetlosti u kvaziperiodičnim fotonskim rešetkama*", za koji je eksperimentalni deo uradila na Institutu za fiziku u Laboratoriji za nelinearnu fotoniku pod mentorstvom Dr Dragane Jović Savić, je odbranila 2014. godine na Prirodno-matematičkom fakultetu Univerziteta u Kragujevcu. Tokom studija bio je stipendista Ministarstva prosvete, nauke i tehnološkog razvoja i Fonda za mlade talente Republike Srbije - Dositeja.

Školske 2014/2015. godine upisala je Doktorske akademske studije na Fizičkom fakultetu Univerziteta u Beogradu, smer kvantna optika i laseri. Od aprila 2015. do novembra 2017. godine bila je stipendista Ministarstva prosvete, nauke i tehnološkog razvoja.

Na Institutu za fiziku u Beogradu zaposlena je od novembra 2017. godine u Laboratoriji za nelinearnu fotoniku. U zvanje istraživač saradnik je izabrana u junu 2019. godine. Od 2015. je angažovana na projektu osnovnih istraživanja OI171036 "Nelinearna fotonika nehomogenih sredina i površin" Ministarstva prosvete, nauke i tehnološkog razvoja Republike Srbije čiji rukovodilac je Dr Dragana Jović Savić.

Pored toga učestvovala je i na bilateralnom projektu između Republike Srbije i Republike Nemačke "Kontrola svetlosti pomoću determinističkih aperiodičnih i kompleksnih fotonskih rešetk" 2016. i 2017. godine, u okviru kog je više puta posetila Institut za primenjenu fiziku, Univerziteta u Minsteru, Nemačka.

Izjava o autorstvu

Ime i prezime autora _____

Broj indeksa _____

Izjavljujem

da je doktorska disertacija pod naslovom

rezultat sopstvenog istraživačkog rada;

da disertacija u celini ni u delovima nije bila predložena za sticanje druge diplome prema studijskim programima drugih visokoškolskih ustanova;

da su rezultati korektno navedeni i

da nisam kršila autorska prava i koristila intelektualnu svojinu drugih lica.

U Beogradu, _____

Potpis autora

Izjava o istovetnosti štampane i elektronske verzije doktorskog rada

Ime i prezime autora _____

Broj indeksa _____

Studijski program _____

Naslov rada _____

Mentor _____

Izjavljujem da je štampana verzija mog doktorskog rada istovetna elektronskoj verziji koju sam predala radi pohranjivanja u Digitalnom repozitorijumu Univerziteta u Beogradu.

Dozvoljavam da se objave moji lični podaci vezani za dobijanje akademskog naziva doktora nauka, kao što su ime i prezime, godina i mesto rođenja i datum odbrane rada.

Ovi lični podaci mogu se objaviti na mrežnim stranicama digitalne biblioteke, u elektronskom katalogu i u publikacijama Univerziteta u Beogradu.

U Beogradu, _____

Potpis autora

Izjava o korišćenju

Ovlašćujem Univerzitetsku biblioteku "Svetozar Marković" da u Digitalni repozitorijum Univerziteta u Beogradu unese moju doktorsku disertaciju pod naslovom: _____

koja je moje autorsko delo.

Disertaciju sa svim priložima predala sam u elektronskom formatu pogodnom za trajno arhiviranje.

Moju doktorsku disertaciju pohranjenu u Digitalnom repozitorijumu Univerziteta u Beogradu i dostupnu u otvorenom pristupu mogu da koriste svi koji poštuju odredbe sadržane u odabranom tipu licence Kreativne zajednice (Creative Commons) za koju sam se odlučila.

1. Autorstvo (CC BY)

2. Autorstvo - nekomercijalno (CC BY-NC)

3. Autorstvo - nekomercijalno - bez prerada (CC BY-NC-ND)

4. Autorstvo - nekomercijalno - deliti pod istim uslovima (CC BY-NC-SA)

5. Autorstvo - bez prerada (CC BY-ND)

6. Autorstvo - deliti pod istim uslovima (CC BY-SA)

(Molimo da zaokružite samo jednu od šest ponudjenih licenci. Kratak opis licenci je sastavni deo ove izjave).

U Beogradu, _____

Potpis autora

1. **Autorstvo.** Dozvoljavate umnožavanje, distribuciju i javno saopštavanje dela, i prerade, ako se navede ime autora na način određen od strane autora ili davaoca licence, čak i u komercijalne svrhe. Ovo je najslobodnija od svih licenci.
2. **Autorstvo - nekomercijalno.** Dozvoljavate umnožavanje, distribuciju i javno saopštavanje dela, i prerade, ako se navede ime autora na način određen od strane autora ili davaoca licence. Ova licenca ne dozvoljava komercijalnu upotrebu dela.
3. **Autorstvo - nekomercijalno - bez prerada.** Dozvoljavate umnožavanje, distribuciju i javno saopštavanje dela, bez promena, preoblikovanja ili upotrebe dela u svom delu, ako se navede ime autora na način određen od strane autora ili davaoca licence. Ova licenca ne dozvoljava komercijalnu upotrebu dela. U odnosu na sve ostale licence, ovom licencom se ograničava najveći obim prava korišćenja dela.
4. **Autorstvo - nekomercijalno - deliti pod istim uslovima.** Dozvoljavate umnožavanje, distribuciju i javno saopštavanje dela, i prerade, ako se navede ime autora na način određen od strane autora ili davaoca licence i ako se prerada distribuira pod istom ili sličnom licencom. Ova licenca ne dozvoljava komercijalnu upotrebu dela i prerada.
5. **Autorstvo - bez prerada.** Dozvoljavate umnožavanje, distribuciju i javno saopštavanje dela, bez promena, preoblikovanja ili upotrebe dela u svom delu, ako se navede ime autora na način određen od strane autora ili davaoca licence. Ova licenca dozvoljava komercijalnu upotrebu dela.
6. **Autorstvo - deliti pod istim uslovima.** Dozvoljavate umnožavanje, distribuciju i javno saopštavanje dela, i prerade, ako se navede ime autora na način određen od strane autora ili davaoca licence i ako se prerada distribuira pod istom ili sličnom licencom. Ova licenca dozvoljava komercijalnu upotrebu dela i prerada. Slična je softverskim licencama, odnosno licencama otvorenog koda.